

Washington University in St. Louis

Washington University Open Scholarship

All Theses and Dissertations (ETDs)

January 2009

Improving Biocompatibility By Controlling Protein Adsorption: Modification And Design Of Biomaterials Using Poly(Ethylene Glycol) Microgels And Microspheres

Evan Scott

Washington University in St. Louis

Follow this and additional works at: <https://openscholarship.wustl.edu/etd>

Recommended Citation

Scott, Evan, "Improving Biocompatibility By Controlling Protein Adsorption: Modification And Design Of Biomaterials Using Poly(Ethylene Glycol) Microgels And Microspheres" (2009). *All Theses and Dissertations (ETDs)*. 316.

<https://openscholarship.wustl.edu/etd/316>

This Dissertation is brought to you for free and open access by Washington University Open Scholarship. It has been accepted for inclusion in All Theses and Dissertations (ETDs) by an authorized administrator of Washington University Open Scholarship. For more information, please contact digital@wumail.wustl.edu.

WASHINGTON UNIVERSITY IN ST. LOUIS
Sever Institute
School of Engineering and Applied Science
Department of Biomedical Engineering

Dissertation Examination Committee:

Donald L. Elbert, Chair
Frank C.P. Yin, M.D., Ph.D.
Garland R. Marshall, Ph.D.
Rohit V. Pappu, Ph.D.
R. Reid Townsend, M.D., Ph.D.
Radhakrishna Sureshkumar, Ph.D.

IMPROVING BIOCOMPATIBILITY BY CONTROLLING PROTEIN
ADSORPTION: MODIFICATION AND DESIGN OF BIOMATERIALS
USING POLY(ETHYLENE GLYCOL) MICROGELS AND
MICROSPHERES

By

Evan Alexander Scott, Sc.B.

A dissertation presented to the
Graduate School of Arts and Sciences of
Washington University in partial fulfillment
of the requirements for the degree of
DOCTOR OF PHILOSOPHY

June, 2009
Saint Louis, Missouri

Acknowledgements

I would first like to sincerely thank my advisor, Donald Elbert, for all of his support and guidance. He has provided me with experimental freedom and insight that has helped foster my enthusiasm for science and research. I would also like to thank my thesis committee (Frank Yin, Garland Marshall, Rohit Pappu, Reid Townsend, and Radhakrishna Sureshkumar) for taking the time to advise and evaluate this work.

I want to thank everyone that I worked with in the Elbert lab. I will always treasure my first few years in graduate school working with Shannon Alford, Megan Kaneda, and Brad Wacker. A special thanks to Casey Donahoe, Peter Nguyen, Megan Flake, and Xioli (Lily) He for providing such an enjoyable work environment and interesting discussions. I would especially like to thank Michael Nichols who worked side-by-side with me on several projects.

Finally, I would like to dedicate this work to my parents and sisters to whom I owe everything. I want to particularly stress the essential work ethic and studious nature that was instilled in me by my Mom, as well as my Dad's passion for bad sci-fi movies that likely sparked my initial interest in science as well as my imagination at a very young age. Thanks to all the friends I made at Wash U. (Paul Watkins, Stephanie Willerth, Gary Escudero, Eric Welsh, Dan Kuster, Paul Wanda, Keith Decker, Ben Filas, Nick Anderson, Ken Borrelli, Philip Johnson, and Matthew Wood).

Evan Alexander Scott

Washington University in St. Louis

June, 2009

Table of Contents

| | |
|--------------------------------|-----|
| Acknowledgements | ii |
| List of Tables | vi |
| List of Figures | vii |
| Abstract of Dissertation | xi |

Chapter 1

| | |
|---|----------|
| Introduction | 1 |
| 1.1 Synopsis and Objectives of Thesis | 5 |
| 1.2 Protein Films on Biomaterials: Biological Implications & Characterization of Adsorbed Fibrinogen | 5 |
| 1.2.1 Relevance of Protein Films in Biomaterials Science | 5 |
| 1.2.2 Fibrinogen Structure and Surface Activity | 8 |
| 1.2.3 Post-Adsorptive Structure of Fibrinogen | 11 |
| 1.3 Controlling Protein Adsorption and Bioactivity Via Surface Treatments of Biomaterials..... | 14 |
| 1.3.1 Progression of Biomaterials Design: Improving the Biocompatibility of Poly(ethylene terephthalate)..... | 14 |
| 1.3.2 Directing Cell Adhesion & Migration: Integrin-Binding Motifs & Sphingosine 1-Phosphate Delivery | 18 |
| 1.3.3 Layer-by-layer Methods | 22 |
| 1.3.4 Radio Frequency Glow Discharge Plasma Treatments | 24 |
| 1.4 Poly(Ethylene Glycol) Hydrogels as Biomaterials | 26 |
| 1.4.1 Poly(Ethylene Glycol): Resistance to Protein Adsorption & Chemical Functionalization | 26 |
| 1.4.2 Poly(Ethylene Glycol) Surface Coatings | 29 |
| 1.4.3 Poly(Ethylene Glycol) Scaffolds | 30 |

Chapter 2

| | |
|--|-----------|
| Mass Spectrometric Mapping of Fibrinogen Conformations at Poly(Ethylene Terephthalate) Interfaces | 33 |
| 2.1 Abstract | 33 |
| 2.2 Introduction | 34 |
| 2.3 Materials and Methods | 39 |
| 2.3.1 Spin Coating | 39 |
| 2.3.2 OWLS Analysis | 40 |
| 2.3.3 Analysis of OWLS Results | 40 |
| 2.3.4 PET Particle Fabrication | 41 |
| 2.3.5 Biotinylation | 42 |
| 2.3.6 MALDI-TOF Analysis | 43 |
| 2.3.7 Liquid Chromatography Electrospray-Ionization Ion Trap Tandem Mass Spectrometry..... | 44 |

| | | |
|--------|---|----|
| 2.3.8 | Expression of HepG2 Proteins | 45 |
| 2.3.9 | Quantification of $^{13}\text{C}_6, ^{15}\text{N}_2$ -Fibrinogen Concentrations in Media..... | 46 |
| 2.3.10 | $^{13}\text{C}_6, ^{15}\text{N}_2$ -Fibrinogen Purification | 46 |
| 2.3.11 | Preparation of $^{13}\text{C}_6, ^{15}\text{N}_2$ -HepG2 Protein Standards | 47 |
| 2.4 | Results | 47 |
| 2.4.1 | Characterization of PET Films | 47 |
| 2.4.2 | OWLS Analysis of Fibrinogen Adsorption onto PET | 50 |
| 2.4.3 | MALDI-TOF Sequence Coverage | 50 |
| 2.4.4 | PET Particle Fabrication | 53 |
| 2.4.5 | Biotinylation of Surface-Adsorbed Fibrinogen | 55 |
| 2.4.6 | Identification of Biotinylated Residues | 58 |
| 2.4.7 | Quantification of Complement C3, α_2 -Macroglobulin, & Fibrinogen.. | 65 |
| 2.5 | Discussion | 74 |
| 2.6 | Conclusion | 81 |

Chapter 3

Protein Adsorption & Cell Adhesion on Nanoscale Bioactive Coatings

| | | |
|--|--|-----------|
| Formed from Poly(Ethylene Glycol) & Albumin Microgels | | 83 |
| 3.1 | Abstract | 83 |
| 3.2 | Introduction | 84 |
| 3.3 | Materials and Methods | 86 |
| 3.3.1 | Synthesis of Poly(Ethylene Glycol) Vinylsulfone | 86 |
| 3.3.2 | Microgel Syntheses | 87 |
| 3.3.3 | Characterization of Microgel Formation | 88 |
| 3.3.4 | Reaction with Surfaces | 90 |
| 3.3.5 | Cell Culture and Adhesion Experiments | 93 |
| 3.3.6 | OWLS Measurements and Analysis | 94 |
| 3.3.7 | QCM-D Measurements and Analysis | 95 |
| 3.4 | Results | 97 |
| 3.4.1 | PEG-OVS Synthesis..... | 97 |
| 3.4.2 | Characterization of Microgel Formation | 99 |
| 3.4.3 | Covalent Attachment of Microgels to Glass Surfaces | 103 |
| 3.4.4 | Properties & Protein Adsorption Resistance of PEG-OVS/BSA Microgel Coatings | 108 |
| 3.4.5 | Resistance of Microgel-Coated Glass to Cell Adhesion | 110 |
| 3.4.6 | Application of Microgel Coating to PET surfaces | 119 |
| 3.5 | Discussion | 121 |
| 3.6 | Conclusion | 125 |

Chapter 4

Modular Scaffolds Assembled Around Living Cells Using Poly(Ethylene Glycol) Microspheres with Macroporation Via a Non-Cytotoxic Porogen

| | | |
|--------------|---|------------|
| | | 126 |
| 4.1 | Abstract | 126 |
| 4.2 | Introduction | 127 |
| 4.3 | Materials and Methods | 134 |
| 4.3.1 | Poly(Ethylene Glycol) Derivatives | 134 |
| 4.3.2 | Dynamic Light Scattering | 134 |

| | | |
|-----------------------------|--|------------|
| 4.3.3 | Microsphere Fabrication & Characterization | 135 |
| 4.3.4 | Microsphere Fabrication for Scaffolds | 136 |
| 4.3.5 | Scaffold Assembly & Cell Seeding | 136 |
| 4.3.6 | Confocal Microscopy | 137 |
| 4.3.7 | Rheometry | 137 |
| 4.3.8 | Statistics | 138 |
| 4.4 | Results | 138 |
| 4.4.1 | Formation of PEG ₈ -VS/PEG ₈ -Amine Microspheres | 138 |
| 4.4.2 | Formation of PEG ₈ -Acrylate/PEG ₈ -Amine & PEG ₈ -VS/BSA Microspheres | 145 |
| 4.4.3 | Microsphere Ripening & Coalescence | 146 |
| 4.4.4 | Assembly of Modular Scaffolds | 151 |
| 4.4.5 | Cell Interactions with Scaffolds | 158 |
| 4.5 | Discussion | 167 |
| 4.6 | Conclusion | 171 |
| Chapter 5 | | |
| Conclusions | | 173 |
| 5.1 | Summary of Dissertation | 173 |
| 5.2 | Future Directions | 177 |
| References | | 182 |
| Vita | | 204 |

List of Tables

| | |
|---|-----|
| Chapter 2 | 49 |
| Table 2.1: XPS analysis of PET coated silicon wafers..... | 51 |
| Table 2.2: Summary of bFg m/a values estimated from OWLS and AFM experiments | 60 |
| Table 2.3: Biotin-labeled bFg peptides identified by liquid chromatography electrospray-ionization ion trap tandem mass spectrometry | 64 |
| Table 2.4: Sequence coverage and percentage of labeled lysines observed after MALDI-TOF analysis of tryptic bFg peptides | |
| Chapter 3 | 106 |
| Table 3.1: Elemental composition of treated glass surfaces, as determined by XPS... | 112 |
| Table 3.2: Physical properties of PEG-OVS/ BSA microgels measured with OWLS and QCM | |
| Chapter 4 | 141 |
| Table 4.1: Summary of products resulting from microsphere fabrication methods ... | |

List of Figures

Chapter 2

| | |
|---|----|
| Figure 2.1: Ellipsometry measurements of polyethylene terephthalate (PET) layer thickness and uniformity on silicon wafers..... | 48 |
| Figure 2.2: Sequence coverage obtained for A α , B β , and γ chain in-gel trypsin digests of biotinylated bFg | 52 |
| Figure 2.3: Scanning electron microscopy (SEM) of fabricated PET particles | 54 |
| Figure 2.4: Workflow diagram for bFg surface adsorption experiments | 56 |
| Figure 2.5: SDS-PAGE gel of bFg before and after reaction with the Sulfo-NHS-LC-Biotin label | 57 |
| Figure 2.6: Centroided MALDI spectra corresponding to bFg trypsin digest fragment masses from the 0.5 mg/mL adsorption experiments | 59 |
| Figure 2.7. Normalized MALDI-TOF spectral peaks corresponding to biotinylated lysine residues within bFg A α , B β , and γ chains, labeled while in a 0.5 mg/mL solution | 61 |
| Figure 2.8. Normalized MALDI-TOF spectral peak intensities of lysine residues within bFg A α , B β , and γ chains that were biotinylated after adsorption to a PET surface from 1, 0.5 and 0.1 mg/mL solutions | 63 |
| Figure 2.9: 3D image of bFg displaying the locations of labeled lysines after adsorption to a PET surface from a 0.1 mg/mL solution | 66 |
| Figure 2.10: SDS-PAGE gel displaying proteins expressed by HepG2 cells grown in serum-free media | 68 |
| Figure 2.11: SDS-PAGE gel demonstrating the purification of carbon-13 labeled hFg from HepG2 media by immunoprecipitation | 69 |
| Figure 2.12: Workflow diagram for fibrinogen peptide quantification using $^{13}\text{C}_6$, $^{15}\text{N}_2$ -labeled fibrinogen internal standards | 70 |
| Figure 2.13: Tandem spectra of unlabeled and $^{13}\text{C}_6$, $^{15}\text{N}_2$ -labeled fibrinogen gamma chain dodecapeptide | 71 |

| | |
|--|----|
| Figure 2.14: Tandem spectra of untagged and acetylated fibrinogen gamma chain dodecapeptide | 72 |
|--|----|

| | |
|---|----|
| Figure 2.15: Standard curves for isotopically labeled HepG2 proteins generated using SILT-MS | 73 |
|---|----|

Chapter 3

| | |
|---|----|
| Figure 3.1: Vapor-silanization procedure | 92 |
|---|----|

| | |
|---|----|
| Figure 3.2: NMR spectra of PEG-OVS | 98 |
|---|----|

| | |
|--|-----|
| Figure 3.3: Crosslinking of bovine serum albumin and poly(ethylene glycol)-octavinylsulfone may lead to microgel formation if the principle of equal end-group reactivity does not apply..... | 100 |
|--|-----|

| | |
|---|-----|
| Figure 3.4: Evidence for formation of microgels during the crosslinking reaction ... | 101 |
|---|-----|

| | |
|--|-----|
| Figure 3.5: Gel permeation chromatography of PEG ₈ -VS and PEG ₈ -amine pre-reacted to $d_{PCS} \cong 100$ nm | 102 |
|--|-----|

| | |
|--|-----|
| Figure 3.6: Kinetics of the crosslinking reaction between PEG-OVS and BSA | 104 |
|--|-----|

| | |
|--|-----|
| Figure 3.7: AFM analysis of microgel coatings | 107 |
|--|-----|

| | |
|---|-----|
| Figure 3.8: OWLS analysis of fibrinogen adsorption to microgel-coated surfaces ... | 109 |
|---|-----|

| | |
|--|-----|
| Figure 3.9: QCM-D frequency and dissipation changes illustrating the attachment of microgels to the MPTS-silanized crystal and subsequent resistance to non-specific protein adsorption | 111 |
|--|-----|

| | |
|--|-----|
| Figure 3.10: Cell adhesion on microgel-coated glass at 10X magnification after a 24 h incubation with endothelial, CHO, or fibroblast cells | 114 |
|--|-----|

| | |
|--|-----|
| Figure 3.11: Cell adhesion to microgel-coated glass at 10X magnification after repeated seedings with fibroblasts | 115 |
|--|-----|

| | |
|--|-----|
| Figure 3.12: Cell counting results for CHO and fibroblast adhesion to microgel surfaces | 116 |
|--|-----|

| | |
|---|-----|
| Figure 3.13: CHO cell adhesion to MPTS-silanized glass reacted with PEG coatings | 117 |
|---|-----|

| | |
|---|-----|
| Figure 3.14: 10X magnification of CHO cell adhesion on glass slides for 24 h demonstrating the effects of the crosslinker and final capping step | 118 |
|---|-----|

| | |
|---|-----|
| Figure 3.15: CHO cell adhesion at 24 h to air RFGD-treated PET films | 120 |
|---|-----|

Chapter 4

| | |
|---|-----|
| Figure 4.1: Production of PEG microspheres in aqueous sodium sulfate solutions... | 132 |
| Figure 4.2: Assembly of microspheres into bioactive modular scaffolds in the presence of living cells | 135 |
| Figure 4.3: PEG or PEG/BSA microspheres were formed above the cloud point and then buffer exchanged into PBS | 139 |
| Figure 4.4: Formation of microspheres was influenced by pre-reaction of PEG derivatives below the cloud point | 142 |
| Figure 4.5: Crosslinking with vortexing during the initial reaction produced bulk hydrogels | 143 |
| Figure 4.6: DLS of PEG solutions above their cloud points | 144 |
| Figure 4.7: Zeta potentials of microspheres were determined by the charge of the crosslinker | 147 |
| Figure 4.8: The formation of PEG ₈ -VS/PEG ₈ -amine microspheres was monitored by confocal microscopy at 20X magnification using fluorescently labeled PEG | 148 |
| Figure 4.9: PEG-rich droplets before and after coalescence | 149 |
| Figure 4.10: Water-rich droplets were observed while monitoring the formation of PEG ₈ -VS/PEG ₈ -amine microspheres by confocal microscopy at 20X magnification.. | 150 |
| Figure 4.11: PEG ₈ -VS and PEG ₈ -amine domains were found to form multiple emulsions following coalescence | 152 |
| Figure 4.12: To visualize the porous structure, larger microspheres were produced... | 153 |
| Figure 4.13: Scaffolds may be formed by centrifuging microspheres in the presence of 2% serum | 155 |
| Figure 4.14: Photographs of modular scaffolds | 156 |
| Figure 4.15: Scaffolds could be fabricated with gradients of microspheres | 157 |

| | |
|---|-----|
| Figure 4.16: Macroporosity was introduced in the presence of cells via dissolution of porogenic microspheres | 156 |
| Figure 4.17: Confocal microscopy at 10X of a macroporous scaffold composed of PEG ₈ -VS/PEG ₈ -amine microspheres, PEG ₈ -acrylate/PEG ₈ -amine microspheres PEG ₈ -VS/BSA microspheres, 48 h after formation | 160 |
| Figure 4.18: Scaffolds could be formed in the presence of cells | 161 |
| Figure 4.19: Modular scaffolds formed tight seals with the walls of UV/vis cuvettes in which they were fabricated | 163 |
| Figure 4.20: Penetration of endothelial cells into surface pores of a modular scaffold | 164 |
| Figure 4.21: S1P, porosity, and RGD peptide affected endothelial cell migration in modular scaffolds | 165 |
| Figure 4.22: Cell migration into scaffolds containing HepG2 cells | 164 |

SEVER INSTITUTE
SCHOOL OF ENGINEERING AND APPLIED SCIENCE
DEPARTMENT OF BIOMEDICAL ENGINEERING

ABSTRACT OF DISSERTATION

IMPROVING BIOCOMPATIBILITY BY CONTROLLING PROTEIN
ADSORPTION: MODIFICATION AND DESIGN OF BIOMATERIALS
USING POLY(ETHYLENE GLYCOL) MICROGELS AND
MICROSPHERES

by

Evan Alexander Scott

Doctor of Philosophy in Biomedical Engineering
Washington University in St. Louis, 2009
Professor Donald L. Elbert, Chairperson

Guided by the clinical needs of patients and developments in biology and materials science, the primary focus of the biomaterials field remains at the solid/liquid interface between biomaterial surfaces and biological fluids. For blood-contacting devices, biological responses are initially elicited and directed by proteins that adsorb from this multicomponent solution to form thin films on their surfaces. The identity, conformation, and quantity of adsorbed proteins are related to the properties of a material's surface. For example, hydrophobic surfaces tend to be thrombotic via interactions between platelets and adsorbed fibrinogen, while surface-activation of specific enzymes initiates the coagulation cascade on hydrophilic surfaces. The objective of this thesis is to improve the design of biomaterials through the analysis and control of adsorbing protein layers. This goal is approached through three separate strategies. First, a proteomics-based methodology is presented for the assessment of protein conformation at the residue level after adsorption to biomaterial

surfaces. A quantitative mass spectrometric technique is additionally suggested for the identification and quantification of proteins within adsorbed protein layers. Second, a method is described for the covalent attachment of poly(ethylene glycol) (PEG)-based hydrogel coatings onto biomaterials surfaces for the minimization of protein adsorption. The coatings are applied using partially crosslinked PEG solutions containing polymer and protein oligomers and microgels that can be designed to control cell adhesion. Finally, a modular strategy is proposed for the assembly of bioactive PEG-based hydrogel scaffolds. This was accomplished using novel PEG microspheres with diverse characteristics that individually contribute to the ability of the scaffold to direct cellular infiltration. The methodologies proposed by this thesis contribute to the recent shift in biomaterials and tissue engineering strategies towards directed cellular responses at the molecular level.

CHAPTER 1

Introduction

1.1 Synopsis and Objectives of Thesis

Upon exposure to blood implanted materials immediately adsorb a thin layer of proteins onto their surfaces, and host cells and biochemical defenses are unable to interact with the foreign material itself (Baier and Dutton 1969; Brash and Davidson 1976; Andrade and Hlady 1986). Instead, the identity and conformation of the proteins that compose these adsorbed layers govern the immunological, coagulatory, thrombotic, and inflammatory responses that result (Zucker and Vroman 1969; Mohammad, Hardison et al. 1974; Kottke-Marchant, Anderson et al. 1987; Anderson, Bonfield et al. 1990; Scott 1991; Tang and Eaton 1995; Shen and Horbett 2001). These responses ultimately determine the biocompatibility and longevity of stents, vascular grafts, artificial heart valves and other blood-contacting devices (Edmunds, Hessel II et al. 2003). The properties of adsorbed protein layers are predominantly dependent on the composition of the solution from which the proteins adsorb and on the characteristics of the material surface, such as chemical functionality, charge, hydrophobicity, and topography (Slack, Posso et al. 1991). As a result, different materials can elicit different cellular responses when exposed to the same protein solution, and the same material can elicit different responses when exposed to solutions with different compositions (Boisson-Vidal, Jozefonvicz et al. 1991; Brash and Ten Hove 1993; Horbett 2004; Krishnan, Liu et al. 2006). The quantity and conformation of certain proteins within adsorbed protein layers can indicate the type and severity of the biological response induced by a particular material. By developing materials with surfaces that prevent protein adsorption and techniques to characterize individual proteins within adsorbed protein layers,

it may be possible to design more compatible biomaterials and to predict complications that may occur post-implantation.

This thesis has two main objectives. First, a proteomics-based methodology was developed capable of assessing materials compatibility *in vitro* by measuring the composition and conformation of adsorbed protein layers. The relationship between material surface properties and thrombogenic potential remains poorly understood (Sarkar, Sales et al. 2007) and few methods exist for the *in vitro* assessment of material compatibility. Many cardiovascular devices, such as artificial heart valves, require the use of anticoagulant drug therapies to prevent coronary thrombosis. Small diameter implants (diameter <6 mm) are easily occluded and thus highly susceptible to thrombus formation and neointimal hyperplasia. Neointimal hyperplasia can be well controlled with antiproliferative agents such as sirolimus and paclitaxel, but as evidenced by the increased number of late thrombosis related fatalities in patients with drug-eluting stents, thrombosis is much more difficult to manage (Axel, Kunert et al. 1997; Parry, Brosius et al. 2005). By characterizing the adsorption of proteins onto material surfaces, this research may further the understanding of the link between material properties and thrombosis as well as determine which biological responses could potentially be elicited by a particular implantable device. We focused on monitoring the post-adsorptive characteristics of fibrinogen, a blood protein whose quantity and conformation within adsorbed protein layers is indicative of thrombus formation and the adhesion and attachment of both leukocytes and platelets (Salzman, Lindon et al. 1987; Tang and Eaton 1993). A qualitative mass spectrometric mapping technique was devised to probe the changes in exposure of locations within adsorbed fibrinogen. This methodology was tested on a clinically relevant model poly(ethylene terephthalate) (PET) surface and permitted a residue-level analysis of the exposure of cell-adhesion motifs within fibrinogen

after adsorption (Scott and Elbert 2007). Results supported the presence of both post-adsorptive spreading effects and a thrombogenic potential for PET that were dependent on the concentration of the adsorbing fibrinogen solution. Additionally, isotopically labeled internal standards were developed to allow quantification of common blood proteins expressed by hepatocytes that are known to participate in the surface activation of blood-contacting devices. The quantification of internal standards were verified using stable isotope-labeling tandem mass spectrometry (SILT-MS) and reproducibly resulted in relative errors ranging between 2.9% -9.8% (Elbert, Mawuenyega et al. 2008).

The second, and primary goal of this thesis was to exploit the protein adsorption resistant properties of poly(ethylene glycol) (PEG) hydrogels to develop methods of modifying and fabricating materials with improved biocompatibility and specific bioactivity. Separate strategies were developed to both modify existing cardiovascular biomaterial surfaces with nanoscale PEG coatings as well as to fabricate modular 100% PEG constructs for tissue engineering applications. PEG derivatives were synthesized to permit gel formation with an amine or thiol containing crosslinker, and thus gels could be crosslinked with or conjugated to any biomolecule containing solution-exposed lysine or cystine residues. Through the use PEG and/or albumin crosslinkers and careful monitoring of the kinetics of gel formation, partially crosslinked PEG solutions containing oligomers and microgels were covalently attached to material surfaces. The grafting of PEG to material surfaces at the high densities required for effective protein resistance has been attempted unsuccessfully for many years. These oligomer/microgel solutions were able to provide high density PEG layers to material surfaces that have low levels of functionalization. Compared to the surface-grafting of individual PEG chains, these large macromonomers are able to cover significantly larger portions of surfaces with only a single covalent attachment.

Covalent oligomer/microgel coatings were applied to relatively inert PET surfaces using a practical plasma-etching strategy that could potentially be applied to a variety of different polymer surfaces. Multiple surface analysis techniques in addition to cell adhesion assessments confirmed the formation of stable coatings that minimized protein adsorption and allowed controllable bioactivity.

We additionally used these oligomer/microgel solutions in the fabrication of multiple types of PEG microspheres with diverse properties and functionalities that were assembled into modular scaffolds. Partially crosslinked solutions were further reacted after phase separation into spherical PEG-rich domains by raising the solution temperature above the cloud point/lower critical solution temperature (LCST), which was lowered to below 37°C using aqueous sodium sulfate solutions. The resulting microspheres displayed a porous structure and were prepared without the use of other monomers, polymers, surfactants or solvents that could decrease biocompatibility or cell survival. Without surfactants and emulsifiers, microsphere formation required control over the kinetics of PEG phase coarsening relative to the rate of gelation. Three separate microsphere types were fabricated: one type of PEG microsphere provided mechanical support and cell adhesion, a second type provided controlled delivery of the angiogenesis-promoting molecule, sphingosine 1-phosphate (S1P), and a third type served as a slowly dissolving non-toxic porogen. These microspheres were crosslinked around hepatocytes via serum proteins present in cell media with a simple centrifugation methodology. The porogenic microspheres dissolved within two days, producing macropores in the scaffold with >90% viability of the liver cells. This small library of PEG microspheres permitted for the first time, to the best of our knowledge, the fabrication of macroporous scaffolds in the presence of living cells. Bioactivity of the modular scaffolds was demonstrated through conjugation of RGD peptides for the directed

infiltration of endothelial cells, and the rate of migration was shown to double in the presence of SIP-loaded microspheres.

1.2 Protein Films on Biomaterials: Biological Implications and Characterization of Adsorbed Fibrinogen

1.2.1 Relevance of Protein Films in Biomaterials Science

Proteins are present in all bodily fluids and thus coat materials regardless of the location of implantation. The dynamics and specificity of protein adsorption is influenced by the properties of the material surface such as charge, hydrophobicity, and roughness (Luck, Paulke et al. 1998; Qiu, Sayer et al. 1998; Dufrene, Marchal et al. 1999; McGurk, Green et al. 1999). Adsorbed biofilms consequently function as a mechanism of recognition for the direction of biological responses to foreign materials. Proteins are well suited for this purpose as they contain a wide range of properties incorporated within hydrophobic, hydrophilic, cationic, and anionic domains. The proteins found in blood alone contain a diversity of chemical properties extensive enough to interact with all known materials surfaces. Detailed knowledge of the process of protein adsorption is therefore essential to the design of implanted devices, and extensive research has been performed in this area.

Proteins are believed to initially adsorb to surfaces in their native state/structure due to ionic, polar, or van der waals forces (Andrade and Hlady 1986; Norde 1986). During adsorption, proteins likely go through the following three processes originally proposed by Soderquist and Walton: 1) rapid and reversible adsorption (up to 50-60% surface coverage) in the native conformation 2) slow conformational change and unfolding that leads to a decreasing rate of desorption and increasing surface contact to achieve irreversible binding,

and 3) irreversible binding in a denatured state and extremely slow rate of irreversible desorption (Soderquist and Walton 1980; Norde, MacRitchie et al. 1986; Morton, Myszka et al. 1995; Engel, Visser et al. 2004). From the simplest perspective, this process is often represented by two structural states for adsorbed proteins: folded (reversible surface-binding and folding) and denatured (irreversible surface-binding and denaturation) (Agnihotri and Siedlecki 2004). The rate of protein unfolding can be estimated from the rate of surface-induced spreading and appears to be on the order of the time required to approach the 'jamming' limit on surfaces (Ramsden 1993). As a result, proteins do not have adequate time to reach their maximum spread area if proteins are adsorbed from highly-concentrated solutions, due to the filling of space required for major conformational changes (Schaaf and Talbot 1989). Irreversible binding of the more surface-active proteins results in a heterogeneous biofilm composed of spread and unspread proteins, which is a consequence of proteins that spread early in the adsorption process decreasing the available spreading area for proteins that adsorb later (Morrissey 1977; Van Tassel and Viot 1997; Zoungrana, Findenegg et al. 1997).

The degree of conformational change and the strength of attachment to material surfaces not only increase with the time allowed for adsorption, but also with the hydrophobicity of the surface (Bohnert and Horbett 1986; Santore and Wertz 2005). The Siedlecki group recently used water contact angle measurements and atomic force microscopy (AFM) to demonstrate a step-like response between surface tension and the adhesive force of adsorbed proteins (Xu and Siedlecki 2007; Xu and Siedlecki 2009). For all proteins tested, a sharp increase in adhesive force occurred when the water contact angle transitioned across the region of $\sim 60-65^\circ$, further supporting the proposed definition of hydrophobic "protein adherent" surfaces (water contact angle $> \sim 60-65^\circ$) and hydrophilic

“protein nonadherent” surfaces (water contact angle $<60^\circ$) (Vogler 1999; Sethuraman, Han et al. 2004).

The kinetics of protein adsorption determines the dynamic composition of biological films. Since 2982 proteins can currently be reproducibly detected in human blood, the adsorption process is highly competitive (Liu, Valentine et al. 2007). The majority of theories used to describe this process represent adsorbed protein layers as a two-dimensional monolayer that can be described in units of surface density (mass or moles per unit area). Early depictions such as the Random Sequential Adsorption (RSA) model based on the Langmuir isotherm have progressed into more complex representations that account for surface exclusion, convection, surface diffusion, and Brownian dynamics (Feder 1980; Schaaf and Talbot 1989; Ramsden 1993; Magan and Sureshkumar 2006). Diffusion controlled transport favors the adsorption of higher concentration proteins first (Andrade and Hlady 1987). Consequently biofilms are initially dominated by “the big twelve”, which are proteins with blood concentrations higher than 1 mg/mL: albumin (40 mg/mL), IgG (8-17 mg/mL), α 1-antitrypsin (2 mg/mL), transferrin (2.3 mg/mL), haptoglobin (1.2-3.0 mg/mL), LDL (4 mg/mL), HDL (3 mg/mL), IgA (1-4 mg/mL), complement C3 (1.6 mg/mL), fibrinogen (2-3 mg/mL), and α 2-macroglobulin (2.7 mg/mL) (Blomback ; Schultze 1966; Andrade and Hlady 1987). Over time, these proteins can desorb from the surface to be replaced by lower concentration proteins of higher surface activity, and in the case of fibrinogen, desorption results in selective replacement with proteins involved in contact activation (Scott 1991). Leo Vroman is widely regarded as the first to link the dynamics of this competitive adsorption process with clinically relevant biological responses (Vroman and Adams 1969). His investigations into the adsorptive and desorptive characteristics of fibrinogen were essential to unraveling the mechanisms behind coagulation and thrombosis

(Vroman, Adams et al. 1980). The biological implications of fibrinogen conformation and competitive adsorption make it a model protein for the general study of protein adsorption as well as for the verification of the clinical relevance of new materials and analytical techniques.

1.2.2 Fibrinogen Structure and Surface Activity

Fibrinogen is a 340 kDa dimeric glycoprotein composed of $A\alpha$, $B\beta$, and γ chains containing globular and α -helical coiled-coil secondary structures held together by 29 disulfide bonds (Figure 2.9). The structure is trinodular, composed of one inner and two outer globular domains linked by regions of coiled-coils (Hall and Slayter 1959). The inner domain (E domain) contains the amino termini of the $A\alpha$, $B\beta$, and γ chains, while the two outer domains (D domains) consist of the carboxyl termini of the $B\beta$, and γ chains (Spraggon, Everse et al. 1997; Madrazo, Brown et al. 2001). Extending from the D domains, beginning near $A\alpha 224$ in bFg, are the mobile and highly flexible αC domains that associate non-covalently with the E domain (Veklich, Gorkun et al. 1993). Fibrinogen possesses several cell adhesion and protein interaction domains in all three of its major chains, including RGD integrin binding motifs in the $A\alpha$ chain, a heparin and cadherin binding domain in the $B\beta$ chain, and a dodecapeptide essential for platelet aggregation in the γ chain (Kloczewiak, Timmons et al. 1984; Andrieux, Hudry-Clergeon et al. 1989; Bach, Barsigian et al. 1998; Yakovlev, Gorlatov et al. 2003).

The principle biological responses to adsorbed protein layers are thrombosis, coagulation, complement activation, and inflammation (Andrade and Hlady 1986; Farrell, Thiagarajan et al. 1992; Tang and Eaton 1993). Fibrinogen contains binding domains that contribute to almost all of these responses. In the $A\alpha$ chain, RGDF and RGDS motifs that

bind several cell receptors, including GPIIb-IIIa integrins on platelets, are located at A α 95-98 and A α 572-575 respectively (Cheresh 1987; Bennett 2001). The B β chain contains domains linked to cadherin binding (B β 15-42) and heparin binding (B β 15-57) (Bach, Barsigian et al. 1998; Yakovlev, Gorlatov et al. 2003). The MAC-1 leukocyte binding sites at γ 190-202 and γ 377-395, the RIBS-I epitope at γ 373-385, the GPIIb-IIIa platelet binding site within γ 370-385, and the platelet binding dodecapeptide at γ 400-411 are all located in the γ chain, which is highly conserved between different species (Hawiger, Timmons et al. 1982; Zamarron, Ginsberg et al. 1990; Podolnikova, Yakubenko et al. 2003; Flick, Du et al. 2004). Antibody and platelet activation/adhesion studies have demonstrated that most of these sites are not accessible when fibrinogen is in solution, and only become accessible after adsorption and denaturation on material surfaces (Cierniewski, Plow et al. 1984; Shiba, Lindon et al. 1991).

The thrombogenicity of materials in contact with blood often correlates with hydrophobicity and the amount of adsorbed fibrinogen within protein layers on the surface (Brash 1979). Shiba et al. examined the ability of antibodies specific for integrin binding domains to bind fibrinogen adsorbed to polymer surfaces, and concluded that surface-dependent conformational changes influenced the exposure of platelet interaction sites within fibrinogen (Shiba, Lindon et al. 1991). Furthermore, antibodies specific for solution conformations of fibrinogen were less able to bind the plasma adsorbed fibrinogen on the more hydrophobic surfaces. Thus extensive spreading on hydrophobic surfaces may allow fibrinogen to denature and unfold into post-adsorptive conformations that expose peptide sequences conducive to platelet adhesion and activation (Zucker and Vroman 1969; Mohammad, Hardison et al. 1974; Shiba, Lindon et al. 1991; Farrell, Thiagarajan et al. 1992). Due to differences in the conformation and surface expression of the α I**b** β ₃ receptor, only

ADP or thrombin-stimulated platelets can bind fibrinogen in solution (Plow and Marguerie 1980; Litvinov, Shuman et al. 2002; Li, Mitra et al. 2003). Surprisingly, both activated and unactivated platelets can bind to adsorbed fibrinogen (Savage and Ruggeri 1991). This is particularly striking considering that only activated platelets can bind to other adsorbed prothrombotic factors such as vitronectin, von Willibrand factor, and fibronectin (Savage and Ruggeri 1991). Furthermore, platelet adhesion to some material surfaces has been shown to be greatly reduced in the presence of afibrinogenemic plasma (Tsai, Grunkemeier et al. 1999). Even surfaces that do not significantly alter the conformation of fibrinogen can lead to the activation and aggregation of platelets (Lindon, McManama et al. 1986). This is possibly due to the multivalency of available sites that could enhance binding to platelet receptors (Ganguly and Gould 1979). The ability of soluble fibrinogen aggregates held together by anti-E domain F(ab') fragments to stimulate platelet aggregation and activation supports this conclusion (McManama, Lindon et al. 1986). The concentration of platelet-binding motifs on fibrinogen-coated surfaces is higher than typically found in solution, and thus receptor clustering may be responsible for the ability of adsorbed fibrinogen to interact with unactivated platelets (Litvinov, Shuman et al. 2002).

Initiation of the coagulation cascade is most prominent on hydrophilic surfaces that weakly adsorb fibrinogen (Vroman and Adams 1969). In the presence of multi-component solutions such as plasma, fibrinogen can be rapidly replaced on some surfaces by lower concentration proteins with higher surface activity in a competitive adsorption process known as the Vroman effect (Brash and ten Hove 1984; Horbett 1984). Similar protein exchanges on surfaces have been found to occur with other proteins, and have been attributed to competition for limited adsorption sites and differences in the surface activation of individual proteins (Brash and ten Hove 1984; Horbett 1984; Slack, Bohnert et

al. 1987; Slack and Horbett 1995). In systems of competitive adsorption, high concentration proteins tend to adsorb first, but are gradually replaced over time as these proteins desorb from the surface and are replaced by proteins with stronger interactions with the surface (Vroman, Adams et al. 1980; Vroman and Adams 1986). On hydrophilic glass surfaces, fibrinogen was found to initially adsorb preferentially over albumin and IgG despite their higher concentrations (Brash, Uniyal et al. 1974). However, fibrinogen was no longer immunologically detectable on surfaces after 10 min when in the presence of factor XII, prekallikrein, and high-molecular-weight-kininogen (HK) (Vroman, Adams et al. 1980; Slack and Horbett 1988). It was later found that fibrinogen was being gradually replaced or ‘converted’ by activated HK, which used factor XII and prekallikrein as cofactors (Schmaier, Silver et al. 1984; Scott, Silver et al. 1984). The activation of these enzymes is the first step in the contact activation (intrinsic) pathway of the coagulation cascade.

1.2.3 Post-Adsorptive Conformation of Fibrinogen

Not unlike most proteins, single component adsorption studies have revealed that the post-adsorptive spreading of fibrinogen increases with hydrophobicity of the surface and is concentration-dependent (Pitt, Spiegelberg et al. 1987; Lu and Park 1991; Ramsden 1993; Wertz and Santore 1999). Circular dichroism (CD) and FTIR of adsorbed fibrinogen that was eluted from hydrophilic, hydrophobic, and charged surfaces revealed extensive post-adsorptive conformational changes marked by decreases in alpha-helical content (>50%) (Soderquist and Walton 1980; Chan and Brash 1981; Roach, Farrar et al. 2005; Steiner, Tunc et al. 2007). Adsorption to hydrophobic surfaces has additionally been shown by FTIR to lower the beta-sheet/turn ratio (Steiner, Tunc et al. 2007). The additional unfolding of fibrinogen on hydrophobic surfaces is indicative of extensive deviation from the solvent-

induced secondary structure of fibrinogen in plasma, and has, therefore, been proposed as a qualitative test for the assessment of material biocompatibility. On a hydrophobic silicon dioxide surface, scanning force microscopy revealed two separate structures for dry fibrinogen: a trinodular form of length 60 nm and a spherical globular shape with a 40 nm diameter, both of which had a maximum height of 6 nm (Wigren, Elwing et al. 1991). These measurements were later verified to also be valid for hydrated fibrinogen molecules (Taatjes, Quinn et al. 1997; Sit and Marchant 1999). The globular shape in combination with the trinodular shapes suggested the presence of extensive post-adsorptive conformational changes due to influences from the hydrophobic surface. Sit et al. additionally used AFM to compare the dimensions of post-adsorptive fibrinogen on surfaces of decreasing hydrophobicity and demonstrated that significantly less spreading occurred on hydrophilic surfaces (Sit and Marchant 1999).

Two distinct surface-bound fibrinogen species have been detected on numerous surfaces, one extremely difficult to elute and one less so. On poly(dimethyl siloxane) (PDMS), 40% of fibrinogen was found to be irreversibly bound and resistant to elution by buffer for 100 h (Lok, Cheng et al. 1983). On polystyrene, 10-15% of adsorbed fibrinogen was highly resistant to elution by sodium dodecyl sulfate and 3-mercaptoethanol and does not participate in fibrin gelation. The percentage of nondesorbable fibrinogen increases with increasing availability of area for spreading and conversion to the nondesorbable species occurs on the same time scale as adsorption (Retzinger, Cook et al. 1994). Fibrinogen adsorption kinetics have been shown to reach a steady state typically between 10 – 20 h, with the majority of surface coverage being obtained before 6 h (Weathersby, Horbett et al. 1977). Using the dimensions of 45 x 6 nm, surface densities of 220 ng/cm² and 1500 ng/cm² are expected at maximum surface coverage if fibrinogen adsorbs with respectively a

side-on or end-on orientation. This suggests a theoretical spread surface area of 20.25 nm^2 for end-on and 212 nm^2 for side-on adsorption (Santore and Wertz 2005). End-on versus side-on conformations depend heavily on the concentration of the adsorbing fibrinogen solutions. Less than 10 ng/cm^2 of fibrinogen is required in order to elicit a physiological response, and thus the density of fibrinogen layers as well as the percentage of irreversibly bound fibrinogen on a variety of surfaces has been examined at different adsorbing concentrations. Such an analysis by Bohnert et al. verified the aforementioned influences of surface properties and adsorbing concentration on fibrinogen surface density and elutability: 593 ng/cm^2 on Silastic with 20% nonelutable at 1.5 mg/mL ; 238 ng/cm^2 on Silastic with 26% nonelutable at $5 \text{ }\mu\text{g/mL}$; 539 ng/cm^2 on Teflon with 12% nonelutable at 1.5 mg/mL ; 176 ng/cm^2 on Teflon with 40% nonelutable at $5 \text{ }\mu\text{g/mL}$; 565 ng/cm^2 on polyethylene with 25% nonelutable at 1.5 mg/mL ; 200 ng/cm^2 on polyethylene with 40% nonelutable at $5 \text{ }\mu\text{g/mL}$.

A comprehensive description of the fibrinogen spreading process has remained elusive. Total internal reflection fluorescence (TIRF) (Wertz and Santore 1999; Santore and Wertz 2005) and atomic force microscopy (AFM) (Agnihotri and Siedlecki 2004) experiments both demonstrate that after an initial rapid spreading event, only a single mode of fibrinogen relaxation can be detected due to the presence of only a single exponential decay. The decay rate of fibrinogen E and D domain heights have been directly measured with AFM and used to extrapolate the initial heights of fibrinogen domains immediately after adsorption and prior to surface-induced spreading. The calculated values were much lower than the known dimensions of fibrinogen, suggesting the presence of a more rapid unfolding rate that occurred prior to analysis by AFM. TIRF confirmed these results by demonstrating that the majority of spreading occurs within the first 15 minutes of adsorption, followed by 2 h of

additional relaxation (Wertz and Santore 1999). The length of the decay was found to be dependent on the hydrophobicity of the surface, as evidenced by TIRF results showing 1735 s on C16-SAM, 2127 s on hydrophobic graphite, and 6740 s on OH-SAM. These results suggest that the two-state (folded versus denatured) single energy barrier model of protein spreading may be inaccurate. Agnihotri et al. proposed a mechanism governed by two separate spreading regimes: an initial rapid spreading event that lasts seconds to minutes followed by a gradual exponential spreading event over the course of ~2 h. This initial event may be due to the initial mechanical impact at the point of contact between amino acids and the surface, while the second event is due to the obtaining of thermodynamic equilibrium whereby the entropy is maximized and the energy of the system is minimized through the increased interaction between hydrophobic domains in fibrinogen and the hydrophobic surface (Agnihotri and Siedlecki 2004).

1.3 Controlling Protein Adsorption and Bioactivity Via Surface Treatments of Biomaterials

1.3.1 Progression of Biomaterial Design: Improving the Biocompatibility of Poly(ethylene terephthalate)

Three separate stages of advancement have been identified for the progression of biomaterials science over the last 50 years, but the underlying objective has remained unchanged: to reproducibly control how biological systems interact with a material surface (Hench and Polak 2002). While the definition has been frequently amended and varies significantly, a biomaterial can be classified in the broadest sense as a “substance other than food or drugs contained in therapeutic or diagnostic systems that are in contact with biological fluids or tissues” (Peppas and Langer 1994). The first stage of polymeric

biomaterials design focused on biological and chemical inertness and material accessibility. Inert materials were considered those that minimized immunologic responses and resisted *in vivo* degradation. Limited development of polymeric biomaterials initially led to the use of accessible polymers that were stable in aqueous environments, such as Dacron-based vascular grafts derived from textiles, poly(methyl methacrylate) originally used in dentistry and for windshields, or poly(ether urethane) taken from women's girdles. While these materials provided temporary solutions to many medical problems, their applications were limited and eventually resulted in severe post-transplantational complications. Dacron, or poly(ethylene terephthalate) (PET), is a classic example of a first-generation biomedical material. Coronary artery bypass surgery has been a common procedure to treat atherosclerotic cardiovascular diseases since the 1960's, but the ideal use of an autologous saphenous vein is not an option for over 30% of all patients (C. William Hall 1967; Mehta and Khan 2002). Mechanically flexible, nontoxic, and chemically inert under physiological conditions, PET was a logical choice for vascular graft design. However, as demonstrated by a water contact angle of 70.0°, the hydrophobic nature of PET supported extensive fibrinogen adsorption and spreading, resulting in inflammation, thrombosis and distal embolization (Roald, Barstad et al. 1994; Chen Jie-Rong 1999). First-generation PET surfaces possessed the structural integrity to maintain compliance under the required 50 mL/min flow rate, but complications stemming from surface activity prevented the development of small diameter vascular grafts with <4 mm internal diameters (Callow 1988).

Second generation polymeric biomaterials evolved to additionally elicit controlled physiological responses, demonstrating degradation or bioactivity that improved the inertness of the surface. The biodegradable and resorbable suture is a notable example of such a material, which by 1984 was used clinically in a variety of procedures. Sutures

composed of poly(lactic-co-glycolic) polymers degrade by hydrolysis at an adjustable rate to allow replacement by host tissues as well as to deliver therapeutic agents (Lim, Poh et al. 2009). Numerous modifications of PET have been attempted to impart bioactivity and inhibit thrombosis and coagulation. For example, PET surfaces have been functionalized with thiol-containing groups to promote the release of nitric oxide (NO) from naturally occurring nitrosated compounds found in the body that are known to inhibit platelet adhesion (Gappa-Fahlenkamp and Lewis 2005). The thrombin-inhibitory activity of antithrombin III is heightened by the glycosaminoglycan heparin, and Bilsen et al. covalently attached heparin to PET surfaces that were first grafted with poly(ethylene imine) (Rosenberg and Damus 1973; Parish 2006). The heparin coatings decreased surface hydrophobicity, and results demonstrated a reduction in inflammatory cell adhesion due to minimizing fibrinogen spreading and preventing exposure of the P2 epitope. Since PET is a “protein adherent” surface, the preadsorption of protein coatings that do not support platelet and cell adhesion has been frequently attempted. Surfaces that preferentially adsorb albumin tend to resist platelet adhesion *in vitro*, and preadsorbed albumin coatings have been shown to temporarily passivate materials surfaces *in vivo* (Chang 1969; Imai, Tajima et al. 1971; Kim, Lee et al. 1974). Albumin is a lipid carrier that possess a high affinity for fatty acids and has demonstrated strong adhesion to alkylated surfaces (Munro, Quattrone et al. 1981). A variety of techniques have been attempted to coat PET with albumin, including chemical crosslinking, surface alkylation, and heat denaturation (Domurado, Guidoin et al. 1978; Tingey 1983; Rumisek, Wade et al. 1986). Although coatings reduced embolization and improved endothelial cell attachment, they were found to be rapidly removed in fluid flow and by protein degradation, and slow tissue incorporation resulted in long-term, thrombus-related complications (Rumisek, Wade et al. 1986; Ben Slimane, Guidoin et al.

1988; Jensen, Lindblad et al. 1996). Other protein coatings have been attempted including collagen, fibronectin, and gelatin without substantial improvement (Drury, Ashton et al. 1987; Noishiki and Chvapil 1987; Callow 1988; Gouny, Hocquet-Cheynel et al. 1995).

Instead of focusing on inertness, third-generation biomaterials actively utilize molecular interactions to direct cell adhesion, migration, differentiation, or proliferation. As evidenced by the aforementioned late-term thrombosis on drug-eluting stents, sustained biocompatibility will likely not be achieved with static polymeric surfaces that solely inhibit biochemical or cellular interactions, and more biologically based strategies that recruit dynamic endotheliums *in vivo* may be more favorable (Axel, Kunert et al. 1997; Hench and Polak 2002; Parry, Brosius et al. 2005). It has been proposed that such a material should: 1) have receptor-based recognition reactions optimized through computer modeling, 2) be well characterized, 3) induce specific healing pathways, 4) not exhibit non-specific interactions, 5) be sufficiently robust to withstand sterilization, storage, and *in vivo* conditions, and 6) be manufacturable (Ratner 1996). Unsuccessful attempts were made in the late 1970's and 1980's to seed PET and poly(tetrafluoroethylene) vascular grafts with endothelial cells *in vitro* prior to implantation (Herring, Gardner et al. 1984; Fasol, Zilla et al. 1989). These early experiments achieved marginal if any improvement over unmodified PET surfaces, and failure was attributed to insufficient cell seeding and formation of unstable endothelium. Several groups have recently revisited these early experiments and utilized improved cell culture techniques, only to again produce marginal improvements (Deutsch, Meinhart et al. 2009). Thrombosis was found between 30 days to 3 years and histology revealed inflamed connective tissue below the endothelium. In all of these prior experiments, cells were directly applied to unmodified polymer surfaces. Such protocols could be improved through the incorporation of adhesion peptides to promote cell attachment and spreading.

Additionally, the delivery of therapeutic agents may be needed to inhibit inflammation and improve endothelial cell migration while limiting the proliferation of smooth muscle cells. Adhesion peptide conjugation and the delivery of chemotactic agents are two promising mechanisms through which material surfaces could exhibit bioactivity and are discussed in section 1.3.2. An overview of two methods that alone or in conjunction could impart this bioactivity to a variety of material surfaces are discussed in section 1.3.3 and 1.3.4. This thesis endeavors to add to the expanding biomaterials literature by presenting a highly versatile strategy for covalently attaching bioactive coatings to most polymeric surfaces. The method is described and demonstrated in Chapter 3 for the imparting of third-generation properties to a first-generation PET surface.

1.3.2 Directing Cell Adhesion and Migration: Integrin-Binding Motifs and Sphingosine 1-Phosphate Delivery

Cell adhesion and migration in the extracellular matrix is mediated through the transient binding of cell-surface receptors and the *in situ* enzymatic degradation of matrix proteins. Several classes of receptors are responsible for cell-surface contacts, but biomaterials are most frequently functionalized to incorporate small integrin-binding motifs. Human integrin receptors are transmembrane heterodimers composed of 24 different matched pairs from a pool of 18 α and 8 β subunits (Shimaoka and Springer 2003). The heterodimers have been categorized as RGD-recognizing ($\alpha_5\beta_1$, $\alpha_V\beta_1$, $\alpha_V\beta_3$, $\alpha_V\beta_5$, $\alpha_V\beta_6$, $\alpha_V\beta_8$, $\alpha_{IIb}\beta_3$), laminin-binding ($\alpha_1\beta_1$, $\alpha_2\beta_1$, $\alpha_3\beta_1$, $\alpha_6\beta_1$, $\alpha_7\beta_1$, $\alpha_6\beta_4$), collagen-binding ($\alpha_1\beta_1$, $\alpha_2\beta_1$, $\alpha_3\beta_1$, $\alpha_{10}\beta_1$, $\alpha_{11}\beta_1$), and leukocyte integrins ($\alpha_L\beta_2$, $\alpha_M\beta_2$, $\alpha_X\beta_2$, $\alpha_D\beta_2$) (Takada, Ye et al. 2007). Inside-out signaling regulates receptor conformation and affinity, which, for example, can modulate platelet aggregation, neutrophil rolling, and the biphasic endothelial cell adhesion

that permits migration (DiMilla, Barbee et al. 1991; Farrell, Thiagarajan et al. 1992; Ginsberg, Partridge et al. 2005; Green, Schaff et al. 2006; Wegener, Partridge et al. 2007). Outside-in signaling through integrins primarily influences the cell cytoskeleton to modulate cell adhesion, proliferation, differentiation, gene expression, shape, migration, polarity, and survival (Takada, Ye et al. 2007). The short peptide sequences present within protein ligands that bind integrins can be fabricated using solid phase peptide synthesis and have been used to impart a diverse range of bioactivities onto material surfaces (Pierschbacher and Ruoslahti 1984). Peptides may be synthesized to contain nucleophilic cystine or lysine residues that can readily react with electrophilic end-groups of functionalized polymers under mild conditions (Elbert and Hubbell 2001). In addition to promoting cell adhesion, conjugation and crosslinking of peptides into materials have also been used for cell-mediated degradation to allow improved integration and replacement of materials by host tissues (Kouvroukoglou, Dee et al. 2000; Lutolf 2003; Lutolf 2003; Lutolf and Hubbell 2005).

Cell adhesion motifs present in fibrinogen were outlined in section 1.2.2, but many other extracellular matrix- and serum-based proteins contain adhesion motifs that have been mimicked by biomaterial surfaces. The most important of these protein ligands include fibronectin, vitronectin, laminin, collagen, thrombospondin, and von Willebrand factor. As with fibrinogen, protein conformation and surface adsorption play a significant role in the presentation of their motifs, and thus the surface properties of materials can be tuned to preferentially adsorb certain proteins to direct cell adhesion. One example of this is the adhesion of cells to tissue culture polystyrene (TCPS), which is currently the standard adhesive surface used in cell culture. TCPS is plasma-treated to possess a highly oxygenated surface, and both antibody assays and radiolabeling studies have demonstrated that this surface preferentially adsorbs vitronectin from serum present in the culture medium (Steele,

Dalton et al. 1993). Adjusting the surface treatment to include equal parts of both nitrogen and oxygen groups shifts the adsorption preference to fibronectin (Steele, Dalton et al. 1995). Fibronectin uses the sequences RGDS, LDV, and REDV to interact primarily with the $\alpha_5\beta_1$ integrin, while vitronectin binds the $\alpha V\beta_3$ integrin via the RGDV sequence. While RGD sequences bind integrin receptors such as $\alpha V\beta_3$ that are well distributed in various tissues, some motifs are highly specific to integrins found only on certain cell types (Pierschbacher and Ruoslahti 1984). Notable examples include $\alpha IIb\beta_3$ on platelets, $\alpha_4\beta_1$ and β_2 integrins on leukocytes, and $\alpha E\beta_7$ on dendritic, mast and T cells (Andrieux, Hudry-Clergeon et al. 1989; Farstad, Halstensen et al. 1996; Rose, Alon et al. 2007). Thus adjusting material surface properties to influence the exposure of various integrin motifs within adsorbed proteins can permit control over the adhesion, migration, and activation of cell types that influence materials compatibility.

The controlled delivery of growth factors and chemotactic agents may also aid in the proliferation and recruitment of cells for *in situ* tissue regeneration on third-generation material surfaces. For example, the Sakiyama-Elbert group has used the controlled delivery of neurotrophin-3 and platelet derived growth factor from fibrin matrices to direct the differentiation of stem cells into specific cells types for neural tissue regeneration (Willerth, Arendas et al. 2006; Willerth, Rader et al. 2008). Our laboratory has previously demonstrated that endothelial cell migration rates on bioactive hydrogel surfaces can be optimized by adjusting the surface concentration of RGD peptide in the presence of sphingosine 1-phosphate (S1P) (Wacker, Alford et al. 2008). S1P is a signaling lipid that participates in a broad spectrum of biological responses and is actively researched as a chemotactic agent in both vascular biology and immunology (Chun and Rosen 2006; Yatomi 2006). Activation of the G protein coupled receptor S1P₁ is the primary mechanism for S1P

manipulation of both lymphocytes and endothelial cells (Van Brocklyn, Lee et al. 1998; Matloubian, Lo et al. 2004). The effects of S1P on endothelial cells regulates multiple stages of vasculogenesis, including an initial promotion of endothelial cell migration and proliferation as well as subsequent endothelial cell entubulation into stable blood vessels (Lee, Thangada et al. 1999; Bayless and Davis 2003; Langlois, Gingras et al. 2004). Additionally, smooth muscle cell migration that often results in stenosis of small diameter vascular devices has been shown to be inhibited in the presence of physiological concentrations of S1P via binding of the chemorepellant S1P₂ receptor (Takuwa 2002; Hla 2004).

S1P levels in blood are regulated by enzymatic, cellular, and protein-based mechanisms. The enzymes sphingosine kinase and sphingosine lyase respectively mediate the phosphorylation of sphingosine into S1P and the degradation of S1P into phosphoethanolamine and fatty aldehyde (Kohama, Olivera et al. 1998; Yatomi, Ozaki et al. 2001). Platelets and red blood cells (RBCs) express sphingosine kinase but not S1P lyase, and thus store large quantities of S1P (Yatomi, Ozaki et al. 2001; Ito, Anada et al. 2007). RBCs constitutively release S1P and are thought to be responsible for the basal level plasma concentrations, while platelets only release S1P upon stimulation by physiological cues such as shear stress and thrombin activation (Yatomi, Yamamura et al. 1997; Yang, Yatomi et al. 1999; Aoki, Osada et al. 2007). Due to poor water solubility, nearly 100% of S1P in blood is bound to the lipid-carriers albumin ($39.5 \pm 7.9\%$), high density lipoprotein ($53.3 \pm 6.4\%$), and low density lipoprotein ($7.2 \pm 3.8\%$) (Aoki, Yatomi et al. 2005). Thus S1P levels in blood are tightly regulated, and the localized delivery of S1P from biomaterials is a practical option for the design of vascular devices. The incorporation of albumin as a lipid carrier for the controlled release of S1P from hydrogels has been achieved, and a variation of this

methodology is utilized to increase the migration rate of endothelial cells through the third-generation scaffolds discussed in Chapter 4 (Hla 2004; Wacker, Scott et al. 2006).

1.3.3 Layer-by-Layer Methods

Layer-by-layer (LbL) methods generate films on surfaces by alternately adsorbing different macromolecules possessing complementary and attractive functionalities. Electrostatic, van der Waals, hydrogen bonding, and covalent interactions have all been employed to maintain the structural integrity of multi-layered coatings of desired thickness on material surfaces (Decher 1997; Stockton and Rubner 1997; Serizawa, Hamada et al. 2000; Kim, Wacker et al. 2007). The coatings can function as barriers between material surfaces and protein solutions, allowing control over protein adsorption and spreading. An LbL methodology is beneficial in that the protocol is usually simple and performed under mild aqueous conditions, often requiring only incubation and washing steps that can be performed on substrates of complex geometries. The films are frequently used in biological applications, and modifications have been developed to elicit specific cellular interactions for third-generation biomaterials. Polyelectrolyte multilayer (PEM) films generated by alternating a cationic poly(allylamine hydrochloride) solution with an anionic poly(sodium 4-styrenesulfonate) solution have shown promise in controlling both the amount and conformation of fibronectin adsorption (Ngankam, Mao et al. 2004). Depending on whether the outermost polymer layer was positively or negatively charged, the adsorbed fibronectin shifted from a side-on to an end-on conformation and the bioactivity changed as evidenced by decreased antibody binding.

A preference for polyelectrolytes in LbL methodologies exists due to the more stringent requirements of sequential covalent reactions (Decher 1997; Z. Tang 2006).

Covalent chemistry has a high steric demand, making consistently dense multilayers difficult to achieve with an LbL strategy that requires high conversion percentages at each step. Electrostatic interaction have the least steric demand of all chemical bonds and the resulting charge reversal at each layering step produces monolayers of consistent density. However, LbL protocols dependent on electrostatic interactions are not well suited for long-term biological applications due to *in vivo* flow conditions and exposure to bodily fluids containing charged molecules and ions that could disrupt the non-covalent bonds between polymer layers (Dubas and Schlenoff 2001). Richert et al. worked around this issue to produce a covalently crosslinked biomimetic surface using a polyelectrolyte LbL method. They formed poly(L-lysine)/hyaluronan multilayers using a standard LbL protocol, but then covalently crosslinked the coating with a mixture of 1-ethyl-3-(3-dimethyl-aminopropyl) carbodiimide and N-hydroxysulfo-succinimide. The hyaluronan component in combination with the increased rigidity of the film due to the crosslinking supported chondrocyte adhesion and spreading. They later switched to a photo-crosslinkable system using sequential poly(L-lysine) and photoreactive vinylbenzene-grafted hyaluronan layers that could produce variable gel stiffnesses to influence cell adhesion (Vazquez, Boudou et al. 2009). Bioactive LbL coatings have also been developed using a “click”-type reaction wherein polyamine was reacted with the azlactone functionality present in poly(2-vinyl-4,4'-dimethylazlactone) to form covalently attached multilayers (Buck, Breitbach et al. 2009). By reacting the free azlactone groups on the surface of the coatings with different biomolecules, they could control the types of proteins that adsorbed to the surface and thus specify cell adhesion. The simplicity of the protocols and mild reaction conditions make LbL strategies an attractive option for imparting bioactivity and biocompatibility to material surfaces.

1.3.4 Radio Frequency Glow Discharge Plasma Treatments

Radio frequency glow discharge (RFGD) plasma may be employed to rapidly modify the surfaces of polymers to both increase biocompatibility and direct cellular responses. Electrical discharges in the presence of low pressure gasses can produce a mixture of low-temperature reactive gaseous species including electrons, free radicals, ions, photons, and excited molecules (Chan, Ko et al. 1996). These highly reactive gas-phase species permit surface etching, functionalization, and grafting on surfaces that may normally be considered chemically inert. As a result, plasma-based protocols can be applied on a variety of different surfaces that would otherwise require separate and often chemically harsh reaction schemes. Furthermore, plasma etching allows functionalization of any surface on a device exposed to the ionized gas, allowing uniform functionalization of materials with complex geometries. This has proven to be quite useful for the industrial sterilization and modification of medical devices such as small diameter vascular grafts (Lauer, Shohet et al. 2004).

Plasma treatments can produce third-generation material surfaces by influencing protein spreading and limiting the exposure of attachment sites within adsorbed proteins containing cell adhesion motifs. Functionalization of PET surfaces with hydrophilic groups has been performed via RFGD plasma treatments with the intention of increasing surface wettability (Ramires, Mirengi et al. 2000). Ammonia gas treatment was found to be particularly beneficial for endothelial cell attachment and spreading. Dekker et al. used nitrogen and oxygen plasma treatments to decrease the water contact angle of poly(tetrafluoroethylene) from 96° to between 15-58 degrees, which supported the formation of endothelial cell monolayers in the presence of 20% serum (Dekker, Reitsma et al. 1991). The utility of nitrogen plasma treatments was further strengthened by Griesser et al., who found polymer surfaces functionalized with amide groups to support fibroblast and

endothelial cell adhesion more effectively than oxygen or amine functionalization (Griesser, Chatelier et al. 1994).

Plasma treatments have additionally been used to functionalize surfaces in preparation for chemical grafting. This strategy has allowed grafting of proteins and polysaccharides to polymer surfaces as described in section 1.3.1 to enhance inertness on second generation material surfaces. The development of biomimetic third-generation materials via the direct grafting of adhesion peptides onto materials surfaces has been attempted, but requires complex and often harsh chemistries that are specific to each polymer surface (Massia and Hubbell 1990; Biltresse, Attolini et al. 2005; Chollet, Chanseau et al. 2007). Recently, a reaction scheme was developed to graft different densities of RGD peptides onto PET to promote osteoblast and endothelial cell adhesion (Chollet, Chanseau et al. 2009). While promising, this protocol cannot be easily adapted for use on other material surfaces, and it would be extremely beneficial if a universal plasma-based protocol could be developed to graft peptides and bioactive coatings to multiple types of polymers. Massia et al. established that a spacing of 440 nm (1 fmol/cm^2) between grafted RGD peptides led to fibroblast spreading via $\alpha V\beta_3$ integrin receptors, and a spacing of 140 nm (10 fmol/cm^2) led to the formation of focal contacts (Massia and Hubbell 1991). Achievement of such high densities of surface functionalization is difficult with plasma-based strategies due to the medley of reactive species present in cold plasmas. Valdes et al. addressed this issue by using plasma polymerization to apply a tetraethylene glycol dimethyl ether (tetraglyme) and (2) 2-hydroxyethyl methacrylate (HEMA) coating that was reacted with 1,1'-carbonyldiimidazole to allow grafting of adhesion peptides to a Nafion surface. A 2.5% HEMA/97.5% tetraglyme surface greatly increased the surface concentration of reactive groups to allow the grafting of approximately 1 nmol/cm^2 of adhesion peptide. While

tetraglyme surfaces are relatively nonfouling, the 2.5% HEMA component may adsorb protein (Cao, Chang et al. 2007). Furthermore, the peptide-grafted surface has yet to be tested for cell adhesion, and tetraglyme surfaces have been shown to increase monocyte adhesion during *in vivo* tests (Shen, Martinson et al. 2002). As an alternative to using complex plasma-based strategies to increase the surface concentration of reactive groups, it may be more practical to instead increase the size and functionality of the grafted molecule. Grafting large (50-180 nm diameter), highly functionalized, bioactive, hydrated, and crosslinkable oligomers/microgels to an air or nitrogen plasma-etched surface may allow extensive covalent surface coverage despite the minimal functionalization that can be achieved via standard plasma-treatments. This strategy is presented in Chapter 3 of this thesis, wherein high density bioactive PEG/albumin or 100% PEG coatings were applied to surfaces following short (10 min) air plasma-treatments.

1.4 Poly(Ethylene Glycol) Hydrogels as Biomaterials

1.4.1 Poly(Ethylene Glycol): Resistance to Protein Adsorption and Chemical Functionalization

PEG, also referred to as poly(ethylene) oxide at high molecular weights, is a synthetic FDA-approved polymer composed of ethylene oxide monomers. PEG has a general formula of $\text{HO}-(\text{CH}_2-\text{CH}_2-\text{O})_n-\text{H}$ and is strongly hydrophilic. Raman scattering and NMR analysis both indicate that three water molecules hydrate each PEG unit, and this extensive hydrogen bonding results in the formation of a hydration shell that may extend several hundred angstroms from the PEG backbone (Liu and Parsons 1969; Horne, Almeida et al. 1971;

Maxfield and Shepherd 1975; Kjellander and Florin 1981; Muller and Rasmussen 1991). The hydration shell and steric repulsive forces of the polymer chains are both thought to provide PEG with considerable resistance to non-specific protein adsorption (Jeon, Lee et al. 1991; McPherson, Shim et al. 1997). Longer lengths and increased packing of the polymer chains enhances the effects of these repulsive forces, and accordingly, the resistance of PEG to protein adsorption is amplified as the molecular weight and density are increased (Jeon and Andrade 1991). Additionally, PEG has an overall neutral charge, which in combination with the hydration shell provides very few binding sites for proteins to attach via electrostatic forces (Harris 1992; Ostuni, Chapman et al. 2001). Studies have demonstrated that reacting the surfaces of proteins and enzymes with PEG chains prevent immunologic recognition as well as clearance of these biomolecules when injected into the blood stream (Abuchowski, McCoy et al. 1977; Abuchowski, van Es et al. 1977). As expected, the covalent attachment of higher molecular weight PEG chains required lower densities of coupling in order to obtain immunologic resistance.

PEG is desirable for use as a biomaterial due to its resistance to protein adsorption, but it does not possess the structural properties of other polymers that are currently used in the manufacturing of implanted devices. As a result, PEG is frequently grafted or coated onto the surfaces of other materials (McPherson, Shim et al. 1997; Burchenal, Deible et al. 2002; Ma, Hyun et al. 2004; Heuberger, Drobek et al. 2005) or used in the formation of hydrogels (Sawhney, Pathak et al. 1993; Zisch, Lutolf et al. 2003; Wacker, Scott et al. 2006). Since the hydroxyl moiety is not highly reactive, PEG derivatives are commonly used in the development of PEG-based materials. Harris et al. developed numerous methods for the highly efficient synthesis of PEG derivatives based on the initial formation of either a PEG-tosylate or PEG-mesylate that could be displaced in subsequent reactions with minimal

chain cleavage (J. Milton Harris 1984). PEG-diisocyanate has been grafted onto Dacron surfaces and was shown to significantly decrease platelet adhesion and fibrinogen adsorption (Burchenal, Deible et al. 2002). Graft polymerization has also been applied for the attachment of PEG to Dacron by generating surface radicals with UV light (Uchida, Uyama et al. 1994). Four-arm PEG-VS hydrogels have been used in the formation of cell in-growth matrices by covalently retaining integrin-binding RGD peptides and substrates for matrix metalloproteinases (Zisch, Lutolf et al. 2003). Despite a plethora of such chemical modifications and applications, few implanted devices currently utilize PEG-based materials, primarily due to an inability to graft a sufficiently high density layer of PEG onto surfaces and partially due to cost restrictions stemming from prohibitively complex chemistries and strategies (Elbert and Hubbell 1996).

Chemical modification of the hydroxyl end-groups of PEG with vinyl-sulfone functionality allows crosslinking for hydrogel formation, retention of biological factors, or covalent attachment to material surfaces under mild physiological conditions (Zisch, Lutolf et al. 2003; Wacker, Scott et al. 2006). α,β conjugated compounds undergo Michael-type nucleophilic addition reactions in the presence of nucleophiles, and vinyl sulfone has been shown to participate in such reactions in a pH dependent manner (Masri and Friedman 1988). Thus PEG-VS can be readily alkylated by thiol-containing molecules under neutral conditions and amine-containing molecules under slightly basic conditions, allowing selective reactivity with either cysteines or lysines within proteins. Since these reactions occur under mild physiological conditions, biological factors can be crosslinked into or retained within PEG-VS gels without fear of denaturation or unwanted side-reactions. This ability has generated a variety of bioactive hydrogel coatings that, for example, allow conjugation of cell adhesion peptides or crosslinking with enzymatically degradable peptides (Lutolf 2003).

Furthermore, these mild reaction conditions can be used to incorporate versatile proteins such as albumin, which is known to passivate material surfaces and function as a lipid carrier for bioactive lipids such as sphingosine 1-phosphate (Amiji, Park et al. 1992; English, Welch et al. 2000; Wacker, Scott et al. 2006). RGD-peptide-containing PEG hydrogels crosslinked with S1P-loaded albumin have been optimized to allow control over the biphasic migration of endothelial cells across hydrogel surfaces (Wacker, Alford et al. 2008). Thus PEG-VS functions as an adaptable and convenient synthetic polymer for the fabrication of bioactive coatings and scaffolds.

1.4.2 Poly(Ethylene Glycol) Coatings

A number of strategies have been explored to produce thin PEG-based coatings. Glow discharge treatment of surfaces with tetraglyme produces surfaces that exhibit low amounts of fibrinogen adsorption (Lopez, Ratner et al. 1992; Cao, Sivaprasad et al. 2006). Surface-initiated free-radical polymerization of hydrophilic monomers promotes polymerization and crosslinking in a limited region above the substrate (Hill-West, Chowdhury et al. 1994; Kizilel, Sawardecker et al. 2006). Adsorption of high molecular weight PEG/polylysine copolymers onto endovascular stents reduces restenosis after implantation, although long-term stability of the adsorbed copolymers may be a concern (Billinger, Buddeberg et al. 2006; Lussi, Falconnet et al. 2006). Copolymers of methyl methacrylate and PEG are also quite effective in reducing non-specific cell adhesion on a variety of surfaces (Banerjee, Irvine et al. 2000; Irvine, Mayes et al. 2001; Hyun, Ma et al. 2003; Zhang, Ma et al. 2005). A single or very thin crosslinked layer of “star” (multiarm) PEG reduces non-specific cell adhesion on surfaces (Kuhl and Griffith-Cima 1996; Groll, Haubensak et al. 2005; Hoffmann, Groll et al. 2006). Covalent layer-by-layer methods have

also been described, in some cases yielding coatings with resistance to protein adsorption and cell adhesion (Lackowski, Ghosh et al. 1999; Ghosh, Lackowski et al. 2001). Amirpour et al. combined micro-contact printing-based lithography and polymer grafting to generate patterns of poly(acrylic acid) layers coated with PEG on gold substrates. The 3D patterns of polymeric “fences” that resulted could direct cell adhesion and spreading (Amirpour, Ghosh et al. 2001).

Our research group has previously attempted the covalent LbL assembly of nanoscale PEG hydrogels by repeatedly alternating surface incubations between PEG-VS and a dithiothreitol crosslinker. However, these efforts to apply dense coatings of PEG to surfaces proved to be quite laborious and afforded only a moderate reduction in cell adhesion (Kim, Wacker et al. 2007). As explained previously, the difficulty in achieving 100% conversion at each reaction step results in progressively inconsistent densities of polymer within layers. Consequently, gaps exist in the coating through which protein can migrate to the underlying material surface, and the thickness of the film eventually reaches a maximum due to decreasing availability of functional groups for further reaction. This suggested that the use of higher molecular weight polymers or larger polymer aggregates (oligomers/microgels) may more readily achieve dense PEG coverage, especially on surfaces with low densities of reactive groups. Such an approach has proven to be quite successful as demonstrated by data presented in Chapter 3 of this thesis.

1.4.3 Poly(Ethylene Glycol) Scaffolds

Tissue engineering scaffolds are structures designed to promote tissue healing and/or regeneration by providing the mechanical and biochemical cues required to maintain cell viability and direct cell proliferation and differentiation (Place, George et al. 2009). The

recent shift in the general focus of the biomaterials field towards the employment of third-generation biomedical materials has carried over into the design of tissue engineering scaffolds. Accordingly, advanced scaffolds are composed of biomaterials designed to elicit specific cellular interactions and responses at the molecular level while minimizing unfavorable nonspecific biological activity (Hench and Polak 2002). As a result, a variety of different scaffold strategies have emerged to take advantage of the chemical versatility and specificity of PEG derivatives and copolymers. Photopolymerizable poly(ethylene glycol) diacrylate (PEG-DA) is certainly the most utilized PEG derivative. It is particularly amenable to template-based lithographic methods that can produce hydrogel modules with well-defined 3D structures for the assembly of larger tissue engineering constructs. For example, cells encapsulated within hydrogels formed by crosslinking PEG-DA with hyaluronic acid within microwells have permitted immense control over 3D scaffold shape (Yeh, Ling et al. 2006). PEG-DA has also served as an injectable cell-laden scaffold for adipogenesis and has been particularly successful when crosslinked with peptides containing LGPA collagenase-degradable and YIGSR cell adhesion motifs (Patel, Gobin et al. 2005). Halstenberg et al. developed hydrogels composed of PEG-DA that were grafted to artificial protein prior to photopolymerization. The protein component was able to provide multiple functions in addition to cell adhesion, including heparin binding and plasmin degradation (Halstenberg, Panitch et al. 2002). A technique designed for precise control over hydrogel porosity was developed by Stachowiak et al., who photopolymerized PEG-DA around poly(methyl methacrylate) microspheres that could be arranged in ordered structures and dissolved with acetic acid to generate interconnected macroporosity (Stachowiak, Bershteyn et al. 2005). The vinylsulfone derivative of PEG has been primarily utilized by the Hubbell group to fabricate PEG hydrogel scaffolds under mild conditions without

photopolymerization. The group developed cell-laden PEG-VS hydrogels crosslinked with MMP-degradable peptides to achieve in situ formation of cell niches as cells migrated and proliferated within the scaffold (Lutolf 2003). Completely synthetic PEG copolymers have been utilized to enhance scaffold stiffness, as demonstrated by poly(ethylene glycol)-terephthalate fibers used in porous scaffolds that can achieve elastic moduli up to 4.33 MPa for the engineering of articular cartilage (Malda, Woodfield et al. 2004; Malda, Woodfield et al. 2005). Thus third-generation scaffolds with a wide range of physical and chemical properties can be generated through the use of PEG.

From this prior work, a description of the optimal tissue engineering scaffold can be envisioned. The scaffold composition should contain as high a percentage of PEG as possible to minimize nonspecific protein adsorption and cell adhesion. A hydrogel structure is desired to achieve high levels of water content and nutrient transfer. Porosity is needed at multiple length scales to provide niches for embedded cells and routes of vascularization. Scaffolds should allow incorporation of biomolecules either at the backbone level or in the form of end-group conjugation to impart specific bioactivity and/or cell-initiated mechanisms of degradation. The stiffness should be adjustable to mimic the physical characteristics of different types of tissues. And finally, scaffolds should be able to accomplish these goals with a rapid, scalable, and modular fabrication process. What is missing from this literature is a methodology to form modular, porous scaffolds under mild conditions that would allow assembly in the presence of cells and not require mobility-impeding cell encapsulation. The creation of such a process was one objective of this thesis, and preliminary data towards achieving this goal are discussed in Chapter 4.

CHAPTER 2[†]

Mass Spectrometric Mapping of Fibrinogen Conformations at Poly(Ethylene Terephthalate) Interfaces

2.1 Abstract

We have characterized the adsorption of bovine fibrinogen onto the biomedical polymer polyethylene terephthalate (PET) by performing mass spectrometric mapping with a lysine-reactive biotin label. After digestion with trypsin, MALDI-TOF mass spectrometry was used to detect peptides from biotinylated bovine fibrinogen, with the goal of identifying lysines that were more accessible for reaction with the chemical label after adsorption. Peptides within domains that are believed to contribute to heparin binding, leukocyte activation, and platelet adhesion were found to be biotin labeled only after bovine fibrinogen adsorbed to the PET surface. Additionally, the accessibility of lysine residues throughout the entire molecule was observed to increase as the concentration of the adsorbing bovine fibrinogen solution decreased, suggesting that the proximity of biologically active motifs to hydrophilic residues leads to their exposure. The surface area per adsorbed bovine fibrinogen molecule was quantified on PET using optical waveguide lightmode spectroscopy (OWLS), which revealed higher surface densities for bovine fibrinogen adsorbed from higher concentration solutions. Preliminary work towards a quantitative variation of the

[†] Chapter 2 has been adapted from the following published manuscripts:
Scott EA, Elbert DL. Mass spectrometric mapping of fibrinogen conformations at poly(ethylene terephthalate) interfaces. *Biomaterials*. 2007 Sep;28(27):3904-17.
Elbert DL, Mawuenyega K, Scott EA, Bateman RJ. Stable isotope labeling tandem mass spectrometry (SILT): Integration with peptide identification and extension to data-dependent scans. *J. Proteome Res*. 2008 Sep 6;7 (10), pp 4546–4556.

mass spectrometric method is additionally presented. A protocol was developed for the expression of isotopically labeled proteins from HepG2 hepatocarcinoma cells. Stable isotope labeling tandem mass spectrometry (SIL/T-MS) was utilized to generate standard curves for the quantification of complement C3, α_2 -macroglobulin, and human fibrinogen. By measuring changes in the identity, conformation, and quantity of proteins that adsorb from complex mixtures such as blood or plasma, the methods presented here may have applications in fundamental studies of protein adsorption and may allow for more accurate predictions of the biocompatibility of materials.

2.2 Introduction

The first biological response to the implantation of foreign materials is the adsorption of a thin layer of proteins onto their surfaces (Baier and Dutton 1969; Brash and Davidson 1976; Andrade and Hlady 1986). The rate of adsorption and the chemical properties of the surface influence protein conformations and surface coverage as the adsorbed proteins denature and unfold at this solid/liquid interface. Some adsorbed proteins expose previously hidden binding domains that participate in inflammatory, thrombotic, and immunologic responses (Zucker and Vroman 1969; Mohammad, Hardison et al. 1974; Kottke-Marchant, Anderson et al. 1987; Anderson, Bonfield et al. 1990; Shen and Horbett 2001). The post-adsorptive conformations of fibrinogen have been investigated on surfaces of varying surface energy and these transformations expose sites responsible for platelet activation and aggregation (Shiba, Lindon et al. 1991; Farrell, Thiagarajan et al. 1992; Liu, Rooney et al. 1998; Tang, Wu et al. 1998; Sit and Marchant 1999; Bennett 2001). Here, we introduce mass spectrometric mapping to probe local conformational changes within

bovine fibrinogen (bFg) following adsorption to the biomedical polymer polyethylene terephthalate (PET).

When proteins are reacted with a chemical label prior to enzymatic digestion, labeled peptides with increased masses can be identified by mass spectrometry. Since the rate of reaction of protein functional groups is dependent on their degree of solution exposure (Suckau, Mak et al. 1992), mass spectrometry can be used to map changes in protein conformation by varying the experimental conditions and tracking the accessibility of specific residues to chemical modification. Mass spectrometric mapping has been previously utilized to discern protein-protein interactions and protein conformations in solution (Robinson, Gross et al. 1994; Bennett, Matthiesen et al. 2000; Carven and Stern 2005). Arginine, lysine, tryptophan, and tyrosine are the most common targets of amino acid modification (Bennett, Matthiesen et al. 2000; Hager-Braun and Tomer 2002; Carven and Stern 2005). Since lysines occur frequently throughout proteins, are charged and have a high degree of solution exposure, amine-specific N-hydroxysuccinimide (NHS) ester labels have been used in various applications, including isotope-tagging for relative absolute quantification (TTRAQ) (Ross, Huang et al. 2004; Roesli, Elia et al. 2006). The availability of water-soluble derivatives of NHS-esters provides an advantage over most other reagents used for protein labeling, in that the reaction can be performed under physiologic conditions (Staros 1982).

Techniques such as antibody labeling, atomic force microscopy (AFM), circular dichroism, sum frequency generation (SFG), total internal reflectance fluorescence (TIRF) and Fourier transform infrared spectroscopy (FTIR) have demonstrated structural changes in fibrinogen after adsorption onto surfaces (Lu and Park 1991; Shiba, Lindon et al. 1991; Buijs, Norde et al. 1996; Sit and Marchant 1999; Cacciafesta, Humphris et al. 2000; Holland

and Marchant 2000; Lu, Huang et al. 2003; Clarke, Wang et al. 2005; Hylton, Shalaby et al. 2005; Tunc, Maitz et al. 2005; Toscano and Santore 2006). Each of these techniques has advantages for elucidating protein structural changes, but generally provides information at the domain-level. Antibody binding can be used to correlate the exposure of cell interaction motifs to post-adsorptive changes in fibrinogen conformation (Shiba, Lindon et al. 1991). While antibody binding verifies the exposure of previously inaccessible domains of fibrinogen, it is dependent on the availability of specific antibodies and can only reveal changes in protein conformation in areas of the protein complementary to these antibodies. AFM has provided detailed information on the overall post-adsorptive structure of fibrinogen by revealing the dimensions of the fibrinogen D and E domains on various surfaces. However, AFM is not well suited for discerning transitions in dense monolayers of protein. Detailed studies on the global changes in fibrinogen secondary structure after adsorption have been performed using SFG, TIRF, and FTIR, also yielding information at the domain-level (Clarke, Wang et al. 2005; Roach, Farrar et al. 2005; Toscano and Santore 2006). We believe that mass spectrometric mapping may contribute to the study of adsorbed proteins by providing residue-specific information on surface-dependent conformational changes under physiologically relevant experimental conditions.

Although protein molecular weights can be routinely determined within ± 0.1 Da, accurate quantification of protein concentrations by mass spectrometry (MS) has remained elusive. The intensities of signals observed in MS are influenced not only by the quantity of the analyte, but also by its ionization efficiency, which is dependent on numerous factors including charge and composition, and can thus vary significantly between different peptides. The most accurate methods of quantifying proteins with MS involve the incorporation of stable isotopes into peptides, usually ^{13}C , ^2H , or ^{15}N . Isotopic labeling does not affect the

chromatographic properties of molecules, and thus permits the direct comparison between the intensities of the heavy and light versions of peptides as they coelute during liquid chromatography. Stable isotopes can be incorporated into peptides with either chemical or metabolic strategies. Chemical strategies have primarily focused on the mass tagging of amino-acid side chains within proteins. The most widely used techniques are the cysteine-specific isotope-encoded affinity tags (ICAT), and the lysine-specific isobaric tags for iTRAQ mentioned earlier (Gygi, Rist et al. 1999; Ross, Huang et al. 2004). Metabolic strategies use the efficient biological machinery of cultured cells to achieve 99%-100% labeling of all expressed proteins. Originally, entire proteomes of cell lines were metabolically labeled by carefully removing all sources of nitrogen except for ^{15}N -substituted food (Oda, Huang et al. 1999). Current metabolic strategies have shifted towards stable isotope labeling by amino acids in cell culture (SILAC), in which specific amino-acids in the cell culture medium are replaced by their heavy counterparts. Since SILAC labels only select amino acid throughout the proteome, the data analysis is greatly simplified (Ong, Blagoev et al. 2002; Mann 2006).

Stable isotope labeling tandem mass spectrometry (SILT-MS) is a metabolic labeling technique that improves upon previous methodology by utilizing LC-ESI-MS/MS in a manner that significantly increases the accuracy of peptide quantification (Bateman, Munsell et al. 2006; Bateman, Munsell et al. 2007; Elbert, Mawuenyega et al. 2008). The technique is similar to SILAC, in that it requires the metabolic labeling of proteins with stable isotopes. In SILAC, the integrated intensities of parent ions of the MS^1 scan are compared for quantification, which introduces significant error from background noise stemming from peptides that coelute with the peptides of interest. SILT-MS takes advantage of the MS^2 scan, which is performed after the rf-field of the ion-trap is adjusted to eject all peptides

from the trap except for peptides with a specific mass to charge ratio. The mass spectrometer can be programmed to follow the MS² scan of each parent ion with a second MS² scan in which the same parent ion mass is increased by the mass of one isotope-labeled amino acid. For each parent ion and their heavy counterpart, the ratio of the sum of the intensities of b-ions (N-terminus fragments) and y-ions (C-terminus fragments) in the MS² spectra may be calculated. This ratio can be used to calculate the quantity of the sample protein based on the known quantity of an internal standard within $\pm 1\%$ error. Previous quantitative MS methods that used MS¹ precursor ions instead of MS² tandem ions could only quantify protein levels within $\pm 30\text{-}50\%$ error.

We have developed a proteomics-based strategy to analyze the adsorption of bFg onto PET, which supplements our earlier proteomic studies on the adsorption of serum and plasma proteins on biomaterials (Kim, Scott et al. 2005). The conformational changes that occur upon fibrinogen adsorption were examined by comparing the mass spectra of bFg that was biotin-labeled in solution to bFg that was labeled after adsorption to the surfaces of PET particles. We hypothesized that there was a tendency for sections of bFg to be exposed to solution during the adsorption process, and that peptides at these locations would be biotinylated at higher rates. We targeted primary amines with a chemical label due to their reactive properties and presence at 107 sites throughout the bFg molecule, which could be analyzed with respect to their location in three dimensional space due to the availability of the nearly complete bFg crystal structure. The reactions were performed under physiological conditions with an NHS-ester label. These residue-specific mass spectrometric mapping experiments correlated well with optical waveguide lightmode spectroscopy (OWLS) results, both of which demonstrated concentration-dependent changes in fibrinogen spreading on PET surfaces. Our data support previous findings that large scale changes in fibrinogen

conformation occur upon adsorption from dilute solutions, evidenced by enhanced exposure of hydrophilic lysine groups throughout the protein. Furthermore, post-adsorptive increases in lysine exposure were detected for several residues localized within biologically relevant fibrinogen motifs. Thus this method may be useful in localizing adsorption-induced conformational changes to specific sites within proteins with a residue-level resolution. Finally, a strategy was developed for the MS-based quantification of plasma proteins expressed by HepG2 hepatocellular carcinoma cells. SILT-MS was used to generate standard curves that demonstrated the quantification of human fibrinogen, complement C3, and α 2-macroglobulin. This technique may prove to be a safe and non-radioactive method of quantifying protein within adsorbed protein layers.

2.3 Materials and Methods

2.3.1 Spin Coating

Unless otherwise noted, all reagents were purchased from Sigma. Glass OWLS chips coated with a Si/Ti/O₂ waveguide layer (48 x 16 x 0.5 mm, MicroVacuum Ltd.) and silicon wafers (48 x 16 x 0.5 mm) were cleaned by immersion in piranha solution (3:1 H₂SO₄ and H₂O₂) for 5 min followed by rinsing in deionized (DI) water. Polyethylene terephthalate (PET, 0.05 mm thick, McMaster Carr, Chicago, IL) sheets were dissolved in chloroform with 5% (w/v) trifluoroacetic acid (TFA) to make 0.8% solutions of PET. The PET solution (100 μ L) was applied to the surfaces of either the wafers or OWLS chips and spun at 4500 RPM for 50 s with a model KW-4A spin coater (CHEMAT Technology). PET layer thicknesses on the silicon wafers were confirmed with a variable angle Stokes ellipsometer (Gaertner Scientific Corporation). X-ray photoelectron spectroscopy (XPS, Kratos

Analytical Axis 165 spectrometer, University of Missouri Rolla) was performed to verify the composition of the layers.

2.3.2 OWLS Analysis

PET coated waveguide chips were placed inside the flow chamber of a MicroVacuum OWLS 110 optical waveguide lightmode spectrometer. The adsorption of bFg from 1, 0.5 and 0.1 mg/mL solutions in phosphate buffered saline (PBS; 0.2 g/L KCl, 0.2 g/L KH₂PO₄, 8 g/L NaCl, 1.15 g/L anhydrous Na₂HPO₄, pH 7.4) was monitored with a time step of 30 sec. PBS was flowed over the surface of the chips for at least 1 h, or until a baseline with a transverse magnetic mode refractive index variation less than 1×10^{-6} was obtained. Solutions of bFg (0.1, 0.5, or 1 mg/mL) were allowed to flow over the surface for 4 h at 0.15 mL/min. The surface was then washed with PBS at 0.15 mL/min until a steady baseline was again reached. The thickness and density of the adsorbed layers were determined for each time point using MicroVacuum BioSense software.

2.3.3 Analysis of OWLS Results

The density and the change in density with time (dM/dt) were fit to a random sequential adsorption (RSA) model of the protein adsorption process (Ramsden 1993), using MathWorks MATLAB version 6.1. The OWLS data was fit to the equation:

$$\frac{d\theta}{dt} = K_a C_b \varphi(\theta) \quad (1)$$

where θ is the fractional surface coverage, K_a is the deposition rate constant, C_b is the bulk solution protein concentration, and φ is a surface coverage dependent function that

represents exclusion effects due to previously adsorbed proteins. The fractional surface coverage is defined by:

$$\theta = \frac{Ma}{m} \quad (2)$$

where M is the adsorbed surface density, m is the mass of a single fibrinogen molecule, and a is the surface area covered by one fibrinogen molecule. The dM/dt data were fit to the RSA equation previously derived using statistical mechanics of hard sphere adsorption to a two dimensional surface (Schaaf and Talbot 1989):

$$\frac{dM}{dt} = K \left[1 - 4\theta + \left(\frac{6\sqrt{3}}{\pi} \right) \theta^2 + \left(\frac{40}{\sqrt{3}\pi} - \frac{176}{3\pi^2} \right) \theta^3 \right] \quad (3)$$

The maximum θ , or jamming limit, resulting from the adsorption process for spheres is 0.547 (Hinrichsen, Feder et al. 1986). By substituting this maximum coverage into equation (2), the protein surface density at the jamming limit, M_∞ , was calculated for each adsorption experiment. M_∞ was used to directly convert OWLS surface density measurements into fractional surface coverages. Statistical significance (p-value < 0.05) between the fibrinogen concentrations was determined by ANOVA followed by a Scheffe post-hoc test.

2.3.4 PET Particle Fabrication

PET solutions (1%) were obtained by dissolving polymer sheets in dichloromethane with 5% (v/v) TFA. Each sample was filtered with a 0.5 μm PTFE filter (Millipore) and poured into 1 L of DI water while stirring. Emulsions were stirred overnight and PET particles were removed by filtration. The particles were washed in ethanol and DI water and stored under vacuum until use. The surface area per gram of particles was determined for

three separate fabrications using BET (Micrometrics Brunauer Emmett Teller model Gemini 2375).

2.3.5 Biotinylation

PET particles were placed in 1.5 mL silicone-coated polypropylene Eppendorf tubes and washed 3X in ethanol and 3X in PBS. Disposable polystyrene columns (Fisher Scientific) with 2 mL bed volumes were filled with the PET particles (150 mg) in PBS and allowed to settle for 30 min. PBS (3 mL) was added to the columns for washing, followed by 2 mL of 1, 0.5, or 0.1 mg/mL bFg in PBS. The PET surfaces were incubated with the bFg solutions for 2 h and then washed with 5 mL of PBS. The PBS washes were collected in 1 mL samples for analysis with a GENESYS 10 spectrophotometer (Spectronic) at 280 nm to monitor the decrease in protein concentration and to ensure that the non-adsorbed bFg solution was completely removed. A 10 mg/mL solution of Sulfo-NHS-LC-Biotin (Pierce) in PBS was added to the column and incubated for 1 h to allow reaction with the adsorbed bFg. PBS (5 mL) was then flowed through the column to remove excess NHS solution. The adsorbed protein was eluted from the column with 500 μ L of an elution buffer (4% SDS, 40 mM Tris, 8M urea, pH 8.5). The elution buffer was allowed to incubate in the column overnight. Protein was collected by acetone precipitation and dried in an Eppendorf Vacufuge concentrator. Adsorption experiments were performed in triplicate for each concentration.

SDS-PAGE was used to monitor the extent of labeling in biotinylated samples. To maintain a similar degree of labeling between solution-labeled and surface-labeled samples, 0.5 mg/mL of bFg was biotinylated in solution with 1 mg/mL of Sulfo-NHS-LC-Biotin for 1 h at room temperature. The labeled bFg was concentrated and desalted by acetone

precipitation. The solution-labeled samples were not exposed to PET surfaces nor the elution buffer. Solution-labeling experiments were performed in triplicate.

Each surface-labeled and solution-labeled fibrinogen precipitation was resuspended in DI water and separated into 3 samples. The samples were reduced with 100 mM DTT, alkylated with 100 mM iodoacetamide and separated by SDS-PAGE using Tris-HCl linear gradient 8-16% gels (Pierce). Fibrinogen A α , B β , and γ chains were stained with SYPRO Ruby stain and excised from the gels. In-gel trypsin digestions were performed overnight for 16 h at 37°C. The peptides were purified for MALDI-TOF analysis using ZipTips (Fisher Scientific) with elution by 15 mg/mL α -cyano-4-hydroxycinnamic acid matrix solution in 0.1% TFA/50% acetonitrile.

2.3.6 MALDI-TOF Analysis

Mass spectrometry was performed with an Applied Biosystems Voyager System 4254 MALDI-TOF in positive-ion reflectron mode to produce centroided spectra. Each bFg sample was divided into three separate aliquots prior to in-gel trypsin digestion and thus each sample was analyzed with MALDI-TOF three times (see workflow diagram, Figure 2.4). The three spectra obtained for each sample were normalized to each other using internal bFg peptide standards. Peptides common to each trypsin digest that did not contain lysines were selected as standards. Trypsin-digested bFg peptide masses were predicted using the ExPASy proteomics server (Gasteiger, Gattiker et al. 2003). Peptides with up to three missed cleavages ranging in size from 700 – 4000 Da were found in MALDI-TOF spectra with in-house Perl scripts that identified peaks consistent with tryptic bFg peptides. A tolerance of \pm 0.1% was utilized with a maximum upper deviation of 2 Da and a maximum lower deviation of 1 Da was utilized. Biotin-labeled peptides were identified by the

following criteria: 1) the peptide contained at least one missed cleavage, 2) the peptide mass increased by the size of the Sulfo-NHS-LC-Biotin label (+339.452 Da), and, 3) the peptide contained at least one lysine residue that was not located at the carboxyl terminus, since trypsin cleavage after labeled lysines should be unfavorable. If two separate peaks corresponded to different peptides that contained the same labeled lysine location due to incomplete trypsin digestion, the normalized intensities were summed. The summed normalized intensities of peptides containing each lysine residue were averaged across the three trypsin digests. These average lysine intensities were then averaged across three separate experiments for each of the tested conditions. Non-parametric Mann-Whitney pairwise comparisons were used to identify statistically significant (p -value < 0.05) changes in intensity. Labeled bFg locations were visualized using PDB file 1DEQ (Brown, Volkmann et al. 2000) with Visual Molecular Dynamics version 1.8.3 (Humphrey, Dalke et al. 1996). A sequence comparison between human and bovine fibrinogen was performed using CLUSTAL W version 1.83 (Thompson, Higgins et al. 1994).

2.3.7 Liquid Chromatography Electrospray-Ionization Ion Trap Tandem Mass Spectrometry

The reliability of labeled peptide detection was confirmed by processing some solution-labeled samples with liquid chromatography electrospray-ionization ion trap tandem mass spectrometry (LC-ESI-MS/MS). After biotinylation, PBS solutions of bFg were buffer exchanged using microcentrifuge filters (NMWL 10,000, PLGC cellulosic membrane, Millipore Corp.) into 25 mM ammonium bicarbonate and digested with sequence grade trypsin overnight at 37°C. The ammonium bicarbonate was evaporated in a Vacufuge and samples were stored at -20°C. Tryptic peptides were dissolved in 25 μ L of 5%

acetonitrile/0.02% N-heptafluorobutyric acid (HFBA). The peptide solutions (4 μ L) were injected into a nano-HPLC system (Agilent 1100 capillary pump) connected to a Picoview nanoelectrospray head (New Objective, Woburn, MA) attached to an ion trap mass spectrometer (LCQ DECA, ThermoFinnigan, San Jose, CA). The peptides in the mixture were separated at a flow rate of 300 nL/min. A gradient of 5% acetonitrile/0.02% HFBA to 80% acetonitrile/0.02% HFBA was run over 60 min, with peptides separated on a 75 μ m \times 5 cm C18 Biobasic column (New Objective). The LCQ-DECA was operated in positive ion mode using a capillary voltage of 12 V, a capillary temperature of 150°C, and a spray voltage of 2.2 kV. Each experiment was immediately followed by a blank injection to ensure that proteins were not carried over from previous injections. Data were collected in full MS/MS mode and biotin-labeled peptides were identified using an in-house program as described previously (Kim, Scott et al. 2005).

2.3.8 Expression of HepG2 Proteins

HepG2 cells were cultured in lysine-free medium (Washington University School of Medicine Tissue Culture Support Center) containing either 105 μ g/mL of L-lysine or $^{13}\text{C}_6, ^{15}\text{N}_2$ - L-lysine hydrochloride . Cells were initially grown in medium supplemented with 10% dialyzed fetal calf serum and 1 μ M all-trans retinoic acid until reaching 50-60% confluency. The culture medium was then switched to serum free medium containing primary hepatocyte growth supplements (Lonza), 1 μ M all-trans retinoic acid, and 1 μ g/mL aprotinin. Medium was collected every 2 days, supplemented with protease inhibitor cocktail (Roche) and filtered through a 0.22 μ m filter (Millipore). The filtered media was concentrated to about 1 mL using 10K MWCO centrifuge filters and stored at -80°C.

2.3.9 Quantification of $^{13}\text{C}_6, ^{15}\text{N}_2$ -Fibrinogen Concentrations in Media

The concentration of $^{13}\text{C}_6, ^{15}\text{N}_2$ -fibrinogen in the HepG2 media was determined with an ELISA kit (AssayMax Human Fibrinogen ELISA Kit). Media was added to a 96-well plate that were pre-coated with a murine anti-human fibrinogen antibody and allowed to incubate for 2 h. After washing, each well was incubated with a biotinylated fibrinogen standard. A streptavidin-peroxidase conjugate was then added to each well to report the amount of bound biotinylated fibrinogen standard. The absorbance was then be read at a wavelength of 450 nm. Lower absorbances indicate higher concentrations of bound $^{13}\text{C}_6, ^{15}\text{N}_2$ -fibrinogen. According to the manufacturer, the minimum detectable dose of fibrinogen for the ELISA kit is 100 ng/mL.

2.3.10 $^{13}\text{C}_6, ^{15}\text{N}_2$ -Fibrinogen Purification

$^{13}\text{C}_6, ^{15}\text{N}_2$ -fibrinogen in HepG2 media was immunoprecipitated with fibrinogen polyclonal rabbit anti-human IgG (Dako North America, Inc.) that were covalently attached to sepharose beads (Amersham Biosciences). Antibody beads were prepared according to the manufacturer's protocol and stored at 4°C in a 50% slurry of PBS and 0.02% sodium azide. Media (1 mL) was incubated with the antibody beads overnight at 4°C in an Eppendorf micro-centrifuge tube and then rinsed 3X with radioimmuno precipitation assay (RIPA) buffer containing protease inhibitors. The bound $^{13}\text{C}_6, ^{15}\text{N}_2$ -fibrinogen was eluted from the beads by boiling in SDS-PAGE loading buffer without a reducing agent at 100°C. Separate fibrinogen purifications in SDS-PAGE loading buffer were pooled together and stored at -20°C.

2.3.11 Preparation of $^{13}\text{C}_6$, $^{15}\text{N}_2$ -HepG2 Protein Standards

Concentrated isotope-labeled and unlabeled media or fibrinogen in SDS-PAGE loading buffer were mixed into 10 μL volumes at various ratios. Media samples were additionally mixed with 10 μL of 2X SDS-PAGE loading buffer, boiled for 5 min at 100°C . Samples were separated by SDS-PAGE, and individual bands were excised, reduced with 50 mM TCEP, and alkylated with 100 mM iodoacetamide. Additionally, an extra 1 h incubation step in a 10 mg/mL sulfo-NHS acetate (Pierce) or 100 mM acetic anhydride was performed for some fibrinogen samples to achieve extensive acetylation of the reduced protein prior to digestion. In-gel digestion was performed with 250 ng of sequence-grade trypsin (Princeton Separations) for 16 h at 37°C . The trypsin reaction was stopped by the addition of 0.1% TFA in DI water and the peptide solutions were evaporated to dryness in an Eppendorf Vacuufuge. Dried samples were stored at -20°C until analysis by mass spectrometry. The percentage of labeled peptide was determined using the SILT-MS software assuming a mass difference of 8 amu between labeled and unlabeled peptides (Elbert, Mawuenyega et al. 2008). Acetylated peptides were detected assuming mass increases of amu after the reaction.

2.4 Results

2.4.1 Characterization of PET Films

The spin coating of PET layers was initially characterized on silicon wafers. Ellipsometry showed consistent thicknesses of between 45 and 50 nm across the surfaces of the silicon wafers (Figure 2.1). XPS analysis verified the composition of these layers (Table

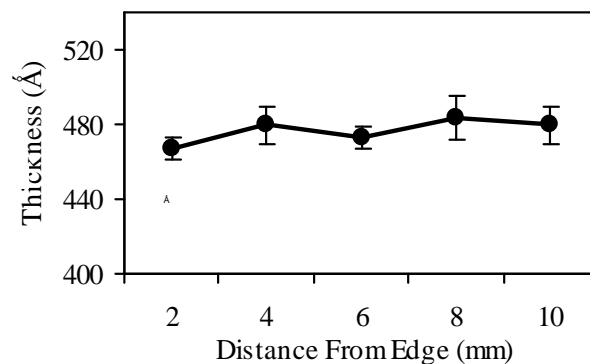


Figure 2.1: Ellipsometry measurements of polyethylene terephthalate (PET) layer thickness and uniformity on silicon wafers. PET coatings were applied to surfaces using spin coating, and ellipsometry was used to determine the layer thickness at 2 mm increments across a wafer. Error bars represent standard deviations of four samples.

Table 2.1: XPS analysis of PET coated silicon wafers.

| Peak | Position BE (eV) | Atomic Conc. % |
|------|------------------|----------------|
| O | 530.5 | 24.80 |
| Ti | 464 | 0.02 |
| N | 397 | 0.19 |
| C | 283 | 71.48 |
| S | 167 | 0.12 |
| Si | 100.5 | 3.05 |
| Cl | 99.5 | 0.00 |

2.1). Peaks at 283.5 eV for carbon and 530.5 eV for oxygen revealed their respective atomic compositions to be approximately 71.0% and 24.8%, which corresponded well with the expected amounts for a PET layer of 72% for carbon and 28% for oxygen. OWLS waveguide chips were coated using the protocol developed for the silicon wafers and the changes in thickness were verified by OWLS to be between 50 and 75 nm.

2.4.2 OWLS Analysis of Fibrinogen Adsorption onto PET

A random sequential adsorption model was used to determine the average surface area of individual bFg molecules on PET-coated OWLS chips at the jamming limit (Table 2.2). Changes in protein surface density over time for the bulk solution concentrations of 0.1, 0.5 and 1 mg/mL were non-linear least-squares fit to equation (3) by adjusting the a/m and K parameters. Statistically significant differences in surface density were found when comparing the 1 mg/mL samples to either the 0.5 mg/mL or the 0.1 mg/mL samples. The 0.5 mg/mL and 0.1 mg/mL samples were not significantly different.

2.4.3 MALDI-TOF Sequence Coverage

The bFg peptides identified in the MALDI-TOF spectra of the solution-labeled samples revealed the sequence coverages of the A α , B β , and γ chains to be 69%, 68%, and 61%, respectively (Figure 2.2). Within these regions, 81 of the 107 lysine locations in bFg were identified. Due to the lack of lysines present in certain sections (e.g. a 128 amino acid span between A α 272-400), several large segments of bFg were neither available for MALDI-TOF detection after trypsin digestion nor accessible for labeling with biotin.

To determine whether the sequences spanned by the recovered peptides included areas of the protein that were complementary to binding motifs previously studied in human

Table 2.2: Summary of bFg m/a values estimated from OWLS and AFM experiments. OWLS analysis of PET coated waveguide chips was performed under flowing bFg solutions in PBS. A random sequential adsorption model was used to determine the m/a from measured changes in surface density during the adsorption process. Statistically significant differences were determined by ANOVA with a Scheffe post-hoc test. OWLS samples that are significantly different (p-value < 0.05) from the 1 mg/mL samples are marked with an (*). AFM Calculations were made using fibrinogen volume and height measurements obtained from Sit et al. (Sit and Marchant 1999).

| Instrument | Material | Bovine | m/a (ng/cm ²) |
|------------|----------|--------------------------|-----------------------------|
| | | fibrinogen Concentration | |
| OWLS | PET | 1 mg/ml | 275.48 ± 4.34 |
| | PET | 0.5 mg/ml | *129.68 ± 51.73 |
| | PET | 0.1 mg/ml | *119.63 ± 22.82 |
| AFM | Mica | 50 ng/ml | 162.31 ± 19.28 |
| | APTES | 50 ng/ml | 124 ± 17.96 |
| | OTS | 50 ng/ml | 79.82 ± 13.19 |

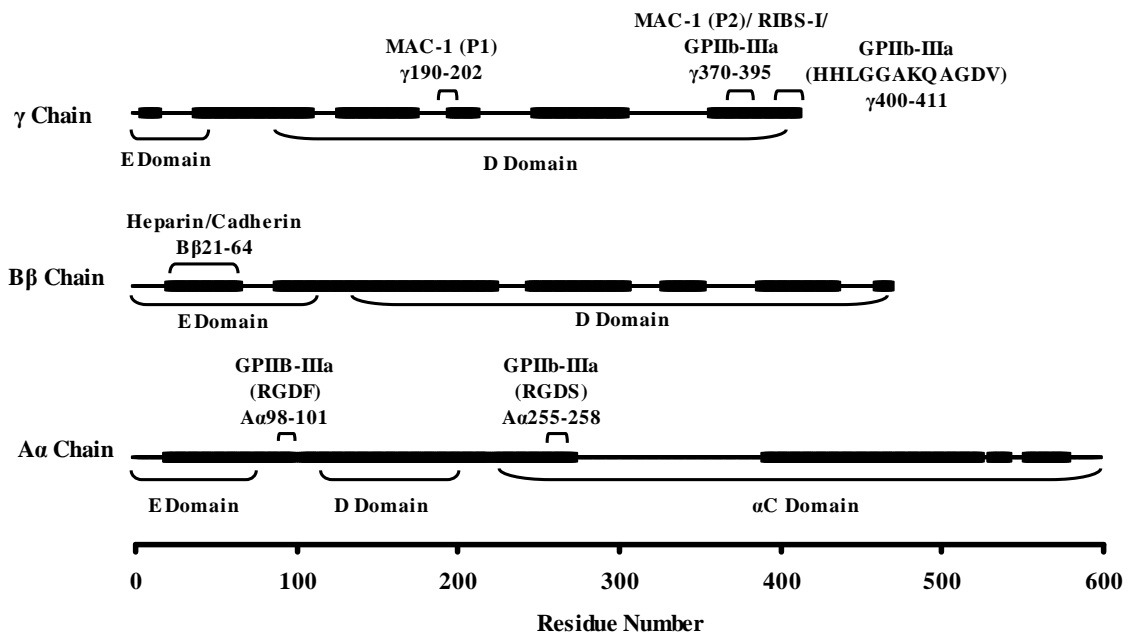


Figure 2.2: Sequence coverage obtained for α , β , and γ chain in-gel trypsin digests of biotinylated bFg. Residues that were found in peptides recovered after the trypsin digests are represented with thick lines, while residues that were not found are represented with thin lines. Locations of important binding motifs are indicated. Sequence coverages of 69%, 68%, and 61% were obtained for the α , β , and γ chains, respectively.

fibrinogen, the sequences of human and bovine fibrinogen were compared using multiple sequence alignments with CLUSTAL W. Although only approximately 66% of the entire bFg molecule was observable by MALDI-TOF, identified regions included several locations of interest, which are labeled in Figure 2.2. In the A α chain, an RGDF platelet binding domain for $\alpha_{\text{IIb}}\beta_3$ integrins at A α 98-101 was found to be complementary to A α 95-98 in human fibrinogen and was found in the MALDI-TOF sequence coverage. A region containing an RGGG motif at A α 541-544 in bFg that was not found in the sequence coverage had high sequence complementarity to a region in human fibrinogen containing an RGDS (A α 572-575). An RGDS motif is present in bFg at A α 255-258 and was within the sequence coverage, but an RGDS is not present in human fibrinogen at the complementary site. The B β chain of human fibrinogen contains domains linked to cadherin binding (B β 15-42) and heparin binding (B β 15-57), which were respectively located in bFg at B β 21-49 and B β 21-64. Both sequences were identified in bFg by MALDI-TOF after trypsin digestion. The binding domains of the γ chain are highly conserved between species. The MAC-1 leukocyte binding sites at γ 190-202 and γ 377-395, the RIBS-I epitope at γ 373-385, the $\alpha_{\text{IIb}}\beta_3$ platelet-binding site within γ 370-385, and the platelet-binding dodecapeptide at γ 400-411 were in similar locations for human and bovine fibrinogen. The biologically-active γ chain binding domains were within the sequence coverage except for the MAC-1 leukocyte motif.

2.4.4 PET Particle Fabrication

SEM analysis revealed mostly spherical particles with diameters ranging from 1 - 200 μm that tended to aggregate in PBS solution (Figure 2.3). Higher percentages of spherical particles were obtained when the surface tension was adjusted with surfactant during formation, but this step was not performed to eliminate the possibility of unwanted

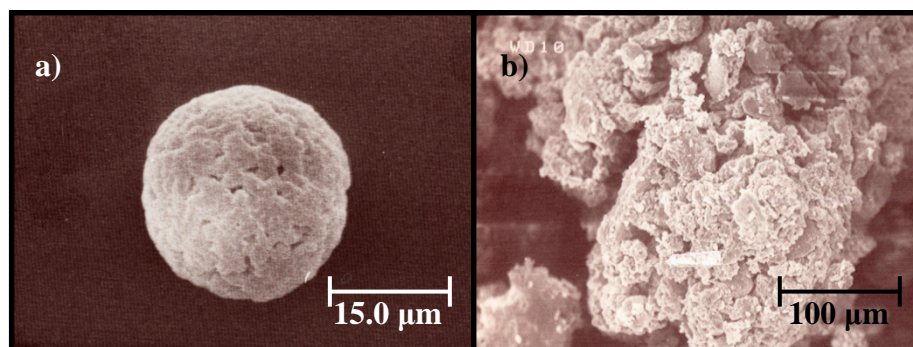


Figure 2.3: Scanning electron microscopy (SEM) of fabricated PET particles. (a) An individual PET particle at 2000x magnification. (b) SEM image of an aggregate of PET particles at 300x magnification. Particle sizes ranged from 1 to 200 μm .

influences of surfactant on protein adsorption. BET analysis determined the surface area of the particles to be $20.1 \pm 2.9 \text{ cm}^2/\text{mg}$.

2.4.5 Biotinylation of Surface-Adsorbed Fibrinogen

The biotinylation protocol used for labeling and analyzing bFg after adsorption to PET surfaces is outlined in Figure 2.4. Plastic disposable chromatography columns were packed with 150 mg of PET particles to provide approximately 3000 cm^2 of surface area. Based on OWLS measurements of adsorbed bFg surface density, this surface area was estimated to adsorb between 0.3 – 0.9 mg of bFg as the solution concentration increased from 0.1 mg/mL to 1mg/mL. Decreased reaction between surface-adsorbed bFg and the biotin label was expected when compared to the reaction of bFg in solution with the biotin label. Therefore, a 10-fold higher concentration of Sulfo-NHS-LC-Biotin was used for the surface adsorption experiments to maintain similar levels of biotin labeling between surface and solution samples (Figure 2.5a). SDS-PAGE of bFg eluted from the PET columns revealed differences in molecular weights between labeled and unlabeled bFg chains. The changes in mass of solution-labeled and surface-labeled samples were compared to verify similar levels of biotin incorporation. The size of each band was determined via the linear relationship between the mobility of proteins in SDS-PAGE gels and the logarithms of their molecular weights (Weber and Osborn 1969). Using the molecular weight standards to produce a standard curve, the $A\alpha$, $B\beta$, and γ chains were found to correlate well with their expected molecular weights of 63.5 kDa, 56 kDa, and 47 kDa (Fig 5b). The changes in molecular weight of the bFg chains in the solution-labeled samples corresponded to the binding of approximately $68.4\% \pm 17.0\%$, $53.8\% \pm 11.0\%$, and $52.1\% \pm 17.1\%$ of the lysines in each respective chain. For the surface-labeled samples, the respective changes in

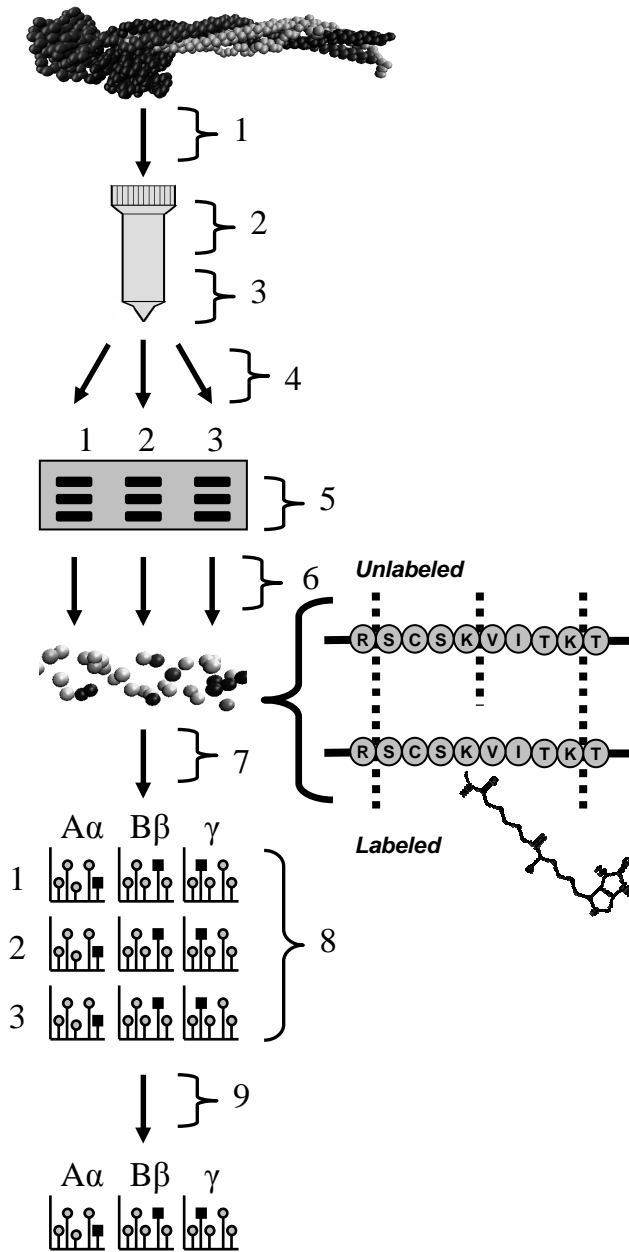
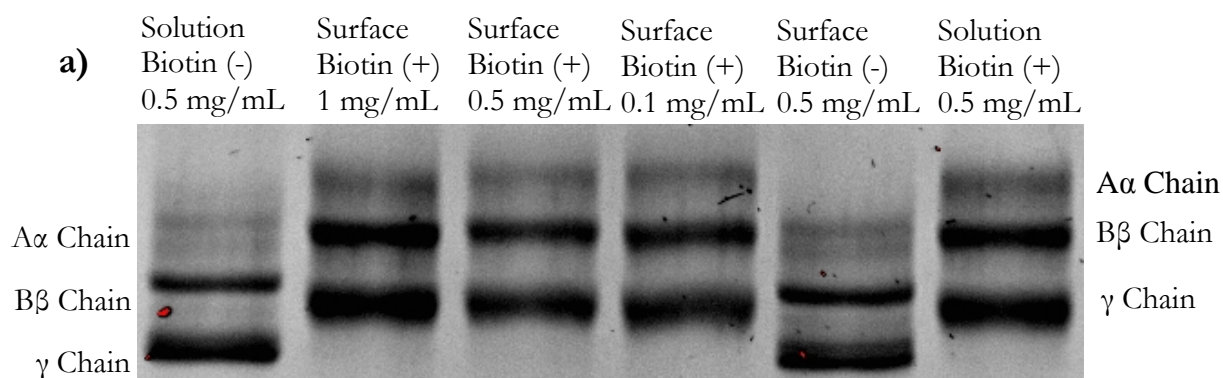


Figure 2.4: Workflow diagram for bFg surface adsorption experiments. Diagram is labeled as follows: (1) Adsorption of bFg onto PET beads packed in a column from 0.1, 0.5, or 1 mg/mL solutions. Each concentration was tested in triplicate, (2) Incubation of adsorbed bFg with Sulfo-NHS-LC-Biotin for 1 h, (3) Elution of adsorbed bFg with 4% SDS, 100 mM DTT and 8 M urea elution buffer. Elutions were separated into three samples for separate trypsin digestion, (4) bFg purification by acetone precipitation, (5) bFg chain separation by SDS-PAGE, (6) In-gel trypsin digestion, (7) Peptide purification with ZipTips, (8) MALDI-TOF analysis, (each PET column yielded three separate samples, and bFg A α , B β , and γ chains were analyzed for each sample), (9) Intensities of peptides containing labeled lysine residues were averaged across the three separate digests.



b)

| | A α chain | B β Chain | γ Chain |
|-----------------------------|------------------|-----------------|----------------|
| Theoretical MW (kDa) | 63.5 | 56 | 47 |
| Experimental MW (kDa) | 64.8 \pm 2.9 | 57.5 \pm 3.3 | 50.9 \pm 3.3 |
| Solution: MW Increase (kDa) | 9.1 \pm 2.3 | 6.9 \pm 1.4 | 5.3 \pm 1.7 |
| Surface: MW Increase (kDa) | 9.1 \pm 1.7 | 7.0 \pm 1.8 | 4.9 \pm 2.2 |

Figure 2.5: SDS-PAGE gel of bFg before and after reaction with the Sulfo-NHS-LC-Biotin label. The concentration of the label was adjusted to achieve the same degree of labeling for both bFg in solution and bFg adsorbed to PET. **(a)** A α , B β , and γ chains were separated by SDS-PAGE and stained with SYPRO Ruby stain to compare the increases in molecular weight due to labeling. Lanes are labeled as follows: Unlabeled bFg in solution (lane 1); labeled bFg eluted from the surfaces of PET particles after adsorption from 1 mg/mL (lane 2), 0.5 mg/mL (lane 3), and 0.1 mg/mL (lane 4); unlabeled bFg eluted from PET surfaces (lane 5); and bFg labeled in solution (lane 6). **(b)** The increases in molecular weight due to labeling were determined from the changes in migration the distances of the protein bands.

molecular weight of the A α , B β , and γ chains corresponded to the reaction of approximately 68.7% \pm 12.8%, 50.6% \pm 14.0%, and 41.6% \pm 21.5% of the lysines. An ANOVA revealed no statistically significant differences in the extent of biotinylation between the solution-labeled and surface-labeled fibrinogen chains.

2.4.6 Identification of Biotinylated Residues

After excision from SDS-PAGE gels and digestion with trypsin, the labeled and unlabeled fibrinogen chains were analyzed with MALDI-TOF and fibrinogen peptides were identified based on the expected molecular weights of tryptic fragments. Figure 2.6 demonstrates the detection of labeled and unlabeled peptides for fibrinogen biotinylated in solution and fibrinogen biotinylated after adsorption onto a PET surface. Trypsin should not cleave after lysines that have been labeled, and thus all Sulfo-NHS-LC-Biotin labeled peptides contained at least one missed cleavage. As a result, the average peptide mass increased as the number of biotinylated peptides increased, and the majority of labeled peptides had molecular weights above 2000 Da.

The ability to discern labeled from unlabeled peptides based on peptide molecular weight was verified with LC-ESI-MS/MS sequence analysis after an in-solution trypsin digestion. Table 2.3 lists the peptide sequences that were detected and the locations of the labeled lysines within them. These lysine locations and peptide masses were used to verify solution-labeled peptides that were identified with MALDI-TOF (Figure 2.7 (✓)). A total of 19 of the 81 lysine residues spanned by the MALDI-TOF sequence coverage were identified as biotin-labeled, and 11 of these lysines were also detected as labeled by LC-ESI-MS/MS.

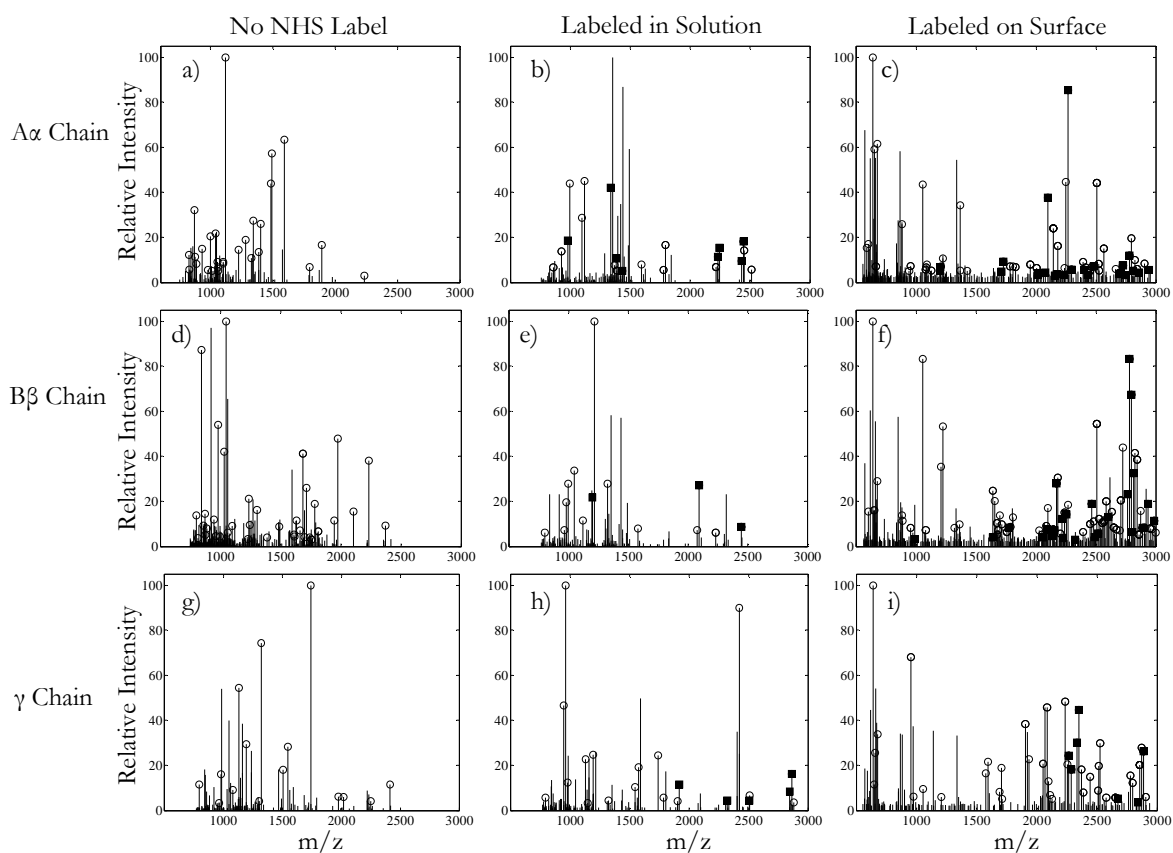


Figure 2.6: Centroided MALDI spectra corresponding to bFg trypsin digest fragment masses from the 0.5 mg/mL adsorption experiments. Open circles indicate the identification of masses that correspond to unlabeled bFg trypsin fragments. Black squares mark peaks that match an expected peptide after the Sulfo-NHS-LC-Biotin label was added to the mass. Spectra are shown for: (a) Unlabeled bFg A α chain, (b) A α chain labeled with biotin, (c) A α chain labeled with biotin after adsorption onto PET, (d) Unlabeled B β chain, (e) B β chain labeled with biotin, (f) B β chain labeled with biotin after adsorption onto PET, (g) Unlabeled γ chain, (h) γ chain labeled with biotin, (i) γ chain labeled with biotin after adsorption onto PET.

Table 2.3: Biotin-labeled bFg peptides identified by liquid chromatography electrospray-ionization ion trap tandem mass spectrometry. bFg was labeled with biotin while in a 0.5 mg/mL solution. Collision-induced dissociation fragmentation spectra of tryptic bFg peptides were compared to the predicted spectra of tryptic peptides from a database of 1×10^6 proteins. Only peptides that matched bFg peptides with p-values $< 1 \times 10^{-7}$ were considered significant. Labeled lysine locations are displayed in lowercase italics.

| Peptide Sequence | Lysine Location | Mol. Wt. (Da) | p-value of match |
|---|------------------------------|---------------|------------------------|
| M <i>K</i> GLIDEVDQDFTSR | A α 55 | 2093.63 | 1×10^{-15} |
| GDF <i>A</i> KANNNDNTFK | A α 103 | 1895.43 | 2.45×10^{-12} |
| ANNNDNTF <i>A</i> QISEDLR | A α 112 | 2218.23 | 6.66×10^{-11} |
| <i>K</i> VIEQVQR | A α 128 | 1339.54 | 2.32×10^{-09} |
| LEV <i>D</i> I <i>D</i> I <i>K</i> R | A α 160 | 1554.08 | 8.49×10^{-12} |
| ALEH <i>K</i> VDLEDYK | A α 175 | 1799.48 | 4.14×10^{-12} |
| NQQ <i>K</i> QLEQVIAINLLPSR | A α 186 | 2432.49 | 2.6×10^{-14} |
| EF <i>K</i> SQLQEAPLEWK | A α 222 | 2072.62 | 1.21×10^{-12} |
| ALLEMQQT <i>K</i> MVLETFGGDGHAR | A α 242 | 2772.7 | 1.98×10^{-10} |
| SCS <i>K</i> VIT <i>K</i> VTNADGR | A α 438 | 2415.95 | 6.73×10^{-10} |
| VIT <i>K</i> VTNADGR | A α 442 | 1614.47 | 2.21×10^{-12} |
| TETT <i>K</i> EVVK | A α 455 | 1374.64 | 2.69×10^{-09} |
| D <i>K</i> DDFFTR | A α 491 | 1383.43 | 5.06×10^{-09} |
| <i>K</i> PPDADGCLHADPDLGVLCPTGC | B β 65 | 2933.07 | 1.91×10^{-11} |
| <i>K</i> SIEDLR | B β 102 | 1200.23 | 5.38×10^{-10} |
| VYCDM <i>K</i> TEK | B β 250 | 1513.58 | 6.69×10^{-11} |
| VYCDM <i>K</i> TE <i>K</i> GGWTVIQNR | B β 250, B β 253 | 2865.09 | 3.8×10^{-09} |
| TE <i>K</i> GGWTVIQNR | B β 253 | 1727.93 | 7.66×10^{-13} |
| QGFGNIATNAEG <i>K</i> K | B β 290 | 1774.73 | 4.34×10^{-08} |
| ISQLTNMGPT <i>K</i> LLIEMEDWK | B β 316 | 2687.71 | 3.64×10^{-13} |
| DNDGW <i>K</i> ITDPR | B β 393 | 1644.27 | 4.96×10^{-11} |
| <i>K</i> QCS <i>K</i> EDGGGWYNR | B β 399, B β 403 | 2550.37 | 5.22×10^{-15} |
| NS <i>K</i> SMMEEIMK | γ 87 | 1667.27 | 3.57×10^{-11} |
| D <i>K</i> VVQLEANCQEPCQDTV <i>K</i> IHDV | γ 127, γ 144 | 3719.16 | 1.62×10^{-08} |
| DCQDVAN <i>K</i> GAK | γ 159 | 1544.92 | 8.48×10^{-13} |
| LDGSLDF <i>K</i> K | γ 205 | 1362.57 | 2.57×10^{-10} |
| LAIGEGQQHQLGG <i>A</i> KQAGDV | γ 406 | 2316.76 | 3.77×10^{-09} |

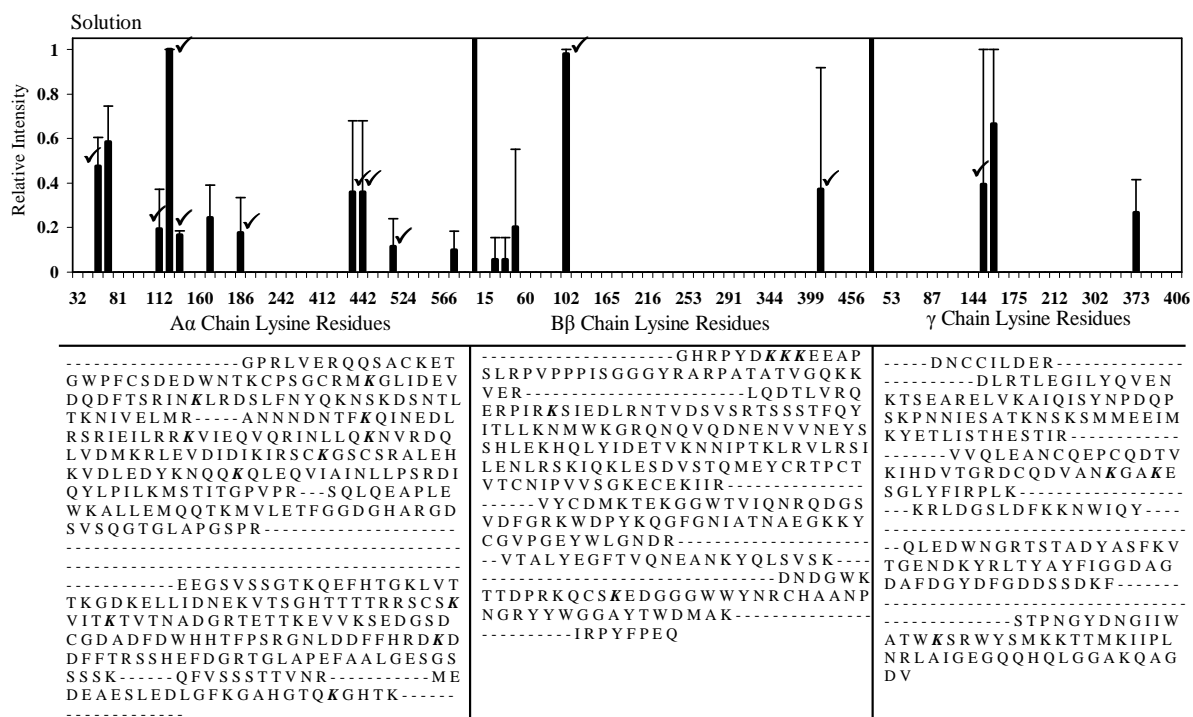


Figure 2.7: Normalized MALDI-TOF spectral peaks corresponding to biotinylated lysine residues within bFg α , β , and γ chains, labeled while in a 0.5 mg/mL solution. A cumulative sum of the intensities of all the labeled peptides that contained the listed lysine residues was determined, normalized relative to the highest intensity obtained, and averaged across three separate experiments. Error bars represent one standard deviation. Peaks that were also found to be labeled by the more accurate LC-ESI-MS/MS sequence analysis are marked with a (✓). The MALDI-TOF sequence coverages for each chain are displayed below each graph. Labeled lysine locations are in italics.

The lysine residues that were labeled after bFg was adsorbed onto PET from 1, 0.5, and 0.1 mg/mL solutions are displayed in Figure 2.8. The exposure of lysine residues was higher for the 0.5 mg/mL and 0.1 mg/mL samples when compared to the 1 mg/mL samples. Both the degree of label incorporation and the surface coverage of the MALDI-TOF spectra increased after adsorption onto PET (Table 2.4). A statistical comparison between solution-labeled and the 1 mg/mL surface-labeled samples revealed a significant decrease in the relative intensity of A α 128 and a significant increase in exposure of A α 438 and A α 442 following adsorption. Several biotin-labeled locations found for the 1 mg/mL surface sample were within the sequence coverage of the solution-labeled samples, yet were not found labeled in solution. Overall, 7 labeled lysines were found in the A α chain only in the adsorbed protein, along with 10 in the B β chain, and 9 in the γ chain. Two of these residues were B β 60, which is located within a heparin/cadherin binding domain, and γ 196, which is located within a MAC-1 binding motif.

After adsorption from 0.5 mg/mL solutions, there were 17 biotinylated locations each in the A α and γ chains and 21 locations in the B β chain that were within the sequence coverage of the solution samples, but were not labeled while in solution. When the 0.5 mg/mL samples were compared to the solution samples, statistically significant decreases in intensity were found for A α 55, A α 71, A α 128 and A α 165, while A α 141 increased in intensity. In addition to B β 60 and γ 196, a multitude of previously inaccessible lysine residues were found labeled, including γ 380, γ 381, γ 385, and γ 406 which all contained binding motifs essential for platelet adhesion.

For adsorption from 0.1 mg/mL solutions, statistically significant decreases in lysine exposure were seen for A α 71, and A α 128, and an increase in ranked intensity was observed for A α 141. As seen in the 0.5 mg/mL samples, previously inaccessible locations were



Figure 2.8: Normalized MALDI-TOF spectral peak intensities of lysine residues within bFg A α , B β , and γ chains that were biotinylated after adsorption to a PET surface from 1, 0.5 and 0.1 mg/mL solutions. Error bars represent one standard deviation. Locations that were labeled both in solution and after adsorption to a PET surface are represented by grey bars. Locations that were labeled only after adsorption to a PET surface are represented by black bars. Pairwise Mann-Whitney comparisons were used to determine statistically significant differences in intensity (p -value <0.05) between solution-labeled samples and surface-labeled samples (*) and between the high concentration (1 mg/mL) surface-labeled samples and the low concentration (0.5 mg/mL, 0.1 mg/mL) surface-labeled samples (†).

Table 2.4: Sequence coverage and percentage of labeled lysines observed after MALDI-TOF analysis of tryptic bFg peptides. Peptides originated from bFg that was labeled with Sulfo-NHS-LC-Biotin while in solution or after adsorption onto PET from different solution concentrations.

| | Sequence Coverage | Lysines Labeled in A α Chain | Lysines Labeled in B β Chain | Lysines Labeled in γ Chain |
|-----------|-------------------|-------------------------------------|------------------------------------|-----------------------------------|
| Solution | 66% | 28% | 13% | 10% |
| 1 mg/mL | 74% | 51% | 39% | 53% |
| 0.5 mg/mL | 89% | 77% | 92% | 93% |
| 0.1 mg/mL | 84% | 69% | 84% | 50% |

labeled in all three chains, with notable exposures of γ 380, γ 381, and γ 385. Increased labeling in the $A\alpha$ chain was mainly localized at the carboxyl terminus, while residues throughout the $B\beta$ chain increased in exposure. Within these locations, a total of 12 residues in the $A\alpha$ chain, 18 in the $B\beta$ chain, and 9 in the γ chain were found to have reacted with biotin exclusively in the surface-labeled samples.

Protein visualization software was utilized to display the three-dimensional locations of biotinylation sites (Figure 2.9). Lysines labeled while in solution were found primarily within the coiled coils of the $A\alpha$ chain and the globular domains of the $B\beta$ and γ chains. Several locations in the α C domain and in the coiled coil regions of the $B\beta$ chain were biotin labeled as well, but these residues were not present in the bFg crystal structure. After adsorption, lysines throughout both the globular and coiled regions of the $B\beta$ and γ chains were labeled, including several locations within the protein interior that are not normally solution-exposed.

2.4.7 Quantification of Complement C3, α_2 -Macroglobulin, and Fibrinogen

To test the quantitative ability of our SILT-MS technique, we cultured HepG2 cells in lysine-free, serum free-media to which we added either carbon-13 labeled lysine or standard carbon-12 lysine. The initial protocol used HepG2 media consisting of lysine-free DMEM containing 10% FCS, 1 μ M all-trans retinoic acid, and 105 μ g/mL. $^{13}\text{C}_6, ^{15}\text{N}_2$ -fibrinogen expression was unaffected under these culture conditions and was improved by the addition of aprotinin to the culture media. ELISA results demonstrated $^{13}\text{C}_6, ^{15}\text{N}_2$ -fibrinogen concentrations after two days of incubation during which cells typically grew

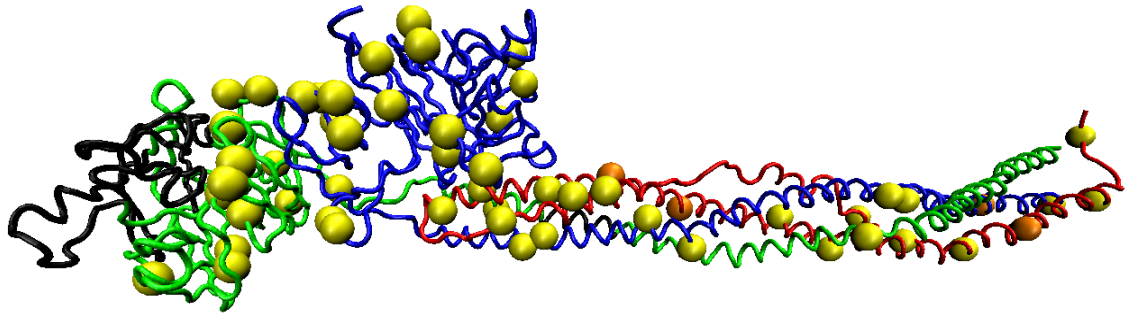


Figure 2.9: 3D image of bFg displaying the locations of labeled lysines after adsorption to a PET surface from a 0.1 mg/mL solution. The image is labeled as follows: A α chain, red; B β chain, blue; γ chain, green; residues not included in sequence coverage, black; labeled lysine residues, yellow spheres; lysine residues with statistically significant changes in relative intensity after adsorption to PET surface, orange spheres. Image was generated using the bFg PDB file 1DEQ and Visual Molecular Dynamics version 1.8.3.

from 50-75% confluency to be 0.8 +/- 0.6 ug/mL, 5.1 +/- 3.1 ug/mL, and 10.8 +/- 7.5 ug/mL respectively for lysine-free MEM with 10% FCS, serum free media with all-trans retinoic acid, and serum free media with all-trans retinoic acid and aprotinin. These levels of $^{13}\text{C}_6$, $^{15}\text{N}_2$ -fibrinogen were too low for SDS-PAGE isolation, and fibrinogen was thus immunoprecipitated with CNBr sepharose beads with conjugated anti-human fibrinogen IgG.

Complement C3 and α_2 -macroglobulin were expressed at much higher levels than fibrinogen and were purified solely through SDS-PAGE. This allowed concentrated stocks of media to be directly stored and to serve as internal standards for these proteins. $^{13}\text{C}_6$, $^{15}\text{N}_2$ -fibrinogen stored in the nonreducing SDS-PAGE buffer used for elution from CNBr resin served as the labeled fibrinogen stocks. Bands corresponding to $^{13}\text{C}_6$, $^{15}\text{N}_2$ -lysine-labeled and unlabeled complement C3 and α_2 -macroglobulin were excised from SDS-PAGE gels after separation from other media proteins under reducing conditions (Fig 10). Fibrinogen bands were excised after separation under nonreducing conditions, which allowed better purification from small amounts of IgG that coeluted from the CNBr resin (Fig 11).

The protocol for quantifying proteins using isopically labeled HepG2 protein internal standards is outlined in Figure 2.12. For quantification of complement C3 and α_2 -macroglobulin, small aliquots of labeled and unlabeled stocks were mixed at various ratios and separated using SDS-PAGE. Quantification via fibrinogen internal standards was tested by adding known amounts of unlabeled commercially available fibrinogen to aliquots of the $^{13}\text{C}_6$, $^{15}\text{N}_2$ -fibrinogen stock prior to separation by SDS-PAGE. After LC-ESI-MS/MS analysis of excised and digested bands, $^{13}\text{C}_6$, $^{15}\text{N}_2$ -lysine-labeled and acetylated fibrinogen peptides corresponding to the fibrinogen gamma chain peptide were detectible (Figure 2.13 & 2.14). Standard curves for complement C3, α_2 -macroglobulin, and $^{13}\text{C}_6$, $^{15}\text{N}_2$ -fibrinogen

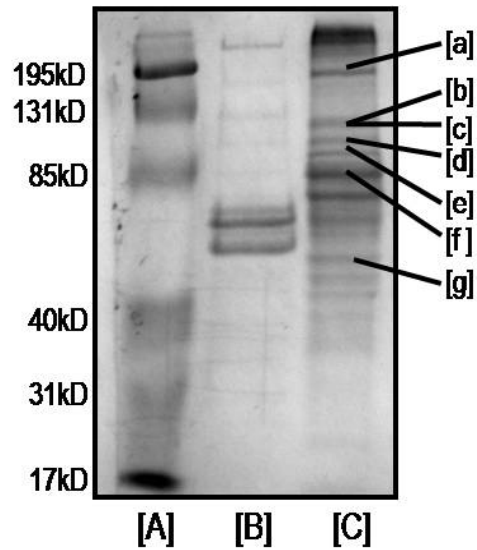


Figure 2.10: SDS-PAGE gel displaying proteins expressed by HepG2 cells grown in serum-free media. HepG2 cells were grown in lysine-free MEM supplemented with 10% dialyzed FCS and 1 μ M all-trans retinoic acid. After reaching 50%-60% confluency, the media was replaced with lysine-free MEM containing primary hepatocyte growth supplements (Lonza), 105 μ g/mL L-lysine- $^{13}\text{C}_6,^{15}\text{N}_2$ hydrochloride, 1 μ M all-trans retinoic acid, and 1 μ g/mL aprotinin. Media was collected every 2 days and concentrated with 10K MWCO centrifuge filters prior to protein separation with SDS-PAGE. Marked bands were analyzed for identity and carbon-13 incorporation using ion-trap mass spectrometry. [A] Molecular weight marker, [B] control containing 5 μ g of hFg under reducing conditions, [C] 10 μ g of HepG2 media proteins, [a] alpha-2 macroglobulin (100% labeled), [b] complement C3 (100% labeled), [c] inter-alpha-trypsin inhibitor (100% labeled), [d] bovine serum albumin (0% labeled), [e] heat shock protein hsp84 (100% labeled), [f] transferrin (0% labeled), [g] alpha-1-antitrypsin (100% labeled).

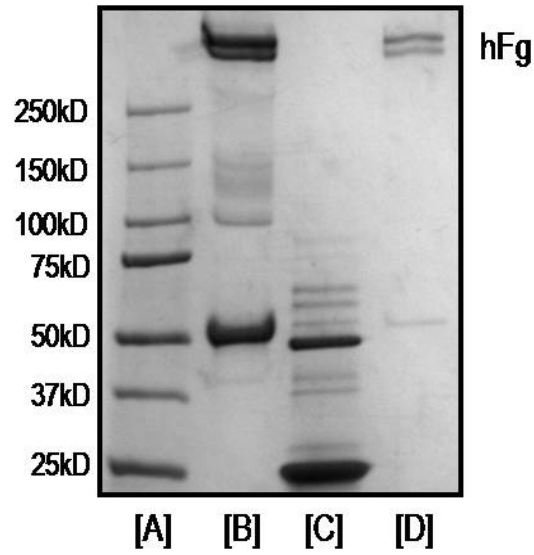


Figure 2.11: SDS-PAGE gel demonstrating the purification of carbon-13 labeled hFg from HepG2 media by immunoprecipitation. [A] Molecular weight marker, [B] control containing 5 ug each of hFg and bovine serum albumin under nonreducing conditions, [C] elution of hFg from CNBr IgG beads with SDS-PAGE sample buffer under reducing conditions, [D] elution of hFg from CNBr IgG beads with 5mM EDTA under nonreducing conditions.

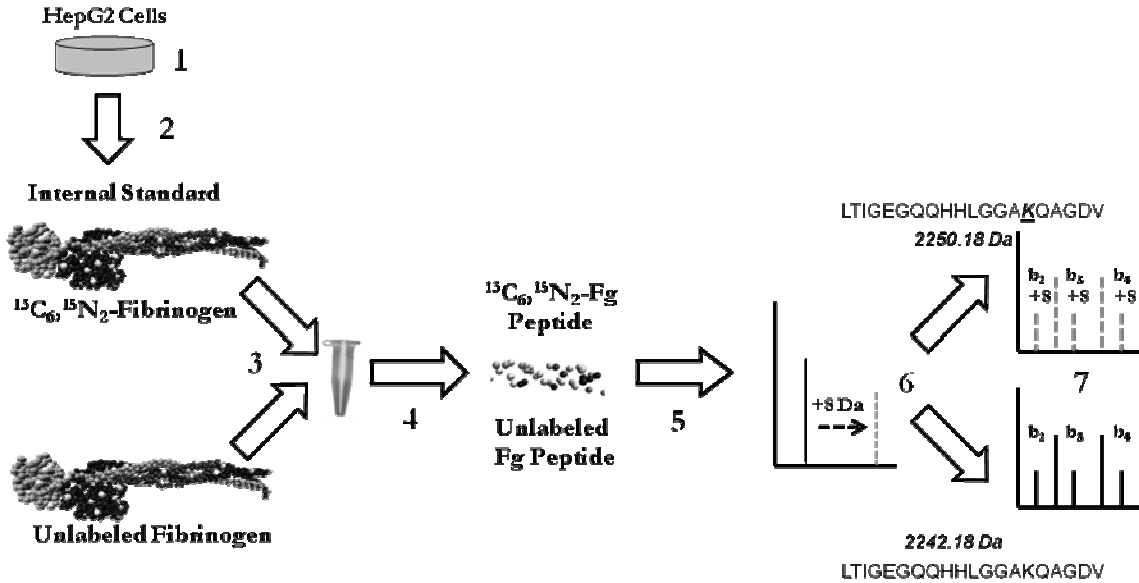


Figure 2.12: Workflow diagram for fibrinogen peptide quantification using $^{13}\text{C}_6, ^{15}\text{N}_2$ -labeled fibrinogen internal standards. Diagram is labeled as follows: (1) Culture of HepG2 cells in serum-free medium supplemented with L-lysine- $^{13}\text{C}_6, ^{15}\text{N}_2$ hydrochloride, all-trans retinoic acid, and aprotinin. (2) Immunoprecipitation, (3) Spiking of unlabeled fibrinogen sample with internal standard of known concentration, (4) SDS-PAGE and trypsin digestion of fibrinogen bands, (5) Liquid chromatography followed by mass spectrometry to generate parent ions, (6) Collision induced dissociation of selected peptides and corresponding $^{13}\text{C}_6, ^{15}\text{N}_2$ -labeled variants, (7) Analysis of tandem ions by SILT-MS for sequencing and quantification.

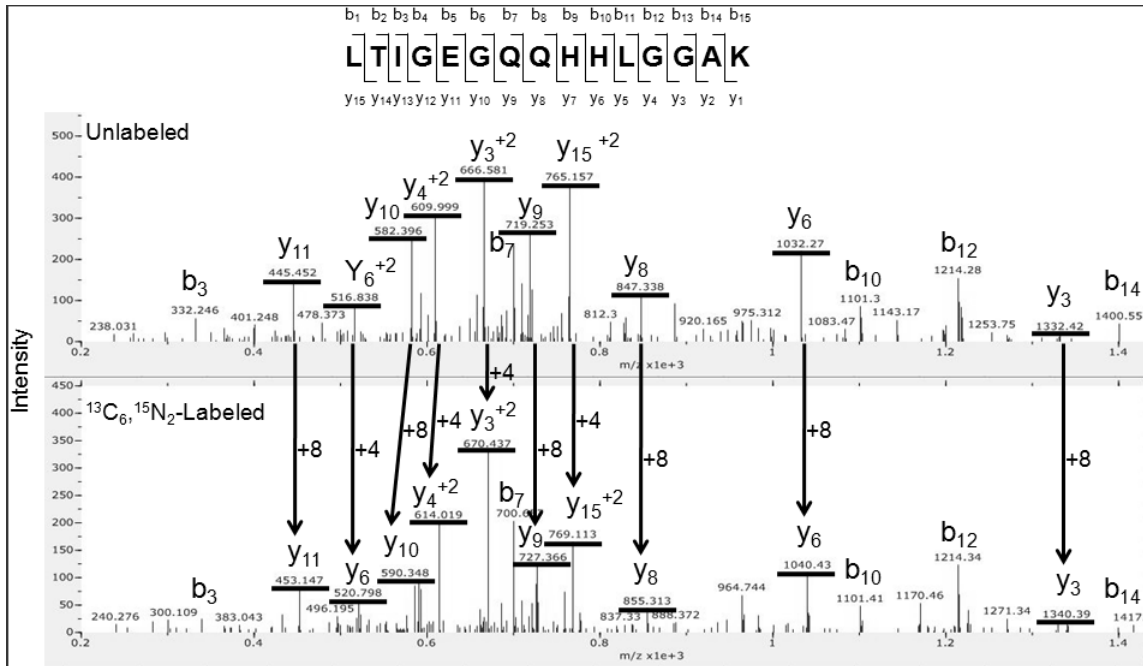


Figure 2.13: Tandem spectra of unlabeled (**top**) and $^{13}\text{C}_6, ^{15}\text{N}_2$ -labeled (**bottom**) fibrinogen gamma chain dodecapeptide. The amino-terminal amino acid of the fibrinogen dodecapeptide is a lysine, and thus all y-ions (underlined) of the peptide increased in mass by 8 amu. Doubly charged ions increased in mass by 4 amu. Arrows point from the unlabeled dodecapeptide y-ions the corresponding $^{13}\text{C}_6, ^{15}\text{N}_2$ -labeled dodecapeptide ions. Spectra was generated by the SILT-MS software package.

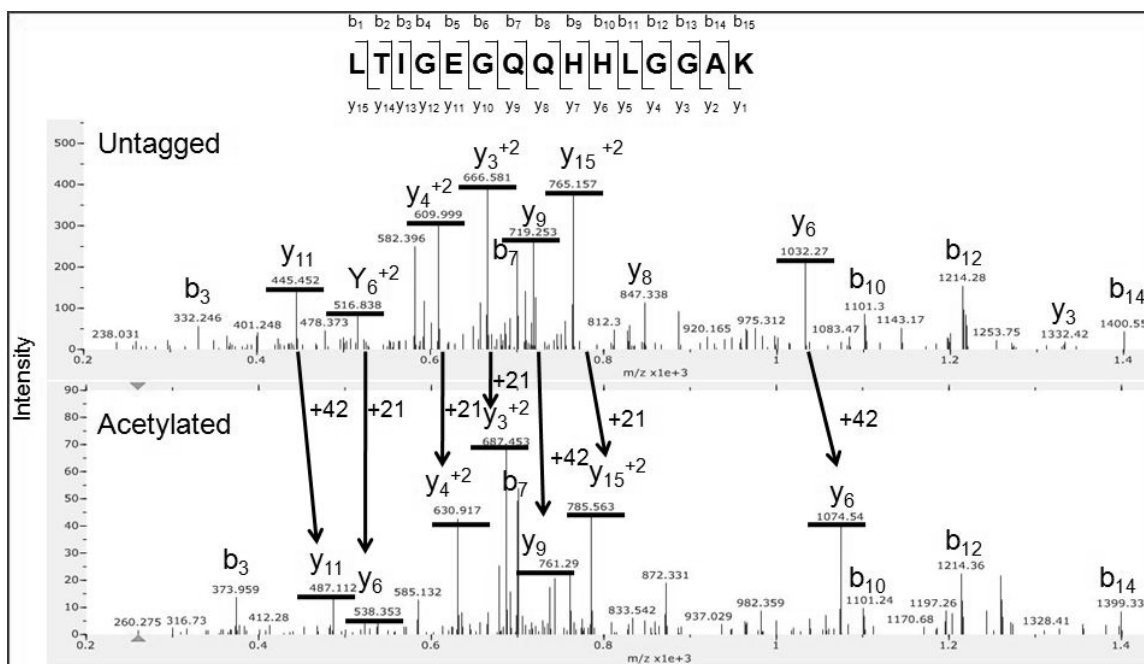


Figure 2.14: Tandem spectra of untagged (**top**) and acetylated (**bottom**) fibrinogen gamma chain dodecapeptide. The amino-terminal amino acid of the fibrinogen dodecapeptide is a lysine, and thus all y-ions (underlined) of the peptide increased in mass by 42 amu after reaction with sulfo-NHS-acetate. Doubly charged ions increased in mass by 21 amu. Arrows point from the untagged dodecapeptide y-ions to the corresponding acetylated dodecapeptide ions. Spectra was generated by the SILT-MS software package.

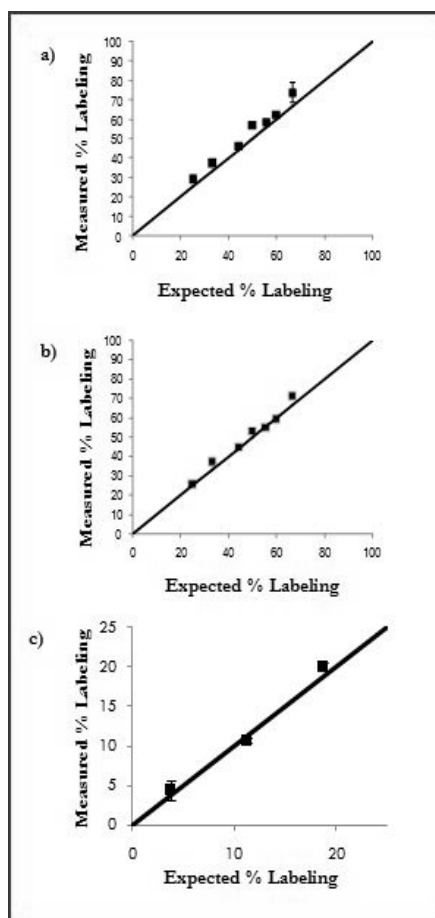


Figure 2.15: Standard curves for isotopically labeled HepG2 proteins generated using SILT-MS. An experimental protocol similar to SILAC was followed using proteins secreted by HepG2 cells, mixing a $^{13}\text{C}_6,^{15}\text{N}_2$ -labeled protein with an unlabeled protein in different ratios. Complement C3 (a) and alpha-2 macroglobulin (b) are secreted in large amounts by HepG2 cells and are readily purified using SDS-PAGE alone. Fibrinogen (c) was purified by immunoprecipitation. HepG2 cells were incubated with unlabeled medium or medium containing $^{13}\text{C}_6,^{15}\text{N}_2$ -lysine. Cell lysates were mixed and purified by SDS-PAGE. $^{13}\text{C}_6,^{15}\text{N}_2$ -fibrinogen was mixed with unlabeled commercially available fibrinogen at different ratios prior to SDS-PAGE. The bands were excised and analyzed by data dependent mass spectrometry. Error bars (standard deviations) are present on all datapoints, with $n = 3$.

were generated by comparing the known ratios of labeled and unlabeled protein with the measured ratios as determined by the SILT-MS software (Figure 2.15) (Elbert, Mawuenyega et al. 2008). Relative errors ranged from 2.9%- 9.5%, and the linear fit of the standard curve had a slope of 0.988 and an R^2 value of 0.986.

2.5 Discussion

Conformational changes can occur in proteins after adsorption to biomaterial surfaces. These changes can influence protein surface coverage with time and expose binding sites that are responsible for eliciting biological responses (Zucker and Vroman 1969; Mohammad, Hardison et al. 1974; Kottke-Marchant, Anderson et al. 1987; Anderson, Bonfield et al. 1990; Shen and Horbett 2001). Since fibrinogen adsorbed on biomaterials directs numerous cellular and thrombotic responses (Weisel 2005), a better understanding of fibrinogen conformational changes at the molecular level may provide information useful in the development of devices with enhanced biocompatibility. We are developing methods to allow a more complete analysis of the fibrinogen structure-function relationship at solid/liquid interfaces by using mass spectrometric mapping to probe changes in the exposure of individual residues. These methods may be beneficial for studying conformation changes in proteins adsorbed from complex mixtures, such as blood or plasma.

Prior to performing the chemical labeling experiments, we used optical waveguide lightmode spectroscopy (OWLS) to measure the extent of bFg spreading on PET as a function of solution protein concentration. OWLS has the ability to measure the surface density of protein layers *in situ* with a 30 s time-step, which permits the determination of parameters in kinetic models of molecular interactions with surfaces (Ramsden 1993; Voros,

Ramsden et al. 2002). Since our interest lies in the interactions of proteins at the solid/liquid interface between blood and biomaterial surfaces, we modified the surfaces of OWLS waveguide chips by spin coating to study the frequently used biomaterial PET.

OWLS results for bFg adsorbed onto PET demonstrated the post-adsorptive spreading of the protein in a concentration-dependent manner, consistent with previous results on other surfaces (Ramsden 1993; Wertz and Santore 1999). During protein adsorption, the rate of protein unfolding appears to be on the order of the time required to approach the RSA jamming limit on surfaces (Ramsden 1993). Proteins thus will not have adequate time to reach their maximum spread area when adsorbed from highly-concentrated solutions, due to the filling of adjacent spaces required for major conformational changes (Schaaf and Talbot 1989). Statistical analysis of OWLS results showed that the 0.5 and 0.1 mg/mL samples were not different from each other, while both were significantly different from the 1 mg/mL samples. The RSA model does not account for the kinetics of spreading, diffusion or hydrodynamic effects on the adsorption process. However, diffusion and hydrodynamic influences have been shown to be counteractive (Bafaluy, Senger et al. 1993). A model that incorporates multiple states of protein denaturation may improve the measurement of protein unfolding kinetics on surfaces, but would require the curve-fitting of additional parameters to the OWLS surface density measurements, which may introduce additional inaccuracies.

Atomic force microscopy (AFM) has previously provided a detailed picture of fibrinogen's post-adsorptive conformations. We compared our OWLS results with published AFM experiments, estimating fibrinogen m/a values from reported volume measurements (Sit and Marchant 1999) (Table 2.2). The m/a estimates were calculated based on dimensions of fibrinogen obtained by Sit et al, who used AFM to study the structure of

fibrinogen adsorbed onto hydrophobic (octadecyltrichlorosilane, OTS), negatively charged (mica), and positively charged (3-aminopropyltriethoxysilane, APTES) surfaces. Their results were obtained under experimental conditions that differed from ours, allowing spreading to occur only over a 1 h period, while our studies allowed 4 h of spreading. We monitored adsorption only on PET, a surface with a higher surface energy than OTS and lower surface energy than mica and APTES (Baier, Shafrin et al. 1968). Moreover, Sit et al. used a much lower fibrinogen concentration (50 ng/mL), so that the jamming limit would not be reached. The OTS surface resulted in a lower m/a in the AFM experiments than the PET used in our OWLS experiments, which was expected due to the higher surface energy of PET and the more concentrated fibrinogen solutions that we tested. PET in the presence of 0.5 and 0.1 mg/mL fibrinogen solutions showed larger spread areas than the hydrophilic mica surfaces exposed to a 50 ng/mL bulk concentration. Wertz et al. showed that the majority of post-adsorptive conformational changes occurred within the first 15 minutes after adsorption (Wertz and Santore 1999), and thus the measurements of Sit et al. may represent the maximum obtainable surface coverage for individual fibrinogen molecules on the surfaces tested. Assuming that bFg has a rod-shaped geometry with dimensions of 6.0 x 6.0 x 45 nm, the theoretical unspread end-on and side-on close packing densities for adsorbed bFg at complete surface coverage are 1.57 and 0.21 $\mu\text{g}/\text{cm}^2$ (Lassen and Malmsten 1996). Thus, even at the highest concentration tested, bFg adsorption levels were in the vicinity of a side-on molecular packing arrangement. These adsorption densities were even lower than the 0.4 – 0.5 $\mu\text{g}/\text{cm}^2$ achieved on low energy methylated surfaces (Wojciechowski and Brash 1993; Malmsten 1994; Lassen and Malmsten 1996), which may reflect extensive spreading of fibrinogen on the PET surface.

Our OWLS experiments revealed increases in the average area per bFg molecule as the solution concentration decreased from 1 mg/mL to 0.1 mg/mL, indicating that different degrees of conformational change occurred between these concentrations. By proteomic methods, we were then able to determine the specific residues within bFg that were susceptible to biotinylation after adsorption to the surfaces of PET particles. These small PET particles were fabricated with high surface areas using emulsion chemistry to increase the amount of adsorbed protein for the labeling experiments. Our hypothesis was that if a predisposition existed for certain biologically active domains within bFg to be exposed upon adsorption, then lysine residues found near these sites would have a higher tendency to react with the chemical label and could be detected by changes in MALDI-TOF peak intensities. Based on the OWLS results, we expected to observe differences in labeling between higher concentration, 1 mg/mL, and lower concentration, 0.5 and 0.1 mg/mL, samples. While only a few statistically significant changes in intensities were found, large differences in the number of biotin labeled lysines were observed. These qualitative results suggest that conformational changes influenced by the energetically more favorable interactions of hydrophilic residues with the solution over the PET surface may be driving the exposure of biologically active motifs. This is evidenced by the drastic increase in accessibility of lysines within the highly interspecies conserved γ chain, which coincides with the exposure of several cell interaction motifs essential to thrombosis and inflammation. Overall, our results are consistent with previous experiments examining the interactions of proteins with low energy surfaces, but at a higher level of resolution and revealing additional complexity.

Although SDS-PAGE showed equivalent increases in molecular weight between solution-labeled and surface-labeled samples, mass spectrometric analysis may have revealed considerable differences in the *distribution* of the label throughout the bFg molecule.

MALDI-TOF has a strong bias for higher concentration peptides (Knochenmuss, Stortelder et al. 2000), and, consequently, many solution-labeled peptides originating from sterically-hindered locations may have been overshadowed by highly labeled locations. However, the non-linear nature of MALDI-TOF intensity may have amplified the differences in labeling between solution and surface biotinylated samples. LC-ESI-MS/MS demonstrated the presence of several labeled peptides that were never detected in the MALDI-TOF spectra of solution-labeled samples. More quantitative mass spectrometric methods will be required to definitively show that such differences between surface and solution labeled fibrinogen exist.

Increases in lysine exposure within the A α chain appeared to occur most prominently in the α C domain. Previous immunochemical studies of the human fibrinogen A α chain performed by Cierniewski et al. revealed that in solution, the majority of the immunogenic surface resided between A α 1-238, with moderate immunogenicity between 239-476 and minimal antibody binding at the C-terminus between A α 518-584 (Cierniewski, Plow et al. 1984). Since the inaccessible areas of the α C domain were readily bound by antibody after plasmin cleavage, they concluded that this region was integrated into the native fibrinogen molecule in a manner that influenced epitope exposure. Mass spectrometric mapping of the bFg A α chain displayed similar distributions of accessibility to the biotin label. Of the 11 lysines biotinylated to a high degree in the A α chain, only one location was found labeled near the carboxyl terminus in the solution-labeled samples. The surface-labeled samples showed that post-adsorptive conformational changes readily exposed these minimally accessible carboxyl-terminal domains, possibly due to decreased interaction between the α C domain and the E domain.

Binding of an antibody that recognizes human A α 572-575 has been correlated with platelet adhesion to adsorbed human fibrinogen (Tsai and Horbett 1999). A region within

the bFg α C domain containing an RGGS site ($A\alpha$ 541-544) has high sequence homology with a region in the human fibrinogen sequence that contains an RGDS motif ($A\alpha$ 572-575). A lysine ($A\alpha$ 549) near this site was shown to increase in exposure after adsorption to PET from the lower concentration solutions. Similarly, a lysine ($A\alpha$ 103) in close proximity to the $A\alpha$ 98-101 RGDF site in the bovine fibrinogen, which is synonymous to RGDF $A\alpha$ 95-98 in human fibrinogen, was found to increase in exposure upon adsorption to PET as the solution concentration decreased. While biotinylated $A\alpha$ 103 was detected in the LC-ESI-MS/MS analysis of solution-labeled samples, $A\alpha$ 549 was only found to be biotinylated in the surface-labeled samples by MALDI-TOF.

Although similar percentages of labeled lysines was found in the γ chain when comparing the high concentration and low concentration adsorption experiments (Table 2.4), the labeling in the low concentration samples shifted towards the carboxyl terminus. In the 0.5 and the 0.1 mg/mL samples, residues were labeled within the sequence γ 370-383, which has been shown to have an essential role in platelet adhesion (Podolnikova, Yakubenko et al. 2003). Sites located in the γ 377-395 sequence, thought to bind the $\alpha_M\beta_2$ /Mac-1 leukocyte integrin and participate in inflammation, were also found labeled (Flick, Du et al. 2004). LC-ESI-MS/MS analysis revealed that γ 406 within the platelet adhesion dodecapeptide (400-411) was accessible while in solution. This lysine was not found labeled in MALDI-TOF analysis of solution samples nor the 1 and 0.1 mg/mL surface-labeled samples. However, this residue was detected as labeled after adsorption to PET from the 0.5 mg/mL solutions (Bennett 2001). These results suggest that the peptide containing this lysine either does not ionize well in MALDI-TOF or is present at very low amounts.

It has been shown that nonactivated platelets bind less to human fibrinogen fragments containing only γ 400-411, only $A\alpha$ 95-98, or without $A\alpha$ 572-575 (Savage and Ruggeri 1991). These previous findings are supported by our data that suggest a post-adsorptive exposure of the locations in bFg that are synonymous to these platelet binding human fibrinogen sites. Furthermore, a lysine near the bovine complement to $A\alpha$ 572-575 in human fibrinogen was only found exposed after adsorption, while a lysine near the bovine complement to $A\alpha$ 95-98 in human fibrinogen was accessible both in solution and on the surface. Thus our data also supports previously performed experiments that suggest that $A\alpha$ 572-575 may be more specific to post-adsorptive platelet binding than $A\alpha$ 95-98.

MALDI-TOF was selected for our initial mass spectrometric mapping experiments because of the quickness and ease of sample preparation and analysis. Unlike MALDI-TOF, more sensitive electrospray ion-trap and Fourier transform mass spectrometry can take advantage of quantitative techniques such as SILAC or ITRAQ, as well as provide more reliable peptide identification by MS². With mass spectrometry coupled to liquid chromatography, adsorption from multicomponent protein solutions or even whole blood could potentially be analyzed, which would have novel applications in the study of post-adsorptive processes such as the Vroman effect (Vroman and Adams 1969; Slack and Horbett 1989). Since the majority of the highest concentration plasma proteins are produced in the liver, we developed a metabolic labeling strategy to express ¹³C₆, ¹⁵N₂-lysine-labeled fibrinogen from HepG2 cells. HepG2 cells express a variety of proteins other than fibrinogen that participate in coagulation and innate immunity, including α ₂-macroglobulin, fibronectin, and complement C3 (Knowles, Howe et al. 1980; Borth 1992). We thought that it would be advantageous to use proteomic methods to isolate these proteins as well, without

the need for immunoprecipitation. Thus we developed a protocol for culturing HepG2 cells in serum-free media to minimize albumin interference during protein purification.

SILAC-based strategies typically quantify protein by comparing the ratios of the parent ions of isotopically labeled and unlabeled protein (Ong, Blagoev et al. 2002). Experiments are simultaneously performed on cells cultured in media with and without isotopically labeled amino acids and specific proteins are immunoprecipitated from each culture for comparison. Here, we have demonstrated that stocks of internal standards can be stored and utilized for the repeated and accurate quantification of multiple proteins within individual samples purified either with immunoprecipitation or SDS-PAGE. From a multicomponent protein sample, we were able to excise and quantify individual protein brands containing less than 1 μg of protein after separation by electrophoresis. Considering the microgram levels of protein that were eluted previously from the PET beads, this method may be quite useful in the quantification of proteins within adsorbed protein layers. The SILT-MS software also permitted the identification of acetylated locations within the gamma chain dodecapeptide of fibrinogen, suggesting that this method may also be useful to probe the exposure of fibrinogen cell-adhesion motifs.

2.5 Conclusion

In summary, we have applied OWLS and mass spectrometric mapping in the study of proteins at solid/liquid interfaces. We have shown that OWLS waveguide chips can be coated with PET and that substantial differences in protein spread area are found between bFg adsorbed at 1 and 0.1 mg/mL. Using chemical labeling and proteomic methods, we compared the differences in exposure of lysines between bFg in solution and bFg adsorbed to PET. Our results suggested extensive

conformational changes in all three chains and specific increases in the exposure of biologically relevant residues in the A α and γ chains during the unfolding process on PET.

Based on these results, we pursued a more quantitative adaptation of this methodology by expressing isotopically labeled fibrinogen from HepG2 cells. The inclusion of aprotinin and all-trans retinoic acid was found to more than double fibrinogen expression. While immunoprecipitation was still required to purify labeled fibrinogen internal standards, the HepG2 media itself proved to be a suitable stock of internal standards for quantification of both complement C3 and α_2 -macroglobulin. The SILT-MS software package was able to both identify the locations of the $^{13}\text{C}_6$, $^{15}\text{N}_2$ -lysine-labels as well as sites of acetylation within proteins. Together, these results suggest that with further development, it may be possible to simultaneously monitor the conformation and abundance of individual proteins within adsorbed protein layers on material surfaces.

CHAPTER 3[†]

Protein Adsorption and Cell Adhesion on Nanoscale Bioactive Coatings Formed from Poly(Ethylene Glycol) and Albumin Microgels

3.1 Abstract

Late-term thrombosis on drug-eluting stents is an emerging problem that might be addressed using extremely thin, biologically-active hydrogel coatings. We report a dip-coating strategy to covalently link poly(ethylene glycol) (PEG) to substrates, producing coatings with ≈ 100 nm thickness. Gelation of PEG-octavinylsulfone with amines in either bovine serum albumin (BSA) or PEG-octaamine was monitored by dynamic light scattering (DLS), revealing the presence of microgels before macrogelation. NMR suggested extremely high end-group conversions prior to macrogelation, which was supported by gel permeation chromatography (GPC) results that revealed that only 12% of the monomer remained unreacted after approximately 90% of the gelation time had passed. Before macrogelation, the reacting solutions were diluted and incubated with nucleophile-functionalized surfaces. Using optical waveguide lightmode spectroscopy (OWLS) and quartz crystal microbalance with dissipation (QCM-D), we identified a highly hydrated, protein-resistant layer with a thickness of approximately 75 nm. Atomic force microscopy in buffered water revealed the presence of coalesced spheres of various sizes but with diameters less than about 100 nm. Microgel-coated glass or poly(ethylene terephthalate) exhibited reduced protein adsorption

[†] Chapter 3 has been adapted from the following published manuscript:
Scott EA, Nichols MD, Cordova LH, George BJ, Jun YS, Elbert DL. Protein adsorption and cell adhesion on nanoscale bioactive coatings formed from poly(ethylene glycol) and albumin microgels. *Biomaterials*. 2008 Dec;29(34):4481-93.

and cell adhesion. Cellular interactions with the surface could be controlled by using different proteins to cap unreacted vinylsulfone groups within the coating.

3.2 Introduction

Thin hydrogel coatings may prove to be useful for reducing coagulation and thrombosis on blood-contacting devices with complex geometries, such as endovascular stents. However, the density of poly(ethylene glycol) (PEG) in the coating must be quite high to achieve a substantial reduction in protein adsorption (Jeon, Lee et al. 1991; Elbert and Hubbell 1996). We have found that single layers or even multiple layers of PEG coated on a surface do not provide the required cell adhesion resistance for long-term effectiveness (Kim, Wacker et al. 2007). This suggested to us that the use of relatively large aggregates containing high densities of PEG to form the thin coatings may ensure adequate surface coverage even with a limited number of attachment sites on the material.

Microgels have been used extensively to produce or enhance surface coatings (e.g. latex paints) (Funke, Okay et al. 1998). The definition of microgel by IUPAC has evolved from “a network of microscopic dimensions”(Metanomski 1991) to the more recent recommendation: “particle of gel of any shape with an equivalent diameter of approximately 0.1 to 100 μm ” (Aleman, Chadwick et al. 2007). ‘Nanogel’ is now “a gel with an equivalent diameter in the range of 1-100 nm”. For simplicity, microgel will herein refer to both the nano- and microscale regimes. Microgels can be readily produced by emulsion polymerization, in which macrogel formation is hindered by the segregation of initiator, monomer and/or polymer in the heterogeneous solution (Smith and Ewart 1948; Baker 1949; Funke, Okay et al. 1998). However, many examples exist in which microgels form in homogenous solutions. For example, polymerization of N-isopropylacrylamide in water at

high temperatures leads to microgel formation due to precipitation (Gan and Lyon 2002; Nolan, Reyes et al. 2005; Singh, Bridges et al. 2007). Other examples exist where microgels form during polymerization, likely due to steric or electrostatic stabilization rather than precipitation (Graham and Mao 1996; Graham, Mao et al. 1996; Graham and Cameron 1998; de Groot, Zurutuza et al. 2001). By manipulating solvent quality, some systems can produce stable microgels without gelation even after complete reaction of end-groups (Graham and Cameron 1998).

Using PEG-octavinylsulfone (PEG-OVS) and either bovine serum albumin (BSA) or PEG-octaamine (PEG-OA) as crosslinkers, we found evidence for substantial microgel formation before macrogelation. The reaction between amines and vinylsulfones is somewhat sluggish, allowing us to maintain a well-mixed system with reproducible sizes of microgels observed by dynamic light scattering (DLS). The crosslinking reaction could be further slowed by dilution or freezing. Taking advantage of the higher reactivity of vinylsulfones with thiols, the crosslinking-solutions containing PEG microgels could be reacted with thiol-functionalized surfaces without macrogelation. Optical waveguide lightmode spectroscopy (OWLS) and quartz crystal microbalance with dissipation (QCM-D) measurements demonstrated the presence of thin hydrogel layers that were extremely resistant to fibrinogen adsorption. A single incubation of the surface with a microgel solution reduced non-specific cell adhesion to an extent that was much greater than 20 layers of PEG applied via a covalent layer-by-layer method (Kim, Wacker et al. 2007). Overall, the resistance to cell adhesion indicates that partially crosslinked multi-arm PEG may be useful in producing thin, but dense, PEG films on a variety of surfaces.

3.3 Materials and Methods

3.3.1 Synthesis of Poly(ethylene glycol) Vinylsulfone

Poly(ethylene glycol) vinylsulfone (PEG-OVS) was synthesized from PEG-OH using a variation of a previously described synthesis (Morpurgo, Veronese et al. 1996). The four-step synthesis began with the preparation of a PEG mesylate. A 10% (w/v) solution of 8-arm PEG MW 10,000 was obtained in toluene. The solution was dried by azeotropic distillation and after cooling to room temperature, dichloromethane was added to 20% (v/v). Methane sulfonyl chloride (4 equiv.) and triethylamine (4 equiv.) were added after cooling in an ice bath while stirring. After 24 hours, the cloudy white product was filtered using a vacuum flask and filter paper to remove the almost completely clear and transparent PEG solution from the solid salt byproduct. The solution volume was then reduced to approximately 20 ml with a roto-evaporator and the polymer was precipitated with the addition of dry diethyl ether after cooling to near 0°C. The final PEG mesylate product was dried overnight *in vacuo*. The mesylate was then dissolved at 10% (w/v) in deionized (DI) water after which 1M NaOH solution (4 equiv.) and β -mercaptoethanol (4 equiv.) were added. The reaction was carried out at reflux for 3 hours while stirring. The product was cooled in an ice bath and extracted twice with dichloromethane and dried over anhydrous sodium sulfate. The sodium sulfate was removed by filtration and the polymer solution was reduced to 20 ml with a rotoevaporator. The PEG was precipitated with the addition of dry diethyl ether after cooling to near 0°C. The final PEG hydroxyethyl sulfide product was dried overnight *in vacuo*. The hydroxyethyl sulfone was completely dissolved at 25% (w/v) in 0.123 M sodium tungstate in distilled water. The solution was cooled to 0°C in an ice bath and 30% hydrogen peroxide (2 equiv.) was added. The reaction continued overnight while stirring, and the product was extracted twice with dichloromethane. After drying over

anhydrous sodium sulfate, the solution was filtered and reduced to 20 ml with a rotoevaporator. The PEG was precipitated with the addition of dry diethyl ether after cooling to near 0°C. The final PEG hydroxyethyl sulfone product was dried overnight *in vacuo*. The hydroxyethyl sulfone was dissolved at 10% (w/v) in toluene and dried through azeotropic distillation. After cooling, dichloromethane was added to 20% (v/v) mesyl chloride (1.5 equiv.) and triethylamine (3 equiv.) were added. The reaction was carried out overnight in an ice bath after which mesyl chloride (1.5 equiv.) and triethylamine (3 equiv.) were again added. After another 24 hours, the solution was filtered and reduced to 20 ml with a rotoevaporator. The PEG was precipitated with the addition of dry diethyl ether after cooling to near 0°C. The final PEG vinylsulfone product was dried overnight *in vacuo*. Before NMR analysis was performed, the product was purified twice by dissolving in dichloromethane followed by filtration and precipitation with diethyl ether. The final product was recovered at 30% with an overall PEG-OVS composition of 96%.

3.3.2 Microgel Syntheses

Unless otherwise noted, all reagents were purchased from Sigma Aldrich. PEG-octaamine (PEG-OA, 91% end-group conversion) were synthesized from 8-arm PEG-OH (mol wt 10,000, Shearwater Polymers, Huntsville, AL) as described previously (Elbert and Hubbell 2001; Wacker, Scott et al. 2006). PEG-OVS, PEG-OA, and bovine serum albumin (BSA) solutions were prepared at 200 mg/mL in phosphate buffered saline (PBS; 0.2 g/L KCl, 0.2 g/L KH₂PO₄, 8 g/L NaCl, 1.15 g/L anhydrous Na₂HPO₄, pH 7.4) and sterile filtered with 0.22 µm sterile syringe tip filters (Millipore). PEG-OVS/BSA or PEG-OVS/PEG-OA microgel solutions were formed through Michael-type conjugate addition reactions by respectively mixing PEG-OVS with either BSA or PEG-OA solutions at 0.4:1

or 1:1 ratios of amine to vinylsulfone groups. Ratios were prepared assuming that 8 moles of accessible functional groups per mole of PEG-OVS or PEG-OA were available and that bovine serum albumin had approximately 36 lysines sterically accessible for reaction (Wacker, Scott et al. 2006). Microgel solutions were maintained at 37°C and rotated at 40 RPM until the desired mean effective diameters were reached, as recorded by DLS.

3.3.3 Characterization of Microgel Formation

Mean effective hydrodynamic diameters (d_{PCS}) were determined by dynamic light scattering/photon correlation spectroscopy (DLS/PCS; 90Plus Particle Size Analyzer, Brookhaven Instruments, Holtsville, NY) at a scattering angle of 90° and wavelength of 658 nm. Disposable polystyrene cuvettes (Brookhaven Instruments) were cleaned 1x with 95% ethanol and 2x with DI water prior to use. Polymerizing samples (30 μL) were collected at regular intervals and diluted with PBS (3 mL) in cleaned cuvettes and analyzed at 25°C. Data presented represent the average results of 3 measurements for each microgel synthesis with acquisition times of 1 min. Calculation of d_{PCS} and statistical analysis of the results were performed using Brookhaven Instruments Particle Sizing Software (version 2.34, Brookhaven Instruments), which uses an intensity-weighted model assuming a log-normal distribution of particle sizes. We also used the software to calculate volume-weighted mean effective diameters.

Increases in BSA molecular weight over the time course of gelation was monitored with SDS-PAGE. BSA and PEG-OVS were mixed at amine to vinylsulfone ratios of 0.4:1 and aliquots (20 μg) were collected every hour and mixed with Laemmli sample buffer (0.01% bromophenol blue, 2% sodium dodecyl sulfate, 25% glycerol, 62.5 mM Tris-HCl, pH

6.8) and separated by gel electrophoresis using standard protocols. ImageJ software (NIH) was used to quantify the relative intensities of 66 kD unreacted BSA monomer bands stained with Coomassie Blue (Bio-Rad Laboratories, Inc.), which were in turn used to calculate the fraction of reacted BSA. 2nd-order kinetic analysis was performed to determine the rate of free BSA monomer consumption (Laidler 1987). Equation 2, valid for a 2nd order reaction, was evaluated and plotted against corresponding time points.

$$k_A t = \frac{1}{a_o - b_o} \ln \left[\frac{b_o(a_o - x)}{a_o(b_o - x)} \right] \quad [2]$$

Parameters a_o and b_o represent the initial concentrations of BSA and PEG-OVS, and x represents the amount of consumed BSA. A linear best-fit determined k_A from the slope, which is the rate of reaction for free BSA monomer.

Nuclear magnetic resonance spectroscopy (NMR) was used to determine the percentage of reacted vinylsulfone groups while PEG-OVS was crosslinked with PEG-OA. The PEG-OVS/PEG-OA microgels are well-suited for ¹H NMR analysis due to the simplicity of the signal from the PEG backbone. PEG-OVS and PEG-OA solutions (200 mg/mL) were prepared in 20 mM potassium phosphate in D₂O and mixed at a 1:1 (v/v) ratio. At various timepoints before gelation, samples of the microgel solution (10 mg of total polymer) were collected and dissolved in deuterated chloroform containing 0.71% N,N-dimethylformamide (DMF; used as an internal standard) prior to analysis on a 300 MHz Varian Mercury-300 NMR. Integrated vinylsulfone peaks at 6.27 ppm (d, 2H, =CH₂) and 6.16 ppm (d, 2H, =CH₂) were normalized against the integrated DMF peak at 7.76 ppm (s, 1H, -OCH) in each NMR spectra.

For gel permeation chromatography, PEG₈-VS was reacted with PEG₈-amine to a $d_{PCS} \cong 100$. The reaction was stopped by incubation with 2-mercaptoethanol for 1 h at 37°C

at a thiol:vinylsulfone ratio of 2:1. After reaction with 2-mercaptoethanol, the d_{PCS} was unchanged. GPC was performed by PolyAnalytik (London, ON, Canada) using a Viscotek Model 302-050 detector (detecting light scattering, viscosity and refractive index). Samples (0.5 mg PEG) were dissolved in 0.05 M sodium nitrate. Three columns were used in series (PolyAnalytik High Resolution Aqueous Columns: PAA-202.5, exclusion limit 10 kDa; PAA-203, exclusion limit 100 kDa; PAA-206M, exclusion limit 20 MDa) calibrated with poly(ethylene oxide) standards.

3.3.4 Reaction with Surfaces

Round glass coverslips (12 mm dia., Ted Pella Inc.) were functionalized with mercaptopropyltrimethoxysilane (MPTS) for covalent reaction with unreacted vinylsulfone groups in microgel solutions. Coverslips were cleaned by washing 3x in DI water and 3x in ethanol prior to oxygen-plasma etching, which was performed at 50% power for 10 min with a 40 kHz, 100 W plasma etcher (Diener Electronic, Femto model). The hydroxylated coverslips were then washed 3x in acetone and reacted for 1 h at 25°C with a 5% (v/v) solution of MPTS in acetone. Surfaces were washed 3x in acetone and cured for 1 h at 100°C under nitrogen. MPTS coverslips were incubated for 1 h with microgel solutions ($d_{\text{PCS}} = 100\text{-}120$ nm), washed 3x in PBS, and incubated overnight with PBS, BSA (50 mg/mL), or bovine fibrinogen (bFg, 2.5 mg/mL) at 37°C to respectively form uncapped, BSA-capped, or fibrinogen-capped microgel-coated surfaces.

Oxygen-plasma treated OWLS waveguide chips (MicroVacuum Ltd.) were vapor silanized with MPTS in preparation for covalent reaction with microgel solutions. After hydroxylation with oxygen plasma for 10 min at 50% power, the waveguide chips were placed on a polyethylene rack within a 100 mL Pyrex bottle attached to a Liebig condenser

(Figure 1). A 5% solution of MPTS in acetone was boiled at reflux for 24 h to provide a continuous silane vapor for reaction with the hydroxylated Si/Ti/O₂ waveguide chip surface. Silanized waveguide chips were cured for 20 min at 100°C under nitrogen, and PEG-OVS/BSA microgel coatings were applied to surfaces as described above for MPTS-silanized coverslips.

QCM-D crystals with silicon dioxide coatings (Q-Sense, QSX 303, Gothenburg, Sweden) were O₃-cleaned for 15 min in a homemade O₃ chamber and immersed in an initially-boiling solution of 5:1:1 DI water:ammonium hydroxide:hydrogen peroxide for 30 min while the solution cooled to remove organics from the substrate surfaces. Cleaned crystals were immediately silanized by placement into 5% (v/v) MPTS in acetone for 1 h at room temperature and subsequently baked at 100 °C for 1 h. Silanized crystals were stored under nitrogen until use, which was always within 24 h.

Poly(ethylene terephthalate) films (PET, 0.05 mm thick, McMaster Carr, Chicago, IL) were functionalized with air-plasma prior to coating with microgel solutions. Circular sections (12 mm dia.) were cut from PET sheets and washed 3x in DI water and ethanol prior to radio frequency glow discharge air plasma (RFGD) treatments for 10 min at 50% power. Air-plasma etched PET (RFGD-PET) surfaces were incubated with 1:3 dilutions of microgels ($d_{\text{PCS}}=40\text{-}50$ nm) in PBS for 12 h. Coated RFGD-PET was washed and stored in PBS until use in cell adhesion assays.

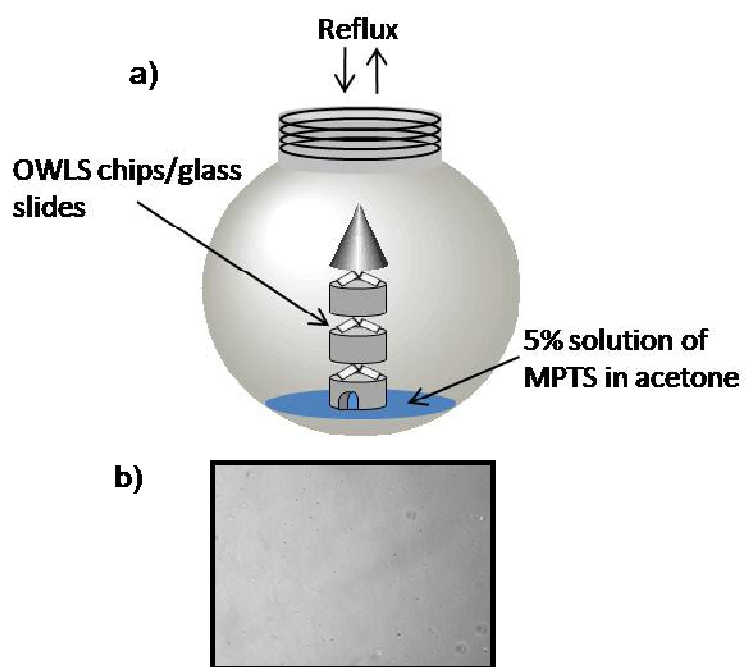


Figure 3.1: Vapor-silanzation procedure: (a) Samples within a covered polyethylene rack were placed inside a glass chamber containing 20 mL of 5% MPTS in acetone that was heated under reflux. (b) Photomicrograph of vapor-silanized MPTS glass reacted with microgels and seeded with CHO cells. No significant differences in resistance to cell adhesion were observed with vapor and solution-silanized glass.

3.3.5 Cell Culture and Adhesion Experiments

Chinese hamster ovary (CHO) cells (ATCC, Manassas, VA) were cultured in F-12 Kaighn's medium (Gibco) supplemented with 10% fetal bovine serum (FBS) and 1% antibiotic-antimycotic (ABAM). Human aortic endothelial cells (HAEC; Lonza, Walkersville, MD) were cultured in endothelial growth medium (EGM, MCDB 131 medium) supplemented with 10 ng/ml epidermal growth factor, 10 µg/mL heparin, 1.0 µg/mL hydrocortisone, 1% penicillin-streptomycin, 5% FBS, and 12 µg/mL bovine brain extract (Clonetics). 3T3 fibroblasts were cultured in Dulbecco's Modified Eagle's Medium (DMEM, Gibco) supplemented with 4.5 g/L D-glucose, L-glutamine, 110 mg/L sodium pyruvate, 10% FBS and 1% penicillin-streptomycin. Microgel-coated coverslips were placed into 24-well plates of tissue-culture polystyrene (Becton Dickinson Labware, Franklin Lakes, NJ) and washed 3x with PBS and 1x with the appropriate cell media. Wells were seeded with cells and incubated for 12 h at 37 °C. CHO cells and fibroblasts were seeded at 2.5×10^5 cells/cm², while endothelial cells were seeded at the lower surface concentration of 3.5×10^4 cells/cm². After incubation, surfaces were washed 3x with media and cell adhesion was assessed by phase contrast microscopy. Photomicrographs were taken at 10X magnification and the number of attached cells was counted manually. The cell adhesion experiments were modified slightly for the long-term fibroblast reseeding experiments. Surfaces were washed and seeded with cells at 2.5×10^5 cells/cm² every 48 h and observed by microscopy every 24 h. Microscopy was performed on unwashed surfaces to observe the aggregation of non-adherent fibroblasts in solution.

3.3.6 OWLS Measurements and Analysis

Si/Ti/O₂, MPTS-silanized, and BSA-capped PEG-OVS/BSA microgel-coated OWLS waveguide chips were analyzed inside the flow chamber of a MicroVacuum OWLS 110 optical waveguide lightmode spectrometer (MicroVacuum Ltd). All experiments were performed at a flow rate of 0.1 mL/min at 37°C and with a time step of 30 s. Waveguide surfaces were first equilibrated under DI water until a transverse magnetic mode refractive index variation of $< 1 \times 10^{-6}$ was obtained. For microgel characterization at each step of the coating process, MPTS-silanized waveguide chips were coated with microgels *in situ* and tested for fibrinogen adsorption using the following sequence of flowing solutions: 1) DI water, 2) PBS, 3) 2 h incubation with PEG-OVS/BSA microgel solutions ($d_{\text{PCS}} = 100\text{-}120$ nm) in PBS, 4) PBS wash/equilibration, 5) overnight incubation with BSA in PBS, 6) PBS wash/equilibration, 7) 2 h incubation with 2.5 mg/mL bFg in PBS, 8) PBS wash/equilibration, and 9) DI water wash/equilibration. Waveguide chips precoated with BSA-capped PEG-OVS/BSA microgels were analyzed specifically for fibrinogen adsorption using the following series of solutions: 1) DI water, 2) PBS, 3) 2 h incubation with 2.5 mg/mL or 20 mg/mL bFg in PBS, 4) PBS wash/equilibration, and 5) DI water wash/equilibration.

Measured effective refractive indices were analyzed with MicroVacuum BioSense Software (MicroVacuum Ltd), which calculated mass on the waveguide surfaces using de Feijter's formula (de Feijter, Benjamins et al. 1978):

$$M = d_A \frac{n_A - n_c}{dn/dc} \quad [3]$$

where M is the adsorbed mass, d_A is the thickness of the adsorbed layer, dn/dc is the refractive index increment of the adsorbate, n_A is the refractive index of the adsorbed layer,

and n_c is the refractive index of the cover medium. To calculate the amount of attached microgels on the waveguide surfaces, a refractometer was used to determine the value of the refractive index increment for PEG-OVS/BSA microgel solutions ($dn/dc = 0.150 \text{ g/cm}^3$). A value of $dn/dc = 0.182 \text{ g/cm}^3$ was used for the analysis of adsorbed fibrinogen (de Feijter, Benjamins et al. 1978).

3.3.7 QCM-D Measurements and Analysis¹

A quartz crystal microbalance with dissipation monitoring (QCM-D, model Q-Sense D300) was used to monitor mass deposition on quartz crystals. Frequency (F) and dissipation (D) were recorded at the fundamental frequency ($f = 5 \text{ MHz}$) and the 3rd, 5th, and 7th overtones ($f = 15, 25, \text{ and } 35 \text{ MHz}$) as functions of time. During all experiments, incubation solutions and the crystal were preheated to and maintained at $37 \text{ }^\circ\text{C}$.

After F and D reached steady state in PBS, 0.5 mL PEG-OVS/BSA microgels ($d_{\text{PCS}} = 100\text{-}120 \text{ nm}$) were diluted by 50% with PBS and incubated with the crystal for 1 h. The crystal was then thoroughly washed with 30 mL PBS. After F and D again reached steady state, the crystal was incubated with 0.5 mL 100 mg/mL BSA (0.22 μm -filtered) for approximately 2 h. Following another 30 mL PBS wash, the crystal was incubated with 0.5 mL 2.5 mg/mL bFg (0.22 μm -filtered) for 90 min. A final wash with 30 mL PBS was conducted until steady state. Control experiments were conducted similarly, with 100 mg/mL BSA substituted for microgels. Between all experiments, the instrument was thoroughly cleaned with a 1% SDS solution and DI water to remove any residual material.

¹ QCM data was gathered by Michael D. Nichols using equipment located at Duke University in the laboratory of Ashutosh Chilkoti.

F and D results corresponding to the 3rd, 5th, and 7th overtones were analyzed using Q-Tools software (version 2.1.6.134, Q-Sense) using a single-layer Voight (viscoelastic) model. Fluid density (1000 kg/m³) and fluid viscosity (6.915 x 10⁻⁴ kg/m-s), corresponding to PBS at 37°C, were kept fixed. Using optical densities obtained from OWLS (m_{OWLS}) analysis in conjunction with modeled Voight masses (m_{QCM}), (Hook, Kasemo et al. 2001; Voros 2004) corresponding layer densities were estimated as:

$$\rho_{\text{layer}} = \frac{m_{\text{QCM}}}{\frac{m_{\text{OWLS}}}{\rho_{\text{macrogel}}} + \frac{m_{\text{QCM}} - m_{\text{OWLS}}}{\rho_{\text{water}}}} \quad [4]$$

Our previous measurement of the volume fraction solid for PEG-OVS/BSA macrogels was used to estimate $\rho_{\text{macrogel}} = 1.0335 \text{ g/cm}^3$. Initially assuming layer densities of 1100 kg/m³, thickness, shear modulus, viscosity, and Voight mass of a deposited layer were modeled. In an iterative fashion, a new effective density was calculated from the Voight mass using equation 4 and used in the model to update parameters until solutions converged.

Atomic force microscopy (AFM, Nanoscope V multimode SPM, Veeco Instruments) was utilized in tapping mode in PBS. PEG-OVS/BSA coatings were applied to MPTS glass surfaces as described, with and without BSA capping. In situ surface imaging was performed using silicon nitride tips (Nanoprobe, Veeco) with drive frequencies of $7.5 \pm 0.4 \text{ kHz}$, a nominal spring constant of 0.06 N m^{-1} , and scan rates of 1-1.2 Hz.

3.4 Results

3.4.1 PEG Synthesis

We developed a four-step synthesis of 10,000 MW eight-arm PEG-VS that did not require the use of highly toxic divinylsulfone. The reaction scheme was a modification of a method developed by Morpurgo *et al* (Morpurgo, Veronese et al. 1996). The first stage of the synthesis required the reaction of PEG with methane sulfonyl chloride (4 eq) and triethylamine (4 eq). The second step produces PEG hydroxyethyl sulfide from the reaction between PEG mesylate and β -mercaptoethanol (4 eq). The desired product of the third step was PEG hydroxyethyl sulfone, resulting from the oxidation of PEG hydroxyethyl sulfide with 30% hydrogen peroxide in a sodium tungstic solution. The fourth and final step produced PEG vinylsulfone by reacting the hydroxyethyl sulfone with methane sulfonyl chloride in the presence of excess triethylamine. This step of the synthesis utilized an optimized procedure requiring the addition of 1.5 equivalents of methane sulfonyl chloride in the presence of 3 equivalents of triethylamine in an ice bath followed by the addition of these same volumes of reagent again after 24 hours. Thus the total reaction time for this step was 48 hours and resulted in a final product that was 96% PEG-VS after purification. Essential NMR peaks for vinylsulfone were seen at 5.96 ppm (d, 2H, =CH₂), 6.25 ppm (d, 2H, =CH₂), 6.73 ppm (t, 1H, =CHSO₂-), and 3.47 ppm (s, PEG backbone, -OCH₂-) (Figure 3.2).

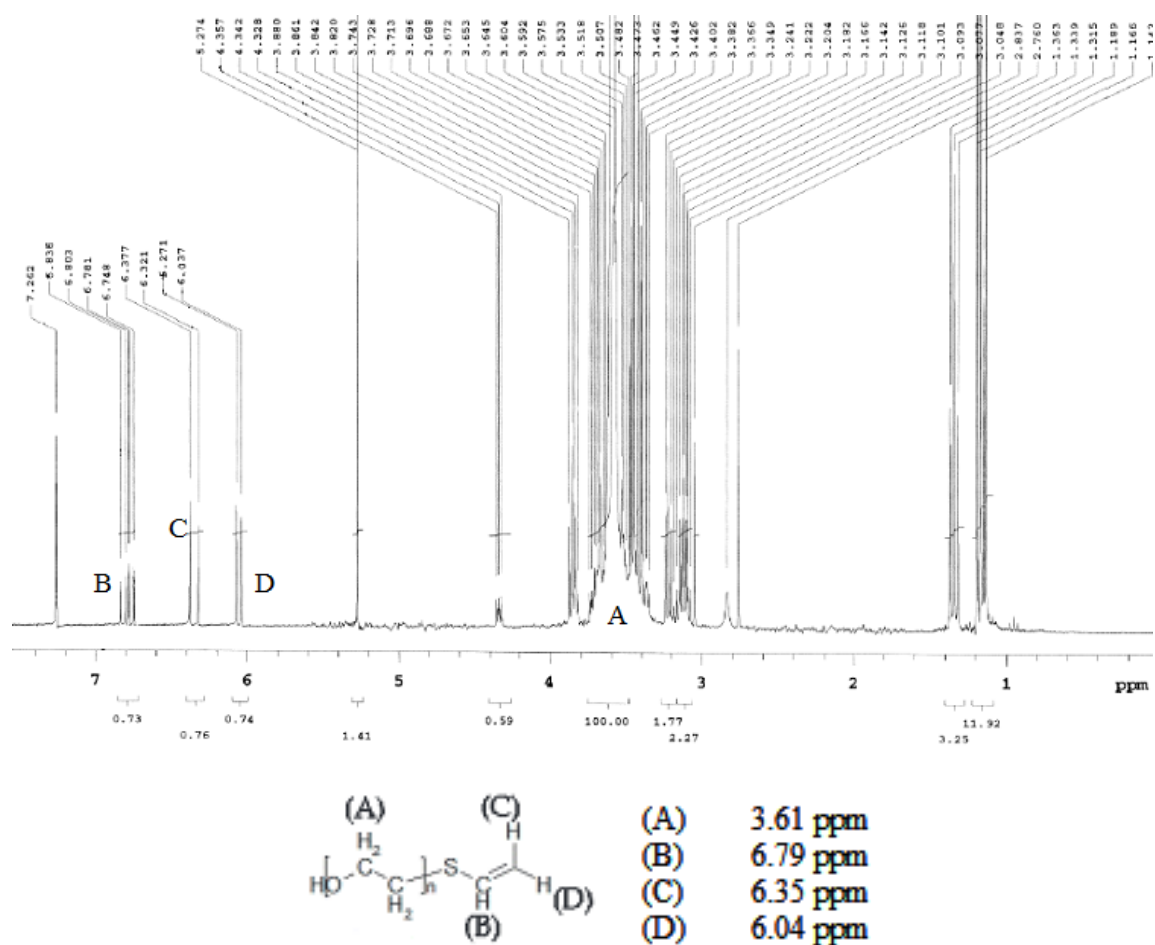


Figure 3.2: NMR spectra of PEG-OVS. A four-step synthesis was used to derivatize PEG-OH with vinylsulfone functionality. The final product was recovered at 30% with an overall conversion to PEG-OVS of 96%. (A) Location of PEG backbone peak. (B-D) Location of vinylsulfone peaks.

3.4.2 Characterization of Microgel Formation

Amines within BSA or PEG-OA were crosslinked with vinylsulfone end-groups of PEG-OVS through a Michael-type conjugate addition reaction, forming PEG-OVS/BSA or PEG-OVS/PEG-OA microgel solutions, respectively. The protocol for microgel formation and covalent attachment to glass surfaces is outlined in Figure 3.3. Microgels were formed by combining 200 mg/mL solutions of either BSA or PEG-OA with 200 mg/mL PEG-OVS at an amine to vinylsulfone ratio of 1:1. Additionally, some PEG-OVS/BSA microgels were formed at an amine to vinylsulfone ratio of 0.4:1. When rotated at 37°C, the 0.4:1 and the 1:1 ratio PEG-OVS/BSA solutions reached the gel point after 44.6 ± 0.6 h and 7.0 ± 0.5 h, respectively. PEG-OVS/PEG-OA solutions mixed at a 1:1 ratio formed gels in 6.7 ± 0.3 h. The longer gelation time of the 0.4:1 ratio was beneficial for microgel characterization, while the 1:1 ratio was employed for a more rapid microgel formation protocol. Regardless of the ratio used, an exponential increase in PEG-OVS/BSA microgel mean effective diameter with time was observed by dynamic light scattering (DLS) until gelation (Figure 3.4a,b). PEG-OVS/BSA microgels were not detected by DLS until reaching a d_{PCS} of 31.6 ± 4.5 nm, which occurred after approximately 50% of the total gelation time. The largest detectable PEG-OVS/BSA d_{PCS} prior to gelation was 159.3 ± 16.5 nm. Note that the measured mean effective diameters (d_{PCS}) are intensity-weighted and thus monomers, dimers and other small aggregates will contribute very little to this average. The intensity-weighted measurement was a highly reproducible measure of microgel formation, but the d_{PCS} should not be confused with the more physically meaningful number-weighted or volume-weighted mean particle sizes. Characterization of a $d_{\text{PCS}} \cong 100$ nm solution by GPC revealed that PEG microgels with >10 nm hydrodynamic radius constituted 46.6 wt% of the PEG

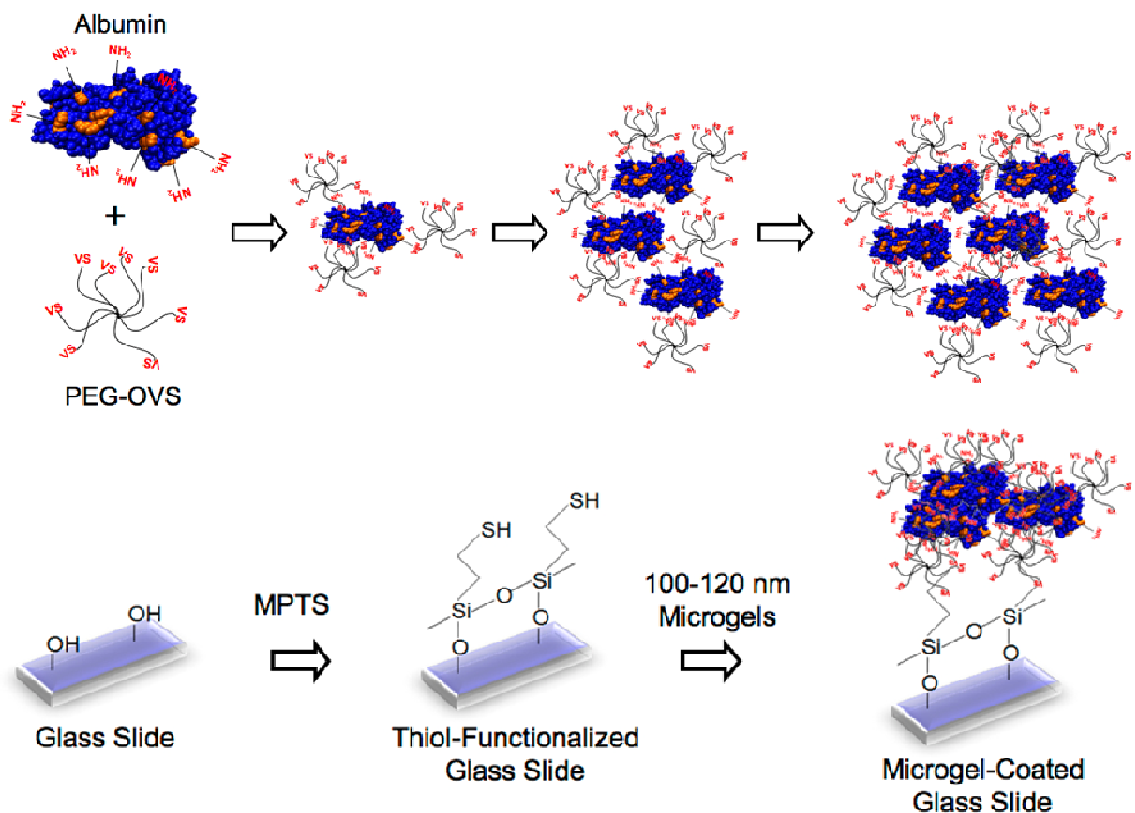


Figure 3.3: Crosslinking of bovine serum albumin (BSA) and poly(ethylene glycol)-octavinylsulfone (PEG-OVS, MW 10,000) may lead to microgel formation if the principle of equal end-group reactivity does not apply. Vinylsulfone groups on PEG molecules undergo a Michael-type addition with solvent-exposed and sterically accessible lysines on BSA, forming covalent linkages at neutral pH. If the crosslinking reaction is slowed before the gel point by dilution, microgel-containing solutions can be rapidly reacted with nucleophile-derivatized surfaces, such as thiol-silanized glass.

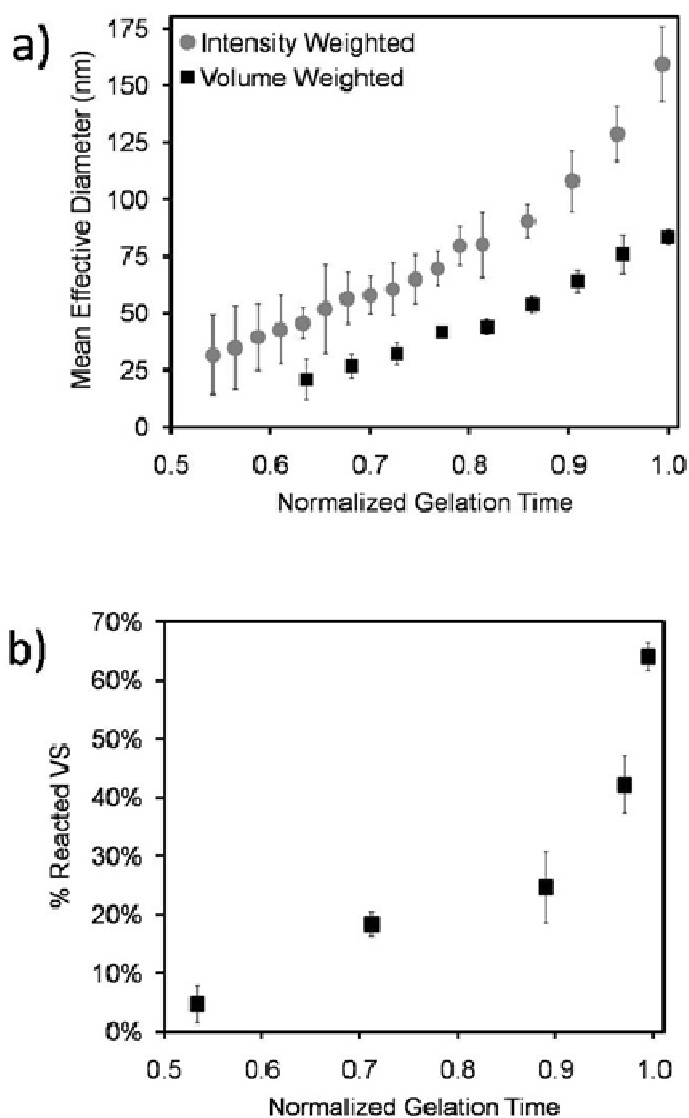


Figure 3.4: Evidence for formation of microgels during the crosslinking reaction: (a) Dynamic light scattering (DLS) with intensity-weighted (d_{PCS}) and volume-weighted mean effective diameters of reacting PEG-OVS/BSA solutions (0.4:1 ratio of BSA amine groups to PEG vinylsulfone groups, 44 h gel time). (b) NMR was used to measure the kinetics of end-group conversion during the reaction of PEG-OVS with PEG-octaamine (both MW 10,000; 1:1 ratio of PEG-OA to PEG-OVS, 6.5 h gel time). The time scales of both (a) and (b) were normalized relative to their respective gel times and error bars display the standard deviations for 4 separate reactions.

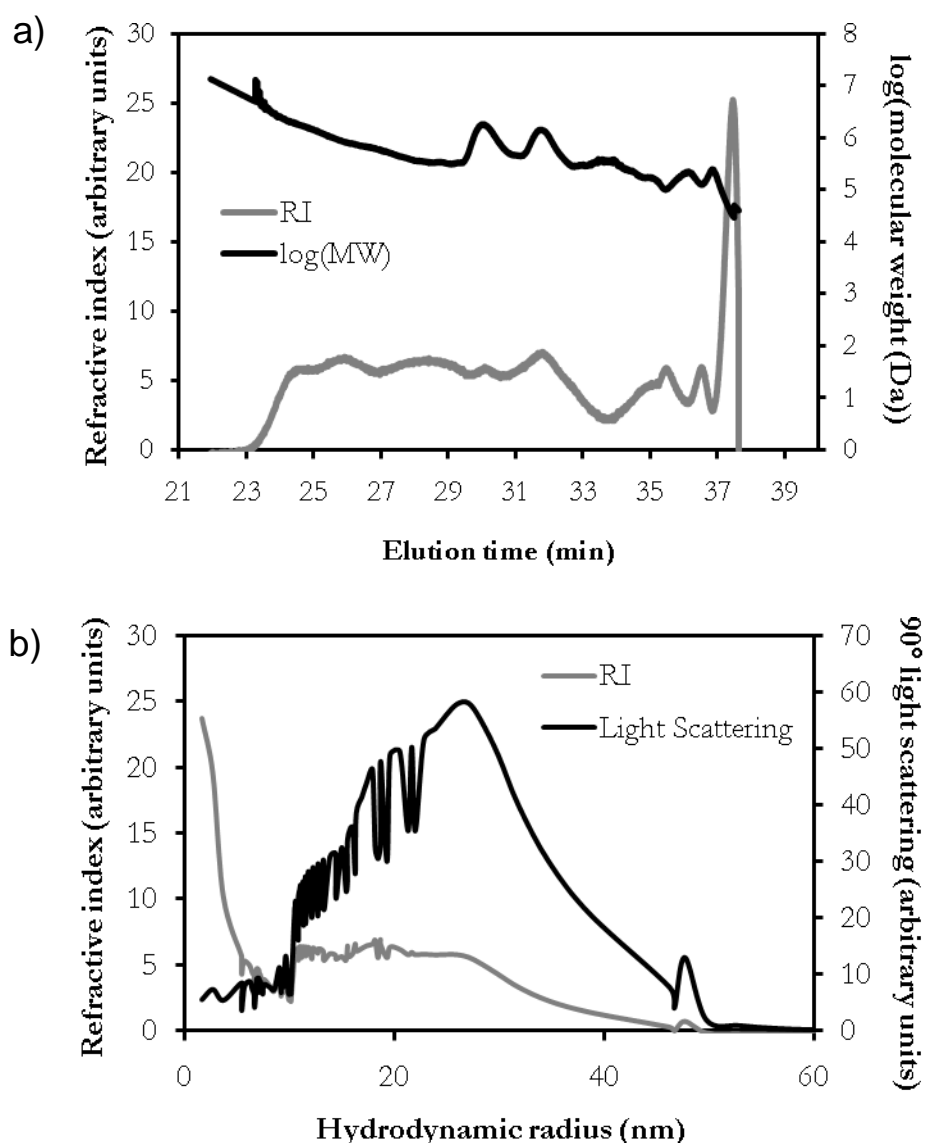


Figure 3.5: Gel permeation chromatography of PEG₈-VS and PEG₈-amine pre-reacted to $d_{\text{PCS}} \cong 100$ nm. The reaction was halted by capping remaining vinylsulfone groups with 2-mercaptoethanol. The absolute molecular weight was determined by triple detection of light scattering, viscosity and refractive index. (a) Molecular weight (black) and refractive index (gray) of eluted polymers. The peak at 37.4 min was confirmed to be monomeric vinylsulfone in a separate run. (b) Intensity of right angle light scattering (black) plotted against hydrodynamic radius. Refractive index (gray) is shown for comparison.

(Figure 3.5). Monomeric (i.e. unreacted) PEG comprised 12.0 wt% of the PEG, with the remainder of solution being oligomers of PEG₈-VS and PEG₈-amine.

An exponential increase in the percentage of reacted vinylsulfone groups was observed by NMR during the formation of PEG-OVS/PEG-OA microgels (Figure 3.4a,b). Only $4.6\% \pm 3.3\%$ of available vinylsulfone groups had reacted after reaching 50% of the gelation time, while $64.0\% \pm 2.4\%$ was the highest detectable end-group conversion prior to gelation. The rate of reaction of BSA with PEG-OVS was calculated from SDS-PAGE. BSA was reacted with PEG-OVS at the 0.4:1 amine to vinylsulfone ratio, and samples were collected at various timepoints for separation by SDS-PAGE. Crosslinking of BSA with PEG-OVS was apparent within 1 min of the start of the reaction, while unreacted BSA was no longer evident after 20 h, corresponding to the time at which correlograms became reliable by DLS (Figure 3.6a). After 84% of the gelation time had passed (38 h), there was no detectable BSA with a molecular weight below 131 kD. This timepoint corresponded to a d_{pCS} of about 100 nm, a degree of crosslinking that was used in most subsequent experiments. Concentrations of unreacted BSA were estimated from the SDS-PAGE gels and analyzed using the method of integration for second-order reactions with different stoichiometries (Laidler 1987), revealing a reaction rate constant of $3.15 \pm 0.11 \times 10^{-3} \text{ M}^{-1} \text{ s}^{-1}$ for the reaction of free BSA with PEG-OVS (Figure 3.6b).

3.4.3 Covalent Attachment of Microgels to Glass Surfaces

The following steps were utilized to covalently attach microgel coatings to glass: 1) oxygen-plasma etching, 2) silanization with mercaptopropyltrimethoxysilane (MPTS), 3) 1 h incubation with a dilute microgel suspensions in PBS pH 7.4 at 37°C, and 4) overnight

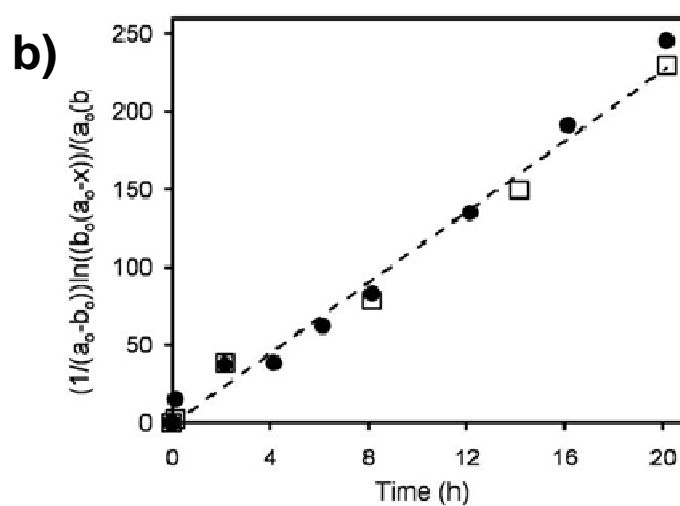
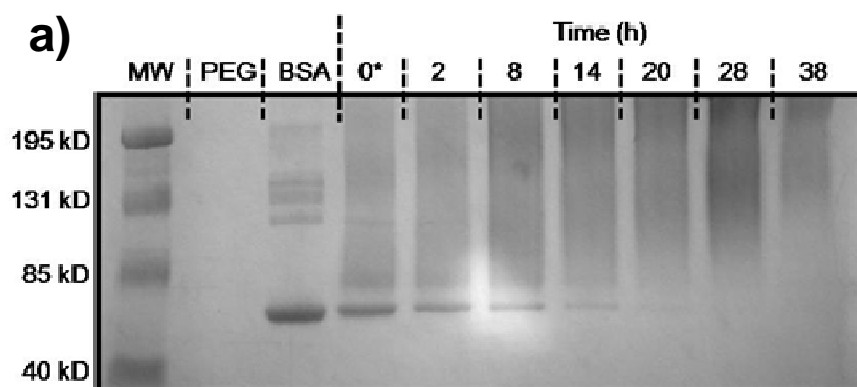


Figure 3.6: Kinetics of the crosslinking reaction between PEG-OVS and BSA. (a) SDS-PAGE of BSA during the crosslinking reaction with PEG-OVS. (b) Analysis of the 2nd order reaction kinetics for part (a) for two separate experiments (circles: first experiment; squares: second experiment; ordinate units: L/mol·h).

incubation with 50 mg/mL BSA. Microgels with d_{PCS} between 100-120 nm were the largest microgels capable of reacting with the MPTS functionalized surfaces at a 1:1 dilution within 1 h without a noticeable increase in size as measured by DLS at the end of the reaction. This d_{PCS} was chosen to maximize the amount of PEG attached to the surface while minimizing the risk of macrogelation on the surface. The presence of microgel coatings on the glass surfaces was verified by XPS (Table 3.1). After application of the microgel coating, the Si atomic concentration of the surfaces decreased from 27.4% to 1.03%, and the N/Si ratio of the surfaces increased by over 600-fold. The microgel-coated surfaces contained more nitrogen than anticipated for PEG alone (theoretical atomic composition of PEG: 66.7% C, 33.3% O, 0% N,) and more carbon than anticipated for BSA alone (theoretical atomic composition of BSA: 63.6% C, 19.4% O, 16.9 % N). Using the measured C/N atomic ratio, a BSA-capped microgel layer was estimated to be 71.4% BSA and 28.6% PEG. The nature of the microgel coating on the surfaces of MPTS functionalized glass was also studied by atomic force microscopy (AFM) in PBS. By AFM, the uncapped PEG-OVS/BSA microgel coatings appeared to consist of coalesced spheres with diameters smaller than 100 nm (Figure 3.7B & 3.7D). Although some areas on the microgel-coated surfaces appear to be uncovered, these areas are only a few nanometers lower than the rest of the surface. After addition of the BSA capping layer, the resolution of the images decreased dramatically, perhaps due to the excess of negative charges on BSA (Figure 3.7C).

Table 3.1: Elemental composition of treated glass surfaces, as determined by XPS.

| Surface | Atomic Conc. (%) | | | | | Atomic Ratios | | |
|-----------------------|------------------|-------|-------|------|-------|---------------|------|-------|
| | O | N | C | S | Si | C/N | C/O | N/Si |
| O ₂ Plasma | 59.16 | 0.59 | 10.34 | 0.47 | 26.52 | 17.53 | 0.17 | 0.02 |
| MPTS | 54.00 | 0.88 | 15.47 | 1.11 | 27.43 | 17.58 | 0.29 | 0.03 |
| Microgel | 18.02 | 12.62 | 67.37 | 0.7 | 1.03 | 5.34 | 3.74 | 12.25 |

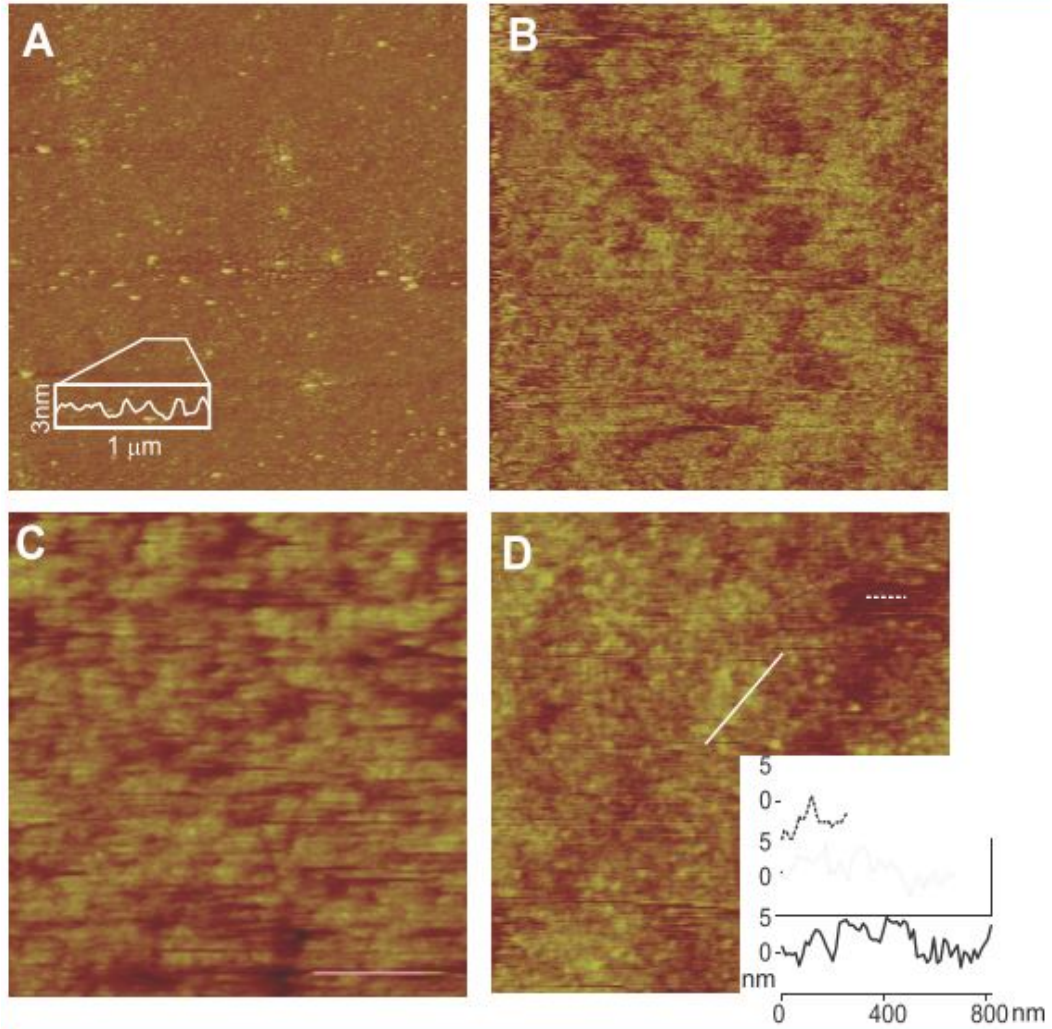


Figure 3.7: AFM analysis of: **(A)** MPTS glass, 10 x 10 microns, **(B)** PEG-OVS/BSA microgel-coated MPTS glass, 10 x 10 microns, **(C)** PEG-OVS/BSA microgel-coated MPTS glass with BSA capping step, 10 x 10 microns, **(D)** PEG-OVS/BSA microgel-coated MPTS glass, 3 x 3 microns with height profiles. The height data scales are 20 nm for (A), 30 nm for (B) and (D), and 120 nm for (C).

3.4.4 Properties and protein adsorption resistance of PEG-OVS/BSA microgel coatings

The optical mass and protein adsorption resistance of microgel coatings was quantified with OWLS. Since OWLS has an upper limit of sensitivity above the waveguide surface (Picart, Gergely et al. 2004), vapor silanization was employed instead of solution silanization, to limit silane aggregation. Solutions of PEG-OVS/BSA microgels ($d_{\text{PCS}} = 100\text{-}120\text{ nm}$) were flowed over Si/Ti/O₂ or MPTS waveguide surfaces, resulting in surface mass densities of $115.0 \pm 0.7\text{ ng/cm}^2$ and $267.38 \pm 8.58\text{ ng/cm}^2$, respectively. Resistance to protein adsorption was tested by comparing the adsorption of bovine fibrinogen (bFg) on MPTS surfaces to BSA-capped PEG-OVS/BSA microgel surfaces. While bFg readily adsorbed to the MPTS surface at $201.9 \pm 1.2\text{ ng/cm}^2$, no detectable change in refractive index was observed for the microgel surface when switching from the PBS solution to the 2.5 mg/mL bFg solution in PBS (Figure 3.8a). To verify that the microgel coated OWLS waveguide chip was still sensitive to refractive index changes above the microgel surface, the adsorption experiment was repeated with an 8-fold higher concentration of bFg (a thick coating, e.g. $> 200\text{ nm}$, could prevent detection of protein on or above the coating) (Lukosz 1991). The refractive index of the 20 mg/mL bFg solution was 0.0042 higher than PBS alone, and this difference in refractive index was detected by OWLS when switching from PBS to 20 mg/mL bFg in PBS on the microgel surface, indicating that the coating was thin enough to detect changes on the surface (Figure 3.8b). After switching the solution back to PBS and DI water for washing, only $4.1 \pm 0.9\text{ ng/cm}^2$ of bFg was detected in comparison to $192 \pm 3.3\text{ ng/cm}^2$ on the MPTS surface under the same conditions.

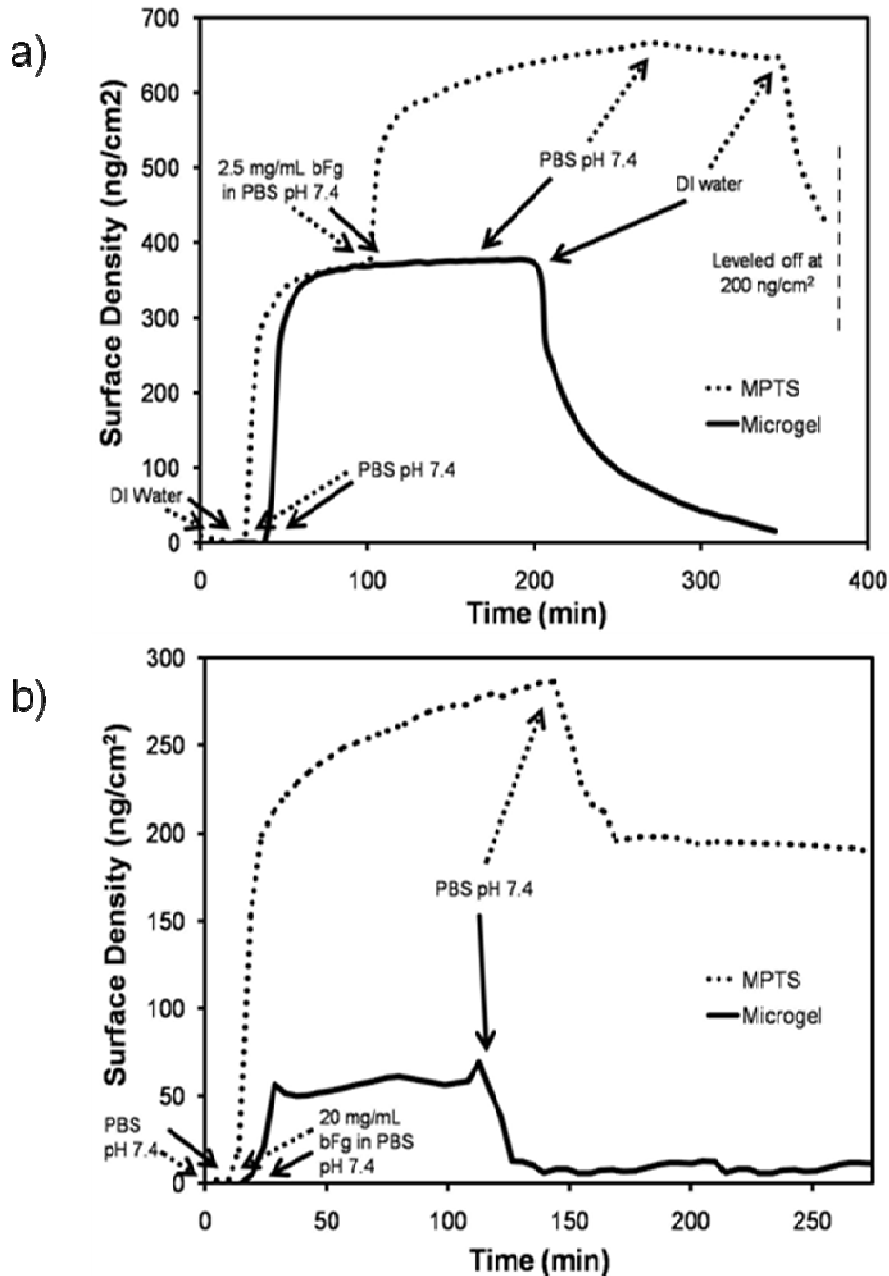


Figure 3.8: OWLS analysis of fibrinogen adsorption to microgel-coated surfaces. Si/Ti/O₂ surfaces of OWLS waveguide chips were oxygen-plasma etched, vapor-silanized with MPTS, and incubated with PEG-OVS/BSA microgels ($d_{\text{PCS}} = 100\text{-}120\text{ nm}$). The adsorption of bovine fibrinogen (bFg) from: (a) 2.5 mg/mL, or (b) 20 mg/mL solutions onto microgel-coated surfaces was monitored. All surfaces were exposed to the same series of solutions flowing at 0.1 mL/min at 37°C: (1) DI water, (2) PBS pH 7.4, (3) 2.5 mg/mL or 20 mg/mL bovine fibrinogen in PBS pH 7.4, (4) wash with PBS, pH 7.4, and (4) wash with DI water. The higher concentration of bovine fibrinogen in part b demonstrated that the microgel layer was thin enough to detect protein above the microgel coating.

QCM-D was used to monitor microgel coatings on MPTS surfaces. Quartz sensors were silanized in solution with MPTS prior to QCM-D analysis. Microgel coatings were formed on the surfaces using the same protocol as for glass slides, including the final capping step with BSA. Incubations with microgel solutions ($d_{\text{PCS}} = 100\text{-}120\text{ nm}$), BSA solutions, and bFg solutions were all performed within the QCM-D itself (Figure 3.9). By combining OWLS-measured optical masses with QCM-D frequency and dissipation measurements, the thickness, Voight mass, shear viscosity, and elastic modulus of the coatings were calculated (Table 2). Comparison between the optical mass and Voight mass for PEG-OVS/BSA microgels revealed the presence of a highly hydrated coating ($\sim 97\%$ water). Measurements of protein adsorption on the microgel-coated surfaces correlated well between OWLS and QCM analysis, revealing negligible changes in effective refractive index or frequency, respectively, after incubation with fibrinogen solutions. None of the differences in the calculated parameters were found to be statistically significant when comparing BSA-capped PEG-OVS/BSA microgels before and after incubation with fibrinogen.

3.4.5 Resistance of Microgel-Coated Glass to Cell Adhesion

Glass slides were coated with microgel solutions and incubated with CHO, fibroblast and endothelial cells to test for resistance to cell adhesion and spreading. CHO cells and fibroblasts readily adhere to materials, while endothelial cells are relevant to use of the coatings on a blood-contacting materials. Phase contrast photomicrographs of cells

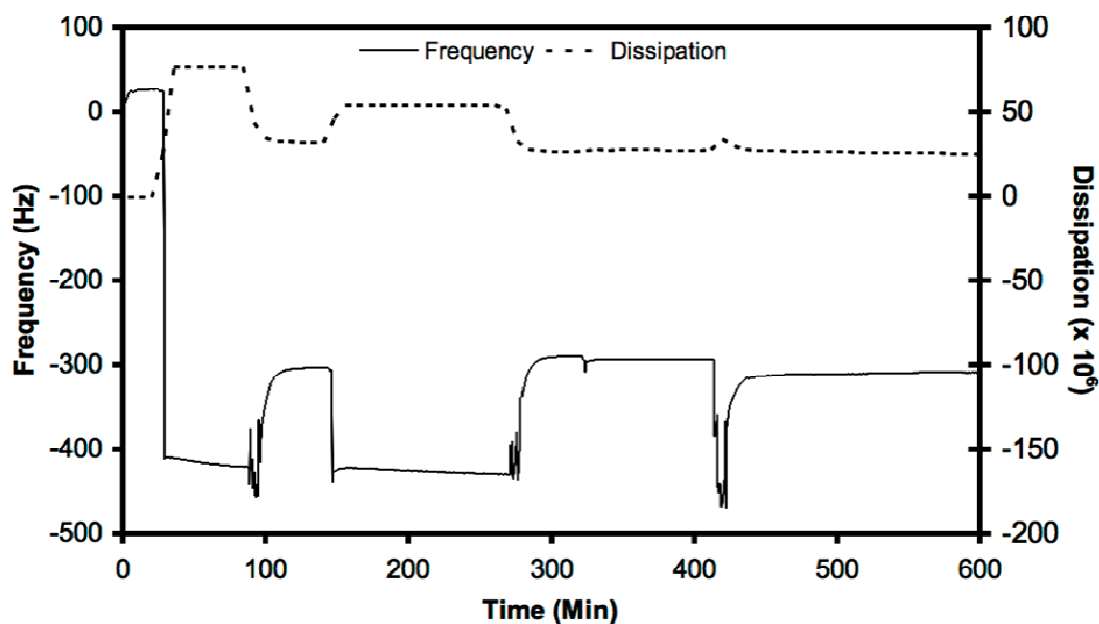


Figure 3.9: QCM-D frequency and dissipation changes illustrating the attachment of microgels to the MPTS-silanized crystal and subsequent resistance to non-specific protein adsorption. The following solutions were flowed over the crystal: (1) 0.5 mL of BSA/PEG-OVS microgels ($d_{\text{PCS}} = 100\text{-}120\text{ nm}$) flowed onto the crystal and then incubated for 60 min. (2) 30 mL wash with PBS and incubation with PBS until readings stabilized. (3) 0.5 mL of 100 mg/mL BSA flowed over the crystal and incubated for about 90 minutes. (4) 30 mL wash with PBS and incubation with PBS until readings stabilized. (5) 0.5 mg/mL of 2.5 mg/mL bovine fibrinogen flowed over crystal and incubated for 2 h. (6) 30 mL wash and incubation with PBS until readings stabilized.

Table 3.2: Physical properties of PEG-OVS/ BSA microgels measured with OWLS and QCM.

| | PEG-OVS/BSA Microgels | PEG-OVS/BSA Microgels (BSA cap) | PEG-OVS/BSA Microgels (BSA cap) + bFg |
|------------------------------------|----------------------------------|--|--|
| Optical mass (ng/cm ²) | 267.3±8.5 | 532.6±77.0 | 579.4±5.9 |
| Density (kg/m ³) | 1001.2±0.1 | 1002.6±0.2 | 1002.7±0.5 |
| Thickness (nm) | 75.2±8.6 | 65.7±5.4 | 71.0±12.0 |
| Voight mass (ng/cm ²) | 7523.7±855.6 | 6582.3±544.5 | 7122.3±1197.1 |
| Elastic Shear Modulus (kPa) | 16.1±11.5 | 16.3±8.8 | 15.9±10.1 |
| Shear Viscosity (cP) | 1.1±0.2 | 1.2±0.2 | 1.2±0.2 |

adhered to PEG-OVS/BSA microgel coatings capped with BSA are displayed in Figure 7. All cell types adhered to and spread on MPTS surfaces and BSA-coated MPTS surfaces during the 24 h incubation period. While fewer cells adhered to the PEG-OVS grafted surfaces, no spread cells and few adhered cells were found on the microgel-coated surfaces (Figure 3.10). Long-term resistance to fibroblast adhesion was tested on BSA-capped PEG-OVS/BSA microgel-coated surfaces by reseeding cells onto surfaces every 2 days. Non-adherent fibroblasts were observed to clump into aggregates above the surfaces and the BSA-capped PEG-OVS/BSA microgels resisted cell adhesion for 19 days (Figure 3.11). In contrast, extensive fibroblast adhesion was observed on non-silanized glass surfaces after the first day of incubation (Figure 3.11, insets).

Cell adhesion and spreading was quantified on the treated surfaces (Figure 3.12a, b). Although fibroblasts tended to spread more on the surfaces than CHO cells, no spread cells of any type were found on the microgel-coated slides. Capping the microgel surfaces with BSA resulted in a small, but insignificant decrease in cell adhesion compared to uncapped microgel coatings (Figure 3.13, Figure 3.14b). PEG-OVS/PEG-OA microgel coatings capped with BSA displayed slightly more cell adhesion than PEG-OVS/BSA gels capped with BSA, but the difference was also not statistically significant (Figure 3.13, Figure 3.14c). The resistance of BSA-capped PEG-OVS/BSA microgel coatings to CHO and fibroblast adhesion was not influenced by preincubation with fibrinogen immediately prior to cell seeding (Figure 3.12a,b, Fig 3.14e). BSA-capped PEG-OVS/PEG-OA microgel coatings were less resistant to cell adhesion after incubation with fibrinogen solutions (Figure 3.14f). Cell adhesion to PEG-OVS/BSA microgel coatings was

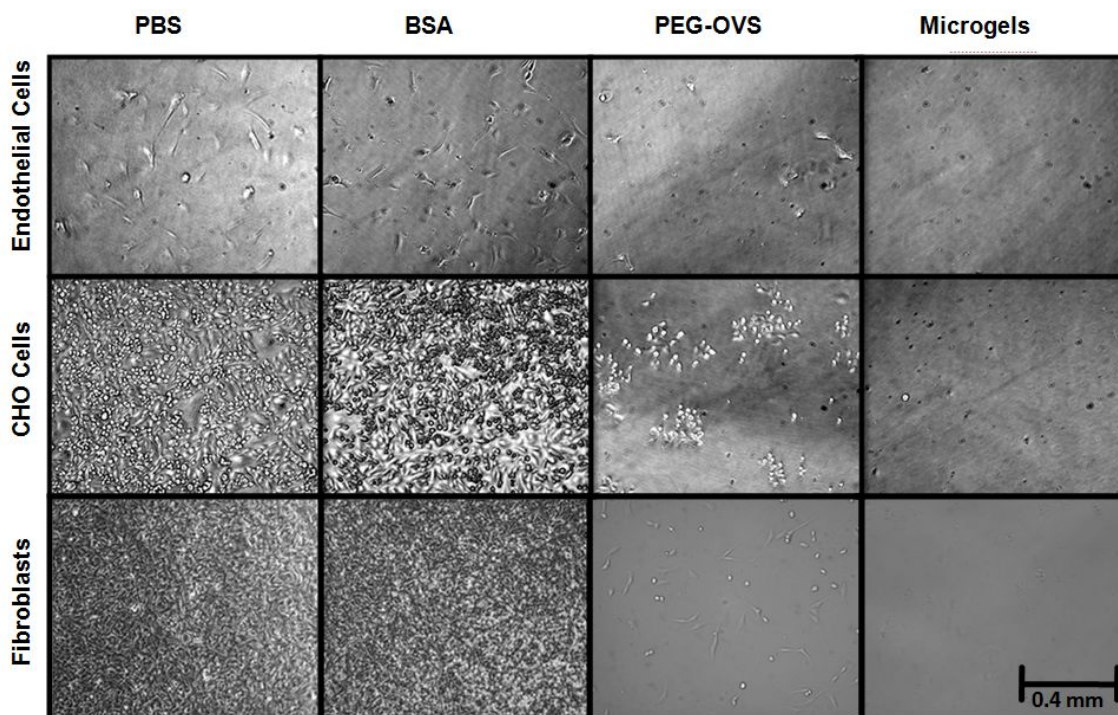


Figure 3.10: Cell adhesion on microgel-coated glass at 10X magnification after a 24 h incubation with endothelial (3.5×10^4 cells/cm²), CHO (2.5×10^5 cells/cm²), or fibroblast (2.5×10^5 cells/cm²) cells. MPTS-silanized glass coverslips were incubated at 37°C with one of the following solutions: PBS for 12 h, 100 mg/mL BSA for 12 h, 100 mg/mL PEG-OVS for 12 h, or PEG-OVS/BSA microgels ($d_{\text{PCS}} = 100\text{-}120$ nm) for 1 h followed by capping with 50 mg/mL BSA for 12 h.

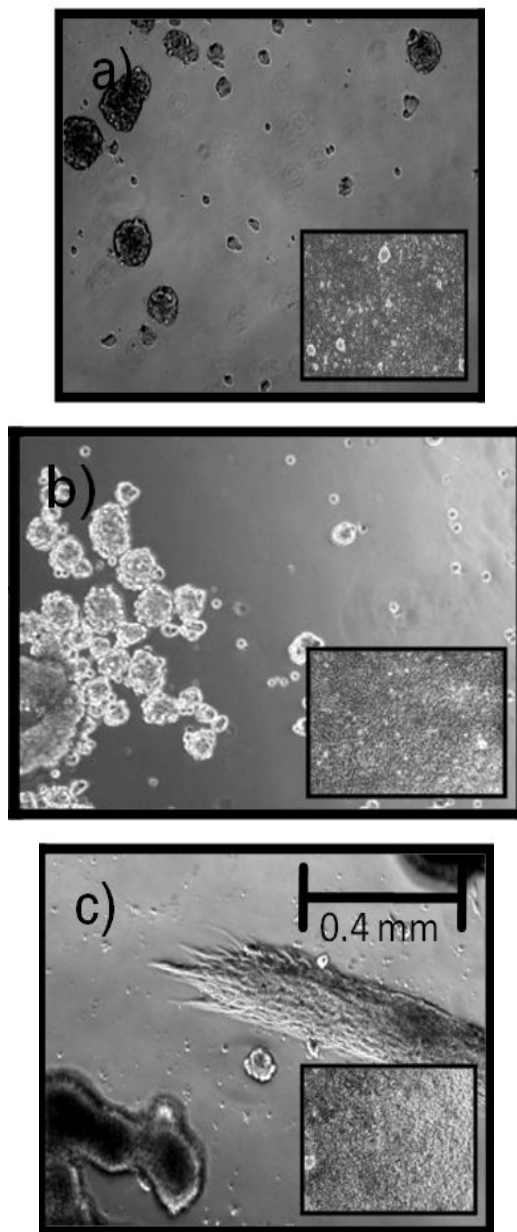


Figure 3.11: Cell adhesion to microgel-coated glass at 10X magnification after repeated seedings with fibroblasts after: (a) 1 day, (b) 5 days, and (c) 19 days. MPTS surfaces coated with BSA-capped BSA/PEG-OVS microgels were washed and reseeded with fibroblasts every 2 days at 2.5×10^5 cells/cm². Cell spreading was not observed until 19 days, at which time aggregates of fibroblasts spread. Controls consisting of non-silanized glass incubated with BSA-capped BSA/PEG-OVS microgels are displayed in the lower right corner of each image at 10X magnification, showing complete cell spreading.

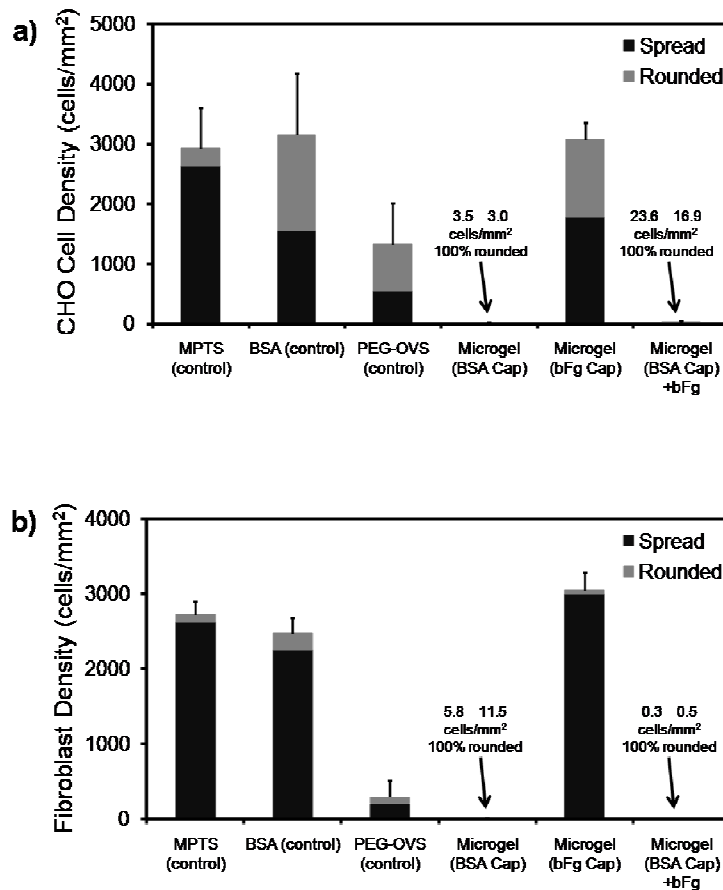
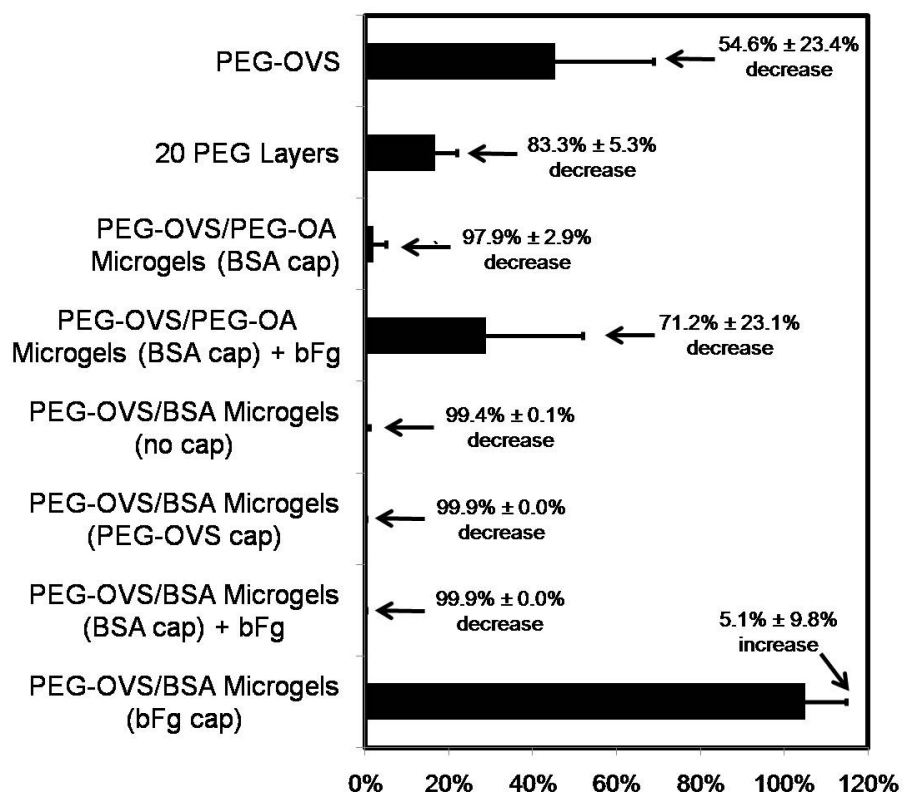


Figure 3.12: Cell counting results for CHO and fibroblast adhesion to microgel surfaces. **(a)** Comparison of CHO cell adhesion to MPTS-silanzed glass incubated overnight with (in order from left to right): (1) PBS pH 7.4; (2) 50 mg/mL bovine serum albumin (BSA) in PBS; (3) 100 mg/mL PEG-OVS in PBS; (4-5) PEG-OVS/BSA microgels ($d_{\text{PCS}} = 100\text{-}120$ nm), capped with (4) BSA or (5) bovine fibrinogen (bFg), and (6) PEG-OVS/BSA microgels ($d_{\text{PCS}} = 100\text{-}120$ nm), capped with BSA then incubated with 2.5 mg/mL bFg in PBS for 2 h at 37°C. **(b)** Fibroblast adhesion after the same surface treatments described in part a. CHO and fibroblast cells were seeded at a density of 2.5×10^5 cells/cm² and incubated with the surfaces for 24 h at 37°C.



CHO Cell Adhesion Relative to Silanated Glass

Figure 3.13: CHO cell adhesion to MPTS-silanized glass reacted with: (in order from top to bottom): (1) 100 mg/mL PEG-OVS in PBS; (2) 20 PEG-OVS layers alternating with DTT applied using a layer-by-layer method; (3-4) PEG-OVS/PEG-OA microgels ($d_{\text{PCS}} = 100\text{-}120$ nm) capped with (3) BSA; (4) BSA then incubated with bFg for 2 h; (5-8) PEG-OVS/BSA microgels ($d_{\text{PCS}} = 100\text{-}120$ nm) that were capped with: (5) PEG-OVS, (6) BSA, (7) BSA, then incubated with bFg for 2 h, or (8) bFg. CHO cells were seeded at a density of 2.5×10^5 cells/cm² and incubated with the surfaces for 24 h at 37°C.

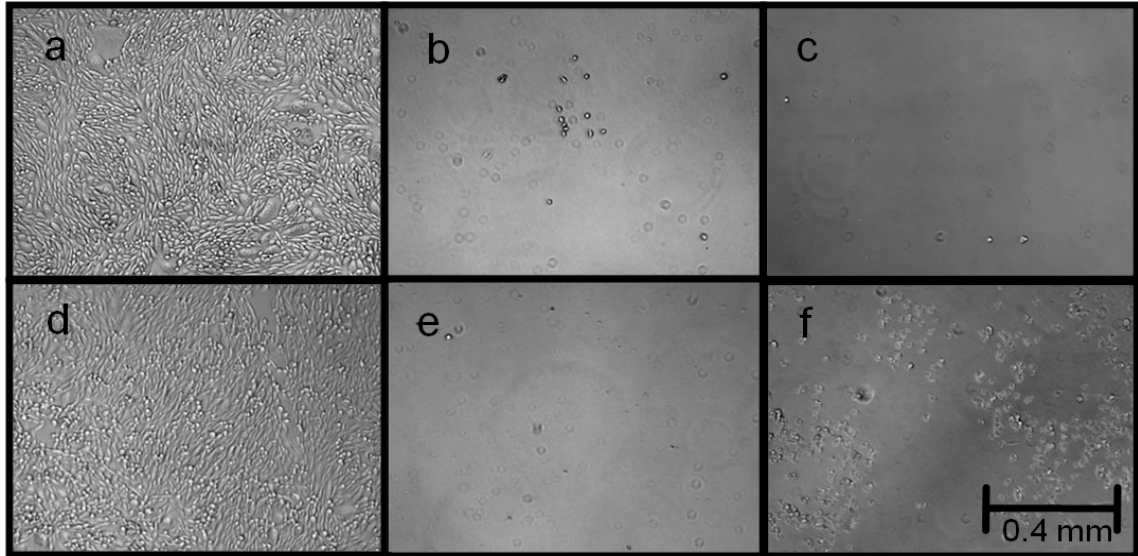


Figure 3.14: 10X magnification of CHO cell adhesion on glass slides for 24 h demonstrating the effects of the crosslinker and final capping step. MPTS-silanized glass was incubated with: (a) 2.5 mg/mL bovine fibrinogen in PBS at pH 7.4 for 2 h, (b) PEG-OVS/BSA microgels overnight in PBS pH 7.4 at 37°C, (c) PEG-OVS/PEG-OA microgels capped overnight with 50 mg/mL BSA in PBS pH 7.4 at 37°C, (d) PEG-OVS/BSA microgels capped overnight at 37°C with 2.5 mg/mL bovine fibrinogen in PBS pH 7.4, (e) PEG-OVS/BSA microgels capped overnight with 50 mg/mL BSA and subsequently incubated for 2 h at 37°C with a 2.5 mg/mL bovine fibrinogen. (f) PEG-OVS/PEG-OA microgels capped overnight with 50 mg/mL BSA and subsequently incubated for 2 h at 37°C with 2.5 mg/mL bovine fibrinogen.

promoted when a bovine fibrinogen cap was used instead of a BSA cap, suggesting the presence of reactive vinylsulfone groups in the coating before the capping step but not after (Figure 3.13, 3.14, & 3.15d). Compared to our previous results with a covalent layer-by-layer method,(Kim, Wacker et al. 2007) the microgel coatings were far superior in preventing cell adhesion (Figure 14c).

3.4.6 Application of Microgel Coating to PET surfaces

Microgel coatings were applied to PET surfaces by a 2-step process and tested for cell adhesion. The first step was etching of the surface with air-plasma to provide a low surface density of amine groups (Riccardi, Barni et al. 2003). The second step was incubation with a 1:3 dilution of PEG-OVS/BSA microgel solutions ($d_{\text{PCS}} = 40.1 \pm 0.99$ nm) for 12 h. A longer incubation time was utilized compared to the coating of thiol-functionalized surfaces due to the slower reaction between vinylsulfone and primary amines.(Friedman 1965) A diluted, smaller d_{PCS} microgel solution was used to limit microgel growth over the 12 h incubation. Mean effective diameters were found to still be below 100 nm after the longer incubation period. Even without a capping step, microgel coatings on RFGD-PET demonstrated considerable resistance to CHO cell adhesion (2.3 ± 3.2 adhered cells/ mm^2) compared to RFGD-PET (1100 ± 216 cells/ mm^2), BSA-adsorbed RFGD-PET (850 ± 129 cells/ mm^2) and PEG-OVS grafted RFGD-PET (975 ± 95 cells/ mm^2) (Figure 3.15).

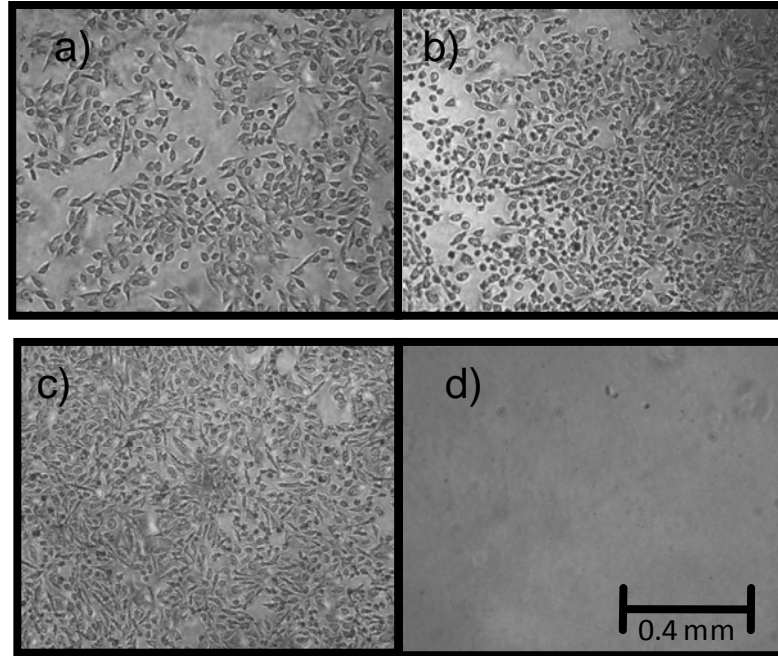


Figure 3.15: CHO cell adhesion at 24 h to air RFGD-treated PET films that were incubated with: (a) PBS, (b) BSA, (c) PEG-OVS, or (d) PEG-OVS/BSA microgels. 10X magnification.

3.5 Discussion

We have previously demonstrated that delivery of a signaling lipid from macroscopic PEG-OVS/BSA gels increased the migration rate of endothelial cells attached to the hydrogel surface via cell adhesion peptides (Wacker, Scott et al. 2006; Wacker, Alford et al. 2008). Here, we present a nanoscale version of this gel that can be covalently attached to biomaterials as a thin coating. The coatings were generated on surfaces by covalently attaching PEG-containing microgels under physiological conditions. This was achieved using a dip-coating methodology wherein thiol-functionalized glass was incubated with dilute microgel solutions to permit rapid attachment to surfaces within a timeframe that permitted minimal growth in microgel mean effective diameters. Compared with strategies that require spin coating, the dip-coating methodology may be useful for coating devices of varying size, shape and geometry. Because the microgels were attached to surfaces during the process of gelation, unreacted VS-groups remained available for additional crosslinking with a capping molecule. Capping of unreacted VS-groups with BSA or PEG-OA may increase the crosslink density within the coating and add a passivating surface layer. Using bioactive capping molecules, cellular responses may also be controlled.

The presence of a very broad distribution of polymer sizes during crosslinking is expected, but the distribution is likely different from that described by Flory and Stockmayer. This was particularly evident from the high end-group conversion measured by NMR, which indicates significant intramolecular crosslinking (i.e. ramification) during crosslinking. The presence of particles with diameters greater than about 30 nm as observed by DLS and the spherical structures with diameters ≈ 100 nm observed by AFM also support the presence of microgels in the crosslinking solutions.

NMR indicated that the rate of reaction actually increased as reactive groups were consumed. The exponential increase in the rate of reaction was correlated with the exponential increase in mean effective diameter measured by DLS. Furthermore, DLS revealed that a $d_{\text{PCS}} \approx 100$ nm was reached after approximately 90% of the gelation time had passed, and GPC analysis demonstrated that only 12.0% of the monomer remained unreacted at this timepoint. While the number of crosslink sites in similar condensation gels has been determined by swelling measurements (Metters and Hubbell 2005), detailed knowledge of the kinetics of crosslinking and microgel formation is sparse. However, NMR should be a useful tool in such studies. Additionally, if solvent conditions could be found such that all of the reactive groups within a microgel could be entirely consumed before gelation occurred, this would enhance the study of microgel size distributions.

We characterized microgel coatings by combining results from OWLS and QCM, which respectively measure the solid and liquid components of highly hydrated layers (Voros 2004; Wittmer, Phelps et al. 2007). Additionally, OWLS provided an independent measurement of optical masses that was used to increase confidence in viscoelastic QCM models (Hook, Kasemo et al. 2001; Voros 2004). PEG-OVS/BSA hydrogel coatings were found to have a higher water content than hydrated protein layers, and the resulting density was much closer to that of water (Voros 2004). In comparison to hydrated laminin films that were previously characterized using the Voight model, the microgel coatings possessed a comparable thickness, but had a higher shear modulus and a slightly lower viscosity (Malmstrom, Agheli et al. 2007). The increased shear modulus likely reflected the effects of covalent crosslinks within the hydrogel coatings versus non-covalent interactions in the multi-domain protein. AFM revealed the presence of coalesced spheres that were consistent with the size range of particles detected by DLS.

The relative role of BSA versus PEG in the resistance of the microgel coatings to cell adhesion is unknown. BSA-capped coatings were similar to PEG-OA-capped coatings in initial cell adhesion (Figure 9c), but BSA-capped PEG-OVS/PEG-OA surfaces that were incubated with fibrinogen before cell seeding displayed some cell adhesion (Figure 10f). The BSA-capped PEG-OVS/BSA microgels were the most robust, but it is possible that with further optimization an all-PEG system could perform equally well. The temporary non-fouling properties of adsorbed albumin films are well-documented in both *in vitro* and *in vivo* studies, (Chang 1969; Imai, Tajima et al. 1971; Eberhart, Munro et al. 1987) so it may emerge that PEG/albumin microgel coatings perform better than all-PEG systems. However, the albumin films may be subject to degradation by proteases and potential immunological responses. Switching the capping protein from BSA to fibrinogen led to cell adhesion, similar to Almany et al. who developed hydrogel scaffolds from PEGylated fibrinogen fragments to support smooth muscle cell and endothelial cell ingrowth (Almany and Seliktar 2005). In the current study, the entire fibrinogen protein was coupled without reduction of disulfide bonds. The use of whole proteins versus cell adhesion peptides may be advantageous in promoting specific cell adhesion and presents a multitude of options for new bioactive coatings.

Strong evidence has emerged for the advantages of high molecular weight, covalently attached PEG-containing polymers, lattices or microgels for producing thin layers that reduce cell adhesion. High molecular weight poly(L-lysine)-graft-poly(ethylene glycol) (PLL-*g*-PEG) adsorbed on surfaces reduces initial cell adhesion, but cell adhesion is observed over a period of two weeks (Lussi, Falconnet et al. 2006). Covalent linkage of PLL-*g*-PEG to aldehyde-functionalized PET may lead to more stable coatings (Blattler, Pasche et al. 2006). Banerjee et al. used a comb copolymer of methyl methacrylate (MMA) and PEG-

methacrylate (PEGMA)/methyl PEGMA, as well as a coalesced PMMA latex, to coat glass substrates to a thickness of 225 nm, which completely inhibited N46 fibroblast adhesion for 24 h (Banerjee, Irvine et al. 2000). More similar to the current study, Groll et al. tested star-PEG molecules with six isocyanate-terminated arms in which crosslinking was initiated just prior to spin-coating on substrates to a thickness of 30 nm. Both osteogenic sarcoma (SaOS) cells and human fibroblasts did not adhere to either of the coated substrates at 24 h (Groll, Fiedler et al. 2005). Crosslinking of star PEG during attachment to surfaces is expected to result in higher coating densities and surface coverage (Gasteier, Reska et al. 2007). Nolan et al. fabricated thermoresponsive microgel particles that were about 200 nm in diameter at 37°C and comprised of poly(*N*-isopropylacrylamide-*co*-acrylic acid) (pNIPAm-*co*-AAc) internally-crosslinked with PEG-diacrylate. When spin coated on aminofunctionalized glass, microgels with 5 mol% PEG 700 significantly reduced 3T3 fibroblast adhesion over 72 h (Nolan, Reyes et al. 2005). More recently, similar microgels were reacted onto benzophenone-functionalized PET discs, which successfully inhibited IC-21 macrophage adhesion over 48 h (Singh, Bridges et al. 2007). Although synthesis and characterization is challenging, the potential for such nanoscale coatings to enhance cell and protein resistance seems particularly promising. However, as improvements in coatings emerge, more challenging cell culture models may be warranted for evaluation prior to *in vivo* testing.

In testing the long-term resistance to cell adhesion *in vitro*, cell reseeding is advantageous. Drumheller et al. demonstrated that semi-interpenetrating network (semi-IPN) thin films containing a PEG-acrylate/acrylic acid copolymer, resisted fibroblasts cell adhesion for over two-weeks with reseeding every three days (Drumheller, Elbert et al. 1994). Additionally, semi-IPN films containing high MW PEG-acrylate or PEG-diol

completely resisted fibroblast adhesion for up to 30 days with weekly reseeding (Drumheller and Hubbell 1995). The microgel coatings presented here, when capped with BSA, exhibited a resistance to cell adhesion for almost three weeks, with reseeding every two days. As more effective PEG coating strategies are developed, it would be advantageous if such reseeding protocols became standard for assessing cell adhesion resistance, as a first step towards *in vivo* testing.

3.6 Conclusion

We have fabricated and characterized PEG-OVS-based microgel solutions for use as protein and cell-resistant bioactive coatings. The microgel solutions were covalently reacted with biomaterial surfaces using a dip-coating methodology. The difference in nucleophilicity of thiols and primary amines was exploited to achieve the slow growth in microgel size and rapid attachment to surfaces. OWLS and QCM analysis demonstrated minimal protein adsorption on the capped films, while DLS, NMR and GPC were used to begin to elucidate the mechanism for microgel formation. Cell adhesion and spreading were inhibited on microgel-coated glass and PET, but cell adhesion was promoted by a fibrinogen-capped coating. If the resistance to cell adhesion translates to blood compatibility, PEG-based microgels could be useful to produce bioactive barriers between blood and vascular devices.

CHAPTER 4[†]

Modular Scaffolds Assembled Around Living Cells Using Poly(Ethylene Glycol) Microspheres with Macroporation Via a Non-Cytotoxic Porogen

4.1 Abstract

The LCST behavior of poly(ethylene glycol) (PEG) in aqueous sodium sulfate solutions was exploited to fabricate microspheres without the use of other monomers, polymers, surfactants or organic solvents. Reactive PEG derivatives underwent thermally induced phase separation to produce spherical PEG-rich domains that coarsened in size pending gelation, resulting in stable hydrogel microspheres between \approx 1-100 microns in size. The time required to reach the gel point during the coarsening process influenced the final microsphere size and morphology. The gel point could be varied by pre-reaction of the PEG derivatives below the cloud point, or by controlling reaction conditions above the cloud point. Pre-reaction brought the PEG derivatives closer to the gel point prior to phase separation, while the temperature influenced the rate of reaction. Dynamic light scattering indicated a percolation-to-cluster transition about 3-5 minutes following phase separation. Three types of PEG microspheres with different functionalities were used to form scaffolds, allowing control over macroporosity and bioactivity. Scaffolds were formed by centrifuging microspheres in the presence of HepG2 hepatoma cells, resulting in a homogenous

[†] Chapter 4 has been adapted from the following unpublished manuscripts:

Scott EA, Nichols MD, Willits RK, Elbert DL. Modular scaffolds assembled around living cells using poly(ethylene glycol) microspheres with macroporation via a non-cytotoxic porogen. *Acta Biomater.* (Under review).

Nichols MD, Scott EA, Elbert DL. Factors affecting size and swelling of poly(ethylene glycol) microspheres formed in aqueous sodium sulfate solutions without surfactants. *Biomaterials.* (Under review).

distribution of cells. Macropores were formed using porogenic PEG microspheres that dissolved within two days without affecting cell viability. Gradients in porosity were produced by varying the density of the porogenic microspheres. Bioactivity was introduced via cell adhesion peptides and delivery of sphingosine 1-phosphate, promoting endothelial cell infiltration through macropores in the scaffolds.

4.2 Introduction

Hydrogels made from synthetic polymers are promising as scaffolds for tissue engineering (Drury and Mooney 2003; Tessmar and Göpferich 2007). PEG-based scaffolds exhibit a high resistance to non-specific protein adsorption and are easily modified with peptides and proteins to impart biological functions such as cell adhesion or cell-initiated degradability (Jeon, Lee et al. 1991; Lutolf and Hubbell 2005). Growth factors and chemotactic factors may also be incorporated within hydrogels to promote cell proliferation, migration or vascularization (Richardson, Peters et al. 2001; DeLong, Moon et al. 2005). However, bulk PEG hydrogels effectively encapsulate the cells in polymer, potentially impacting cell survival, proliferation and migration (Lutolf and Hubbell 2005; Varghese and Elisseeff 2006). Porosity at multiple length scales may thus be desirable, with smaller pores providing a niche for functional cells and larger pores permitting vascularization (Hill, Boontheekul et al. 2006). Such multi-scale porous hydrogels can be formed with a variety of porogens, but a need exists for porogens that dissolve without compromising cell viability (Asnaghi, Giglio et al. 1995; Shapiro and Cohen 1997; Lévesque, Lim et al. 2005; Stachowiak, Bershteyn et al. 2005; Ford, Bertram et al. 2006; Sannino, Netti et al. 2006; Bryant, Cuy et al. 2007; Osathanon, Linnes et al. 2008). A non-cytotoxic porogen would permit incorporation

of cells at the time of scaffold formation, potentially leading to a more homogenous distribution of cells compared to cell seeding after scaffold formation.

Modular assembly of different types of microparticles is also desirable to allow versatility in engineering the properties of the scaffold (McGuigan and Sefton 2006; Yeh, Ling et al. 2006; Rivest, Morrison et al. 2007; Du, Lo et al. 2008; Pautot, Wyart et al. 2008; Serban and Prestwich 2008). Scaffolds for cell transplantation can be formed in a modular manner by assembling microparticles with different functionalities (Rivest, Morrison et al. 2007; Serban and Prestwich 2008). For example, modular scaffolds have been assembled from short tubes of collagen gels containing HepG2 hepatoma cells. The tubes were assembled into a highly porous structure and seeded with endothelial cells to produce a non-thrombogenic scaffold (McGuigan and Sefton 2006). Modular scaffolds may also be assembled from PEG microparticles formed in wells on a silicon wafer or by microfluidics (Yeh, Ling et al. 2006; Du, Lo et al. 2008). However, the scalability of many microparticle production techniques (e.g. micromolding, microfluidics, 3D printing) may be a concern due to the large number of microparticles required to form scaffolds of sufficient size for practical applications (Tsang and Bhatia 2004; Boland, Xu et al. 2006; Lu, Mapili et al. 2006; Yeh, Ling et al. 2006; Kim, Utada et al. 2007; Tan and Takeuchi 2007; Um, Lee et al. 2008).

Formation of hydrogel microspheres in solution addresses the issue of scalability but typically requires the use of organic solvents and surfactants in a two-phase system. These additives stabilize the size of the polymer-rich phases but may be difficult to remove from the formed microspheres, potentially affecting biocompatibility. Hennink and colleagues previously demonstrated that the phase separation of dextran and PEG in water may be used to produce crosslinked dextran or PEG microspheres without a surfactant (Franssen and Hennink 1998; Van Thienen, Demeester et al. 2008; Van Tomme, Mens et al. 2008). In this

system, the phase separated solutions were vigorously shaken before free-radical polymerization was initiated. Alternatively, hydrogel microspheres have been formed in water by copolymerizing PEG with a polymer that exhibits a lower critical solution temperature (LCST) near room temperature. For example, N-isopropylacrylamide monomer has been used to form microspheres that are about 60% PEG by mass via free-radical precipitation polymerization at 70°C (Nolan, Reyes et al. 2005). However, poly(N-isopropylacrylamide) itself is known to promote the adsorption of proteins at physiological temperature and thus maximizing the concentration of PEG in the scaffold is desirable (Kawaguchi, Fujimoto et al. 1992).

The LCST of low molecular weight PEG (up to 100 kDa) is above the boiling point of water but is greatly decreased in the presence of kosmotropic salts (e.g. sulfate, bicarbonate or phosphate anions) (Bailey and Callard 1959; Bae, Lambert et al. 1991). An advantage of using a salt for the formation of microspheres is that salts may be easily removed by washing, particularly when compared to polymers, organic solvents or surfactants. This ability allows the microspheres to be used in a variety of downstream biological applications that are extremely sensitive to hyperosmotic environments. Hennick and colleagues found that vigorous mixing of phase separated PEG/sodium sulfate solutions led to the formation of large aggregates of PEG microspheres upon polymerization, which was ascribed to the low viscosity of the solution (Franssen and Hennink 1998). Here, we report that 100% PEG microspheres can be formed in aqueous solutions without surfactants in the absence of mixing and by timing the gel point to occur prior to extensive coarsening of the phase-separated PEG-rich domains.

Phase separation occurs by nucleation and growth or by spinodal decomposition, dependent upon if the spinodal line is crossed. The binodal and spinodal lines are affected

by the molecular weight of the PEG, such that no single LCST may be associated with a PEG solution undergoing crosslinking. Furthermore, away from the critical concentration, single-phase solutions exist between the LCST and the binodal line. For simplicity, a cloud point temperature corresponding to the binodal line is often reported rather than an LCST (Bae, Lambert et al. 1991). Phase separation by nucleation or spinodal decomposition in a two-phase system results in a polydisperse mixture of phase-separated minority domains within the majority phase (J.D. Gunton 1983). Interfacial instability compels the minority phase droplets to minimize interfacial tension and area by reducing droplet curvature (Lifshitz and Slyozov 1961). Consequently, the minority phase domains grow in size over time, and this coarsening primarily occurs through the mechanisms of coalescence and/or Ostwald ripening (Friedlander 1977; Ratke and Voorhees 2002). In coalescence, droplets grow as they collide and merge while moving through the majority phase due to hydrodynamic flow and Brownian motion (Friedlander and Wang 1966). Ostwald ripening reduces the interfacial area of minority phase domains via the diffusional mass transfer of molecules from regions of high interfacial curvature to regions of low interfacial curvature (Ostwald 1900; Lifshitz and Slyozov 1961; Voorhees 1992). The growth of phase-separated domains through either or both coalescence and Ostwald ripening displays the same time dependence of $\bar{r} \propto \text{time}^{\frac{1}{3}}$, where \bar{r} is the average droplet radius (Lifshitz and Slyozov 1961; Friedlander and Wang 1966; Crist and Nesarikar 1995). Given enough time, the phase domains will coarsen into a single homogenous layer, which in colloidal systems is referred to as a coacervate layer (Bungenberg de Jong 1949).

We have formed PEG hydrogel microspheres in aqueous sodium sulfate solutions by crosslinking PEG derivatives while above the cloud point and during the early stages of coarsening. Gelation was achieved via conjugate addition reactions between electrophilic

vinylsulfone or acrylate groups on eight-arm PEG (PEG₈-vinylsulfone or PEG₈-acrylate, mol. wt. 10 kDa) and nucleophilic amines on eight-arm PEG (PEG₈-amine, mol. wt. 10 kDa) or bovine serum albumin (BSA) (Figure 1a) (Elbert, Pratt et al. 2001; Wacker, Scott et al. 2006). We utilized this reaction to produce three types of microspheres: 1) PEG₈-vinylsulfone/PEG₈-amine microspheres containing RGD peptides for structural support, biocompatibility, and cell adhesion, 2) PEG₈-acrylate/PEG₈-amine microsphere containing hydrolyzable ester bonds to provide porosity, 3) PEG₈-vinylsulfone/BSA microspheres for the delivery of sphingosine 1-phosphate (S1P), a bioactive lipid that enhances endothelial cell migration and is released from PEG/BSA hydrogels in controlled manner due to affinity interactions with BSA (English, Welch et al. 2000; Wacker, Scott et al. 2006) (Figure 4.1). Unreacted vinylsulfone moieties on the surfaces of these microspheres were further crosslinked with serum proteins to form three-dimensional scaffolds in the presence of HepG2 hepatoma cells (Figure 4.2). Within 48 h, the PEG₈-acrylate/PEG₈-amine microspheres dissolved, producing a porous scaffold capable of supporting endothelial cell infiltration. Furthermore, degradable 100% PEG microspheres were shown to be non-cytotoxic, permitting macropore formation in the presence of living cells.

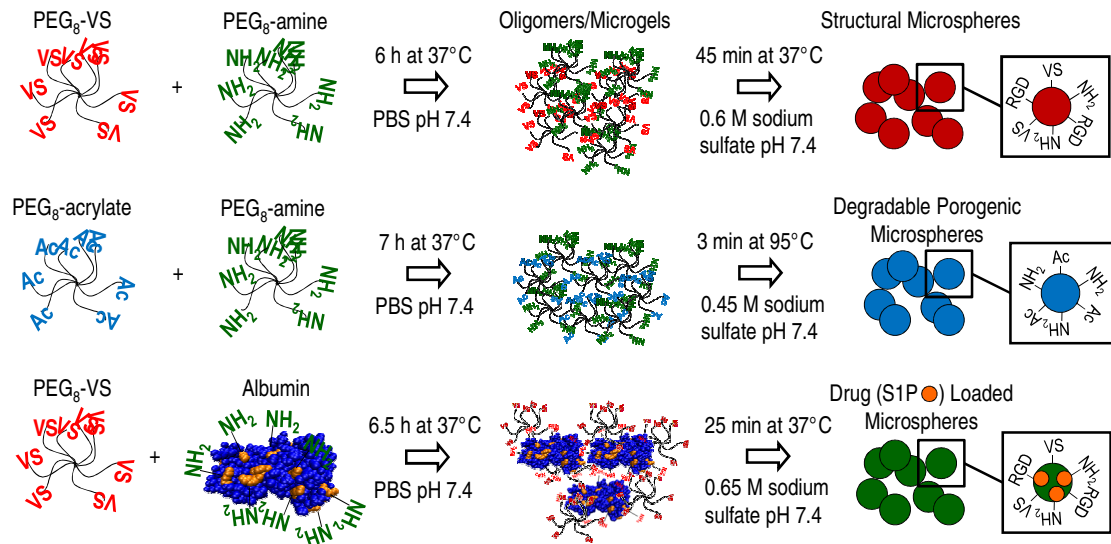


Figure 4.1: Production of PEG microspheres in aqueous sodium sulfate solutions. Eight-arm PEG-vinylsulfone (PEG₈-VS) was reacted with eight-arm PEG-amine (PEG₈-amine) in PBS. The Michael-type reaction was followed by dynamic light scattering to detect the formation of PEG oligomers/microgels during crosslinking. At a certain mean effective diameter (d_{PCS}), sodium sulfate was added and the solution was heated above the cloud point. A similar strategy was followed with eight arm PEG-acrylate (PEG₈-acrylate) and PEG₈-amine to produce porogenic microspheres. Microspheres were produced for the delivery of sphingosine 1-phosphate (S1P) to promote endothelial cell migration by reacting PEG₈-VS with bovine serum albumin (BSA).

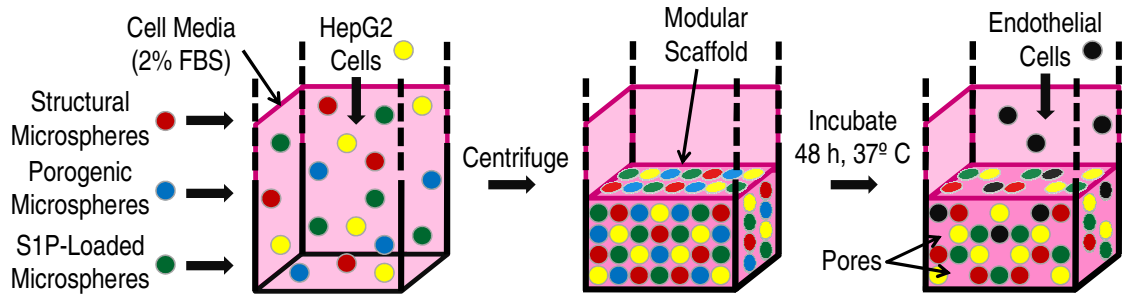


Figure 4.2: Assembly of microspheres into bioactive modular scaffolds in the presence of living cells. Microspheres with different functionalities were mixed with HepG2 hepatoma cells in medium containing 2% serum and centrifuged for 10 min at 1000g and allowed to crosslink overnight at 37°C. Within 48 h, PEG₈-acrylate/PEG₈-amine microspheres dissolved to form macroporous scaffolds. Endothelial cells seeded on the scaffolds adhered via RGD peptide incorporated in the non-degradable microspheres.

4.3 Materials and Methods

4.3.1 PEG Derivatives

Unless otherwise noted, all reagents were purchased from Sigma-Aldrich. Eight-arm PEG-OH (PEG₈-OH; mol. wt. 10,000; Shearwater Polymers, Huntsville, AL) was used to synthesize PEG₈-vinylsulfone (PEG₈-VS), PEG₈-amine, and PEG₈-acrylate as previously described (Elbert and Hubbell 2001; Scott, Nichols et al. 2008). Stock solutions of PEG₈-VS, PEG₈-amine, PEG₈-acrylate, and fatty acid-free bovine serum albumin (BSA) solutions were prepared at 20%(w/v) in Dulbecco's phosphate buffered saline (Pierce) and sterile filtered with 0.22 μm syringe filters. For fluorescent labeling, stock solutions of PEG₈-amine or BSA in PBS were reacted with a 10 mg/mL solution of Dylight-488 or Dylight-633 (Pierce) in dimethylformamide at a 100:1 molar ratio of PEG:dye or BSA:dye overnight at room temperature.

4.3.2 Dynamic Light Scattering

Dynamic light scattering/photon correlation spectroscopy (DLS/PCS; 90Plus Particle Size Analyzer, Brookhaven Instruments, Holtsville, NY) was performed at a scattering angle of 90° and wavelength of 658 nm. Calculation of d_{PCS} and statistical analysis of the results were performed using Brookhaven Instruments Particle Sizing Software (version 2.34, Brookhaven Instruments).

4.3.3 Microsphere Fabrication and Characterization

PEG₈-VS/PEG₈-amine microspheres were fabricated from pre-reacted solutions of PEG₈-VS and PEG₈-amine (20%(w/v) PEG in PBS, 37°C, reacted to $d_{\text{PCS}} \cong 100$ nm unless otherwise stated; pre-reacted solutions could be stored at -80°C for at least five months). Pre-reacted solutions were diluted to 2%(w/v) PEG at room temperature with PBS and PBS + 1.5 M sodium sulfate to achieve a final sodium sulfate concentration of 0.6 M and volume of 50 μ L. The solutions were then heated above the cloud point to 37°C for 45 min unless otherwise stated. Suspensions of microspheres were buffer exchanged into PBS 2x to remove the sodium sulfate, diluting the microsphere solution 3:1 with PBS and titrating and centrifuging at 14,100g for 2 min. For zeta potential measurements, PEG₈-VS and PEG₈-amine microspheres were formed as described above. PEG₈-VS /BSA microspheres were formed by pre-reaction of PEG₈-VS and BSA (12%(w/v) BSA + 8%(w/v) PEG in PBS, 37°C, reacted to $d_{\text{PCS}} \cong 100$ nm), dilution 10x at room temperature to obtain PBS + 0.65 M sodium sulfate and reaction for 25 min at 37°C. The number of reactive amines per BSA was assumed to be 36.(Wacker, Scott et al. 2006) PEG₈-acrylate and PEG₈-amine were pre-reacted (20%(w/v) PEG in PBS, 37°C, reacted to $d_{\text{PCS}} \cong 100$ nm), diluted 10x at room temperature to obtain PBS + 0.45 M sodium sulfate and reacted for 10 min at 95°C. For confocal microscopy, microspheres were formed as described above, except in PBS + 0.8 M sodium sulfate to cause phase separation at room temperature. Samples were held above the cloud point at room temperature for 5 min prior to reaction at the temperature and time stated above.

4.3.4 Microsphere Fabrication for Scaffolds

S1P was dissolved in methanol at 0.5 mg/mL and divided into 287 nmol aliquots in Eppendorf tubes. The methanol solutions were dried under nitrogen. The tubes were filled with 20% (w/v) BSA in PBS (1 nmol S1P/mg BSA) and rotated at 37°C until completely solubilized. Pre-reacted solutions of PEG₈-VS/PEG₈-amine (2:1 VS:amine, $d_{\text{PCS}} \cong 50$ nm, 20%(w/v) PEG) or PEG₈-VS/BSA/S1P (2:1 VS:amine, $d_{\text{PCS}} \cong 50$ nm, 8.5%(w/v) BSA + 11.5%(w/v) PEG) were reacted for 30 min at 37°C with RGD peptide (sequence: GCGYGRGDSPG, Genscript Corp.) at an RGD concentration of 5.5 mM. (Wacker, Scott et al. 2006) Pre-reacted PEG₈-VS/PEG₈-amine solutions (25 μ L) were diluted 10x to obtain PBS + 0.6 M sodium sulfate. PEG₈-VS/PEG₈-amine microspheres were formed by incubation of this solution for 45 min at 37°C. Pre-reacted PEG₈-VS/BSA/S1P solutions (25 μ L) were diluted 10x to obtain PBS + 0.65 mM sodium sulfate. PEG₈-VS/BSA/S1P microspheres were formed by incubation of this solution for 25 min at 37°C. Pre-reacted PEG₈-acrylate/PEG₈-amine solutions (1:1 acrylate:amine, $d_{\text{PCS}} \cong 100$ nm, 20%(w/v) PEG, 25 μ L) were diluted 10x to obtain PBS + 0.45 mM sodium sulfate. PEG₈-acrylate/PEG₈-amine microspheres with low, medium, or high densities were formed by incubation of this solution at 95°C for 3 min, 5 min, or 10 min, respectively. Microsphere suspensions were buffer exchanged first into PBS and then into endothelial growth medium (EGM; MCDB 131 medium supplemented with 10 ng/mL epidermal growth factor, 10 mg/mL heparin, 1.0 mg/mL hydrocortisone, 1% penicillin–streptomycin, 2% FBS, and 12 mg/mL bovine brain extract; Clonetics).

4.3.5 Scaffold Assembly and Cell Seeding

PEG₈-VS/PEG₈-amine microspheres, PEG₈-VS/BSA microspheres and PEG₈-acrylate/PEG₈-amine microspheres (1:1:1 of washed microsphere solutions) were combined and briefly mixed by titration with 5×10^5 HepG2 cells in EGM in UV/vis cuvettes (Brookhaven Instruments Corporation) to a final volume of 1 mL. Microspheres and cells were centrifuged for 10 min at 1000g. Scaffolds were incubated for 48 h at 37°C followed by

replacement of the medium with fresh EGM containing 5×10^5 endothelial cells. Live/dead assays were performed by incubating scaffolds for 30 min at 37°C with EGM containing 12 μM fluorescein diacetate (Sigma) and 250 μM ethidium bromide (Pierce).

4.3.6 Confocal Microscopy

Fluorescence microscopy was performed with a Nikon Eclipse C1/80i confocal microscope. Suspensions of fluorescently-labeled microspheres were imaged on glass microscope slides (Corning Inc.) with a 20X objective (0.45 DIC L WD 7.4). Scaffolds were imaged in EGM and within UV/vis cuvettes with a 10X objective (0.3 DIC L/N1 WD 16.0). Images were processed and rendered in 3D using EZ-C1 3.70 FreeViewer software (Nikon Instruments Inc.).

4.3.7 Rheometry

Storage (G') and loss (G'') moduli of bulk hydrogels and scaffolds were measured at room temperature with oscillatory shear rheometry (25 mm parallel plate) on a fluids rheometer (RFS3, Rheometric Scientific). Viscoelasticity was measured at 5% strain within a frequency range of 1-100 Hz. Scaffolds (1 mm thickness) were formed from PEG₈-VS/PEG₈-amine microspheres (2:1 VS:amine) as above, with centrifugation in silanized (Sigmacote) glass vials (25 mm diameter). Bulk hydrogels were prepared *in situ* on the surface of the 25 mm parallel plate by mixing 200 mg/mL solutions of PEG₈-VS (200 μL) and PEG₈-amine (200 μL) in PBS pH 10.0 at a 1:1 ratio.

4.3.8 Statistics

A p -value < 0.05 was considered significant. Data were mean \pm standard deviation.

4.4 Results

4.4.1 Formation of PEG-VS/PEG-Amine Microspheres

Reaction of PEG derivatives above the cloud point led to microsphere formation only under specific conditions. To form microspheres at pH 7.4 and 37°C within 45 min, initial reaction of the PEG macromonomers below the cloud point was required ('pre-reaction'). We previously demonstrated that the extent of the crosslinking reaction between eight-arm PEG-vinylsulfone (PEG₈-VS; 10 kDa) and eight-arm PEG-amine (PEG₈-amine; 10 kDa) at 20%(w/v) PEG and 37°C in phosphate buffered saline (PBS, pH 7.4) could be monitored with dynamic light scattering (DLS) (Scott, Nichols et al. 2008). Well before gelation, PEG oligomers/microgels with hydrodynamic radii ≥ 10 nm were observed by DLS and reached a mean effective diameter (d_{PCS}) of about 180 nm just prior to bulk gelation, which normally occurred after 6.5 h. To form microspheres, solutions with $d_{\text{PCS}} \cong 100$ nm by DLS were diluted to 2%(w/v) PEG in PBS + 0.6 M sodium sulfate at room temperature and raised above the cloud point to 37°C. These conditions allowed mixing of polymer and salt at room temperature and did not lead to bulk gelation while the solution was heated to the cloud point. Above the cloud point, the spherical PEG-rich domains coarsened and crosslinked over the course of 45 min, resulting in the formation of stable PEG

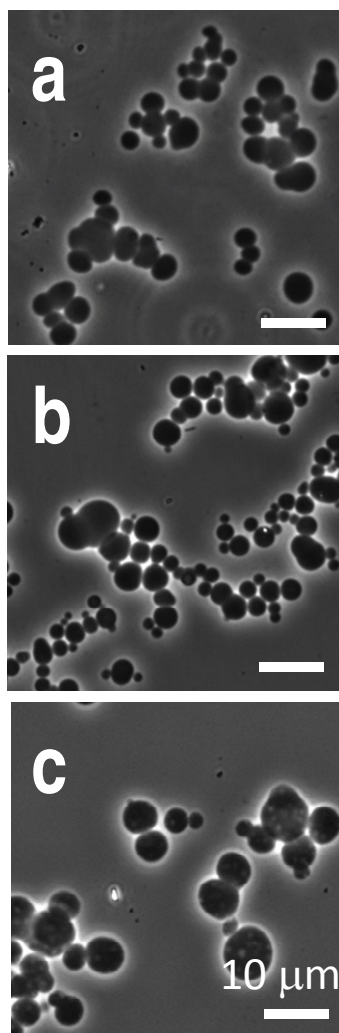


Figure 4.3: PEG or PEG/BSA microspheres were formed above the cloud point and then buffer exchanged into PBS. Phase-contrast photomicrographs with a 20X objective of: (a) PEG₈-VS/PEG₈-amine (b) PEG₈-acrylate/PEG₈-amine and (c) PEG₈-VS/BSA microspheres. Scale bar = 10 μm .

microspheres. Following buffer exchange into PBS, the microspheres had mean diameters of $6.65 \pm 1.65 \mu\text{m}$ and a polydispersity of 1.59^\dagger (Figure 4.3a). In contrast, when PEG₈-VS and PEG₈-amine were mixed and immediately heated above the cloud point (i.e. without pre-reaction), stable microspheres did not form after 45 min and further incubation overnight produced a bulk hydrogel (Table 4.1, Fig 4.4). However, pre-reaction was not necessary to form microspheres if the solution of PEG₈-VS and PEG₈-amine was rapidly heated to 95°C instead of 37°C (Table 4.1 & Figure 4.4). The rate of coarsening affected microsphere formation, as samples formed bulk gels within 45 min when vortexed above the cloud point or when prepared with PBS + 1.5 M sodium sulfate (Table 1, Figure 4.4 & 4.5)[‡]. Presumably, vortexing increased the encounter rate between the phase-separated domains while high salt promoted ‘floating’ of the PEG-rich phase. The critical factor for microsphere formation was thus the balance between the rates of gelation and coarsening.

The importance of pre-reacting the components before phase separation may have been due to the dramatic difference in the cloud point between PEG₈-VS and PEG₈-amine. The cloud point of 2% (w/v) PEG₈-VS in PBS + 0.6 M sodium sulfate was close to room temperature, while the cloud point of the cationic PEG₈-amine was $>100^\circ\text{C}^\dagger$. Eight-arm PEG-acrylate (PEG₈-acrylate, 10 kDa) was found to phase separate at lower temperatures than PEG₈-VS[†]. DLS was used to investigate the effects of the charged PEG₈-amine on the early stages of coarsening above the cloud point of PEG₈-VS (Figure 4.6). A linear relationship was found between the mean diameter of the phase-separated domains and time, which is expected in the early stages of phase separation (Crist 1996). A plateau in

[†] Microsphere sizing was performed by Michael D. Nichols using phase contrast photomicrographs of microspheres at 20X. Briefly, >500 microspheres from three separately prepared samples were manually thresholded and quantified with ImageJ software (NIH).

[‡] Data was collected by Michael D. Nichols

Table 4.1: Summary of products resulting from microsphere fabrication methods

| Salt conc. (M sodium sulfate +PBS; pH 7.4) | Pre-reaction (below the cloud point) (d_{PCS}) | Reaction temperature and time (above the cloud point) | Result | Image |
|--|--|---|-----------------------------------|------------------------|
| PEG ₈ -vinylsulfone/PEG ₈ -amine | | | | |
| 0.6 | None | 37°C, 45 min | No microspheres or gel | Figure 4.4d |
| 0.6 | None | 37°C, overnight | Bulk gel of microspheres | Figure 4.4a |
| 0.6 | None | 95°C, 3 min | Microspheres | Figure 4.4b |
| 0.6 | 100 nm | 95°C, 3 min | Microspheres | Figure 4.4c |
| 0.6 | 100 nm | 37°C, 45 min | Microspheres | Figure 4.3a |
| 0.6 | 100 nm | 37°C, 45 min, with 5 min vortex | Bulk gel with irregular structure | Figure 4.5 |
| 1.5 | None | 95°C, 5 min | Bulk gel of microspheres | Figure 4.4e |
| 1.5 | 100 nm | 95°C, 5 min | Bulk gel of microspheres | Rig. 4.4f |
| PEG ₈ -acrylate/PEG ₈ -amine | | | | |
| 0.45 | 100 nm | 95°C, 10 min | High density microspheres* | Figure 4.15a(i) |
| 0.45 | 100 nm | 95°C, 5 min | Medium density microspheres* | Figure 4.3b, 4.15a(ii) |
| 0.45 | 100 nm | 95°C, 3 min | Low density microspheres* | Figure 4.15a |
| PEG ₈ -vinylsulfone/BSA | | | | |
| 0.65 | 100 nm | 37°C, 25 min | Medium density microspheres* | Figure 4.3c |
| 0.65 | 100 nm | 95°C, 10 min | Denatured BSA | - |

*Density is relative to PEG₈-vinylsulfone/PEG₈-amine microspheres ($d_{PCS} = 100$ nm, 45 min at 37°C in PBS + 0.6 M sodium sulfate)

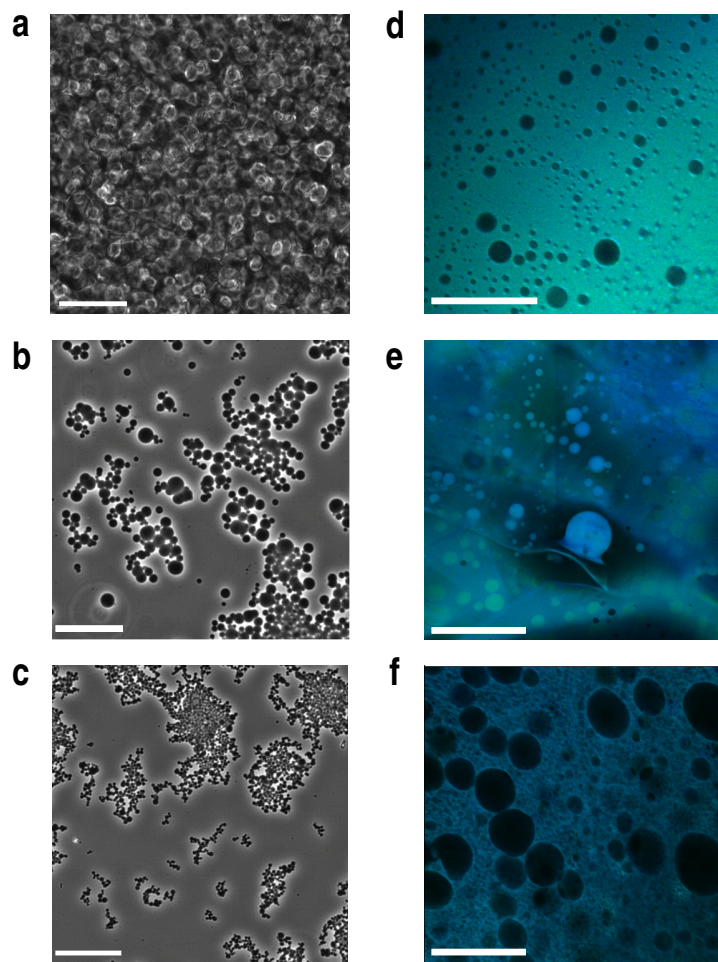


Figure 4.4: Formation of microspheres was influenced by pre-reaction of PEG derivatives below the cloud point. PEG₈-VS/PEG₈-amine microspheres were formed with or without pre-reaction followed by dilution to 2%(w/v) PEG in PBS + sodium sulfate. Phase-contrast photomicrographs at 20X of: (a) Bulk gel formed from aggregated and crosslinked microspheres fabricated without pre-reaction, PBS + 0.6 M sodium sulfate, 37°C for 12 h (scale bar = 100 μm), (b) No pre-reaction, PBS + 0.6 M sodium sulfate, 95°C for 3 min (scale bar = 50 μm), and (c) Pre-reaction to $d_{\text{PCS}} \cong 100$ nm, PBS + 0.6 M sodium sulfate, 95°C for 3 min (scale bar = 50 μm). Confocal microscopy at 10X of fluorescent PEG₈-VS (green) and PEG₈-amine (blue) reacted under different conditions: (d) No pre-reaction, PBS + 0.6 M sodium sulfate, 37°C for 45 min (scale bar = 50 μm), (e) No pre-reaction, PBS + 1.5 M sodium sulfate, 95°C for 5 min (scale bar = 200 μm), (f) Pre-reaction to $d_{\text{PCS}} \cong 100$ nm, PBS + 1.5 M sodium sulfate, 95°C for 5 min (scale bar = 200 μm).

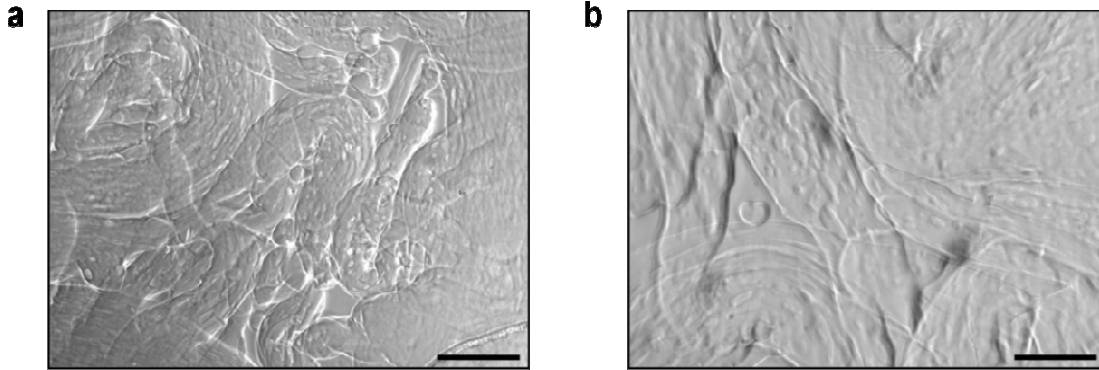


Figure 4.5: Crosslinking with vortexing during the initial reaction produced bulk hydrogels. Pre-reacted PEG₈-VS and PEG₈-amine (1:1 VS:amine, $d_{\text{PCS}} \cong 100$ nm, 20%(w/v)) were diluted 10x to 2%(w/v) in PBS + 0.6 M sodium sulfate. Solutions were vortexed for the first 5 min after the temperature was raised to 37°C, resulting in the formation of white precipitates. The sample was then incubated without mixing at the same temperature for an additional 40 min. Phase-contrast photomicrographs at (a) 10X (scale bar = 100 μm) and (b) 20X (scale bar = 200 μm) reveal a bulk hydrogel with an irregular structure.

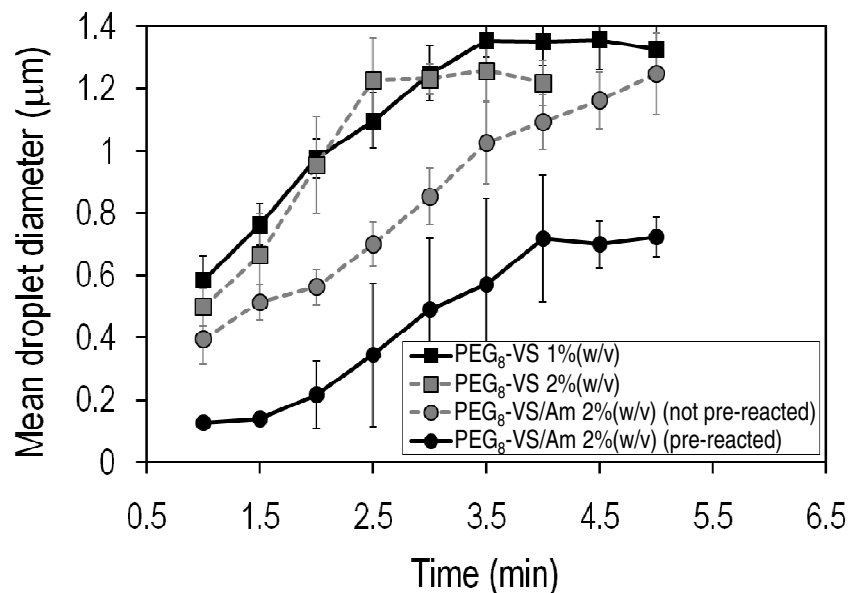


Figure 4.6: DLS of PEG solutions above their cloud points demonstrated that mean effective droplet diameters (d_{PCS} values) increased linearly with time during early stages of coarsening, as expected for this process by coalescence or Ostwald ripening. Later, an apparent regime change to slower growth with time was observed, possibly corresponding to a percolation-to-cluster transition. Both decreasing the concentration of PEG₈-VS and mixing PEG₈-Am with the PEG₈-VS (PEG₈-VS/Am) slowed coarsening. Pre-reaction of these components to $d_{\text{PCS}} \cong 100$ nm further reduced the rate of coarsening. Data represent three independent samples averaged over 10 runs.

coarsening was reached 3-5 minutes after phase separation that may correspond to a percolation-to-cluster transition (Crist 1996). The rate of coarsening of a PEG₈-VS solution was not greatly affected by the presence of PEG₈-amine if the two components were mixed just prior to raising the temperature above the cloud point. However, pre-reaction of PEG₈-VS with PEG₈-amine to a $d_{\text{PCS}} \cong 100$ nm increased the cloud point and produced a plateau in coarsened microsphere size at 700 nm instead of 1400 nm, indicating that PEG₈-amine may have had a stabilizing or emulsifying effect on the phase-separated PEG.

4.4.2 Formation of PEG-Acrylate/PEG-Amine and PEG-VS/BSA Microspheres

Having found suitable conditions for stable microsphere formation, we then produced degradable microspheres for macropore formation and PEG/protein microspheres for drug delivery (Figure 4.3b,c). To fabricate degradable microspheres, eight-arm PEG-acrylate (PEG₈-acrylate; 10 kDa) was reacted with PEG₈-amine. Hydrolysis of the ester bonds present due to the acrylate provided a mechanism for dissolution of the microspheres (Elbert, Pratt et al. 2001). Compared to vinylsulfone, the acrylate group has a slightly lower reactivity towards amines (Friedman 1965). The slower kinetics of the reaction were overcome by pre-reaction to a $d_{\text{PCS}} \cong 100$ nm and incubation for 5 min at 95°C in PBS + 0.45 M sodium sulfate at 2%(w/v) PEG (Table 4.1). PEG/BSA microspheres were produced for delivery of S1P from the scaffolds, since we previously demonstrated that controlled release of S1P from PEG/BSA hydrogels enhances endothelial cell migration (Wacker, Scott et al. 2006). The biocompatibility of PEG/BSA and 100% PEG hydrogel surface coatings was previously compared and both were found to be highly resistant to

non-specific cell adhesion (Scott, Nichols et al. 2008). In contrast to the 100% PEG microspheres, production of PEG/BSA microspheres could not be performed at high temperature due to denaturation of the BSA (Table 1). Formation of microspheres at 37°C required pre-reaction of PEG₈-VS with amine groups on BSA. PEG₈-VS was pre-reacted with BSA to a $d_{\text{PCS}} \cong 100$ nm, followed by incubation for 25 min at 37°C in PBS + 0.65 M sodium sulfate at 0.8%(w/v) PEG and 1.2%(w/v) BSA. A negative zeta potential was observed for the PEG/BSA microspheres due to the presence of BSA, while microspheres made with PEG₈-amine were positively charged (Figure 4.7).

4.4.3 Microsphere Ripening and Coalescence

Microsphere coarsening and crosslinking were further investigated using fluorescently labeled microspheres. To observe Ostwald ripening, solutions of fluorescent PEG₈-vinylsulfone (green) and fluorescent PEG₈-amine (blue) were separately raised above their cloud points in PBS + 1.2 M sodium sulfate and then mixed (Figure 4.8a). Over time, the fluorescent PEG derivatives transferred between the two types of spherical domains without observing coalescence. The exchange must have occurred via mass transfer through the majority phase, indicating that Ostwald ripening occurs during coarsening of the PEG domains. Transfer of fluorescent PEG from smaller to larger droplets was additionally observed to occur (Figure 4.8b). A salt concentration more typical for microsphere formation (PBS + 0.6 M sodium sulfate) was used to observe coalescence. Fluorescent PEG₈-vinylsulfone and fluorescent PEG₈-amine were pre-reacted to a d_{PCS} of 100 nm. The solution was then heated for 15 min at 37°C, followed by visualization on a confocal microscope. PEG-rich domains with different ratios of PEG₈-vinylsulfone (green) and PEG₈-amine (blue) were found, as judged by the relative fluorescence intensities. Some of

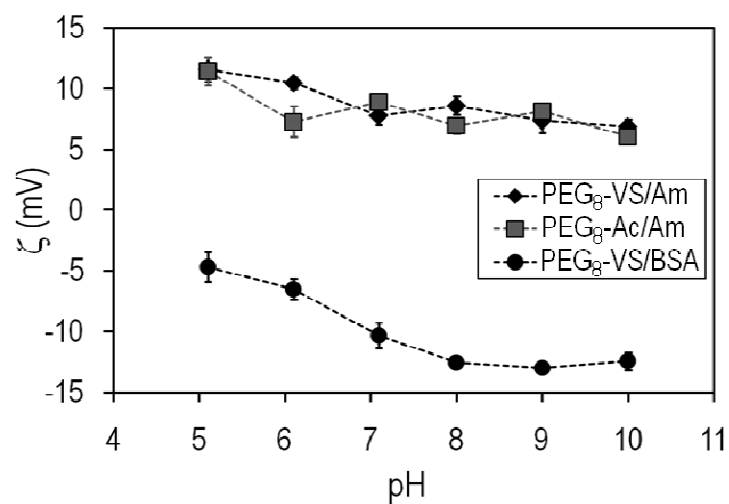


Figure 4.7: Zeta potentials of microspheres were determined by the charge of the crosslinker. Zeta potentials of PEG₈-VS/PEG₈-amine (PEG₈-VS/Am), PEG₈-acrylate/PEG₈-amine (PEG₈-Ac/Am), and PEG₈-VS/BSA microspheres were measured. Net positively charged microspheres formed when crosslinked with PEG₈-amine and net negatively charged microspheres formed when crosslinked with BSA. Data represent $n = 3$ independent samples averaged over 10 runs each.

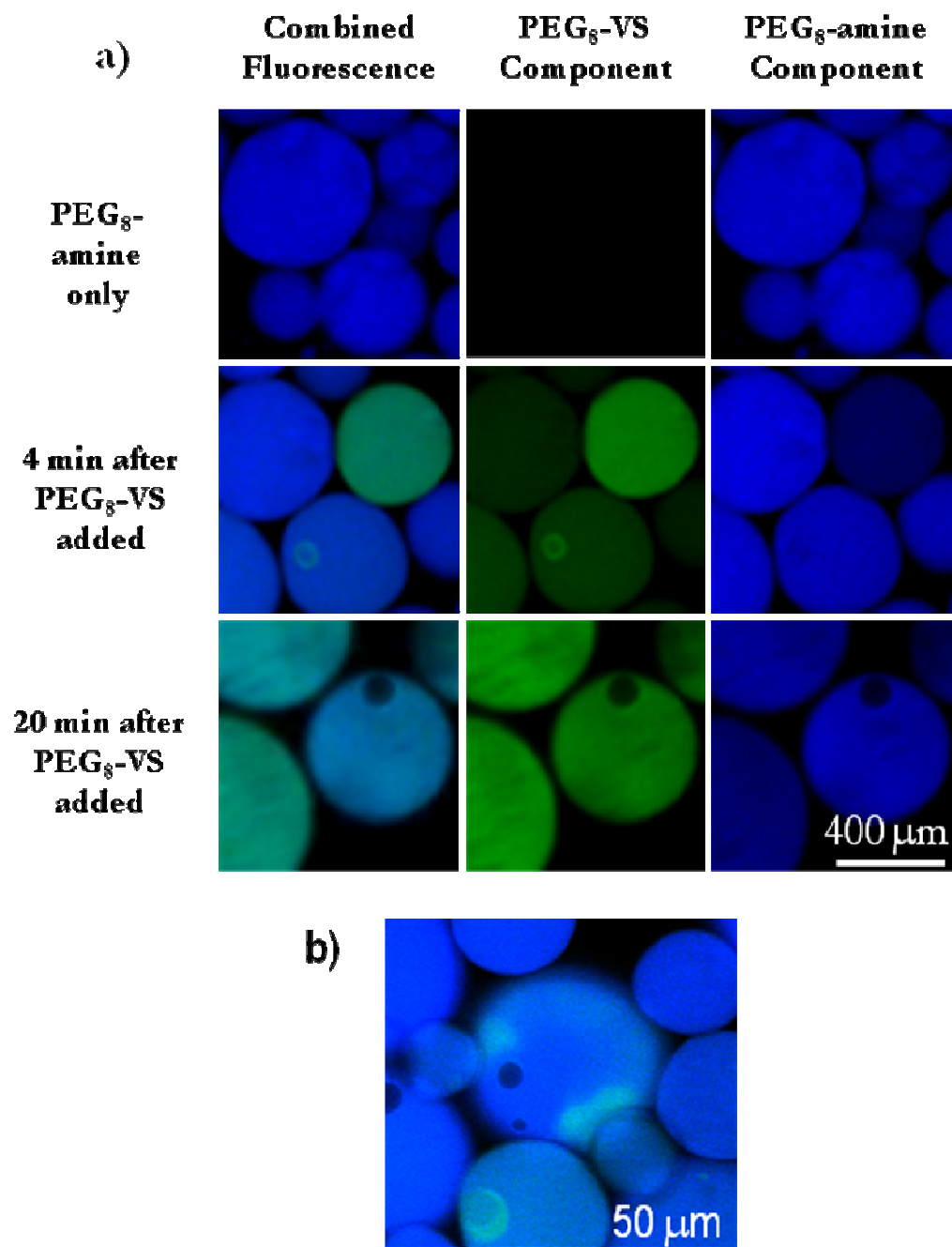


Figure 4.8: The formation of PEG₈-VS/PEG₈-amine microspheres was monitored by confocal microscopy at 20X magnification using fluorescently labeled PEG. (a) PEG₈-VS (green) and PEG₈-amine (PEG₈-Am; blue) were separately added to PBS + 1.2 M sodium sulfate to cause phase separation of both polymers at room temperature. The phase separated solutions were then mixed. Mass transfer occurred between the droplets without coalescence, indicating that Ostwald ripening occurred. (b) Mass transfer was also directly observed under these same conditions between touching PEG-rich droplets.

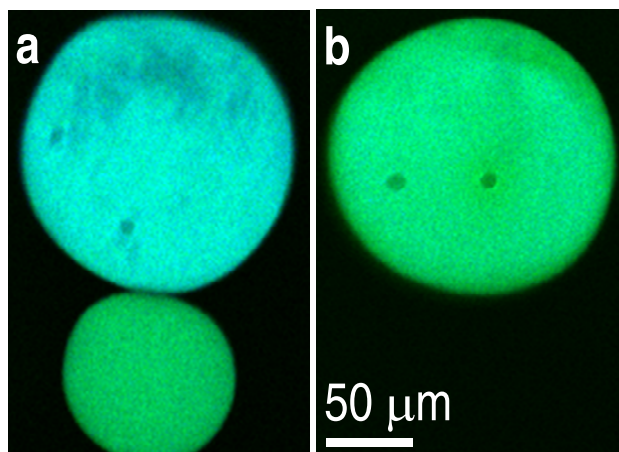


Figure 4.9: PEG-rich droplets before (a) and after (b) coalescence. PEG₈-VS (green) was pre-reacted with PEG₈-amine (blue) to $d_{\text{PCS}} \cong 100$ nm and then crosslinked above the cloud point for 15 min at 37°C in PBS + 0.6 M sodium sulfate.

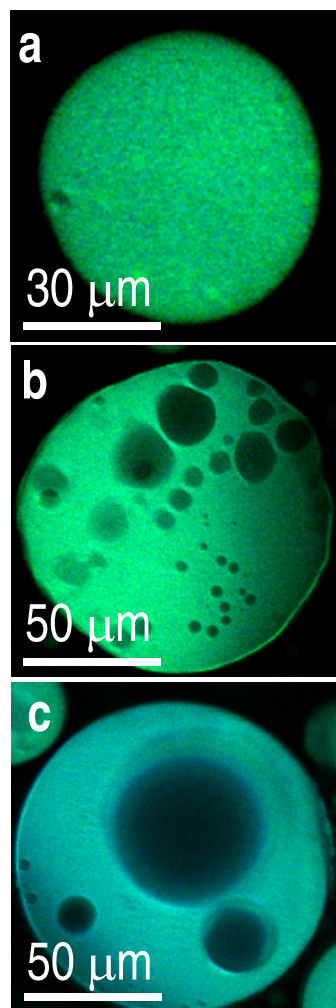


Figure 4.10: Water-rich droplets were observed while monitoring the formation of PEG₈-VS/PEG₈-amine microspheres by confocal microscopy at 20X magnification. Fluorescently labeled PEG₈-VS (green) was mixed with PEG₈-amine (blue) in PBS + 0.6 M sodium sulfate and heated at 37°C for 15 min: (a-c) progression of coarsening of water-rich domains within PEG-rich droplets over 15 min.

these spherical domains were observed to coalesce, forming larger spheres with an intermediate ratio of the two types of PEG (Figure 4.9). Over the course of 20 min, coalescence of PEG-rich domains became less frequent and unlabeled regions began to appear (Figure 4.10). Since both PEG derivatives were fluorescently labeled, the unlabeled regions signified the presence of a water-rich, polymer-poor phase. Water-rich domains grew in size within the PEG-rich spherical domains. Eventually, the water-rich droplets ceased to grow in size suggesting that the PEG-rich domains had reached the gel point. Additionally, small domains of PEG₈-VS were often found to form within larger PEG₈-amine phases and vice versa, sometimes producing multiple emulsions (Figure 4.11). To better visualize the structure of the formed microspheres, relatively large fluorescent microspheres ($\approx 100 \mu\text{m}$ instead of $\approx 10 \mu\text{m}$) were generated by lowering the cloud point to room temperature and allowing the solution to coarsen for 5 min before raising the temperature to 37°C for 45 min. Results revealed that after gelation the water-rich domains became pores in the microspheres (Figure 4.12a). Degradable PEG₈-acrylate/PEG₈-amine and PEG₈-VS/BSA microspheres possessed the same porous structures (Figure 4.12b,c).

4.4.4 Assembly of Modular Scaffolds

After formation, microspheres were buffer exchanged into PBS or cell culture medium and reacted to form scaffolds. Unreacted vinylsulfone and amine groups were present on the surfaces of the microspheres, evidenced by the aggregation and crosslinking of microspheres overnight in PBS. To increase the availability of reactive groups for scaffold formation, microspheres were produced with 2:1 or 1:2 ratios of PEG₈-VS to PEG₈-amine. The 2:1 and 1:2 ratio microspheres were mixed in PBS and compacted by centrifugation in UV/vis cuvettes, permitting *in situ* visualization by confocal microscopy.

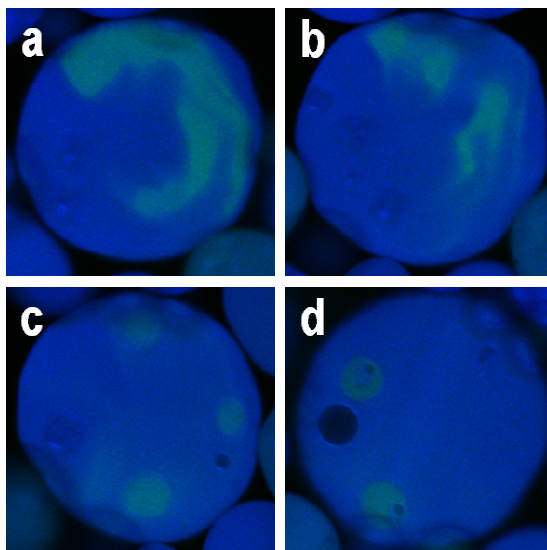


Figure 4.11: PEG₈-VS and PEG₈-amine domains were found to form multiple emulsions following coalescence. (a-d) Progression of multiple emulsion formation within a PEG-amine droplet. The final multiple droplet (d) is a PEG-amine/PEG-VS/PEG-amine/water emulsion.

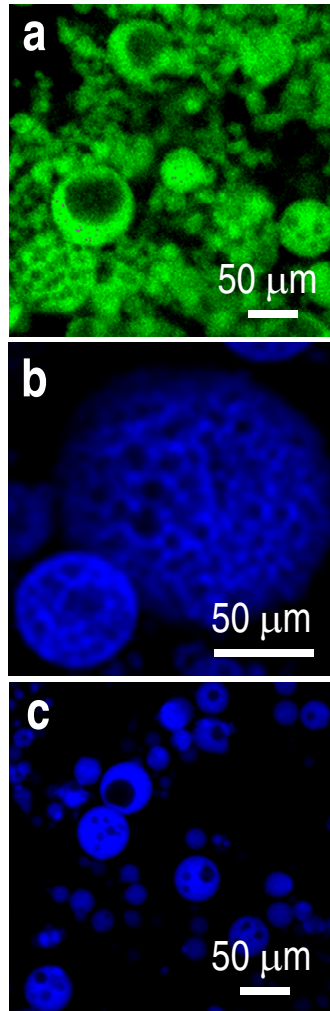


Figure 4.12: To visualize the porous structure, larger microspheres were produced by pre-reacting all samples to $d_{pCS} \cong 100$ nm and diluting in PBS + 0.8 M sodium sulfate, followed by reaction for 5 min above the cloud point at 25°C prior to further reaction as noted: (a) PEG₈-VS/PEG₈-amine (green), 37°C for 45 min (b) PEG₈-acrylate/PEG₈-amine (blue), 95°C for 5 min. (c) PEG₈-VS/BSA (blue), 37°C for 45 min. Scale bar = 50 μm.

Stable scaffolds formed after 200 min at 2000g, conditions that may not be favorable for cell survival. However, 2:1 ratio microspheres formed stable scaffolds when centrifuged for 10 min at 1000g in the presence of cell culture medium containing 2% serum followed by an overnight incubation at 37°C. The presence of 2% serum was necessary for scaffold formation, indicating that serum proteins served to crosslink the microspheres via reaction of amines on the proteins with vinylsulfone groups on the microspheres. Scaffolds supported their own weight in medium (Figure 4.13a) and had storage moduli that were about an order of magnitude lower than bulk hydrogels formed from the same reactants (Figure 4.13b). The storage moduli of the scaffolds were similar to liver tissue and higher than Matrigel or collagen gels (Raeber, Lutolf et al. 2005; Cullen, Lessing et al. 2007; Levental, Georges et al. 2007; Lai, Li et al. 2008). Scaffolds with greater stiffnesses were fabricated by crosslinking microspheres above the cloud point, but these conditions were not amenable to forming scaffolds in the presence of cells (Figure 4.14a). When placed in high concentration salt solutions that decreased the cloud point to \leq room temperature, assembled scaffolds responded by shrinking in size by up to 300%, possibly due to a combination of water extrusion and osmotic pressure (Figure 4.14b).

The distribution of macropores was controlled by the density (i.e. buoyancy) of the porogenic microspheres relative to the other microsphere types. The density of the PEG₈-acrylate/PEG₈-amine microspheres was changed by varying the length of the reaction at 95°C from 3 min to 10 min during their formation. Upon centrifugation, PEG₈-acrylate/PEG₈-amine microspheres migrated to different locations relative to PEG₈-VS/BSA microspheres, producing gradients in porogenic microspheres (Figure 4.15). If the densities of the different microsphere types were matched by selecting appropriate microsphere formation conditions, scaffolds assembled from PEG₈-VS/PEG₈-amine

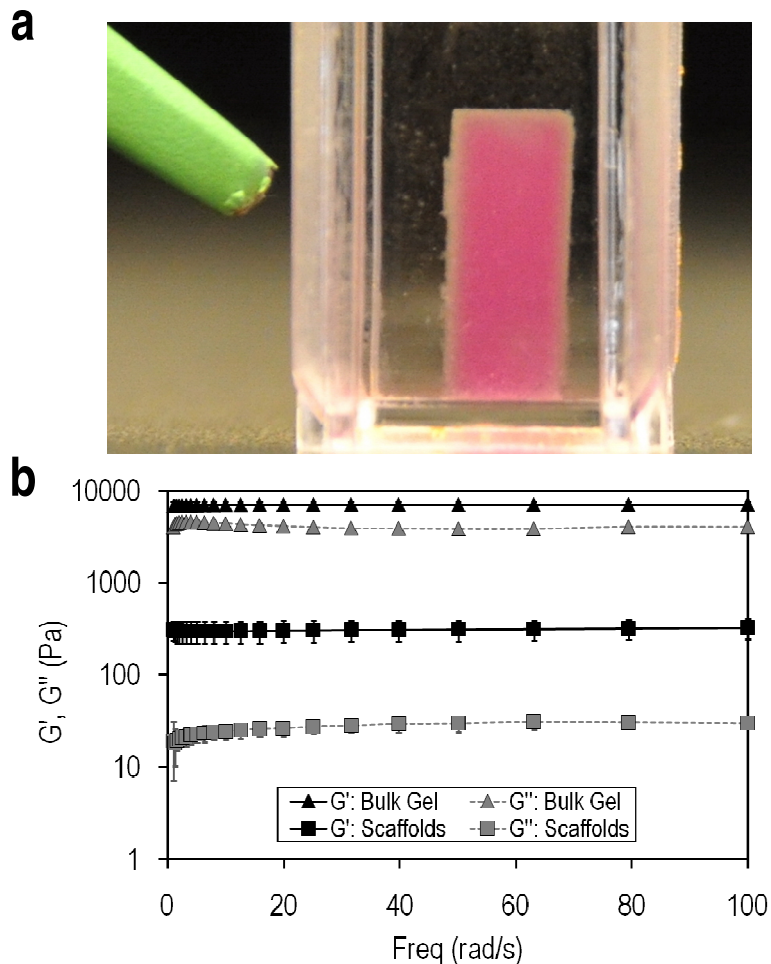


Figure 4.13: Scaffolds may be formed by centrifuging microspheres in the presence of 2% serum. (a) Photograph of a scaffold composed of PEG₈-VS/PEG₈-amine microspheres, PEG₈-acrylate/PEG₈-amine microspheres and PEG₈-VS/BSA microspheres. Microspheres were compacted by centrifugation at 1000g for 10 min in the presence of HepG2 hepatoma cells and then incubated for 12 h at 37°C in medium with 2% FBS. (b) Rheometric measurements of storage (G') and loss (G'') moduli of modular scaffolds formed from PEG₈-VS/PEG₈-amine microspheres compared with bulk hydrogels formed by crosslinking PEG₈-VS with PEG₈-amine below the cloud point.

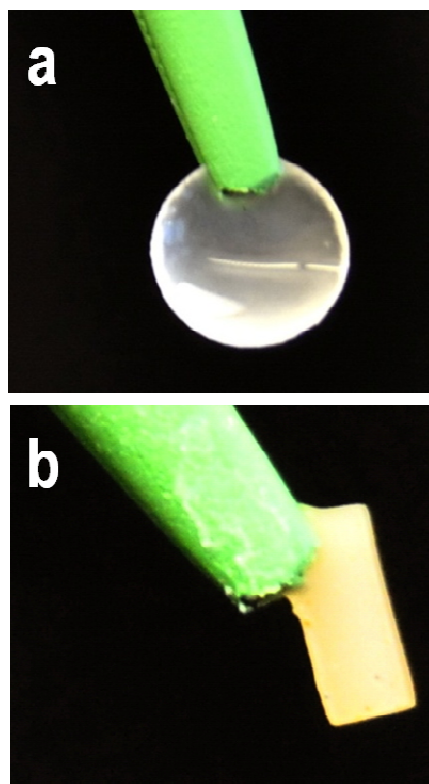


Figure 4.14: Photographs of modular scaffolds. **(a)** Modular scaffold formed overnight in high salt without centrifugation. Photo of a scaffold formed from PEG₈-VS/PEG₈-amine microspheres produced in PBS + 0.6 M sodium sulfate pH 7.4 incubated for 12 h instead of 45 min at 37°C in a 1.5 mL centrifuge tube. Stable microspheres that formed in the solution rose to the top due to their lower densities relative to the solution, allowing crosslinking between unreacted vinylsulfone and amine groups on the microspheres. **(b)** Shrunken modular scaffold that was raised above the cloud point in sodium sulfate solution. Scaffold was formed by centrifugation of PEG₈-VS/PEG₈-amine microspheres at 1000g for 10 min followed by incubation for 12 h at 37°C in medium with 2% FBS.

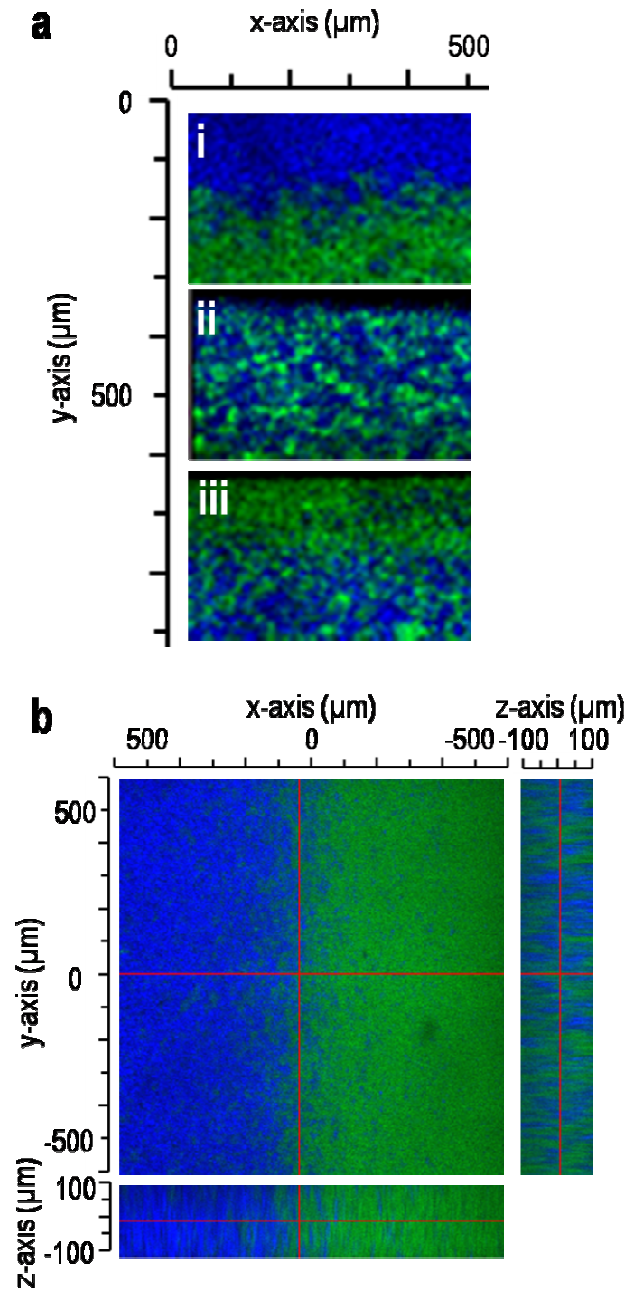


Figure 4.15: Scaffolds could be fabricated with gradients of microspheres. Images were obtained by confocal microscopy with a 10X objective. (a) Scaffolds formed by centrifuging PEG₈-VS/BSA microspheres (green) with (i) low, (ii) medium or (iii) high density PEG₈-acrylate/PEG₈-amine microspheres (blue). The density of the PEG₈-acrylate/PEG₈-amine microspheres was varied by reacting solutions of PEG₈-acrylate and PEG₈-amine in PBS + 0.45 M sodium sulfate at 95°C for: (i) 3 min, (ii) 5 min or (iii) 10 min. (b) 3D section of gradient scaffold from (a(i)).

microspheres and degradable PEG₈-acrylate/PEG₈-amine microspheres demonstrated an even distribution of the two types of microspheres (Figure 4.16a). After incubation at 37°C for 2 days, the PEG₈-acrylate microspheres had completely dissolved, leaving behind a porous scaffold of the PEG₈-VS/PEG₈-amine microspheres (Figure 4.16b). Some microsphere aggregation prior to scaffold formation was generally observed, but this had the desirable effect of increasing the size and connectivity of macropores that eventually formed in the scaffolds. Assembly of all three types of microspheres with matched densities also led to the formation of scaffolds with evenly distributed pores after two days at 37°C (Figure 4.17).

4.4.5 Cell Interactions with Scaffolds

The standard scaffold formation conditions were well-tolerated by living cells (1000g for 10 min in medium with 2% serum followed by incubation at 37°C overnight). To support cell adhesion, cysteine-containing RGD peptide was conjugated to PEG₈-VS during pre-reaction with PEG₈-amine or BSA.(Elbert and Hubbell 2001) Cell-laden scaffolds were formed by mixing the RGD peptide-derivatized microspheres with degradable microspheres and HepG2 hepatoma cells prior to centrifugation. A live/dead assay revealed the viability of HepG2 cells to be minimally impacted by centrifugation in the presence of the microspheres ($93.64 \pm 3.34\%$ live cells). Dissolution of porogenic microspheres over the course of two days had no further effect on the survival of the HepG2 cells ($91.94 \pm 1.87\%$ live cells), demonstrating that the degradation products of the porogenic microspheres were not cytotoxic (Figure 4.18a). The cells were evenly distributed in the scaffolds and surrounded by but not encapsulated within microspheres. Each cell formed its own niche within the scaffold that was further expanded upon dissolution of the porogenic

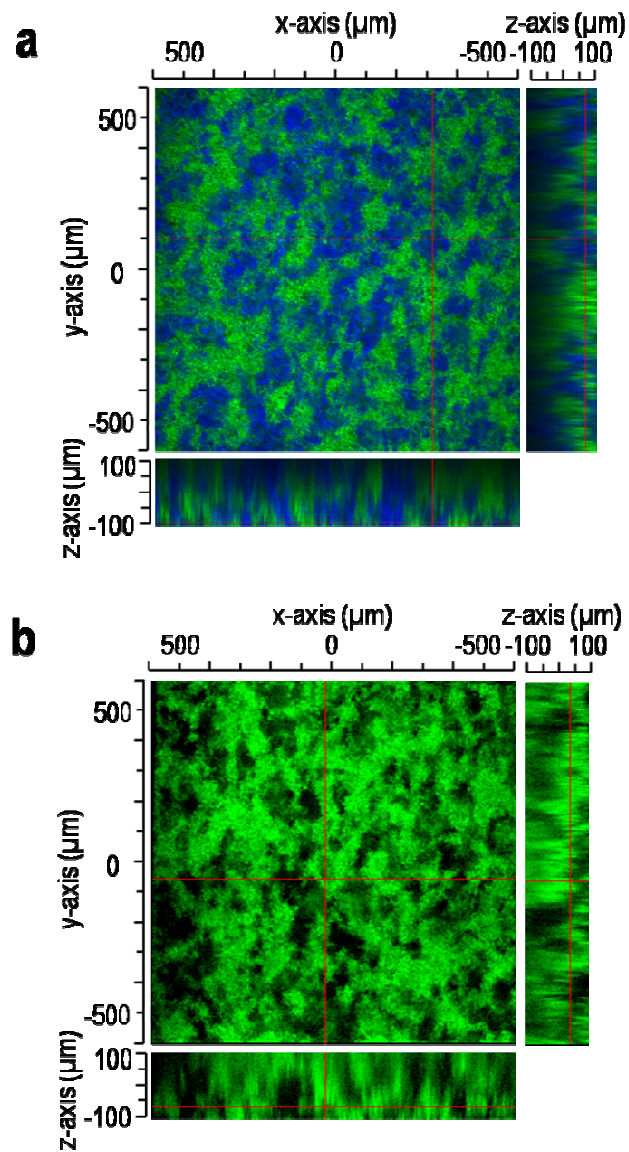


Figure 4.16: Macroporosity was introduced in the presence of cells via dissolution of porogenic microspheres. (a) A scaffold formed from PEG₈-VS/PEG₈-amine microspheres (green) and PEG₈-acrylate/PEG₈-amine microspheres (blue) with matched densities, imaged 12 h after centrifugation in cell culture medium at 37°C. (b) Scaffold from (a) after 48 h in cell culture medium at 37°C. PEG₈-acrylate/PEG₈-amine microspheres (blue) were no longer detectable.

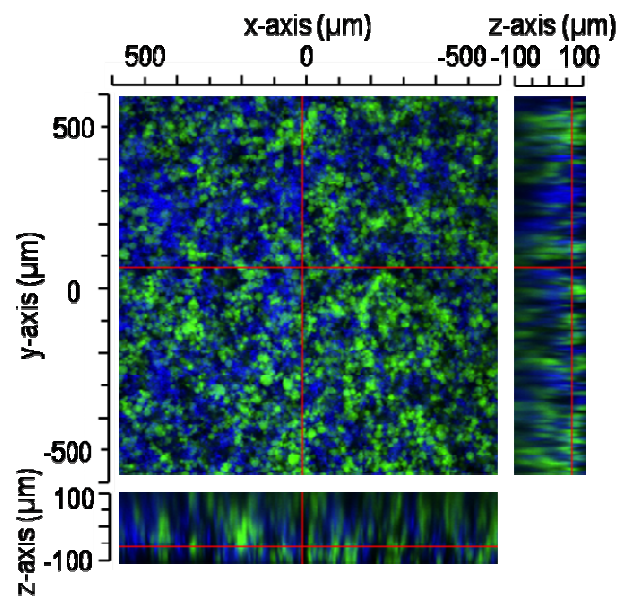


Figure 4.17: Confocal microscopy at 10X of a macroporous scaffold composed of PEG₈-VS/PEG₈-amine microspheres (green), PEG₈-acrylate/PEG₈-amine microspheres PEG₈-VS/BSA microspheres (blue), 48 h after formation. Microsphere densities were matched to produce an even distribution of macropores following dissolution of PEG₈-acrylate/PEG₈-amine microspheres.

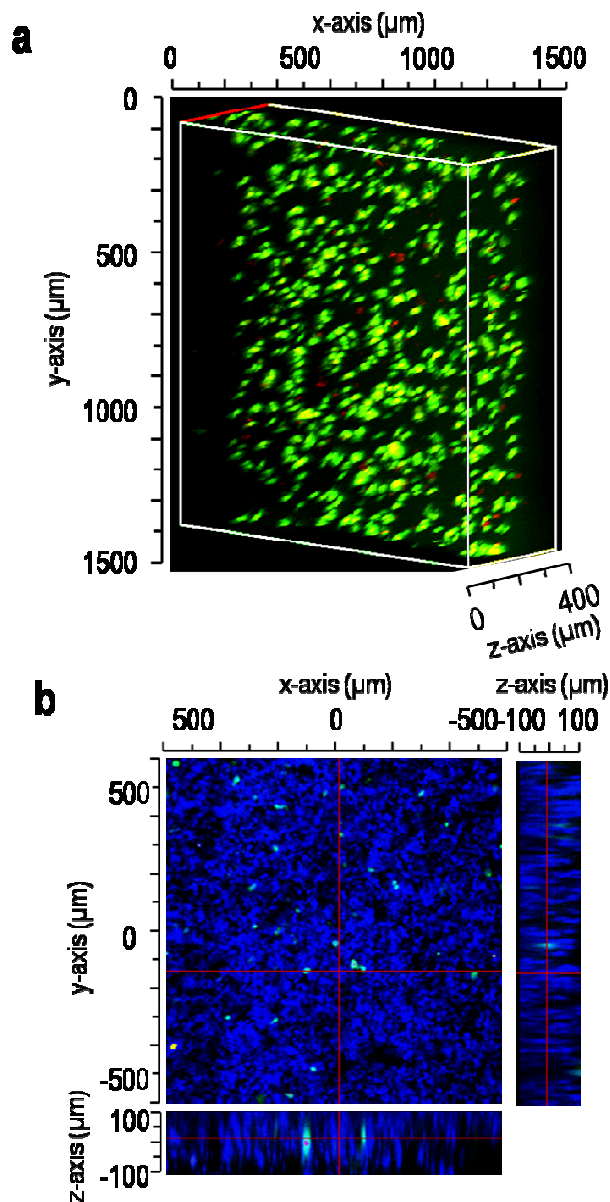


Figure 4.18: Scaffolds could be formed in the presence of cells. **(a)** HepG2 cell viability in a scaffold composed of PEG₈-VS/PEG₈-amine microspheres, PEG₈-acrylate/PEG₈-amine microspheres (blue) and PEG₈-VS/BSA microspheres. The PEG₈-acrylate/PEG₈-amine microspheres were no longer detectable, demonstrating complete hydrolysis of porogenic microspheres. HepG2 cells were stained with fluorescein diacetate (green; live) and ethidium bromide (red; dead). **(b)** HepG2 cell viability in a scaffold similar to (a) but composed of PEG₈-VS/PEG₈-amine microspheres, PEG₈-VS/BSA microspheres (blue) and PEG₈-acrylate/PEG₈-amine microspheres. HepG2 cells were evenly dispersed throughout the macroporous scaffold and were surrounded by microspheres but not encapsulated in them. Live/dead assays were performed 48 h after scaffold formation to allow porogen dissolution, revealing cell viability of $91.9 \pm 1.87\%$ ($n=3$). Cells were imaged by confocal microscopy with a 10X objective.

microspheres (Figure 4.18b). Cell viability decreased to $43.4 \pm 9.7\%$ after three weeks in culture when the medium changes every two days.

The potential for directed vascularization into the modular scaffolds was assessed by observing the infiltration of human aortic endothelial cells after dissolution of the porogen. Due to the formation of a tight seal between the scaffolds and the sides of UV/vis cuvettes, endothelial cell migration only occurred from the top of the scaffold (Figs. 4.19 & 4.20). For confocal microscopy, the cuvettes were turned on their sides to allow imaging along the entire length of the scaffold to a maximum observable depth of about 300 microns. The influence of macroporosity on endothelial cell infiltration was investigated by introducing gradients of porosity into scaffolds, which resulted in a highly porous 250-300 μm upper layer and a less porous lower layer (Figure 4.21a). With RGD peptide incorporated in the scaffold, endothelial cells labeled with Vybrant DiI (red) penetrated throughout the highly porous upper layer within 24 h (Figure 4.21a(i)) and continued to migrate into the less porous lower region by 48 h (Figure 4.21a(ii)). No endothelial cell infiltration was found when the scaffolds were formed without the porogenic microspheres (Figure 4.21a(iii)). With high porosity but no RGD peptide, endothelial cells were found only at the top of the scaffold (Figure 4.21a(iv)). To specifically probe the influence of S1P release, endothelial cell migration rates into scaffolds with uniform porosity were compared with and without loading of S1P into the PEG₈-VS/BSA microspheres (Figure 4.21b). The rate of endothelial cell migration increased from $2.6 \pm 0.8 \mu\text{m}/\text{h}$ to $5.4 \pm 1.0 \mu\text{m}/\text{h}$ when S1P was delivered from PEG/BSA microspheres ($p < 1 \times 10^{-5}$).

Finally, we observed the infiltration of endothelial cells into scaffolds containing HepG2 cells. The scaffolds formed with HepG2 cells and all three microsphere types were cultured for two days to allow pore formation by dissolution of the PEG₈-acrylate/PEG₈-

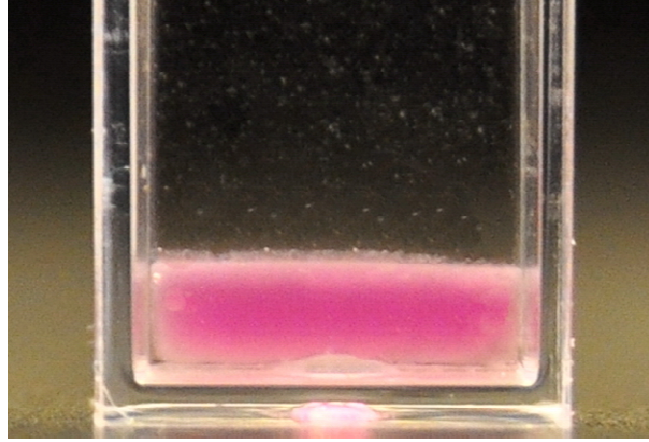


Figure 4.19: Modular scaffolds formed tight seals with the walls of UV/vis cuvettes in which they were fabricated. Photograph of a scaffold fabricated by crosslinking PEG₈-VS/BSA microspheres, PEG₈-VS/PEG₈-amine microspheres, and PEG₈-acrylate/PEG₈-amine microspheres in cell media. The scaffold was not disturbed following formation within the UV/vis cuvettes. A tight seal formed with the walls of the UV/vis cuvette walls, allowing endothelial cell infiltration only from the top surface of the scaffold. Cell migration could thus be measured for the entire height of the scaffold by imaging the scaffold on its side, despite the 300 micron limit to the depth of field of the confocal microscope.

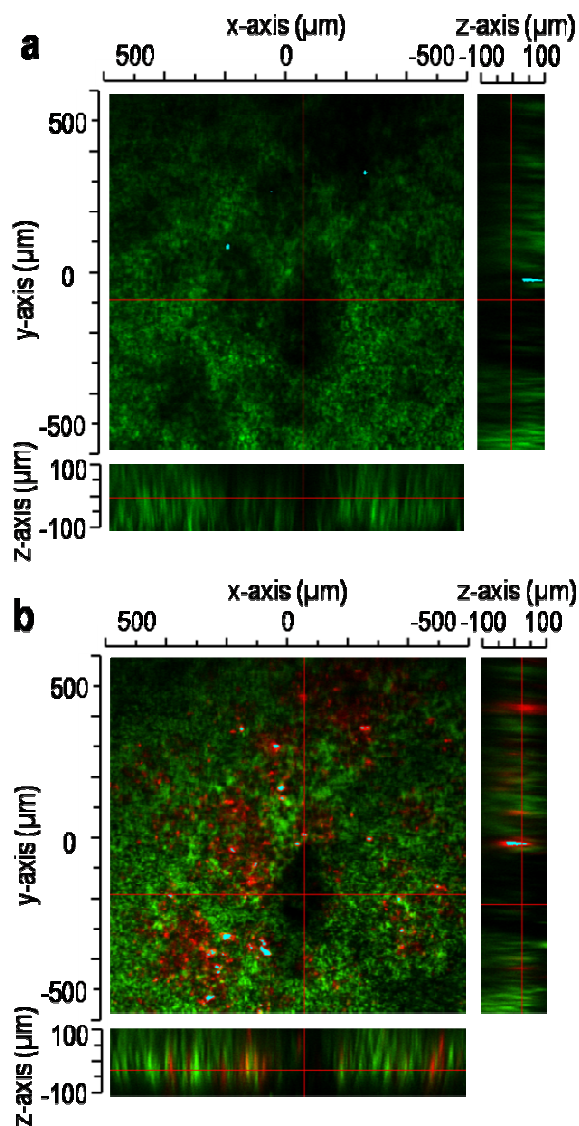


Figure 4.20: Penetration of endothelial cells into surface pores of a modular scaffold. Macropores were visible at the top surface of a modular scaffold composed of PEG₈-VS/PEG₈-amine microspheres, PEG₈-VS/BSA microspheres (green) and PEG₈-acrylate/PEG₈-amine microspheres. Scaffolds were imaged by confocal microscopy at 10X magnification: (a) prior to cell seeding, (b) after seeding Vybrant DiI-stained endothelial cells (red). Endothelial cells adhered to RGD peptide conjugated to microspheres, which allowed migration into macropores.

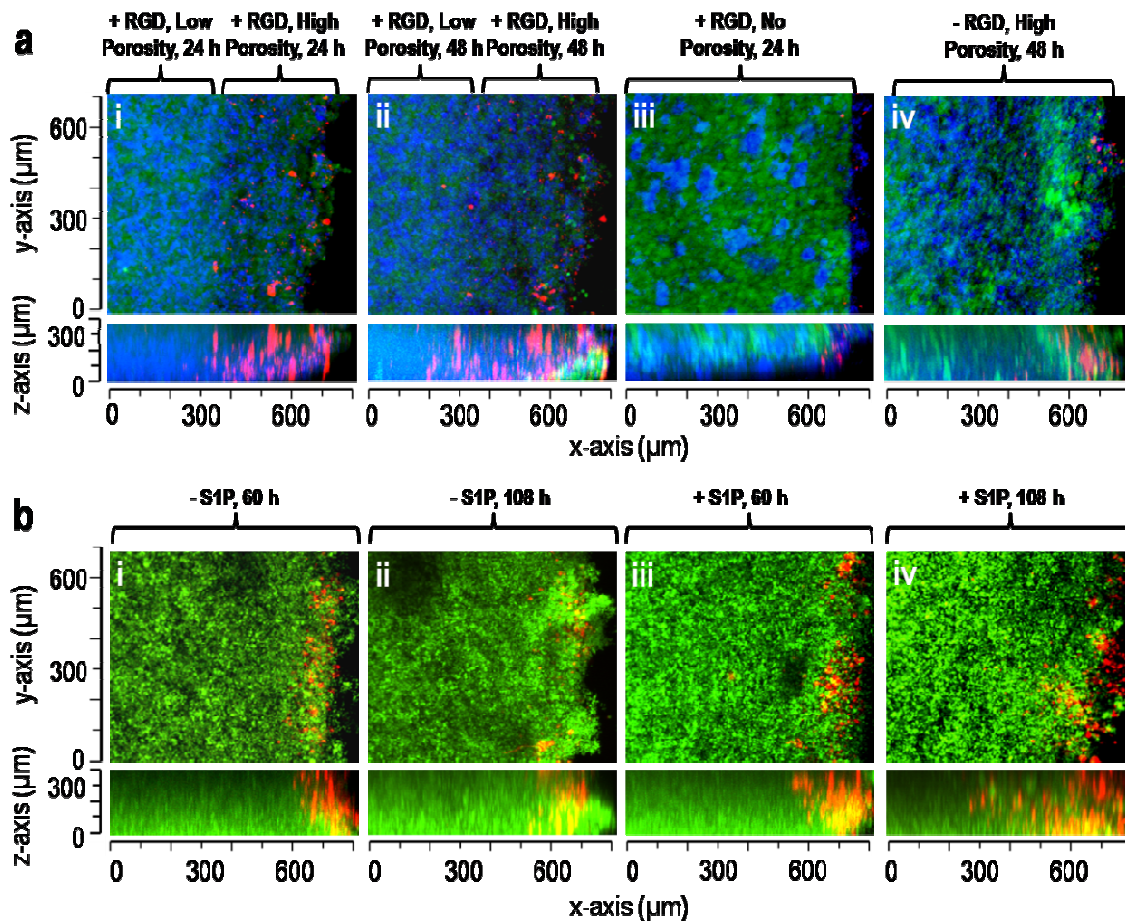


Figure 4.21: S1P, porosity, and RGD peptide affected endothelial cell migration in modular scaffolds. (a) Migration of Vybrant DiI stained endothelial cells (red) into scaffolds composed of PEG₈-VS/PEG₈-amine microspheres (green), PEG₈-acrylate/PEG₈-amine microspheres and PEG₈-VS/BSA microspheres (blue). Scaffolds were formed with: (i) RGD peptide and a highly porous 250-300 μm upper layer, imaged 24 h after cell seeding, (ii) Same location within scaffold from (i) at 48 h, (iii) RGD peptide but no porogenic microspheres, 24 h, (iv) No RGD peptide but with porogenic microspheres, 48 h. (b) Migration of endothelial cells (red) into scaffolds with uniform porosity composed of PEG₈-VS/PEG₈-amine microspheres, PEG₈-acrylate/PEG₈-amine microspheres and PEG₈-VS/BSA microspheres (with or without S1P-loaded, green): (i) 60 h after cell seeding without S1P-loading, (ii) 108 h without S1P-loading, (iii) 60 h with S1P-loading, (iv) 108 h with S1P-loading. The maximum extent of migration of endothelial cells was recorded at 50 μm increments within each scaffold. The average rate of migration increased from $2.57 \pm 0.76 \mu\text{m/h}$ to $5.4 \pm 1.02 \mu\text{m/h}$ when S1P was released from the PEG₈-VS/BSA microspheres.

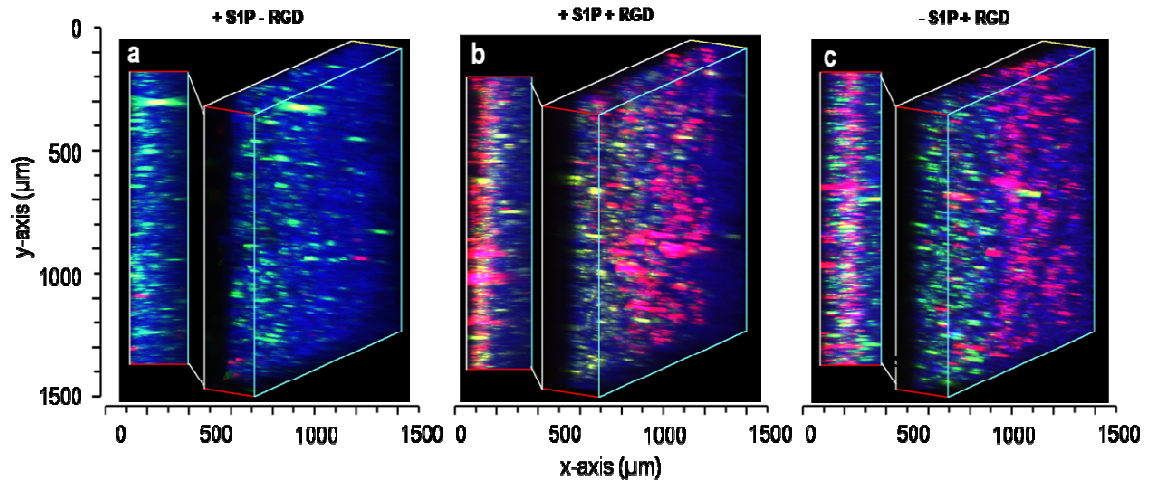


Figure 4.22: Endothelial cell migration into scaffolds containing HepG2 cells. Modular scaffolds were formed from all three types of microspheres in the presence of HepG2 cells stained with Vybrant DiO (green). After crosslinking with media proteins and hydrolysis of porogenic microspheres for 48 h, endothelial cells (red) were seeded onto all sides of the scaffolds. The scaffolds contained: (i) S1P-loaded PEG₈-VS/BSA microspheres (blue) without RGD peptide, (ii) PEG₈-VS/BSA microspheres (blue) loaded with S1P, with RGD, (iii) PEG₈-VS/BSA microspheres (blue) not loaded with S1P, with RGD. Cells were imaged by confocal microscopy with a 10X objective. Endothelial cells migrated to the maximum observable distance (300 μm) within two days with or without S1P delivery. Scaffolds were imaged by confocal microscopy with a 10X objective.

amine microspheres. Scaffolds were dislodged from the cuvettes to permit endothelial cell infiltration from all sides of the scaffolds. The HepG2 cells within these scaffolds were labeled with Vybrant DiO (green) while the endothelial cells were labeled with Vybrant DiI (red). The PEG₈-VS/BSA microspheres were labeled with Dylight 633 (blue). In the absence of RGD peptide, few endothelial cells were observed in the scaffolds by confocal microscopy (Figure 4.22a). With conjugated RGD peptide, endothelial cell migration was observed after two days up to the maximum imaging depth of 300 μm with or without S1P delivery (Figs. 4.22a,b).

4.4 Discussion

In this study, we introduce a new method of constructing tissue engineering scaffolds from novel PEG-based microspheres. The method is highly scalable and amenable to macroporous scaffold formation in the presence of living cells. Rivest et al. recently categorized different methods of forming hydrogel scaffolds as either “top-down”, i.e. pore formation followed by cell seeding, or “bottom-up”, i.e. assembly of cell-laden hydrogel modules (Rivest, Morrison et al. 2007). Our strategy does not fit either description and represents a new methodology that combines beneficial aspects of both top-down and bottom-up strategies. Similar to top-down strategies, macropores for cell infiltration are produced using a degradable porogen, but unlike the commonly used porogens, PEG₈-acrylate/PEG₈-amine microspheres are non-cytotoxic and form macropores in the presence of cells. Similar to bottom-up strategies, the scaffolds are assembled from smaller modules, but our modules may be assembled around cells due to their small size and do not require cell encapsulation within crosslinked bulk hydrogel. Assembly of microspheres around cells may enhance transport of nutrients and facilitate removal of waste products, while

macropore formation may permit directed vascularization of scaffolds. Additionally, the ability to produce microsphere gradients may be useful to introduce gradients in mechanical stiffness or bioactive factors to influence cellular responses to the scaffolds (Engler, Griffin et al. 2004; DeLong, Moon et al. 2005; Moore, Macsween et al. 2006). Gradients in these properties may have applications in both the transplantation of cells *in vivo* and the differentiation of stem cells *in vitro*.

Microsphere formation in aqueous systems without surfactant is rarely attempted due to rapid aggregation and coarsening of the polymer phase prior to solidification or gelation. We also observed some moderate aggregation, which likely resulted from the reaction of residual vinylsulfone and amine groups present within the microspheres. Occasionally, microspheres were observed that appeared to consist of two or more microspheres that gelled while coalescing. Hennink and colleagues demonstrated that vigorously mixed, phase separated all-aqueous solutions of PEG and dextran could be polymerized by free-radical polymerization, resulting in crosslinked dextran or PEG microspheres (Franssen and Hennink 1998; Van Thienen, Demeester et al. 2008; Van Tomme, Mens et al. 2008). A similar method may be used to directly form macroporous dextran scaffolds, as demonstrated by Shoichet and colleagues (Lévesque, Lim et al. 2005). It was proposed that the scaffolds consisted of dextran microspheres gelled together, similar to the bulk gel of microspheres observed under some conditions here (Table 1). To form microspheres, we avoided these conditions by timing gelation to occur early in the coarsening process, and therefore the resulting microspheres sizes were influenced by the time required to reach the gel point. Increasing the solution temperature increased the rate of the crosslinking reaction to allow the gel point to occur sooner. This decreased the time allowed for coarsening and produced smaller microspheres.

Coarsening of PEG-rich droplets following phase separation supported an $\bar{r} \propto \text{time}$ growth law (Figure 4.6b). Such growth is indicative of hydrodynamic interactions that occur in the early stages of spinodal decomposition (Lal and Bansil 1991). After about 4 min, DLS indicated a plateau or asymptote in domain size growth. These findings are consistent with light scattering studies of polymer solutions following thermally induced phase separation, in which an initially linear growth regime was followed by a period of much slower growth (Lauger, Lay et al. 1994). The cessation of domain growth, or “spontaneous pinning”, during spinodal decomposition has been frequently observed for high-molecular weight polymer mixtures away from the critical concentration (Hashimoto, Takenaka et al. 1992). Molecular dynamics simulations suggest that the growth has not in fact ceased, but instead undergone a percolation-to-cluster transition (PCT) from a $\bar{r} \propto \text{time}$ to a $\bar{r} \propto \text{time}^{\frac{1}{4}}$ and finally to a $\bar{r} \propto \text{time}^{\frac{1}{3}}$ growth law (Crist and Nesarikar 1995; Crist 1996; Termonia 1997). The physical occurrence responsible for the shift in growth law has been proposed to be the disbanding of a percolated polymer network, present immediately after spinodal decomposition, into isolated aggregates and droplets that grow by coalescence and Ostwald ripening (Termonia 1997).

DLS results demonstrated a difference in coarsening rate and PCT between the different PEG solutions. The pre-reacted PEG₈-VS/PEG₈-amine samples coarsened at a slower rate and reached the PCT at a smaller d_{PCS} than the PEG-monomers solutions. Several factors may have influenced the coarsening of PEG-rich phases. The buoyancy of PEG-rich droplets caused by the high density salt solutions is a possible explanation. PEG₈-amine has a higher LCST than PEG₈-VS, and crosslinking of the two polymer results in an intermediate cloud point. Thus a higher salt concentration was required to cause phase separation at the same temperature for PEG₈-VS than for PEG₈-VS/PEG₈-amine pre-

reacted solutions, which could cause a discrepancy in the coarsening rate due to differences in density of the salt solutions. Alternatively, the PEG₈-amine may influence coarsening by acting as a surfactant. The higher LCST for more highly charged PEG₈-amine compared to PEG₈-VS is likely reflective of increased hydrogen bonding and may enable PEG₈-amine to function as a surfactant to stabilize PEG₈-VS droplets. This is evidenced by the decrease in coarsening rate that occurs when mixing PEG₈-VS and PEG₈-amine without pre-reaction. In the pre-reacted sample, PEG₈-amine may act as a reactive surfactant, which would improve its ability to stabilize PEG-rich phases. This effect in combination with being initially closer to the gel point could stabilize the PEG-rich domains for the pre-reacted solutions and may contribute to the observed lower d_{PCS} at the PCT.

The microspheres described herein were not only polydisperse but also porous. Similar pores have been observed in gelatin coacervates following a decrease in temperature (Kruyt 1949). In PEG/water biphasic systems, an increase in molecular weight broadens the binodal curve, increasing the PEG equilibrium concentration in the PEG-rich domains (Bae, Lambert et al. 1991). Thus, water should be released during crosslinking to form water-rich domains inside the PEG-rich domain. The water-rich domains coarsen inside the PEG-rich phase, resulting in pores after gelation if the water-rich domains are unable to diffuse to the surface of the PEG-rich phase. This suggests that our method of microsphere formation is similar to the coacervation method commonly used to form gelatin microcapsules for drug encapsulation (Arshady 1990). Coacervates can be used to surround insoluble solid particles or droplets of immiscible phases, making them well suited for microencapsulation strategies (Bungenberg de Jong 1949; Russell E. Phares Jr. 1964). The Mikos group has used this method to encapsulate growth factors within degradable gelatin microparticles for sustained, localized drug release (Holland, Tessmar et al. 2004). When a sufficiently high sodium

sulfate concentration was used to produce a triphasic PEG-VS/PEG-amine/water system, the PEG-amine and PEG-VS domains were shown to envelop each other as well as the water domains to form multiple emulsions. It may be possible to use this methodology in the formation of multi-level PEG-coated drug particles that could perhaps display multiple levels of degradation or drug delivery.

The original coacervation process developed by Bungenberg de Jong and Kruyt involved the addition of ethanol to an aqueous gelatin solution to produce a triphasic system (H. G. Bungenberg de Jon 1929). The more favorable interactions between water and ethanol decreased the gelatin solubility to increase the interactions between the polymer molecules (Reza Arshady 1990). We have observed that in an unreactive aqueous mixture of PEG-OH and PEG-amine containing a sodium sulfate concentration suitable to cause phase separation of PEG-OH but not PEG-amine, the PEG-amine preferentially associates with the resulting PEG-OH coacervate layer. Thus in our standard biphasic system, the interaction between PEG₈-VS and PEG₈-amine is likely to be heightened by the preferential association of the soluble PEG₈-amine with the insoluble PEG₈-VS phase. Such an association would drastically increase the rate of the crosslinking reaction, which was reflected in our ability to decrease a typically 6-7 h reaction time to 45 min at 37°C and less than 3 min at 95°C.

4.5 Conclusion

In summary, the methods presented here for fabricating PEG microspheres allowed us to advance the modular approach to the design of tissue engineering scaffolds. The mechanism of microsphere formation bears a resemblance to classical coacervation processes and may permit adaption to useful techniques such as microencapsulation. By assembling multiple types of hydrogel microspheres with diverse properties, we developed a highly scalable platform designed to enhance biocompatibility while allowing control over bioactivity and porosity. Scalability resulted from solution-phase synthesis of microspheres while biocompatibility was enhanced by the absence of surfactants, organic solvents and copolymers. The enhanced biocompatibility allowed assembly of scaffolds in the presence of cells, resulting in a homogenous cellular distribution. Bioactivity was introduced via RGD peptide conjugation and S1P delivery, both of which promoted endothelial cell infiltration. The use of porogenic microspheres with different densities allowed introduction of gradients in macroporosity, suggesting the potential to develop highly complex scaffolds. Production of PEG microsphere libraries may allow the development of advanced scaffolds with application-specific architectures, bioactivity, mechanical properties and degradation kinetics.

CHAPTER 5

Conclusions

5.1 Summary of Results

Leo Vroman proposed that the adsorption and distortion of proteins on the surfaces of foreign materials exposed to blood may be an intrinsic defense mechanism that has continued to evolve from amoebic origins (Vroman 2003). The contact activation system appears to be a “large-scale Devaux effect”, wherein the hydrophobic cores of certain enzymes become exposed, resulting in a cascade of protein-induced distortions (Vroman 1965). Acceleration of the coagulation cascade is initiated by surface-induced conformational changes in factor XII. By relating the conformations of distorted proteins to their biological responses, it may be possible to assess the biocompatibility of new materials and improve the compatibility of current implantable devices. For this reason, the goal of this thesis was to develop new methodologies for the advancement of biomaterials design by focusing on information gained from the analysis of adsorbed protein films.

A key contributor to the progression of biomaterials design over the last half-century has been the ability to assess the identity and conformation of adsorbed proteins in relation to the properties of a material surface. This ability has been particularly vital to the study of blood/material interfaces, since biological responses are communicated through protein conformation. Hence the first objective of this thesis was to develop a technique capable of probing these conformations to determine the exposure of cell adhesion motifs that elicit thrombotic responses.

Mass spectrometric mapping was presented in Chapter 2 for the assessment of the thrombotic potential of adsorbed fibrinogen on PET surfaces. Fibrinogen solutions were exposed to the surfaces of PET microparticles that were packed within columns to provide extensive surface area for adsorption. After allowing sufficient time for post-adsorptive conformational changes, the fibrinogen was reacted with biotin tags that could only react with solution exposed lysine residues. Locations of the tagged residues were then determined using MALDI-TOF. The experiment was performed at different solution concentrations of fibrinogen and demonstrated a concentration-dependent change in exposure of numerous cell adhesion motifs, of which the most important was the gamma chain dodecapeptide essential to platelet adhesion. The effect of solution concentration on fibrinogen spreading was monitored with OWLS and found to correlate with the mass spectrometric mapping results. Increased exposures of lysines throughout the fibrinogen molecule supported the association of hydrophilic residues with the solution and hydrophobic residues with the PET surface at solid/liquid interfaces. While the MALDI-TOF results were informative, they proved to only be qualitative in nature. As a result, a quantitative strategy was devised using a variation of SILAC entitled SILT-MS. We developed a serum-free culture protocol for the expression of isotopically labeled fibrinogen and other high concentration blood proteins from HepG2 hepatocellular carcinoma cells. To demonstrate the quantitative ability of the technique, standard curves for isotopically labeled fibrinogen, complement C3, and α 2-macroglobulin were generated. The internal standards proved to be highly accurate for relative protein quantification, producing accuracies ranging from 2.9% -9.8%.

As described in section 1.3 of this thesis, history has clearly shown that the *in vivo* environment is too dynamic and chemically diverse to be placated by a material with a

simple first-generation surface. Biomaterials science has recently come to focus on the more realistic aspiration of developing third-generation materials capable of inhibiting undesirable biological responses and promoting specific cellular interactions. Therefore, the second goal of this thesis was to develop materials with pro-active surfaces that could inhibit distortions in protein structure while encouraging specific cell adhesion and migration.

Chapter 3 presented a method of applying covalent PEG coatings onto material surfaces by taking advantage of pre-reacted oligomers and microgels. Surface grafting of PEG chains onto materials typically requires high surface functionalization in order to obtain sufficient surface coverage to prevent nonspecific protein adsorption. We addressed this issue by increasing the size and functionality of the grafted molecule instead of increasing the availability of reactive groups on material surfaces. An electrophilic 8-arm PEG derivative, PEG-OVS, was partially crosslinked with nucleophilic 8-arm PEG-amine or lysines within albumin to form solutions of large oligomers and microgel. Reaction of the macromonomers was monitored with DLS and the reaction was arrested prior to bulk gel formation. The resulting oligomer/microgel solutions were characterized by SDS-PAGE, NMR, and GPC, revealing extensive end-group conversion prior to reaching the gel point. These oligomer/microgels contained reactive vinyl sulfone groups that permitted grafting to thiol or amine functionalized surfaces under mild physiologic conditions. The grafted oligomers and microgels continued to react on the surface to produce dense hydrogel coatings of controlled thickness. OWLS and QCM analysis verified the resistance of the coatings to protein adsorption and, along with AFM, confirmed their nanoscale thickness. With only a single layer, the coatings were shown to resist adhesion of CHO, fibroblast, and endothelial cell lines superior to multi-layer coatings formed by covalently attaching individual PEG monomers with layer-by-layer methodologies. Reaction conditions were

adjusted to allow subsequent attachment of bioactive molecules to these hydrogel coatings to promote cell adhesion. Due to the large size of the partially crosslinked molecules compared to individual monomers, extensive surface coverage could be achieved on surfaces with with low levels of functionalization. Thus simple air-plasma treatments provided sufficient functionalization on PET to apply a covalent film for resistance to cell adhesion.

In Chapter 4, a novel method was described for fabricating 100% PEG microspheres that allowed us to demonstrate the benefits of using a modular strategy in the design of synthetic polymer scaffolds. The reactive PEG oligomers/microgels introduced in Chapter 3 were used in the fabrication of hydrogel microspheres, which were produced in aqueous sodium sulfate solutions without the use of surfactants or copolymers. Microspheres were formed if the gel point was reached following thermally induced phase separation and prior to extensive coarsening of spherical PEG-rich domains. By assembling scaffolds from multiple PEG microspheres with unique properties, we were able to develop a highly scalable platform that presents biocompatibility, macroporosity and biochemical versatility useful for a variety of tissue engineering applications. This solution-phase gelation method allowed rapid fabrication of microspheres in quantities realistic for the development of large scaffolds required during the tissue engineering of organs. The lack of additives maximized the amount of PEG in the microspheres, permitting the fabrication of noncytotoxic PEG-based porogens and possibly improving the overall biocompatibility of assembled scaffolds. Macroporous scaffold formation and cell seeding occurred in a single step, and the distribution and location of cells within the scaffolds was controlled by varying the microsphere density. Use of microspheres with a tunable density allowed formation of gradient and layering effects as demonstrated by the porosity gradient that induced rapid endothelial cell infiltration into the outer edges of some scaffolds. Endothelial cell migration

into the scaffolds was directed and enhanced through conjugation of RGD peptide and delivery of S1P from microspheres crosslinked with albumin, a lipid carrier.

5.2 Future Directions

The mass spectrometric mapping experiments described in Chapter 2 provided qualitative information on the accessibility of fibrinogen cell-interaction motifs after adsorption onto hydrophobic PET surfaces at 1, 0.5, and 0.1 mg/mL. Future experiments should be performed on materials with different surface charge, topography, and hydrophilicity. Lower adsorbing concentrations of fibrinogen should also be tested to further investigate more extensive fibrinogen spreading. Solutions of fibrinogen with other proteins such as albumin should be used to observed post-adsorptive fibrinogen conformation under conditions of competitive adsorption. The SILT-MS experiments proved that labeled lysine locations could be quantified and that acetylated residues could be identified reproducibly. A logical next step would be to analyze mass spectrometric mapping experiments using SILT-MS. Together, the two methods may allow a quantitative analysis of cell adhesion motif exposures. This could be accomplished by acetylating isotopically labeled proteins to form internal standards that are both labeled and tagged. Although our focus was on the adsorption of fibrinogen, our methodology could be utilized for the study of multiple blood proteins simultaneously. Protein separation methods such as 2D SDS-PAGE and multidimensional chromatography are routinely used in the analysis of large proteomes. Thus it could be possible to expose biomaterial surfaces to human plasma and use our labeled HepG2 media internal standards to quantify any blood proteins within adsorbed protein layers that are also expressed by HepG2 cells. By incorporating mass spectrometric mapping, the degree of exposure of protein residues essential for eliciting

cellular interactions could be measured within multiple proteins. Such a comprehensive surface analysis technique could have immense applications in the prediction of the compatibility and longevity of implantable devices, particularly small diameter vascular devices that are prone to thrombus formation. In a broader application, our technique could also be used to accurately quantify changes in the expression and post-translational modification of multiple proteins within cell lines as well as blood samples for the diagnosis of disease.

The nanoscale hydrogel PEG coatings presented in Chapter 3 were found to inhibit nonspecific protein and cell adhesion on PET surfaces using a grafting strategy that could be applied to many different surfaces. Future work with this method should first attempt to generate coatings on other surfaces to demonstrate the versatility of the plasma-based protocol. Although fibrinogen was covalently attached to the surfaces of the hydrogel layers to promote cell adhesion, it would be beneficial to also conjugated specific cell adhesion peptides. Surface functionalization using different plasmas should be attempted to improve the initial surface functionalization step. Surface treatments with ammonia-based plasmas have been shown to be much more effective than air-plasma treatments at functionalizing surfaces with primary amines (Ben Rejeb, Tatoulian et al. 1998). Although the coatings are very thin and likely unable to store therapeutic quantities of growth factors or drugs, it may be possible to adapt the protocol for sustained drug delivery. Only a single layer of oligomer/microgel was required to form a dense uniform coating on surfaces, but it may be possible use this method with a layer-by-layer strategy that could increase coating thickness or form alternating drug-loaded layers. The PEG-amine and PEG-OVS composition of the oligomer/microgel solutions can be adjusted, and 2:1 and 1:2 ratios of PEG-OVS:PEG-OA oligomers/microgels were formed to improve the crosslinking between PEG microspheres

in Chapter 4. Similarly, 2:1 and 1:2 ratio microgels could be sequentially attached to surfaces to form progressively thicker coatings that may be more effective at delivering therapeutic agents than a single 100 nm thick coating. Additionally, due to the mild reaction conditions required for conjugation to PEG-OA, it may be possible to covalently attach active enzymes onto the coatings to allow *in situ* activation of compounds present in blood. Attachment of the enzyme responsible for the phosphorylation of sphingosine into S1P, sphingosine kinase, may prove to be beneficial for the *in vivo* recruitment of neo-intima onto surfaces of small diameter blood-contacting devices. Finally, immediate steps should likely be taken to test the efficacy of the PEG coatings in an animal model. The PEG-OVS/BSA coatings have already been shown to be stable for up to 3 weeks, and by excluding the protein component, the PEG-OVS/PEG-OA coatings may demonstrate improved longevity *in vivo*.

The scaffold strategy outlined in Chapter 4 can be applied to a wide range of tissue engineering applications. An inherent advantage of this modular strategy is the ability to mix and match components from a diverse microsphere library to fabricate customized scaffolds for a particular therapy or experiment. While only three different microsphere types were used in this thesis, it may be desirable to fabricate a large library of different PEG microspheres. One could imagine the potential for stem cell differentiation and proliferation within a macroporous scaffold assembled from a dozen different microspheres, each of which delivers unique growth factors, presents different adhesion molecules, and is displayed at diverse gradients. This biochemical versatility additionally provides freedom in the selection of the molecules used to crosslink the microspheres together. While the proteins present in cell media function as convenient crosslinkers, it is also possible to use enzymatically degradable peptides that could permit transplanted cells to eventually replace the scaffold and become functional tissue (Lutolf 2003). The stiffness of the scaffolds we

utilized was similar to that of liver tissue and will have to be adjusted for other applications. Mild centrifugation conditions were used to form these scaffolds in order to maintain high cell viability, but further compaction may be able to produce stiffnesses up to and including the modulus observed for bulk hydrogels. Increased compaction could be achieved by decreasing the spacer arm length of crosslinking molecules or by allowing microsphere buoyancy to compact microspheres into scaffolds without centrifugation as observed in Fig. 4.14a. The later method would not be amenable to formation in the presence of cells, but other methods of cell seeding should be investigated. When raised above the cloud point, the PEG within formed scaffolds responded by causing the scaffold to extrude water and collapse into a shrunken state (Fig. 4.14b). If such a shrunken scaffold were to be made porous and placed in media containing cells below the cloud point, the scaffold may swell with media as well as the cells, providing a simple and convenient method of cell seeding.

The microspheres themselves may serve a variety of functions other than for the modular assembly of scaffolds. As mentioned in Chapter 4, it may be possible to load drugs into the microspheres using coacervation-based microencapsulation techniques. The degradable PEG₈-acrylate/PEG₈-amine microspheres proved to be noncytotoxic and may therefore serve as vehicles for timed drug release. Antibodies could be conjugated to microsphere surfaces in a similar fashion to the covalent attachment of proteins to CNBr resin, which also binds to lysine residues. Thus the microspheres could be used for immunoprecipitation and possibly achieve higher pull-down specificity due to the superior resistance to nonspecific protein adsorption of PEG. By both loading microspheres with drugs and conjugating antibodies to their surfaces, targeted drug delivery strategies could be developed. Finally, the porous structure, ability to conjugate antibodies, and resistance to nonspecific protein adsorption may make functionalized PEG microspheres suitable as resin

for chromatographic applications. Such a resin may enhance and accelerate the proteomic analysis of biological fluids by removing high abundance proteins.

References

- Abuchowski, A., J. R. McCoy, et al. (1977). "Effect of covalent attachment of polyethylene glycol on immunogenicity and circulating life of bovine liver catalase." J Biol Chem **252**(11): 3582-6.
- Abuchowski, A., T. van Es, et al. (1977). "Alteration of immunological properties of bovine serum albumin by covalent attachment of polyethylene glycol." J Biol Chem **252**(11): 3578-81.
- Agnihotri, A. and C. A. Siedlecki (2004). "Time-dependent conformational changes in fibrinogen measured by atomic force microscopy." Langmuir **20**(20): 8846-8852.
- Aleman, J., A. V. Chadwick, et al. (2007). "Definitions of terms relating to the structure and processing of sols, gels, networks, and inorganic-organic hybrid materials (IUPAC Recommendations 2007)." Pure and Applied Chemistry **79**(10): 1801-1827.
- Almany, L. and D. Seliktar (2005). "Biosynthetic hydrogel scaffolds made from fibrinogen and polyethylene glycol for 3D cell cultures." Biomaterials **26**(15): 2467-77.
- Amiji, M., H. Park, et al. (1992). "Study on the prevention of surface-induced platelet activation by albumin coating." J Biomater Sci Polym Ed **3**(5): 375-88.
- Amirpour, M. L., P. Ghosh, et al. (2001). "Mammalian Cell Cultures on Micropatterned Surfaces of Weak-Acid, Polyelectrolyte Hyperbranched Thin Films on Gold." Analytical Chemistry **73**(7): 1560-1566.
- Anderson, J. M., T. L. Bonfield, et al. (1990). "Protein adsorption and cellular adhesion and activation on biomedical polymers." Int J Artif Organs **13**(6): 375-82.
- Andrade, J. D. and V. Hlady (1986). Protein adsorption and materials biocompatibility: a tutorial review and suggested hypothesis. Adv Polym Sci. **79**: 1-63.
- Andrade, J. D. and V. Hlady (1987). "Plasma protein adsorption: the big twelve." Ann N Y Acad Sci **516**: 158-72.
- Andrieux, A., G. Hudry-Clergeon, et al. (1989). "Amino acid sequences in fibrinogen mediating its interaction with its platelet receptor, GPIIbIIIa." J Biol Chem **264**(16): 9258-65.
- Aoki, S., M. Osada, et al. (2007). "Fluid shear stress enhances the sphingosine 1-phosphate responses in cell-cell interactions between platelets and endothelial cells." Biochem Biophys Res Commun **358**(4): 1054-7.
- Aoki, S., Y. Yatomi, et al. (2005). "Sphingosine 1-phosphate-related metabolism in the blood vessel." J Biochem **138**(1): 47-55.
- Arshady, R. (1990). "Microspheres and microcapsules, a survey of manufacturing techniques .2. coacervation." Polymer Engineering and Science **30**(15): 905-914.
- Asnaghi, D., M. Giglio, et al. (1995). "Large-scale microsegregation in polyacrylamide gels (spinodal gels)." The Journal of Chemical Physics **102**(24): 9736-9742.
- Axel, D. I., W. Kunert, et al. (1997). "Paclitaxel inhibits arterial smooth muscle cell proliferation and migration in vitro and in vivo using local drug delivery." Circulation **96**(2): 636-45.

- Bach, T. L., C. Barsigian, et al. (1998). "Endothelial cell VE-cadherin functions as a receptor for the beta15-42 sequence of fibrin." J Biol Chem **273**(46): 30719-28.
- Bae, Y. C., S. M. Lambert, et al. (1991). "Cloud-Point Curves of Polymer-Solutions from Thermo-optic Measurements." Macromolecules **24**(15): 4403-4407.
- Bafaluy, J., B. Senger, et al. (1993). "Effect of hydrodynamic interactions on the distribution of adhering Brownian particles." Physical Review Letters **70**(5): 623-626.
- Baier, R. E. and R. C. Dutton (1969). "Initial events in interactions of blood with a foreign surface." J Biomed Mater Res **3**(1): 191-206.
- Baier, R. E., E. G. Shafrin, et al. (1968). "Adhesion: mechanisms that assist or impede it." Science **162**(860): 1360-8.
- Bailey, F. E. and R. W. Callard (1959). "Some properties of poly(ethylene oxide) in aqueous solution." J. Appl. Polym. Sci. **1**: 56-62.
- Baker, W. O. (1949). "Microgel, A New Macromolecule - Relation to sol and gel as structural elements of synthetic rubber." Industrial and Engineering Chemistry **41**(3): 511-520.
- Banerjee, P., D. J. Irvine, et al. (2000). "Polymer latexes for cell-resistant and cell-interactive surfaces." Journal of Biomedical Materials Research **50**(3): 331-339.
- Banerjee, P., D. J. Irvine, et al. (2000). "Polymer latexes for cell-resistant and cell-interactive surfaces." J Biomed Mater Res **50**(3): 331-9.
- Bateman, R. J., L. Y. Munsell, et al. (2007). "Stable isotope labeling tandem mass spectrometry (SILT) to quantify protein production and clearance rates." J Am Soc Mass Spectrom **18**(6): 997-1006.
- Bateman, R. J., L. Y. Munsell, et al. (2006). "Human amyloid-beta synthesis and clearance rates as measured in cerebrospinal fluid in vivo." Nat Med **12**(7): 856-61.
- Bayless, K. J. and G. E. Davis (2003). "Sphingosine-1-phosphate markedly induces matrix metalloproteinase and integrin-dependent human endothelial cell invasion and lumen formation in three-dimensional collagen and fibrin matrices." Biochem Biophys Res Commun **312**(4): 903-13.
- Ben Rejeb, S., M. Tatoulian, et al. (1998). "Functionalization of nitrocellulose membranes using ammonia plasma for the covalent attachment of antibodies for use in membrane-based immunoassays." Analytica Chimica Acta **376**(1): 133-138.
- Ben Slimane, S., R. Guidoin, et al. (1988). "Polyester arterial grafts impregnated with cross-linked albumin: the rate of degradation of the coating in vivo." Eur Surg Res **20**(1): 12-7.
- Bennett, J. S. (2001). "Platelet-fibrinogen interactions." Ann N Y Acad Sci **936**: 340-54.
- Bennett, K. L., T. Matthiesen, et al. (2000). "Probing protein surface topology by chemical surface labeling, crosslinking, and mass spectrometry." Methods Mol Biol **146**: 113-31.
- Billinger, M., F. Buddeberg, et al. (2006). "Polymer stent coating for prevention of neointimal hyperplasia." J Invasive Cardiol **18**(9): 423-6; discussion 427.
- Biltresse, S., M. Attolini, et al. (2005). "Cell adhesive PET membranes by surface grafting of RGD peptidomimetics." Biomaterials **26**(22): 4576-87.

- Blattler, T. M., S. Pasche, et al. (2006). "High salt stability and protein resistance of poly(L-lysine)-g-poly(ethylene glycol) copolymers covalently immobilized via aldehyde plasma polymer interlayers on inorganic and polymeric substrates." Langmuir **22**(13): 5760-9.
- Blomback, B., Hanson, L.A. Plasma Proteins. New York, Wiley.
- Bohnert, J. L. and T. A. Horbett (1986). "Changes in adsorbed fibrinogen and albumin interactions with polymers indicated by decreases in detergent elutability." Journal of Colloid and Interface Science **111**(2): 363-377.
- Boisson-Vidal, C., J. Jozefonvicz, et al. (1991). "Interactions of proteins in human plasma with modified polystyrene resins." J Biomed Mater Res **25**(1): 67-84.
- Boland, T., T. Xu, et al. (2006). "Application of inkjet printing to tissue engineering." Biotechnology Journal **1**(9): 910-917.
- Borth, W. (1992). "Alpha 2-macroglobulin, a multifunctional binding protein with targeting characteristics." FASEB J **6**(15): 3345-53.
- Brash, J. L. (1979). "Dependence of albumin-fibrinogen simple and competitive adsorption on surface properties of biomaterials." Journal of Polymer Science: Polymer Symposia **66**(1): 377-389.
- Brash, J. L. and V. J. Davidson (1976). "Adsorption of glass and polyethylene from solutions of fibrinogen and albumin." Thromb Res **9**(3): 249-59.
- Brash, J. L. and P. ten Hove (1984). "Effect of plasma dilution on adsorption of fibrinogen to solid surfaces." Thromb Haemost **51**(3): 326-30.
- Brash, J. L. and P. Ten Hove (1993). "Protein adsorption studies on 'standard' polymeric materials." J Biomater Sci Polym Ed **4**(6): 591-9.
- Brash, J. L., S. Uniyal, et al. (1974). "Exchange of albumin adsorbed on polymer surfaces." Trans Am Soc Artif Intern Organs **20A**: 69-76.
- Brown, J. H., N. Volkmann, et al. (2000). "The crystal structure of modified bovine fibrinogen." Proc Natl Acad Sci U S A **97**(1): 85-90.
- Bryant, S. J., J. L. Cuy, et al. (2007). "Photo-patterning of porous hydrogels for tissue engineering." Biomaterials **28**(19): 2978-2986.
- Buck, M. E., A. S. Breitbach, et al. (2009). "Chemical Modification of Reactive Multilayered Films Fabricated from Poly(2-alkenyl azlactone)s: Design of Surfaces that Prevent or Promote Mammalian Cell Adhesion and Bacterial Biofilm Growth." Biomacromolecules.
- Buijs, J., W. Norde, et al. (1996). "Changes in the secondary structure of adsorbed IgG and F(ab')(2) studied by FTIR spectroscopy." Langmuir **12**(6): 1605-1613.
- Bungenberg de Jong, H. G. (1949). Colloid Science II. New York, Elsevier Publishing Co., Inc.
- Burchenal, J. E., C. R. Deible, et al. (2002). "Polyethylene glycol diisocyanate decreases platelet deposition after balloon injury of rabbit femoral arteries." J Thromb Thrombolysis **13**(1): 27-33.
- C. William Hall, D. L., John J. Ghidoni, Michael E. De Bakey, Donald P. Dressler, (1967). "Velour fabrics applied to medicine." Journal of Biomedical Materials Research **1**(2): 179-196.
- Cacciafesta, P., A. D. L. Humphris, et al. (2000). "Human plasma fibrinogen adsorption on ultraflat titanium oxide surfaces studied with atomic force microscopy." Langmuir **16**(21): 8167-8175.

- Callow, A. D. (1988). "Problems in the construction of a small diameter graft." Int Angiol **7**(3): 246-53.
- Cao, L., M. Chang, et al. (2007). "Plasma-deposited tetraglyme surfaces greatly reduce total blood protein adsorption, contact activation, platelet adhesion, platelet procoagulant activity, and in vitro thrombus deposition." J Biomed Mater Res A **81**(4): 827-37.
- Cao, L., S. Sivaprasad, et al. (2006). "Glow discharge plasma treatment of polyethylene tubing with tetraglyme results in ultralow fibrinogen adsorption and greatly reduced platelet adhesion." Journal of Biomedical Materials Research Part A **79A**(4): 788-803.
- Carven, G. J. and L. J. Stern (2005). "Probing the ligand-induced conformational change in HLA-DR1 by selective chemical modification and mass spectrometric mapping." Biochemistry **44**(42): 13625-13637.
- Chan, B. M. C. and J. L. Brash (1981). "Conformational change in fibrinogen desorbed from glass surface." Journal of Colloid and Interface Science **84**(1): 263-265.
- Chan, C. M., T. M. Ko, et al. (1996). "Polymer surface modification by plasmas and photons." Surface Science Reports **24**(1-2): 1-54.
- Chang, T. M. (1969). "Removal of endogenous and exogenous toxins by a microencapsulated absorbent." Can J Physiol Pharmacol **47**(12): 1043-5.
- Chen Jie-Rong, W. X.-Y., Wakida Tomiji, (1999). "Wettability of poly(ethylene terephthalate) film treated with low-temperature plasma and their surface analysis by ESCA." Journal of Applied Polymer Science **72**(10): 1327-1333.
- Cheresh, D. A. (1987). "Human endothelial cells synthesize and express an Arg-Gly-Asp-directed adhesion receptor involved in attachment to fibrinogen and von Willebrand factor." Proc Natl Acad Sci U S A **84**(18): 6471-5.
- Chollet, C., C. Chanseau, et al. (2007). "RGD peptides grafting onto poly(ethylene terephthalate) with well controlled densities." Biomol Eng **24**(5): 477-82.
- Chollet, C., C. Chanseau, et al. (2009). "The effect of RGD density on osteoblast and endothelial cell behavior on RGD-grafted polyethylene terephthalate surfaces." Biomaterials **30**(5): 711-20.
- Chun, J. and H. Rosen (2006). "Lysophospholipid receptors as potential drug targets in tissue transplantation and autoimmune diseases." Curr Pharm Des **12**(2): 161-71.
- Cierniewski, C. S., E. F. Plow, et al. (1984). "Conformation of the carboxy-terminal region of the A alpha chain of fibrinogen as elucidated by immunochemical analyses." Eur J Biochem **141**(3): 489-96.
- Clarke, M. L., J. Wang, et al. (2005). "Conformational changes of fibrinogen after adsorption." J Phys Chem B Condens Matter Mater Surf Interfaces Biophys **109**(46): 22027-35.
- Crist, B. (1996). "On "pinning" domain growth in two-phase polymer liquids." Macromolecules **29**(22): 7276-7279.
- Crist, B. and A. R. Nesarikar (1995). "Coarsening in Polyethylene Copolymer Blends." Macromolecules **28**(4): 890-896.
- Cullen, D., M. Lessing, et al. (2007). "Collagen-Dependent Neurite Outgrowth and Response to Dynamic Deformation in Three-Dimensional Neuronal Cultures." Annals of Biomedical Engineering **35**(5): 835-846.

- de Feijter, J. A., J. Benjamins, et al. (1978). "Ellipsometry as a tool to study the adsorption of synthetic biopolymers at the air-water interface." *Biopolymers* **17**: 1759-1772.
- de Groot, J. H., A. Zurutuza, et al. (2001). "Water-soluble microgels made by radical polymerization in solution." *Colloid and Polymer Science* **279**(12): 1219-1224.
- Decher, G. (1997). "Fuzzy nanoassemblies: Toward layered polymeric multicomposites." *Science* **277**(5330): 1232-1237.
- Dekker, A., K. Reitsma, et al. (1991). "Adhesion of endothelial cells and adsorption of serum proteins on gas plasma-treated polytetrafluoroethylene." *Biomaterials* **12**(2): 130-8.
- DeLong, S. A., J. J. Moon, et al. (2005). "Covalently immobilized gradients of bFGF on hydrogel scaffolds for directed cell migration." *Biomaterials* **26**(16): 3227-3234.
- Deutsch, M., J. Meinhart, et al. (2009). "Long-term experience in autologous in vitro endothelialization of infrainguinal ePTFE grafts." *Journal of Vascular Surgery* **49**(2): 352-362.
- DiMilla, P. A., K. Barbee, et al. (1991). "Mathematical model for the effects of adhesion and mechanics on cell migration speed." *Biophys. J.* **60**: 15-37.
- Domurado, D., R. Guidoin, et al. (1978). "Albuminated dacron prostheses as improved blood vessel substitutes." *J Bioeng* **2**(1-2): 79-91.
- Drumheller, P. D., D. L. Elbert, et al. (1994). "Multifunctional poly(ethylene glycol) semi-interpenetrating polymer networks as highly selective adhesive substrates for bioadhesive peptide grafting." *Biotechnology and Bioengineering* **43**: 772-780.
- Drumheller, P. D. and J. A. Hubbell (1995). "Densely crosslinked polymer networks of poly(ethylene glycol) in trimethylolpropane triacrylate for cell-adhesion-resistant surfaces." *J Biomed Mater Res* **29**(2): 207-15.
- Drury, J. K., T. R. Ashton, et al. (1987). "Experimental and clinical experience with a gelatin impregnated Dacron prosthesis." *Ann Vasc Surg* **1**(5): 542-7.
- Drury, J. L. and D. J. Mooney (2003). "Hydrogels for tissue engineering: Scaffold design variables and applications." *Biomaterials* **24**: 4337-4351.
- Du, Y., E. Lo, et al. (2008). "Directed assembly of cell-laden microgels for fabrication of 3D tissue constructs." *Proceedings of the National Academy of Sciences* **105**(28): 9522-9527.
- Dubas, S. T. and J. B. Schlenoff (2001). "Polyelectrolyte Multilayers Containing a Weak Polyacid: Construction and Deconstruction." *Macromolecules* **34**(11): 3736-3740.
- Dufrene, Y. F., T. G. Marchal, et al. (1999). "Influence of Substratum Surface Properties on the Organization of Adsorbed Collagen Films: In Situ Characterization by Atomic Force Microscopy." *Langmuir* **15**(8): 2871-2878.
- Eberhart, R. C., M. S. Munro, et al. (1987). "Influence of endogenous albumin binding on blood-material interactions." *Ann N Y Acad Sci* **516**: 78-95.
- Edmunds, L. H., E. A. Hessel II, et al. (2003). "Cardiac Surgery in the Adult, second ed., McGraw-Hill Companies Inc." 315.
- Elbert, D. and J. Hubbell (1996). "Surface treatments of polymers for biocompatibility." *Annual Review of Materials Science* **26**: 365-394.

- Elbert, D. L. and J. A. Hubbell (1996). "Surface treatments of polymers for biocompatibility." Annual Review of Materials Science **26**: 365-394.
- Elbert, D. L. and J. A. Hubbell (2001). "Conjugate Addition Reactions Combined with Free-radical Cross-linking for the Design of Materials for Tissue Engineering." Biomacromolecules **2**: 430-441.
- Elbert, D. L. and J. A. Hubbell (2001). "Conjugate addition reactions combined with free-radical cross-linking for the design of materials for tissue engineering." Biomacromolecules **2**(2): 430-41.
- Elbert, D. L., K. G. Mawuenyega, et al. (2008). "Stable isotope labeling tandem mass spectrometry (SILT): integration with peptide identification and extension to data-dependent scans." J Proteome Res **7**(10): 4546-56.
- Elbert, D. L., A. B. Pratt, et al. (2001). "Protein delivery from materials formed by self-selective conjugate addition reactions." Journal of Controlled Release **76**(1-2): 11-25.
- Engel, M. F., A. J. Visser, et al. (2004). "Conformation and orientation of a protein folding intermediate trapped by adsorption." Proc Natl Acad Sci U S A **101**(31): 11316-21.
- Engler, A. J., M. A. Griffin, et al. (2004). "Myotubes differentiate optimally on substrates with tissue-like stiffness: pathological implications for soft or stiff microenvironments." J. Cell Biol. **166**(6): 877-887.
- English, D., Z. Welch, et al. (2000). "Sphingosine 1-phosphate released from platelets during clotting accounts for the potent endothelial cell chemotactic activity of blood serum and provides a novel link between hemostasis and angiogenesis." FASEB J **14**(14): 2255-65.
- English, D., Z. Welch, et al. (2000). "Sphingosine 1-phosphate released from platelets during clotting accounts for the potent endothelial cell chemotactic activity of blood serum and provides a novel link between hemostasis and angiogenesis." FASEB J. **14**(14): 2255-2265.
- Farrell, D. H., P. Thiagarajan, et al. (1992). "Role of fibrinogen alpha and gamma chain sites in platelet aggregation." Proc Natl Acad Sci U S A **89**(22): 10729-32.
- Farstad, I. N., T. S. Halstensen, et al. (1996). "Distribution of beta 7 integrins in human intestinal mucosa and organized gut-associated lymphoid tissue." Immunology **89**(2): 227-37.
- Fasol, R., P. Zilla, et al. (1989). "Human endothelial cell seeding: evaluation of its effectiveness by platelet parameters after one year." J Vasc Surg **9**(3): 432-6.
- Feder, J. (1980). "Random Sequential Adsorption." Journal of Theoretical Biology **87**(2): 237-254.
- Flick, M. J., X. Du, et al. (2004). "Leukocyte engagement of fibrin(ogen) via the integrin receptor alphaMbeta2/Mac-1 is critical for host inflammatory response in vivo." J Clin Invest **113**(11): 1596-606.
- Ford, M. C., J. P. Bertram, et al. (2006). "A macroporous hydrogel for the coculture of neural progenitor and endothelial cells to form functional vascular networks in vivo." Proceedings of the National Academy of Sciences of the United States of America **103**(8): 2512-2517.

- Franssen, O. and W. E. Hennink (1998). "A novel preparation method for polymeric microparticles without the use of organic solvents." International Journal of Pharmaceutics **168**(1): 1-7.
- Friedlander, S. K. (1977). Smoke, Dust and Haze. New York, Wiley.
- Friedlander, S. K. and C. S. Wang (1966). "The self-preserving particle size distribution for coagulation by brownian motion." Journal of Colloid and Interface Science **22**(2): 126-132.
- Friedman, M., Cavins, J.F., Wall, J.S. (1965). "Relative Nucleophilic Reactivities of Amino Groups and Mercaptride Ions in Addition Reactions with alpha, beta-Unsaturated Compounds." Journal of American Chemical Society **87**(16): 3672-3682.
- Funke, W., O. Okay, et al. (1998). "Microgels - Intramolecularly crosslinked macromolecules with a globular structure." Microencapsulation - Microgels - Iniferters **136**: 139-234.
- Gan, D. J. and L. A. Lyon (2002). "Synthesis and protein adsorption resistance of PEG-modified poly(N-isopropylacrylamide) core/shell microgels." Macromolecules **35**(26): 9634-9639.
- Ganguly, P. and N. L. Gould (1979). "Receptor aggregation: a possible mechanism of platelet stimulation by thrombin." Thromb Res **15**(5-6): 879-84.
- Gappa-Fahlenkamp, H. and R. S. Lewis (2005). "Improved hemocompatibility of poly(ethylene terephthalate) modified with various thiol-containing groups." Biomaterials **26**(17): 3479-85.
- Gasteier, P., A. Reska, et al. (2007). "Surface grafting of PEO-based star-shaped molecules for bioanalytical and biomedical applications." Macromol Biosci **7**(8): 1010-23.
- Gasteiger, E., A. Gattiker, et al. (2003). "ExpASy: The proteomics server for in-depth protein knowledge and analysis." Nucleic Acids Res **31**(13): 3784-8.
- Ghosh, P., W. M. Lackowski, et al. (2001). "Two new approaches for patterning polymer films using templates prepared by microcontact printing." Macromolecules **34**(5): 1230-1236.
- Ginsberg, M. H., A. Partridge, et al. (2005). "Integrin regulation." Curr Opin Cell Biol **17**(5): 509-16.
- Gouny, P., C. Hocquet-Cheynel, et al. (1995). "Incorporation of fibronectin-impregnated vascular prostheses in the pig. Microscope study." J Cardiovasc Surg (Torino) **36**(6): 573-80.
- Graham, N. B. and A. Cameron (1998). "Nanogels and microgels: The new polymeric materials playground." Pure and Applied Chemistry **70**(6): 1271-1275.
- Graham, N. B. and J. W. Mao (1996). "Microgels .2. Solution polymerization using a urethane stepgrowth mechanism." Colloids and Surfaces a-Physicochemical and Engineering Aspects **118**(3): 211-220.
- Graham, N. B., J. W. Mao, et al. (1996). "Microgels .4. The preparation of novel microgels and their applications." Angewandte Makromolekulare Chemie **240**: 113-121.
- Green, C. E., U. Y. Schaff, et al. (2006). "Dynamic shifts in LFA-1 affinity regulate neutrophil rolling, arrest, and transmigration on inflamed endothelium." Blood **107**(5): 2101-11.

- Griesser, H. J., R. C. Chatelier, et al. (1994). "Growth of human cells on plasma polymers: putative role of amine and amide groups." J Biomater Sci Polym Ed **5**(6): 531-54.
- Groll, J., J. Fiedler, et al. (2005). "A novel star PEG-derived surface coating for specific cell adhesion." J Biomed Mater Res A **74**(4): 607-17.
- Groll, J., W. Haubensak, et al. (2005). "Ultrathin coatings from isocyanate terminated star PEG prepolymers: Patterning of proteins on the layers." Langmuir **21**(7): 3076-3083.
- Gygi, S. P., B. Rist, et al. (1999). "Quantitative analysis of complex protein mixtures using isotope-coded affinity tags." Nat Biotechnol **17**(10): 994-9.
- H. G. Bungenberg de Jon, H. R. K. (1929). Proc. Krungl. Ned. Acad. Wetensch **32**: 849.
- Hager-Braun, C. and K. B. Tomer (2002). "Characterization of the tertiary structure of soluble CD4 bound to glycosylated full-length HIVgp120 by chemical modification of arginine residues and mass spectrometric analysis." Biochemistry **41**(6): 1759-66.
- Hall, C. E. and H. S. Slayter (1959). "The fibrinogen molecule: its size, shape, and mode of polymerization." J Biophys Biochem Cytol **5**(1): 11-6.
- Halstenberg, S., A. Panitch, et al. (2002). "Biologically engineered protein-graft-poly(ethylene glycol) hydrogels: a cell adhesive and plasmin-degradable biosynthetic material for tissue repair." Biomacromolecules **3**(4): 710-23.
- Harris, J. M. (1992). Poly(Ethylene Glycol) Chemistry: Biotechnical and Biomedical Applications. New York, Plenum Press.
- Hashimoto, T., M. Takenaka, et al. (1992). "Spontaneous pinning of domain growth during spinodal decomposition of off-critical polymer mixtures." The Journal of Chemical Physics **97**(1): 679-689.
- Hawiger, J., S. Timmons, et al. (1982). "gamma and alpha chains of human fibrinogen possess sites reactive with human platelet receptors." Proc Natl Acad Sci U S A **79**(6): 2068-71.
- Hench, L. L. and J. M. Polak (2002). "Third-generation biomedical materials." Science **295**(5557): 1014-7.
- Herring, M., A. Gardner, et al. (1984). "Seeding human arterial prostheses with mechanically derived endothelium. The detrimental effect of smoking." J Vasc Surg **1**(2): 279-89.
- Heuberger, M., T. Drobek, et al. (2005). "Interaction forces and morphology of a protein-resistant poly(ethylene glycol) layer." Biophys J **88**(1): 495-504.
- Hill-West, J. L., S. M. Chowdhury, et al. (1994). "Inhibition of thrombosis and intimal thickening by in situ photopolymerization of thin hydrogel barriers." Proc Natl Acad Sci U S A **91**(13): 5967-71.
- Hill, E., T. Boontheekul, et al. (2006). "Designing Scaffolds to Enhance Transplanted Myoblast Survival and Migration." Tissue Engineering **12**(5): 1295-1304.
- Hinrichsen, E. L., J. Feder, et al. (1986). "Geometry of random sequential adsorption." J Stat Phys **44**: 793-827.
- Hla, T. (2004). "Physiological and pathological actions of sphingosine 1-phosphate." Semin Cell Dev Biol **15**(5): 513-20.

- Hoffmann, J., J. Groll, et al. (2006). "Blood cell and plasma protein repellent properties of Star-PEG-modified surfaces." Journal of Biomaterials Science-Polymer Edition **17**(9): 985-996.
- Holland, N. B. and R. E. Marchant (2000). "Individual plasma proteins detected on rough biomaterials by phase imaging AFM." J Biomed Mater Res **51**(3): 307-15.
- Holland, T. A., J. K. Tessmar, et al. (2004). "Transforming growth factor-beta 1 release from oligo(poly(ethylene glycol) fumarate) hydrogels in conditions that model the cartilage wound healing environment." J Control Release **94**(1): 101-14.
- Hook, F., B. Kasemo, et al. (2001). "Variations in coupled water, viscoelastic properties, and film thickness of a Mefp-1 protein film during adsorption and cross-linking: a quartz crystal microbalance with dissipation monitoring, ellipsometry, and surface plasmon resonance study." Anal Chem **73**(24): 5796-804.
- Horbett, T. A. (1984). "Mass action effects on competitive adsorption of fibrinogen from hemoglobin solutions and from plasma." Thromb Haemost **51**(2): 174-81.
- Horbett, T. A. (2004). "The role of adsorbed proteins in tissue response to biomaterials. In: Ratner B, Hoffman A, editors. Biomaterials science: an introduction to materials in medicine. 2nd ed. San Diego: Elsevier Academic Press." 237-46.
- Horne, R. A., J. P. Almeida, et al. (1971). "Macromolecule hydration and the effect of solutes on the cloud point of aqueous solutions of polyvinyl methyl ether: a possible model for protein denaturation and temperature control in homeothermic animals." J Colloid Interface Sci **35**(1): 77-84.
- Humphrey, W., A. Dalke, et al. (1996). "VMD: visual molecular dynamics." J Mol Graph **14**(1): 33-8, 27-8.
- Hylton, D. M., S. W. Shalaby, et al. (2005). "Direct correlation between adsorption-induced changes in protein structure and platelet adhesion." J Biomed Mater Res A **73**(3): 349-58.
- Hyun, J., H. Ma, et al. (2003). "Universal Route to Cell Micropatterning Using an Amphiphilic Comb Polymer." Advanced Materials **15**(7-8): 576-579.
- Imai, Y., K. Tajima, et al. (1971). "Biologized materials for cardiovascular prosthesis." Trans Am Soc Artif Intern Organs **17**: 6-9.
- Irvine, D. J., A. M. Mayes, et al. (2001). "Nanoscale Clustering of RGD Peptides at Surfaces Using Comb Polymers. 1. Synthesis and Characterization of Comb Thin Films." Biomacromolecules **2**(1): 85-94.
- Ito, K., Y. Anada, et al. (2007). "Lack of sphingosine 1-phosphate-degrading enzymes in erythrocytes." Biochem Biophys Res Commun **357**(1): 212-7.
- J. Milton Harris, E. C. S. M. G. C. M. S. P. M. Y. J. M. V. A. D. E. B. (1984). "Synthesis and characterization of poly(ethylene glycol) derivatives." Journal of Polymer Science: Polymer Chemistry Edition **22**(2): 341-352.
- J.D. Gunton, M. S. M., P.S Sahni (1983). Phase Transitions and Critical Phenomena. London, Academic.
- Jensen, N., B. Lindblad, et al. (1996). "In vitro attachment of endothelial cells to different graft materials." Eur Surg Res **28**(1): 49-54.
- Jeon, S., J. Lee, et al. (1991). "Protein Surface Interactions in the Presence of Polyethylene Oxide .1. Simplified Theory." Journal of Colloid and Interface Science **142**: 149-158.

- Jeon, S. I. and J. D. Andrade (1991). "Protein Surface Interactions in the Presence of Polyethylene Oxide .2. Effect of Protein Size." Journal of Colloid and Interface Science **142**(1): 159-166.
- Jeon, S. I., J. H. Lee, et al. (1991). "Protein Surface Interactions in the Presence of Polyethylene Oxide .1. Simplified Theory." Journal of Colloid and Interface Science **142**(1): 149-158.
- Kawaguchi, H., K. Fujimoto, et al. (1992). "Hydrogel microspheres III. Temperature-dependent adsorption of proteins on poly-N-isopropylacrylamide hydrogel microspheres." Colloid & Polymer Science **270**(1): 53-57.
- Kim, J., B. K. Wacker, et al. (2007). "Thin polymer layers formed using multiarm poly(ethylene glycol) vinylsulfone by a covalent layer-by-layer method." Biomacromolecules **8**(11): 3682-6.
- Kim, J. K., E. A. Scott, et al. (2005). "Proteomic analysis of protein adsorption: serum amyloid P adsorbs to materials and promotes leukocyte adhesion." J Biomed Mater Res A **75**(1): 199-209.
- Kim, J. W., A. S. Utada, et al. (2007). "Fabrication of monodisperse gel shells and functional microgels in microfluidic devices." Angewandte Chemie-International Edition **46**(11): 1819-1822.
- Kim, S. W., R. G. Lee, et al. (1974). "Platelet adhesion to polymer surfaces." Trans Am Soc Artif Intern Organs **20 B**: 449-55.
- Kizilel, S., E. Sawardecker, et al. (2006). "Sequential formation of covalently bonded hydrogel multilayers through surface initiated photopolymerization." Biomaterials **27**(8): 1209-15.
- Kjellander, R. and E. Florin (1981). "Water Structure and changes in thermal stability of the system poly(ethylene oxide)-water." J. Chem. Soc. Faraday Trans. **77**: 2053-2077.
- Kloczewiak, M., S. Timmons, et al. (1984). "Platelet receptor recognition site on human fibrinogen. Synthesis and structure-function relationship of peptides corresponding to the carboxy-terminal segment of the gamma chain." Biochemistry **23**(8): 1767-74.
- Knochenmuss, R., A. Stortelder, et al. (2000). "Secondary ion-molecule reactions in matrix-assisted laser desorption/ionization." J Mass Spectrom **35**(11): 1237-45.
- Knowles, B. B., C. C. Howe, et al. (1980). "Human hepatocellular carcinoma cell lines secrete the major plasma proteins and hepatitis B surface antigen." Science **209**(4455): 497-9.
- Kohama, T., A. Olivera, et al. (1998). "Molecular cloning and functional characterization of murine sphingosine kinase." J Biol Chem **273**(37): 23722-8.
- Kottke-Marchant, K., J. M. Anderson, et al. (1987). "Vascular graft-associated complement activation and leukocyte adhesion in an artificial circulation." J Biomed Mater Res **21**(3): 379-97.
- Kouvroukoglou, S., K. C. Dee, et al. (2000). "Endothelial cell migration on surfaces modified with immobilized adhesive peptides." Biomaterials **21**(17): 1725-33.
- Krishnan, A., Y. H. Liu, et al. (2006). "Interfacial energetics of globular-blood protein adsorption to a hydrophobic interface from aqueous-buffer solution." J R Soc Interface **3**(7): 283-301.
- Kruyt, H. R. (1949). Colloid Science, Vol. I. Amsterdam, Elsevier.

- Kuhl, P. R. and L. G. Griffith-Cima (1996). "Tethered epidermal growth factor as a paradigm for growth factor-induced stimulation from the solid phase." Nat Med **2**(9): 1022-1027.
- Lackowski, W. M., P. Ghosh, et al. (1999). "Micron-Scale Patterning of Hyperbranched Polymer Films by Micro-Contact Printing." J. Am. Chem. Soc. **121**(6): 1419-1420.
- Lai, G., Y. Li, et al. (2008). "Effect of concentration and temperature on the rheological behavior of collagen solution." International Journal of Biological Macromolecules **42**(3): 285-291.
- Laidler, K. (1987). Chemical Kinetics. New York, Harper & Row, Inc.
- Lal, J. and R. Bansil (1991). "Light-scattering study of kinetics of spinodal decomposition in a polymer solution." Macromolecules **24**(1): 290-297.
- Langlois, S., D. Gingras, et al. (2004). "Membrane type 1-matrix metalloproteinase (MT1-MMP) cooperates with sphingosine 1-phosphate to induce endothelial cell migration and morphogenic differentiation." Blood **103**(8): 3020-8.
- Lassen, B. and M. Malmsten (1996). "Structure of protein layers during competitive adsorption." Journal of Colloid and Interface Science **180**(2): 339-349.
- Lauer, J. L., J. L. Shohet, et al. (2004). Control of uniformity of plasma-surface modification inside of small-diameter polyethylene tubing using microplasma diagnostics. Plasma Science, 2004. ICOPS 2004. IEEE Conference Record - Abstracts. The 31st IEEE International Conference on.
- Lauger, J., R. Lay, et al. (1994). "The percolation-to-cluster transition during spinodal decomposition of an off-critical polymer mixture. Observation by light scattering and optical microscopy." The Journal of Chemical Physics **101**(8): 7181-7184.
- Lee, M. J., S. Thangada, et al. (1999). "Vascular endothelial cell adherens junction assembly and morphogenesis induced by sphingosine-1-phosphate." Cell **99**(3): 301-12.
- Levental, I., P. C. Georges, et al. (2007). "Soft biological materials and their impact on cell function." Soft Matter **3**(3): 299-306.
- Lévesque, S. G., R. M. Lim, et al. (2005). "Macroporous interconnected dextran scaffolds of controlled porosity for tissue-engineering applications." Biomaterials **26**(35): 7436-7446.
- Li, R., N. Mitra, et al. (2003). "Activation of integrin α IIb β 3 by modulation of transmembrane helix associations." Science **300**(5620): 795-8.
- Lifshitz, I. M. and V. V. Slyozov (1961). "The kinetics of precipitation from supersaturated solid solutions." Journal of Physics and Chemistry of Solids **19**(1-2): 35-50.
- Lifshitz, I. M. and V. V. Slyozov (1961). "The Kinetics of Precipitation from Supersaturated Solid Solutions." J. Phys. Chem. Solids **19**: 35-50.
- Lim, T. Y., C. K. Poh, et al. (2009). "Poly (lactic-co-glycolic acid) as a controlled release delivery device." J Mater Sci Mater Med.
- Lindon, J. N., G. McManama, et al. (1986). "Does the conformation of adsorbed fibrinogen dictate platelet interactions with artificial surfaces?" Blood **68**(2): 355-62.

- Litvinov, R. I., H. Shuman, et al. (2002). "Binding strength and activation state of single fibrinogen-integrin pairs on living cells." Proc Natl Acad Sci U S A **99**(11): 7426-31.
- Liu, K.-J. and J. L. Parsons (1969). "Solvent Effects on the Preferred Conformation of Poly(ethylene glycols)." Macromolecules **2**(5): 529-533.
- Liu, Q. D., M. M. Rooney, et al. (1998). "Role of the gamma chain Ala-Gly-Asp-Val and A alpha chain Arg-Gly-Asp-Ser sites of fibrinogen in coaggregation of platelets and fibrinogen-coated beads." Biochimica Et Biophysica Acta-Protein Structure and Molecular Enzymology **1385**(1): 33-42.
- Liu, X., S. J. Valentine, et al. (2007). "Mapping the human plasma proteome by SCX-LC-IMS-MS." J Am Soc Mass Spectrom **18**(7): 1249-64.
- Lok, B. K., Y.-L. Cheng, et al. (1983). "Protein adsorption on crosslinked polydimethylsiloxane using total internal reflection fluorescence." Journal of Colloid and Interface Science **91**(1): 104-116.
- Lopez, G. P., B. D. Ratner, et al. (1992). "Glow discharge plasma deposition of tetraethylene glycol dimethyl ether for fouling-resistant biomaterial surfaces." J Biomed Mater Res **26**(4): 415-39.
- Lu, D. R. and K. Park (1991). "Effect of surface hydrophobicity on the conformational changes of adsorbed fibrinogen." Journal of Colloid and Interface Science **144**(1): 271-281.
- Lu, X. Y., Y. Huang, et al. (2003). "An effective method for quantitative evaluation of proteins adsorbed on biomaterial surfaces." J Biomed Mater Res A **66**(3): 722-7.
- Lu, Y., G. Mapili, et al. (2006). "A digital micro-mirror device-based system for the microfabrication of complex, spatially patterned tissue engineering scaffolds." J Biomed Mater Res A **77**(2): 396-405.
- Luck, M., B. R. Paulke, et al. (1998). "Analysis of plasma protein adsorption on polymeric nanoparticles with different surface characteristics." J Biomed Mater Res **39**(3): 478-85.
- Lukosz, W. (1991). "Principles and Sensitivities of Integrated Optical and Surface-Plasmon Sensors for Direct Affinity Sensing and Immunosensing." Biosensors & Bioelectronics **6**(3): 215-225.
- Lussi, J. W., D. Falconnet, et al. (2006). "Pattern stability under cell culture conditions--a comparative study of patterning methods based on PLL-g-PEG background passivation." Biomaterials **27**(12): 2534-41.
- Lussi, J. W., D. Falconnet, et al. (2006). "Pattern stability under cell culture conditions--A comparative study of patterning methods based on PLL-g-PEG background passivation." Biomaterials **27**(12): 2534-2541.
- Lutolf, M. P. (2003). "Repair of bone defects using synthetic mimetics of collagenous extracellular matrices." Nat. Biotechnol. **21**: 513-518.
- Lutolf, M. P. (2003). "Synthetic matrix metalloproteinase-sensitive hydrogels for the conduction of tissue regeneration: Engineering cell-invasion characteristics." Proc. Natl. Acad. Sci. USA **100**: 5413-5418.
- Lutolf, M. P. and J. A. Hubbell (2005). "Synthetic biomaterials as instructive extracellular microenvironments for morphogenesis in tissue engineering." Nat Biotech **23**(1): 47-55.

- Ma, H. W., J. H. Hyun, et al. (2004). "'Non-fouling" oligo(ethylene glycol)-functionalized polymer brushes synthesized by surface-initiated atom transfer radical polymerization." Advanced Materials **16**(4): 338-+.
- Madrazo, J., J. H. Brown, et al. (2001). "Crystal structure of the central region of bovine fibrinogen (E5 fragment) at 1.4-Å resolution." Proc Natl Acad Sci U S A **98**(21): 11967-72.
- Magan, R. V. and R. Sureshkumar (2006). "Multiscale-linking simulation of irreversible colloidal deposition in the presence of DLVO interactions." J Colloid Interface Sci **297**(2): 389-406.
- Malda, J., T. B. Woodfield, et al. (2004). "The effect of PEGT/PBT scaffold architecture on oxygen gradients in tissue engineered cartilaginous constructs." Biomaterials **25**(26): 5773-80.
- Malda, J., T. B. Woodfield, et al. (2005). "The effect of PEGT/PBT scaffold architecture on the composition of tissue engineered cartilage." Biomaterials **26**(1): 63-72.
- Malmsten, M. (1994). "Ellipsometry Studies of Protein Layers Adsorbed at Hydrophobic Surfaces." Journal of Colloid and Interface Science **166**(2): 333-342.
- Malmstrom, J., H. Agheli, et al. (2007). "Viscoelastic modeling of highly hydrated laminin layers at homogeneous and nanostructured surfaces: quantification of protein layer properties using QCM-D and SPR." Langmuir **23**(19): 9760-8.
- Mann, M. (2006). "Functional and quantitative proteomics using SILAC." Nat Rev Mol Cell Biol **7**(12): 952-8.
- Masri, M. S. and M. Friedman (1988). "Protein reactions with methyl and ethyl vinyl sulfones." J Protein Chem **7**(1): 49-54.
- Massia, S. P. and J. A. Hubbell (1990). "Covalent surface immobilization of Arg-Gly-Asp- and Tyr-Ile-Gly-Ser-Arg-containing peptides to obtain well-defined cell-adhesive substrates." Anal Biochem **187**(2): 292-301.
- Massia, S. P. and J. A. Hubbell (1991). "An RGD spacing of 440 nm is sufficient for integrin alpha V beta 3-mediated fibroblast spreading and 140 nm for focal contact and stress fiber formation." J Cell Biol **114**(5): 1089-100.
- Matloubian, M., C. G. Lo, et al. (2004). "Lymphocyte egress from thymus and peripheral lymphoid organs is dependent on S1P receptor 1." Nature **427**(6972): 355-60.
- Maxfield, J. and I. W. Shepherd (1975). "Conformation of poly(ethylene oxide) in the solid state, melt and solution measured by Raman scattering." Polymer **16**(7): 505-509.
- McGuigan, A. P. and M. V. Sefton (2006). "Vascularized organoid engineered by modular assembly enables blood perfusion." Proceedings of the National Academy of Sciences **103**(31): 11461-11466.
- McGurk, S. L., R. J. Green, et al. (1999). "Molecular Interactions of Biomolecules with Surface-Engineered Interfaces Using Atomic Force Microscopy and Surface Plasmon Resonance." Langmuir **15**(15): 5136-5140.
- McManama, G., J. N. Lindon, et al. (1986). "Platelet aggregation by fibrinogen polymers crosslinked across the E domain." Blood **68**(2): 363-71.
- McPherson, T. B., H. S. Shim, et al. (1997). "Grafting of PEO to glass, nitinol, and pyrolytic carbon surfaces by gamma irradiation." Journal of Biomedical Materials Research **38**(4): 289-302.

- Mehta, N. J. and I. A. Khan (2002). "Cardiology's 10 greatest discoveries of the 20th century." Tex Heart Inst J **29**(3): 164-71.
- Metanovski, W. V. (1991). Compendium of Macromolecular Nomenclature: The Purple Book. Oxford, Blackwell Science.
- Metters, A. and J. Hubbell (2005). "Network Formation and Degradation Behavior of Hydrogels Formed by Michael-Type Addition Reactions." Biomacromolecules **6**(1): 290-301.
- Mohammad, S. F., M. D. Hardison, et al. (1974). "Adhesion of human blood platelets to glass and polymer surfaces. I. Studies with platelets in plasma." Haemostasis **3**(5-6): 257-70.
- Moore, K., M. Macsween, et al. (2006). "Immobilized Concentration Gradients of Neurotrophic Factors Guide Neurite Outgrowth of Primary Neurons in Macroporous Scaffolds." Tissue Engineering **12**(2): 267-278.
- Morpurgo, M., F. M. Veronese, et al. (1996). "Preparation and Characterization of Poly(ethylene glycol) Vinyl Sulfone." Bioconjugate Chem. **7**(3): 363-368.
- Morrissey, B. W. (1977). "THE ADSORPTION AND CONFORMATION OF PLASMA PROTEINS: A PHYSICAL APPROACH*." Annals of the New York Academy of Sciences **283**(1): 50-64.
- Morton, T. A., D. G. Myszka, et al. (1995). "Interpreting complex binding kinetics from optical biosensors: a comparison of analysis by linearization, the integrated rate equation, and numerical integration." Anal Biochem **227**(1): 176-85.
- Muller, E. A. and P. Rasmussen (1991). "Densities and Excess Volumes in Aqueous Poly(Ethylene Glycol) Solutions." Journal of Chemical and Engineering Data **36**(2): 214-217.
- Munro, M. S., A. J. Quattrone, et al. (1981). "Alkyl substituted polymers with enhanced albumin affinity." Trans Am Soc Artif Intern Organs **27**: 499-503.
- Ngankam, A. P., G. Mao, et al. (2004). "Fibronectin Adsorption onto Polyelectrolyte Multilayer Films." Langmuir **20**(8): 3362-3370.
- Noishiki, Y. and M. Chvapil (1987). "Healing Pattern of Collagen-Impregnated and Preclotted Vascular Grafts in Dogs." Vascular and Endovascular Surgery **21**(6): 401-411.
- Nolan, C. M., C. D. Reyes, et al. (2005). "Phase transition behavior, protein adsorption, and cell adhesion resistance of poly(ethylene glycol) cross-linked microgel particles." Biomacromolecules **6**(4): 2032-9.
- Nolan, C. M., C. D. Reyes, et al. (2005). "Phase transition behavior, protein adsorption, and cell adhesion resistance of poly(ethylene glycol) cross-linked microgel particles." Biomacromolecules **6**(4): 2032-2039.
- Norde, W. (1986). "Adsorption of proteins from solution at the solid-liquid interface." Advances in Colloid and Interface Science **25**: 267-340.
- Norde, W., F. MacRitchie, et al. (1986). "Protein adsorption at solid-liquid interfaces: Reversibility and conformation aspects." Journal of Colloid and Interface Science **112**(2): 447-456.
- Oda, Y., K. Huang, et al. (1999). "Accurate quantitation of protein expression and site-specific phosphorylation." Proc Natl Acad Sci U S A **96**(12): 6591-6.

- Ong, S. E., B. Blagoev, et al. (2002). "Stable isotope labeling by amino acids in cell culture, SILAC, as a simple and accurate approach to expression proteomics." Mol Cell Proteomics **1**(5): 376-86.
- Osathanon, T., M. L. Linnes, et al. (2008). "Microporous nanofibrous fibrin-based scaffolds for bone tissue engineering." Biomaterials **29**(30): 4091-4099.
- Ostuni, E., R. G. Chapman, et al. (2001). "A Survey of Structure-Property Relationships of Surfaces that Resist the Adsorption of Protein." Langmuir **17**(18): 5605-5620.
- Ostwald, W. (1900). Z. Phys. Chem. **34**: 495.
- Parish, C. R. (2006). "The role of heparan sulphate in inflammation." Nat Rev Immunol **6**(9): 633-43.
- Parry, T. J., R. Brosius, et al. (2005). "Drug-eluting stents: sirolimus and paclitaxel differentially affect cultured cells and injured arteries." Eur J Pharmacol **524**(1-3): 19-29.
- Patel, P. N., A. S. Gobin, et al. (2005). "Poly(ethylene glycol) hydrogel system supports preadipocyte viability, adhesion, and proliferation." Tissue Eng **11**(9-10): 1498-505.
- Pautot, S., C. Wyart, et al. (2008). "Colloid-guided assembly of oriented 3D neuronal networks." Nat Meth **5**(8): 735-740.
- Peppas, N. A. and R. Langer (1994). "New challenges in biomaterials." Science **263**(5154): 1715-20.
- Picart, C., C. Gergely, et al. (2004). "Measurement of film thickness up to several hundreds of nanometers using optical waveguide lightmode spectroscopy." Biosens Bioelectron **20**(3): 553-61.
- Pierschbacher, M. D. and E. Ruoslahti (1984). "Cell attachment activity of fibronectin can be duplicated by small synthetic fragments of the molecule." Nature **309**(5963): 30-3.
- Pitt, W. G., S. H. Spiegelberg, et al. (1987). Proteins at Interfaces: Physicochemical and Biochemical Studies. Washington DC, American Chemical Society.
- Place, E. S., J. H. George, et al. (2009). "Synthetic polymer scaffolds for tissue engineering." Chem Soc Rev **38**(4): 1139-51.
- Plow, E. F. and G. A. Marguerie (1980). "Participation of ADP in the binding of fibrinogen to thrombin-stimulated platelets." Blood **56**(3): 553-5.
- Podolnikova, N. P., V. P. Yakubenko, et al. (2003). "Identification of a novel binding site for platelet integrins alpha(IIb)beta(3) (GPIIb/IIIa) and alpha(5)beta(1) in the gamma C-domain of fibrinogen." Journal of Biological Chemistry **278**(34): 32251-32258.
- Qiu, Q., M. Sayer, et al. (1998). "Attachment, morphology, and protein expression of rat marrow stromal cells cultured on charged substrate surfaces." J Biomed Mater Res **42**(1): 117-27.
- Raeber, G. P., M. P. Lutolf, et al. (2005). "Molecularly Engineered PEG Hydrogels: A Novel Model System for Proteolytically Mediated Cell Migration." **89**(2): 1374-1388.
- Ramires, P. A., L. Mirengi, et al. (2000). "Plasma-treated PET surfaces improve the biocompatibility of human endothelial cells." J Biomed Mater Res **51**(3): 535-9.
- Ramsden, J. J. (1993). "Concentration scaling of protein deposition kinetics." Physical Review Letters **71**(2): 295-298.

- Ratke, L. and P. W. Voorhees (2002). Growth and Coarsening: Ostwald Ripening in Material Processing. Berlin, Springer-Verlag.
- Ratner, B. D. (1996). "The engineering of biomaterials exhibiting recognition and specificity." J Mol Recognit **9**(5-6): 617-25.
- Retzinger, G. S., B. C. Cook, et al. (1994). "The Binding of Fibrinogen to Surfaces and the Identification of Two Distinct Surface-Bound Species of the Protein." Journal of Colloid and Interface Science **168**(2): 514-521.
- Reza Arshady (1990). "Microspheres and microcapsules, a survey of manufacturing techniques Part II: Coacervation." Polymer Engineering & Science **30**(15): 905-914.
- Riccardi, C., R. Barni, et al. (2003). "Surface modification of poly(ethylene terephthalate) fibers induced by radio frequency air plasma treatment." Applied Surface Science **211**(1-4): 386-397.
- Richardson, T. P., M. C. Peters, et al. (2001). "Polymeric system for dual growth factor delivery." Nat. Biotechnol. **19**: 1029-1034.
- Rivest, C., D. W. G. Morrison, et al. (2007). "Microscale hydrogels for medicine and biology: Synthesis, characteristics and applications." Journal of Mechanics of Materials and Structures **2**(6): 1103-1119.
- Roach, P., D. Farrar, et al. (2005). "Interpretation of protein adsorption: Surface-induced conformational changes." Journal of the American Chemical Society **127**(22): 8168-8173.
- Roald, H. E., R. M. Barstad, et al. (1994). "Initial interactions of platelets and plasma proteins in flowing non-anticoagulated human blood with the artificial surfaces Dacron and PTFE." Blood Coagul Fibrinolysis **5**(3): 355-63.
- Robinson, C. V., M. Gross, et al. (1994). "Conformation of GroEL-bound alpha-lactalbumin probed by mass spectrometry." Nature **372**(6507): 646-51.
- Roesli, C., G. Elia, et al. (2006). "Two-dimensional mass spectrometric mapping." Curr Opin Chem Biol **10**(1): 35-41.
- Rose, D. M., R. Alon, et al. (2007). "Integrin modulation and signaling in leukocyte adhesion and migration." Immunol Rev **218**: 126-34.
- Rosenberg, R. D. and P. S. Damus (1973). "The purification and mechanism of action of human antithrombin-heparin cofactor." J Biol Chem **248**(18): 6490-505.
- Ross, P. L., Y. N. Huang, et al. (2004). "Multiplexed protein quantitation in *Saccharomyces cerevisiae* using amine-reactive isobaric tagging reagents." Mol Cell Proteomics **3**(12): 1154-69.
- Rumisek, J. D., C. E. Wade, et al. (1986). "Heat-denatured albumin-coated Dacron vascular grafts: physical characteristics and in vivo performance." J Vasc Surg **4**(2): 136-43.
- Russell E. Phares Jr., G. J. S. (1964). "Coating pharmaceuticals by coacervation." Journal of Pharmaceutical Sciences **53**(5): 515-518.
- Salzman, E. W., J. Lindon, et al. (1987). "Role of fibrinogen in activation of platelets by artificial surfaces." Ann N Y Acad Sci **516**: 184-95.
- Sannino, A., P. A. Netti, et al. (2006). "Synthesis and characterization of macroporous poly(ethylene glycol)-based hydrogels for tissue engineering application." Journal of Biomedical Materials Research Part A **79A**(2): 229-236.

- Santore, M. M. and C. F. Wertz (2005). "Protein spreading kinetics at liquid-solid interfaces via an adsorption probe method." Langmuir **21**(22): 10172-10178.
- Sarkar, S., K. M. Sales, et al. (2007). "Addressing thrombogenicity in vascular graft construction." J Biomed Mater Res B Appl Biomater **82**(1): 100-8.
- Savage, B. and Z. M. Ruggeri (1991). "Selective recognition of adhesive sites in surface-bound fibrinogen by glycoprotein IIb-IIIa on nonactivated platelets." J Biol Chem **266**(17): 11227-33.
- Sawhney, A. S., C. P. Pathak, et al. (1993). "Interfacial photopolymerization of poly(ethylene glycol)-based hydrogels upon alginate-poly(l-lysine) microcapsules for enhanced biocompatibility." Biomaterials **14**(13): 1008-16.
- Schaaf, P. and J. Talbot (1989). "Kinetics of random sequential adsorption." Physical Review Letters **62**(2): 175-178.
- Schaaf, P. and J. Talbot (1989). "Surface Exclusion Effects in Adsorption Processes." Journal of Chemical Physics **91**(7): 4401-4409.
- Schmaier, A. H., L. Silver, et al. (1984). "The effect of high molecular weight kininogen on surface-adsorbed fibrinogen." Thromb Res **33**(1): 51-67.
- Schultze, H. E., Heremans, J.J. (1966). Molecular Biology of Plasma Proteins. Amsterdam, Elsevier.
- Scott, C. F. (1991). "Mechanism of the participation of the contact system in the Vroman effect. Review and summary." J Biomater Sci Polym Ed **2**(3): 173-81.
- Scott, C. F., L. D. Silver, et al. (1984). "Cleavage of human high molecular weight kininogen markedly enhances its coagulant activity. Evidence that this molecule exists as a procofactor." J Clin Invest **73**(4): 954-62.
- Scott, E. A. and D. L. Elbert (2007). "Mass spectrometric mapping of fibrinogen conformations at poly(ethylene terephthalate) interfaces." Biomaterials **28**(27): 3904-17.
- Scott, E. A., M. D. Nichols, et al. (2008). "Protein adsorption and cell adhesion on nanoscale bioactive coatings formed from poly(ethylene glycol) and albumin microgels." Biomaterials **29**(34): 4481-4493.
- Serban, M. A. and G. D. Prestwich (2008). "Modular extracellular matrices: solutions for the puzzle." Methods **45**(1): 93-8.
- Serizawa, T., K.-i. Hamada, et al. (2000). "Stepwise Stereocomplex Assembly of Stereoregular Poly(methyl methacrylate)s on a Substrate." Journal of the American Chemical Society **122**(9): 1891-1899.
- Sethuraman, A., M. Han, et al. (2004). "Effect of surface wettability on the adhesion of proteins." Langmuir **20**(18): 7779-88.
- Shapiro, L. and S. Cohen (1997). "Novel alginate sponges for cell culture and transplantation." Biomaterials **18**(8): 583-590.
- Shen, M. and T. A. Horbett (2001). "The effects of surface chemistry and adsorbed proteins on monocyte/macrophage adhesion to chemically modified polystyrene surfaces." J Biomed Mater Res **57**(3): 336-45.
- Shen, M., L. Martinson, et al. (2002). "PEO-like plasma polymerized tetraglyme surface interactions with leukocytes and proteins: in vitro and in vivo studies." J Biomater Sci Polym Ed **13**(4): 367-90.

- Shiba, E., J. N. Lindon, et al. (1991). "Antibody-detectable changes in fibrinogen adsorption affecting platelet activation on polymer surfaces." Am J Physiol **260**(5 Pt 1): C965-74.
- Shimaoka, M. and T. A. Springer (2003). "Therapeutic antagonists and conformational regulation of integrin function." Nat Rev Drug Discov **2**(9): 703-16.
- Singh, N., A. W. Bridges, et al. (2007). "Covalent tethering of functional microgel films onto poly(ethylene terephthalate) surfaces." Biomacromolecules **8**(10): 3271-3275.
- Sit, P. S. and R. E. Marchant (1999). "Surface-dependent conformations of human fibrinogen observed by atomic force microscopy under aqueous conditions." Thrombosis and Haemostasis **82**(3): 1053-1060.
- Slack, S. M., J. L. Bohnert, et al. (1987). "The effects of surface chemistry and coagulation factors on fibrinogen adsorption from plasma." Ann N Y Acad Sci **516**: 223-43.
- Slack, S. M. and T. A. Horbett (1988). "Physicochemical and biochemical aspects of fibrinogen adsorption from plasma and binary protein solutions onto polyethylene and glass." Journal of Colloid and Interface Science **124**(2): 535-551.
- Slack, S. M. and T. A. Horbett (1989). "Changes in the Strength of Fibrinogen Attachment to Solid-Surfaces - an Explanation of the Influence of Surface-Chemistry on the Vroman Effect." Journal of Colloid and Interface Science **133**(1): 148-165.
- Slack, S. M. and T. A. Horbett (1995). "The Vroman effect - a critical review." ACS Symp Ser **602**: 112-28.
- Slack, S. M., S. E. Posso, et al. (1991). "Measurement of fibrinogen adsorption from blood plasma using 125I-fibrinogen and a direct ELISA technique." J Biomater Sci Polym Ed **3**(1): 49-67.
- Smith, W. V. and R. H. Ewart (1948). "Kinetics of emulsion polymerization." J. Chem. Phys. **16**: 592-599.
- Soderquist, M. E. and A. G. Walton (1980). "Structural changes in proteins adsorbed on polymer surfaces." Journal of Colloid and Interface Science **75**(2): 386-397.
- Spraggon, G., S. J. Everse, et al. (1997). "Crystal structures of fragment D from human fibrinogen and its crosslinked counterpart from fibrin (vol 389, pg 455, 1997)." Nature **390**(6657): 315-315.
- Stachowiak, A. N., A. Bershteyn, et al. (2005). "Bioactive Hydrogels with an Ordered Cellular Structure Combine Interconnected Macroporosity and Robust Mechanical Properties." Advanced Materials **17**(4): 399-403.
- Staros, J. V. (1982). "N-hydroxysulfosuccinimide active esters: bis(N-hydroxysulfosuccinimide) esters of two dicarboxylic acids are hydrophilic, membrane-impermeant, protein cross-linkers." Biochemistry **21**(17): 3950-5.
- Steele, J. G., B. A. Dalton, et al. (1993). "Polystyrene chemistry affects vitronectin activity: an explanation for cell attachment to tissue culture polystyrene but not to unmodified polystyrene." J Biomed Mater Res **27**(7): 927-40.
- Steele, J. G., B. A. Dalton, et al. (1995). "Adsorption of fibronectin and vitronectin onto Primaria and tissue culture polystyrene and relationship to the mechanism of initial attachment of human vein endothelial cells and BHK-21 fibroblasts." Biomaterials **16**(14): 1057-67.

- Steiner, G., S. Tunc, et al. (2007). "Conformational Changes during Protein Adsorption. FT-IR Spectroscopic Imaging of Adsorbed Fibrinogen Layers." Anal. Chem. **79**(4): 1311-1316.
- Stockton, W. B. and M. F. Rubner (1997). "Molecular-Level Processing of Conjugated Polymers. 4. Layer-by-Layer Manipulation of Polyaniline via Hydrogen-Bonding Interactions." Macromolecules **30**(9): 2717-2725.
- Suckau, D., M. Mak, et al. (1992). "Protein surface topology-probing by selective chemical modification and mass spectrometric peptide mapping." Proc Natl Acad Sci U S A **89**(12): 5630-4.
- Taatjes, D. J., A. S. Quinn, et al. (1997). "Tertiary structure of the hepatic cell protein fibrinogen in fluid revealed by atomic force microscopy." Cell Biol Int **21**(11): 715-26.
- Takada, Y., X. Ye, et al. (2007). "The integrins." Genome Biol **8**(5): 215.
- Takuwa, Y. (2002). "Subtype-specific differential regulation of Rho family G proteins and cell migration by the Edg family sphingosine-1-phosphate receptors." Biochim Biophys Acta **1582**(1-3): 112-20.
- Tan, W. H. and S. Takeuchi (2007). "Monodisperse alginate hydrogel microbeads for cell encapsulation." Advanced Materials **19**(18): 2696-+.
- Tang, L. and J. W. Eaton (1993). "Fibrin(ogen) mediates acute inflammatory responses to biomaterials." J Exp Med **178**(6): 2147-56.
- Tang, L. and J. W. Eaton (1995). "Inflammatory responses to biomaterials." Am J Clin Pathol **103**(4): 466-71.
- Tang, L., Y. Wu, et al. (1998). "Fibrinogen adsorption and host tissue responses to plasma functionalized surfaces." J Biomed Mater Res **42**(1): 156-63.
- Termonia, Y. (1997). "Molecular Modeling of Structure Development upon Quenching of a Polymer Solution." Macromolecules **30**(18): 5367-5371.
- Tessmar, J. K. and A. M. Göpferich (2007). "Customized PEG-Derived Copolymers for Tissue-Engineering Applications." Macromolecular Bioscience **7**(1): 23-39.
- Thompson, J. D., D. G. Higgins, et al. (1994). "CLUSTAL W: improving the sensitivity of progressive multiple sequence alignment through sequence weighting, position-specific gap penalties and weight matrix choice." Nucleic Acids Res **22**(22): 4673-80.
- Tingey, K. G., Frautschi, J. R., Lloyd, D. R., Eberhart, R. C. (1983). "Alkylated polyethylene terephthalate with enhanced albumin affinity." Trans. Soc. Biomater. **9**: 125.
- Toscano, A. and M. M. Santore (2006). "Fibrinogen adsorption on three silica-based surfaces: conformation and kinetics." Langmuir **22**(6): 2588-97.
- Tsai, W. B., J. M. Grunkemeier, et al. (1999). "Human plasma fibrinogen adsorption and platelet adhesion to polystyrene." J Biomed Mater Res **44**(2): 130-9.
- Tsai, W. B. and T. A. Horbett (1999). "The role of fibronectin in platelet adhesion to plasma preadsorbed polystyrene." J Biomater Sci Polym Ed **10**(2): 163-81.
- Tsang, V. L. and S. N. Bhatia (2004). "Three-dimensional tissue fabrication." Advanced Drug Delivery Reviews **56**(11): 1635-1647.
- Tunc, S., M. F. Maitz, et al. (2005). "In situ conformational analysis of fibrinogen adsorbed on Si surfaces." Colloids and Surfaces B: Biointerfaces **42**(3-4): 219-225.

- Uchida, E., Y. Uyama, et al. (1994). "Grafting of Water-Soluble Chains onto a Polymer Surface." Langmuir **10**(2): 481-485.
- Um, E., D.-S. Lee, et al. (2008). "Continuous generation of hydrogel beads and encapsulation of biological materials using a microfluidic droplet-merging channel." Microfluidics and Nanofluidics **5**(4): 541-549.
- Van Brocklyn, J. R., M. J. Lee, et al. (1998). "Dual actions of sphingosine-1-phosphate: extracellular through the Gi-coupled receptor Edg-1 and intracellular to regulate proliferation and survival." J Cell Biol **142**(1): 229-40.
- Van Tassel, P. R. and P. Viot (1997). "A kinetic model of partially reversible protein adsorption." Journal of Chemical Physics **106**(2): 761.
- Van Thienen, T. G., J. Demeester, et al. (2008). "Screening poly(ethyleneglycol) micro- and nanogels for drug delivery purposes." International Journal of Pharmaceutics **351**(1-2): 174-185.
- Van Tomme, S. R., A. Mens, et al. (2008). "Macroscopic Hydrogels by Self-Assembly of Oligolactate-Grafted Dextran Microspheres." Biomacromolecules **9**(1): 158-165.
- Varghese, S. and J. H. Elisseeff (2006). "Hydrogels for musculoskeletal tissue engineering." Polymers for Regenerative Medicine: 95-144.
- Vazquez, C. P., T. Boudou, et al. (2009). "Variation of Polyelectrolyte Film Stiffness by Photo-Cross-Linking: A New Way To Control Cell Adhesion." Langmuir **25**(6): 3556-3563.
- Veklich, Y. I., O. V. Gorkun, et al. (1993). "Carboxyl-terminal portions of the alpha chains of fibrinogen and fibrin. Localization by electron microscopy and the effects of isolated alpha C fragments on polymerization." J Biol Chem **268**(18): 13577-85.
- Vogler, E. A. (1999). "Water and the acute biological response to surfaces." J Biomater Sci Polym Ed **10**(10): 1015-45.
- Voorhees, P. W. (1992). "Ostwald Ripening of Two-Phase Mixtures." Annual Review of Materials Science **22**(1): 197-215.
- Voros, J. (2004). "The density and refractive index of adsorbing protein layers." Biophys J **87**(1): 553-61.
- Voros, J., J. J. Ramsden, et al. (2002). "Optical grating coupler biosensors." Biomaterials **23**(17): 3699-710.
- Vroman, L. (1965). "A Resemblance between the Clotting of Blood Plasma and the Breakdown of Cytoplasm." Nature **205**: 496-7.
- Vroman, L. (2003). "Perspectives on blood/materials interactions." J Biomed Mater Res A **65**(2): 125.
- Vroman, L. and A. L. Adams (1969). "Identification of rapid changes at plasma-solid interfaces." J Biomed Mater Res **3**(1): 43-67.
- Vroman, L. and A. L. Adams (1986). "Rapid identification of proteins on flat surfaces, using antibody-coated metal oxide suspensions." J Immunol Methods **93**(2): 213-6.
- Vroman, L., A. L. Adams, et al. (1980). "Interaction of high molecular weight kininogen, factor XII, and fibrinogen in plasma at interfaces." Blood **55**(1): 156-9.
- Wacker, B. K., S. K. Alford, et al. (2008). "Endothelial cell migration on RGD-peptide-containing PEG hydrogels in the presence of sphingosine 1-phosphate." Biophys J **94**(1): 273-85.

- Wacker, B. K., E. A. Scott, et al. (2006). "Delivery of sphingosine 1-phosphate from poly(ethylene glycol) hydrogels." Biomacromolecules **7**(4): 1335-43.
- Weathersby, P. K., T. A. Horbett, et al. (1977). "Fibrinogen Adsorption to Surfaces of Varying Hydrophobicity." Journal of Bioengineering **1**: 395-409.
- Weber, K. and M. Osborn (1969). "The reliability of molecular weight determinations by dodecyl sulfate-polyacrylamide gel electrophoresis." J Biol Chem **244**(16): 4406-12.
- Wegener, K. L., A. W. Partridge, et al. (2007). "Structural basis of integrin activation by talin." Cell **128**(1): 171-82.
- Weisel, J. W. (2005). "Fibrinogen and fibrin." Adv Protein Chem **70**: 247-99.
- Wertz, C. F. and M. M. Santore (1999). "Adsorption and relaxation kinetics of albumin and fibrinogen on hydrophobic surfaces: Single-species and competitive behavior." Langmuir **15**(26): 8884-8894.
- Wigren, R., H. Elwing, et al. (1991). "Structure of adsorbed fibrinogen obtained by scanning force microscopy." FEBS Letters **280**(2): 225-228.
- Willerth, S. M., K. J. Arendas, et al. (2006). "Optimization of fibrin scaffolds for differentiation of murine embryonic stem cells into neural lineage cells." Biomaterials **27**(36): 5990-6003.
- Willerth, S. M., A. Rader, et al. (2008). "The effect of controlled growth factor delivery on embryonic stem cell differentiation inside fibrin scaffolds." Stem Cell Res **1**(3): 205-18.
- Wittmer, C. R., J. A. Phelps, et al. (2007). "Fibronectin terminated multilayer films: protein adsorption and cell attachment studies." Biomaterials **28**(5): 851-60.
- Wojciechowski, P. W. and J. L. Brash (1993). "Fibrinogen and albumin adsorption from human blood plasma and from buffer onto chemically functionalized silica substrates." Colloids and Surfaces B: Biointerfaces **1**(2): 107-117.
- Xu, L. C. and C. A. Siedlecki (2007). "Effects of surface wettability and contact time on protein adhesion to biomaterial surfaces." Biomaterials **28**(22): 3273-83.
- Xu, L. C. and C. A. Siedlecki (2009). "Atomic Force Microscopy Studies of the Initial Interactions between Fibrinogen and Surfaces." Langmuir **25**(6): 3675-81.
- Yakovlev, S., S. Gorlatov, et al. (2003). "Interaction of fibrin(ogen) with heparin: further characterization and localization of the heparin-binding site." Biochemistry **42**(25): 7709-16.
- Yang, L., Y. Yatomi, et al. (1999). "Metabolism and functional effects of sphingolipids in blood cells." Br J Haematol **107**(2): 282-93.
- Yatomi, Y. (2006). "Sphingosine 1-phosphate in vascular biology: possible therapeutic strategies to control vascular diseases." Curr Pharm Des **12**(5): 575-87.
- Yatomi, Y., Y. Ozaki, et al. (2001). "Sphingosine 1-phosphate: synthesis and release." Prostaglandins Other Lipid Mediat **64**(1-4): 107-22.
- Yatomi, Y., S. Yamamura, et al. (1997). "Sphingosine 1-phosphate induces platelet activation through an extracellular action and shares a platelet surface receptor with lysophosphatidic acid." J Biol Chem **272**(8): 5291-7.
- Yeh, J., Y. Ling, et al. (2006). "Micromolding of shape-controlled, harvestable cell-laden hydrogels." Biomaterials **27**(31): 5391-5398.

- Z. Tang, Y. W., P. Podsiadlo, N. A. Kotov, (2006). "Biomedical Applications of Layer-by-Layer Assembly: From Biomimetics to Tissue Engineering." Advanced Materials **18**(24): 3203-3224.
- Zamarron, C., M. H. Ginsberg, et al. (1990). "Monoclonal antibodies specific for a conformationally altered state of fibrinogen." Thromb Haemost **64**(1): 41-6.
- Zhang, Z., H. Ma, et al. (2005). "Pretreatment of Amphiphilic Comb Polymer Surfaces Dramatically Affects Protein Adsorption." Biomacromolecules **6**(6): 3388-3396.
- Zisch, A. H., M. P. Lutolf, et al. (2003). "Cell-demanded release of VEGF from synthetic, biointeractive cell ingrowth matrices for vascularized tissue growth." FASEB J **17**(15): 2260-2.
- Zoungrana, T., G. H. Findenegg, et al. (1997). "Structure, stability, and activity of adsorbed enzymes." Journal of Colloid and Interface Science **190**(2): 437-448.
- Zucker, M. B. and L. Vroman (1969). "Platelet adhesion induced by fibrinogen adsorbed onto glass." Proc Soc Exp Biol Med **131**(2): 318-20.

Vita

Evan Alexander Scott

Date of Birth June 24, 1979

Place of Birth Baltimore, MD

Degrees Sc.B. Biomedical Engineering, May 2002
Ph.D. Biomedical Engineering, June 2009

Professional Societies Society for Biomaterials
Biomedical Engineering Society
National Society for Black Engineers

Publications Scott EA, Nichols MD, Willits RK, Elbert DL. Modular scaffolds assembled around living cells using poly(ethylene glycol) microspheres with macroporation via a non-cytotoxic porogen. *Acta Biomater.* (Under review).

Nichols MD, Scott EA, Elbert DL. Factors affecting size and swelling of poly(ethylene glycol) microspheres formed in aqueous sodium sulfate solutions without surfactants. *Biomaterials.* (Under review).

Chang SH, Custer PL, Mohadjer Y, Scott E. Use of Lorenz[®] titanium implants in orbital fracture repair. *Ophthalm Plast Reconstr Surg.* 2009 Mar-Apr;25(2):119-22.

Scott EA, Nichols MD, Cordova LH, George BJ, Jun YS, Elbert DL. Protein adsorption and cell adhesion on nanoscale bioactive coatings formed from poly(ethylene glycol) and albumin microgels. *Biomaterials.* 2008 Dec;29(34):4481-93.

Elbert DL, Mawuenyega K, Scott EA, Bateman RJ. Stable isotope labeling tandem mass spectrometry (SILT): Integration with peptide identification and extension to data-dependent scans. *J. Proteome Res.* 2008 Sep 6;7(10), pp 4546–4556.

Wacker BK, Alford SK, Scott EA, Das Thakur M, Longmore GD, Elbert DL. Endothelial cell migration on RGD-peptide containing PEG hydrogels in the presence of sphingosine 1-phosphate. *Biophys J.* 2008 Jan 1;94(1):273-85.

Scott EA, Elbert DL. Mass spectrometric mapping of fibrinogen conformations at poly(ethylene terephthalate) interfaces. *Biomaterials*. 2007 Sep;28(27):3904-17.

Wacker BK, Scott EA, Hughes SK, Elbert DL. Delivery of sphingosine 1-phosphate from poly(ethylene glycol) hydrogels. *Biomacromolecules*. 2006 Apr; 7(4):1335-1343.

Kim JK, Scott EA, Elbert DL. Proteomic analysis of protein adsorption: Serum amyloid P adsorbs to materials and promotes leukocyte adhesion. *J Biomed Mater Res A* 2005 Oct 1;75(1):199-209.

Godbee J, Pattamunuch P, Scott E, Mathiowitz E. Degradation of Multi-Phase Microspheres Fabricated Via Solvent Removal. *J. Microencapsulation*. 21(3) 2004: 331-352.

Godbee J, Scott E, Pattamunuch P, Chen S, Mathiowitz E. The Role of Solvent/Non-Solvent Ratio for Sphere Formation Using the Solvent Removal Method. *J. Microencapsulation*. 21(2) 2004: 151-160.